CRANFIELD UNIVERSITY

Paul Daniel Liddel

Transforming Composite Design by Use of Structural Health Monitoring

School of Aerospace, Transport and Manufacturing (formally SAS)

PhD
Academic Year: 2016 - 2017

Supervisor: Professor Peter Foote
December 2016

CRANFIELD UNIVERSITY

School of Aerospace, Transport and Manufacturing (formally SAS)

PhD

Academic Year 2015 - 2016

Paul Daniel Liddel

Transforming Composite Design by Use of Structural Health Monitoring

Supervisor: Professor Peter Foote
December 2016

© Cranfield University 2016. All rights reserved. No part of this publication may be reproduced without the written permission of the copyright owner.

ABSTRACT

Commercial composite aerospace structure is required to be designed and managed under the damage tolerant principle. Airworthiness is maintained through a process of regulated inspections and if required maintenance. Currently inspections use visual and assisted visual (non-destructive inspection - NDI) techniques. Damage tolerant operation is therefore reliant on inspectability. Unlike metal structure composite and adhesively bonded structure may show few if any recognisable indicators prior to rapid failure, either visually or using NDI. Although stringent manufacturing processes are demanded to best ensure components are fit for service strategies such as reducing stresses by oversizing components or in the case of bonded features additional mechanical fasteners may be included to allow operation with this potential structural uncertainty.

Structural Heath Monitoring (SHM) uses data from in-situ sensors to assess the condition of the structure. If via SHM any uncertainty associated with difficult to inspect components could be eliminated less reliance would be required of additional structure or features allowing lighter and more efficient structure to be viable with no impact on current airworthiness demands. Despite much previous research no SHM system is in use with in-service composite or bonded aerospace components. When operating a structure under Damage-tolerance operational requirements damage must be positively identified to allow repairs to be made whist ensuring appropriate airworthiness demands are maintained. Such demands must also be met by structure inspected using SHM. Unlike previous studies this research combines the process of structural design and in-situ monitoring to address the issues identified. Termed SHM enabled design this approach allows the implementation of monitoring technology and the potential for benefits including the reduced reliance on inefficient additional structure to be viably included in actual structure.

Investigations into previous developments in SHM strategies, performance and design of bonded composite structure and the requirements of certified operation within the aerospace sector were performed. It was also recognised

once stress/strain levels at critical regions of standard bonded double lap/strap joints are exceeded there is a strong tendency for the joint to fail near instantaneously and catastrophically. Critical stress/strain levels are not only dependent on the adhesive used but also the quality of the bond. This may be influenced by manufacturing defects, accidental damage or in-service degradation such as environmental ingress. Rapid failure which shows little or no advanced indicators recognisable by either visual inspection or non-destructive inspection limits the efficient use of purely bonded structure in aerospace structures.

From this a novel SHM enable bonded composite joint was developed based on modified joint geometry. This adaption influences the stress/strain distributions within the bond-line preventing near instantaneous failure and controlling damage growth. The modified structure was used in conjunction with surface mounted strain monitoring, allowing damage to be identified whilst sufficient residual properties remained allowing an inspection (via the in-situ sensors) and maintenance regime to be made possible. Such an approach has not previously been explored. The SHM enabled design has experimentally demonstrated appropriate responses to damage initiation that are easily identified and interpreted. This approach can provide action thresholds for maintenance while significant residual properties are still present. Used in-conjunction with application methods proposed, in the cases investigated, damage and appropriate maintenance action thresholds were identified with 100% detection and zero cases of no-fault-found responses. In the poorest residual strength case an SHM enabled joint reported damage whilst a further 16.8% of the load at which damage was positively identified was required to cause failure. In all other test cases at least a further 74% of the load at which damage was positively reported was required to cause the joint to fail. Such behaviour was present both in joints which failed as a result of problematic ‘adhesive’ type failure as well as mixed mode ‘adhesive/cohesive’ damage. To the best of the author’s knowledge no previous contribution has exploited such a concept.

In conjunction with the application methods proposed the system may be used to aid qualification of bonded components in compliance with current legislation. Once used in this manner the ability for a bonded joint to have a static load capability greater than the structures Design Limit Load (DLL), the highest load expected in service, may be assured even if the performance of the bond degrades over time. The lowest strength joint in this study revealed signs of initial damage positively recognised by the SHM system at only 64% of the DLL, representative of a significantly degraded joint. This structure however continued to transfer load, ultimately failing at 136% of the DLL.

Estimations of the damage size to ≈2mm accuracy in length could be made. As physical damage was present all maintenance actions triggered by the SHM enabled joint have the capability to be confirmed via standard NDI techniques. The influence of the amended geometry used in the specific design tested resulted in a reduction in potential strength of the joint over standard configurations (0.78 knock-down factor). The removal or reduction of similar knockdown factors included on conventional structure to account for uncertainties in the bonds actual performance (made possible by the SHM enabled design) however result in joints with potentially improved design strengths over conventional joint configurations.

Although, as is required of contemporary structure, such joints would not be designed to deliberately fail degradation behaviour appropriate to damage tolerant operation occurs regardless of joint condition and failure type. This approach is therefore suitable for problematic in-service structure which by definition falls outside of required specifications. Strategies and considerations in the application of these SHM enabled joints are put forward. The result is a design of SHM enabled bonded composite joint which meets the demands of aircraft regulators as included in the FAA documentation AC20-107B without the requirement of inefficient additional structural features allowing an alternative to current inspection methods to be viable.

Keywords:

Bonded Joint, Damage tolerance, DIC, FEA, SHM enabled design, Strain

ACKNOWLEDGEMENTS

The author would like to thank the support, assistance and sponsorship provided by BAE Systems, and in particular Jim McFeat, during the research conducted for this thesis.

My deepest thanks and gratitude go to my supervisor Professor Peter Foote for his endless guidance, support and patience.

Many thanks to my friends and colleagues linked to the Cranfield composites centre – Giacomo, Diego, Tassos, Thomas, Vincenzo, Kostas, Lawrence, Ben, Andrew, David, Alex, Sharon, Hameed, Thibault, Lesley-Ann, Sat, Sonia and Luca – for your friendship and support and for listening to my terrible jokes and putting up with me during the good and not so good times. Included and in addition to those above I would also like to thank Jim Hurley for his essential assistance in the laboratory.

Thank you Dad, I hope you would be proud.

My greatest thanks go to Sarah whose love and support has been unwavering over the last few years, both regarding this work and in the greater aspects of life. Thank you Sarah, you are everything to me.

TABLE OF CONTENTS

LIST OF FIGURES

LIST OF TABLES

LIST OF EQUATIONS

LIST OF ABBREVIATIONS

AD	Accidental Damage
AE	Acoustic Emission
A-SHM	Automated SHM
BVID	Barely Visible Impact Damage
CAD	Computer Aided Design
CFRP	Carbon Fibre Reinforced Plastic
CVM	Comparative Vacuum Monitoring
DIC	Digital Image Correlation
DLL	Design Limit Load
DUL	Design Ultimate Load
ED	Environmental Damage
EMI	Electromagnetic Interference
FAA	Federal Aviation Administration
FAR	Federal Aviation Regulations
FBG	Fibre Bragg Grating
FD	Fatigue Damage
FEA	Finite Element Analysis
FOS	Fibre Optic Sensor
FST	Full Scale Test
GA	Genetic Algorithm
GFRP	Glass-Fibre Reinforced Plastic
IDT	Inter-Digital Transducer
ISHM	Integrated Systems Health Management
JAR	Joint Aviation Requirements
KN	Knee
LL	Limit Load
LL	Linear Limit
MAFT	Major Aircraft Fatigue Test
MEMS	Micro-Electro-Mechanical Systems
NDI	Non-Destructive Inspection
NDT	Non-Destructive Testing
OF	Optical Fibre

PABST	Primary Adhesive Bonded Structure Technology
PTFE	Polytetrafluoroethylene
PSE	Principle Structural Element
PZT	Piezoelectric transducer
RSG	Resistance Stain Gauge
RTM	Resin Transfer Moulding
SAE	Society of Automotive Engineers
SHM	Structural Health Monitoring
SMCS	Surface Mountable Crack Gauges
S-SHM	Scheduled SHM
TRL	Technical Readiness Level
UL	Ultimate Load/strength
UV	Ultraviolet
VID	Visual Impact Damage

Glossary of terms

Adherend	A surface or object bonded by an adhesive
Automated SHM	Any SHM technology which does not have a predetermined interval at which maintenance action must take place, but instead relies on the system to inform maintenance personnel that action must take place [1]
Damage tolerance	The attributes of the structure that permits it to retain its required residual strength for a period of use after the structure has sustained a given level of fatigue, corrosion, or accidental or discrete source damage [2]
Damage tolerant design/operation	Design and operation based on consideration of a structures damage tolerance combined with appropriate inspection and maintenance actions
Design Limit Load	The largest loads expected to be experienced during operation by any aircraft of entire fleet of the design type
Design Ultimate Load	Loads to which many aircraft structures are designed to at withstand, usually 1.5 x DLL
Fail-safe	The attribute of the structure that permits it to retain its required residual strength for a period of unrepaired use after the failure or partial failure of a principle structural element
Joint Plate	Representative of structure being joined
Joint Strap	Additional structure forming the overlap of double strap type joints
Primary Structure	The structure which carries flight, ground, or pressurisation loads, and whose failure would reduce the structural integrity of the aircraft [3]
Safe life	The number of events within which a structural has a low probability of degrading below its design ultimate value due to fatigue cracking
Scheduled SHM	To use/run/read out a SHM device at an interval set at a fixed schedule [1]
Structural Health Monitoring	The process of acquiring and analysing data from on-board sensors to determine the health of a structure
SHM enabled design/structure	Structure which could otherwise not be operated and therefore any benefits exploited without the inclusion of SHM

1 Introduction

Composite materials, particularly Carbon Fibre Reinforced Plastics (CFRPs), are being used in more applications than ever largely due to their excellent specific properties and the ability to produce structures specifically tailored for their application. This may allow benefits including lighter or more aerodynamically efficient components to be produced when compared to using traditional materials. As a result composites are of great interest and are finding greater use within the aerospace sector.

Commercial composite aerostructures are required to be designed and operated using damage tolerant principles. This approach ensures continued airworthiness through the action of regular inspections and appropriate maintenance actions. Intervals between routine inspections are selected based on typical rates of damage growth and the ability of inspection by visual and assisted visual (Non-destructive Inspection – NDI) methods to detect potential damage. As such the damage tolerant principle is based on a foundation of inspection and inspectability.

Aerospace damage tolerant designs must conform to either ‘No-growth’, ‘Slow-growth’, or ‘Arrested growth’ philosophies regarding damage. This philosophy was originally developed for metallic structure where damage growth equates to crack growth. Unlike metals composite and adhesively bonded components may reveal little or no visual indicators or other measurand exploited via NDI prior to rapid catastrophic failure. As a result the ‘No-growth’ approach is commonly adopted. As a consequence components may be oversized to reduce stresses or in the case of adhesive bonds supplementary features may be included such as additional mechanical fasteners. This produces airworthy structure but at the cost of increased mass and manufacturing complexity.

Structural Health Monitoring (SHM) is the process of acquiring and analysing data provided by on-board sensors to determine the health of a structure [4]. Such a process has the potential, with appropriate amendment to current legislation, to provide all or part of the inspection requirements needed to manage damage tolerant structure. By building in SHM sensors, the structure can continuously inspect itself hence removing the uncertainties in status of structural integrity that currently

account for deliberate, precautionary over engineering. Despite many years of research no such system has been included within in-service composite or bonded aerospace assemblies to date other than for loads or usage monitoring. Under damage tolerance operation it is essential that any damage must be reliably identified with sufficient warning to ensure maintenance actions may be performed while suitable airworthiness levels remain. This must therefore also be the case for structure inspected by SHM. The problems associated with damage identification in combination with rapid or unpredictable damage growth must therefore be considered if a damage tolerance philosophy based on the incorporation of SHM is to be viable.

This research attempts to combine the process of composite structural design and in-situ monitoring strategy to overcome the issues discussed. Rather than the contemporary approach of developing structure and any retrofitted monitoring system independently it is proposed both should be designed simultaneously as an integrated system. It is believed this approach, termed 'SHM enabled design', will allow benefits gained through the implementation of inspection technology to be achieved. In this thesis the potential benefits applicable to composite structures, the problems currently inhibiting the use of SHM, and the ability to tailor damage behaviour appropriate to damage tolerant operation are considered. On this basis a novel SHM enabled design concept based on bonded composite structure has been developed. Tapered width joint straps tailor the strain experienced by the adhesive in the working bond-line promoting slow damage growth in the event of the structure becoming degraded/experiencing damage or overload. This in conjunction with in-situ sensors allows the damage to be identified prior to catastrophic failure with sufficient warning as to allow an inspection-maintenance regime to be viable. No previous contribution has been identified which exploits such a concept. The long term aim of this research is to eventually reduce or eliminate the requirement of inefficient additional features currently used to account for the uncertainty of the condition of these necessary joints.

This thesis explores the approaches used in aerospace operation and design as well as techniques, methods and technologies currently under development in the field of SHM. From this issues are identified and structure likely to be suitable both for the

implementation as well as providing benefits from the implementation of SHM enable design are selected and their physical characteristics in the presence of damage explored. Using the example of carbon fibre composite with adhesively bonded joints, an iterative design and test program is presented as the SHM enabled design evolves both in developing appropriate structural behaviour as well as sensing strategies. Consideration is made regarding the interpretation and potential consequences of the data produced by such a system and how this may be used in practical applications. A summary of the findings and results are discussed. Potential issues are highlighted and possible routes for further research and development to bring the SHM enabled structure philosophy, with particular focus on adhesively bonded composite structure, are suggested.

1.1 Thesis Structure

A literature review is presented in Chapter 2 which identifies and discusses aerospace design and operational philosophies required of modern aerospace structure. The literature review continues by reviewing the development of structural health monitoring techniques and each approaches effectiveness in monitoring various forms of damage in composite materials and bonded structure. The literature review ultimately appraises current research which considers SMH influenced engineering design.

Based on findings from the literature review defined research objectives are presented in Chapter 3. Focus is made on structure considered appropriate to the inclusion of SHM as an element of design in the form of bonded joints and suitable in-situ monitoring in the form of surface strain measurement. Research questions are presented to address design efficiency and operational shortfalls in current aerospace structure that may be addressed by SHM enabled designs.

Adhesively bonded joints are identified as being likely to benefit from SHM considered design in Chapter 3. Chapter 4 therefore reviews analytical and numeric approaches used in the design and analysis of bonded joints with consideration of how this information may be used to address previously identified issues including rapid catastrophic joint failure.

Chapter 5 details the experimental methodology used in this research. This includes specimen design and fabrication, numerical (FEA) analysis, and mechanical testing and data collection techniques.

Design, testing and analysis of evolutions in SHM enable joint design are presented in Chapters 6, 7, & 8.

Chapter 9 presents methods that may be used in-conjunction with the SHM enabled joint design in practical applications. Methods proposed are designed to enable such structure to be used in close conjunction with current legislation and increase the effectiveness of the SHM/structure system.

Chapter 10 discusses the research findings, addresses research questions set in Chapter 3, and suggests further research based on the work of this thesis.

1.2 Publications

Liddel, P.D., Foote, P., (2015) “SHM Enabled Design: Application to Damage Tolerance Design with Bonded, Composite Joints”, *10th International Workshop on Structural Health Monitoring*, Stanford, CA

Aspirational Papers

Journal papers based on the work presented in this these are hoped to be published in the following publications in the near future:

Mechanical Systems and Signal Processing

Composites Part A: Applied Science and Manufacturing

Composites Part B: Engineering

2 Literature Review

2.1 Introduction

The following chapter details a literary survey used to understand current aerospace structural design philosophies and how the capabilities and implementation of Structural Health Monitoring (SHM) may impact or influence designs therefore creating benefits over unmonitored structure. Initially this review focusses on aerospace design philosophies and how structures designed with these approaches are influenced in terms of structural requirements and operation. This is followed by a review of the development of SHM techniques with focus on studies relevant to composite structure. The final element of this review is an appraisal of existing literature on the topic of SHM influenced structural design.

2.2 Aerospace Structural Design Philosophies

Aero-structure design has evolved throughout the history of manned flight. Currently there are three principle philosophies, that of: 'Safe-life', 'fail-safe' and 'damage tolerant' design. Each approach is considered in detail in the sections below.

2.2.1 Safe-life Design

Introduced during the post war years the safe-life design philosophy takes into account the cyclic stresses experienced by airframes which result in fatigue [5]. The Federal Aviation Administration (FAA) defines safe-life as, "The number of events, such as flight cycles, landings, or flight hours, within which the structural strength has a low probability of degrading below its design ultimate value due to fatigue cracking" [2]. Safe-life designs must therefore experience no significant cracking within this prescribed safe-life [6].

Designs are initially based on fatigue calculations. Although originally developed for metallic airframes the certification of composite structures must meet equivalent structural integrity, safety and durability requirements [7]. The safe-life is calculated by testing at various scales, considering fatigue data (Figure 1), and examination of the expected load spectrum. Evaluations are tested by full scale testing [8].

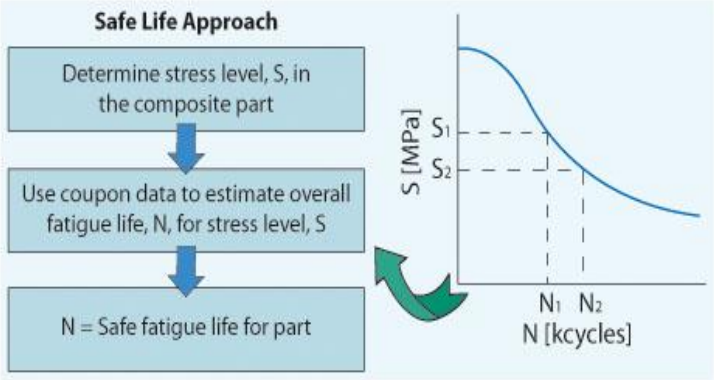

Figure 1: Estimation of safe fatigue life based on coupon tests results for cycles to failure [9]

An example of the safe-life design process is shown below (Figure 2):

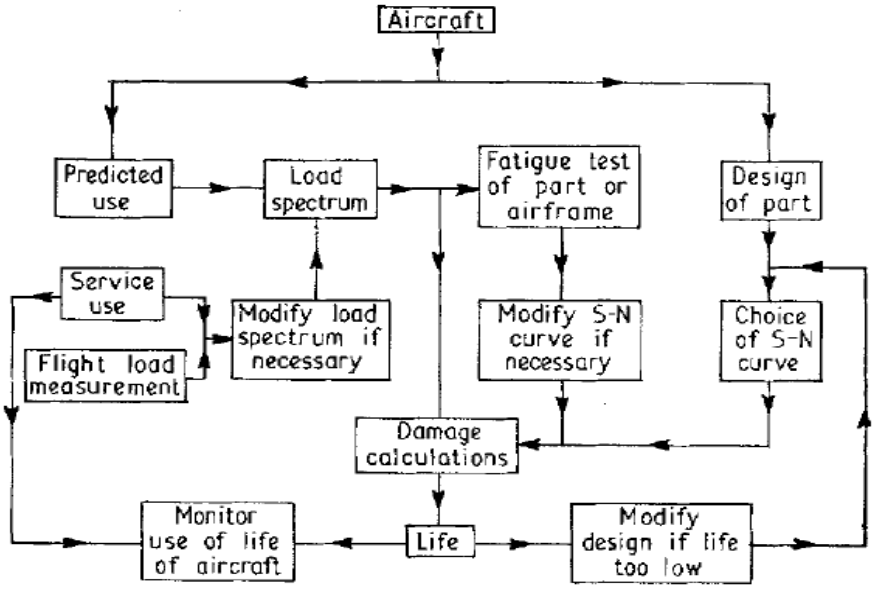

Figure 2: The Safe-life process [10]

The safe-life specified must ensure that the likelihood of failure in-service is less than 1 in 1000 [11]. Safe-life designs/evaluations do not usually consider growth rates or residual strength after fatigue damage [12]. When the safe-life is reached the structure must be taken out of service or replaced. As such a very large percentage of the fleet population (>99.9%) will be removed from service long before the potential useful life has been reached [11]. Currently, in civil aircraft, safe-life designs are only permitted for landing gear components, and some engine parts. Safe-life philosophies are however still commonly used in helicopter design [13]. Some military aircraft also exploit safe-life design [14,15].

‘Scatter values’ are used to make allowances for variability in fatigue performance therefore ensuring an acceptably low probability of failure [11].

In essence [12]:

The safe life = The mean test life ÷ The scatter value

Equation 1

The approach for calculating the mean test life and scatter factor to establish the safe-life of a small, metallic aircraft from full scale tests is shown below:

The statistical distribution of fatigue follows a log-normal statistical distribution therefore the arithmetic mean of tested structure cannot be used as ‘the mean test life’. The logarithmic mean test life is calculated using the equations shown below [12]:

$$\log_{10}(\text{meantest life}) = \frac{1}{n}\sum_{i=1}^{n}\log_{10}(\text{test life}_i)$$

Equation 2

$$\text{meantest life} = 10^{\log_{10}(\text{meantest life})}$$

Equation 3

Note: logarithmic mean values are lower than arithmetic mean values.

A scatter factor is implemented to account for the inherent statistical variability of fatigue performance within built up structures. It is assumed the fatigue life follows a log-normal distribution. The scatter factor is calculated using the equation below [12]:

$$\text{Scatter Factor}_{FST} = 10^{Z_p\sigma\sqrt{\frac{n_s+1}{n_s}}}$$

Equation 4

Where: FST denotes full-scale test

Z_p is the standard normal distribution for the specified probability of a detectable crack-free safe-life.

σ is the standard deviation of the population of fatigue test lives. For use in this equation, σ, is a percentage of the log of the mean test life for the built up or mono-lithic structure.

n_s is the number of fatigue specimens tested.

For small aircraft the FAA stipulate a Zp value of 3.511 [16] equalling a probability of 99.978% that the structural component will reach its safe-life without acquiring a detectable fatigue crack [12]. Different Zp values may be stipulated for different applications, such as helicopters or safe-life structure on commercial aircraft. Details for requirements of large aeroplanes are described in [17].

A comparison of service lives to failure against estimated lives was conducted during the early 1960's. Results are shown in Figure 3. It is apparent a scatter factor (life factor) of 5 may be appropriate when estimating fatigue life. Factors between 6 and 3.5 were used for civil aircraft during this period with values dependent on the number of tests undertaken [10]. The importance of scatter factors can be seen as all but three of the 45 failures failed before the predicted safe-life (life factor = 1).

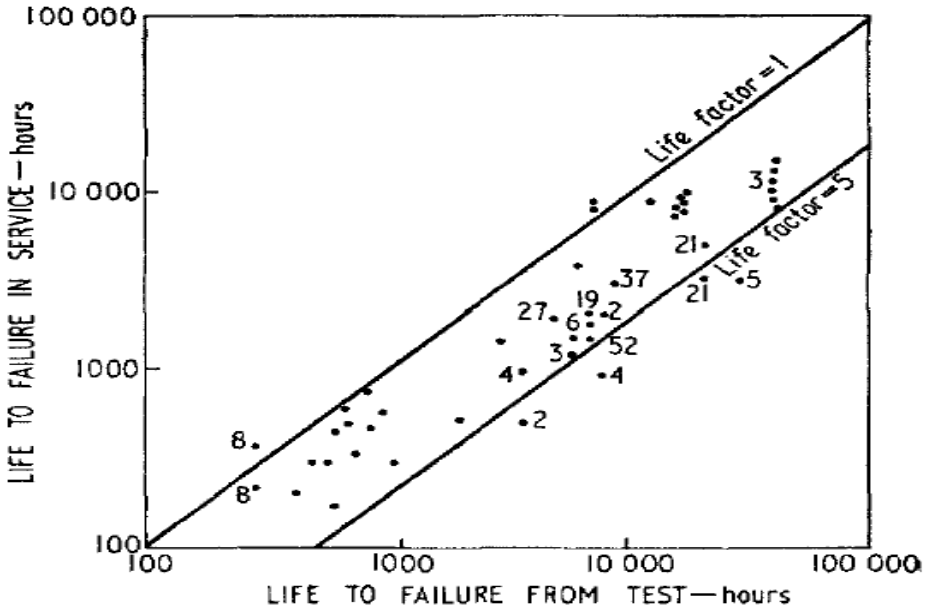

Figure 3: Comparison of failures against lives estimated from full scale tests [10]

2.2.2 Fail-Safe Design

Many issues associated with safe-life design principles were addressed through the implementation of ‘fail-safe’ methods during the late 1950’s [18].

The FAA defines ‘fail-safe’ as “The attribute of the structure that permits it to retain its required residual strength for a period of unrepaired use after the failure or partial failure of a principle structural element” [2]. Cracks [damage] may form, however this is either not permitted to grow to critical dimensions or the failure of a component will not cause failure of the greater structure [10].

Methods to ensure fail-safe structure include crack stoppers – features to limit the growth of cracks to sizes below that which would compromise the structure – and multiple load paths [19]. Multi-load path construction ensures loads are shared by two or more features of the airframe. If one fails the remaining undamaged element(s) must carry the loads designated by fail-safe criteria [19]. Back-up structure is another alternative. In this case a single member may carry the entire load however in the event of failure a secondary member is available to assume the load [12].

After fail-safe failure the remaining structure is required to support 80% of the Design Ultimate Load (DUL) in military aircraft and the Design Limit Load (DLL) on civil aircraft [10]. Excessive deformation must also be prevented [12]. In addition all fail-safe structure must be designed to be at least depot level inspectable [20]. This requirement is essential, as once a component within a fail-safe structure has failed the systems required redundancy is no longer present.

2.2.2.1 Fail-safe evaluation

A typical evaluation is described in the FAA advisory circular AC 23-13A. Although primarily focused on metallic structure of ‘normal, utility, acrobatic, and commuter category aircraft’, the process summarised below would appear applicable when considering fail-safe designs for larger jet powered civil aircraft, as well as fail-safe military airframes.

A typical fail-safe evaluation will generally include the following [12]:

1. Identify the structural components that will need to be made fail-safe. This process will include determining the primary/critical structure and identifying appropriate fail-safe techniques, e.g. crack stopper or redundant load path.

2. Determine the loading conditions. This should include establishing the loads (including that of dynamic loading- see below) experienced by primary as well as redundant structure, both with and without structural damage.

3. Establish the degree of damage for which the fail-safe structure will be designed (for civil aircraft this may be determined by industry legislation).

4. Validate that the fail-safe objective of the structure has been fulfilled through appropriate structural testing and analysis.

5. Design an inspection program suitable for the early detection of structural fatigue/damage.

2.2.3 Damage Tolerant Design

The United States Air force originally developed a damage tolerance philosophy during the early 1970's to address structural failures and cracking problems that had been associated with various safe-life designed military aircraft. A review of failures identified that safe-life principles offered little protection to designs sensitive to damage or defects introduced either during manufacture or in service. In addition not all cracks may be identified during the inspection of older airframes [20]. Examples of safe life failings include the losses of two de Havilland comet 1 aircraft – the world's first commercial jet airliner – in similar circumstances during only their second year of service. Investigation into these accidents revealed failure was caused by structural failure of the pressure cabin as a result of fatigue. Using fracture mechanics approaches not available at the time of the incidents (1954) it has been estimated in one of the cases that the initial defect size was in the region of 100μm in size which is considered to be not incompatible with the methods of manufacture at the time [21]. A further example is the loss of a US air-force F-111A military jet during an exercise in 1969. An undetected manufacturing flaw grew to a

critical size resulting in the loss of the aircraft after only 100 flying hours. Prior to this, representative airframes, components and sub-assemblies had been fatigue tested for 40,000 hours and a scatter factor of four used. This process certified a 'safe-life' of 10,000 hours to the aircraft [5]. In such cases failures occurred due to unidentified or unexpected flaws that were unlikely to be detected before the structure which was not designed to manage such defects rapidly and catastrophically failed. The recognition that undetected defects may potentially be present was in part responsible for the development of damage tolerant design. The damage tolerance approach was adopted by civil transport regulation in 1978 via the FAR & JAR documents 25.571 [22]. The FAA defines damage tolerance as, "The attributes of the structure that permits it to retain its required residual strength for a period of use after the structure has sustained a given level of fatigue, corrosion, or accidental or discrete source damage". The structure should also not suffer excessive structural deformation [2]. Designs should also maintain optimal structural efficiency with minimum weight, manufacturing, maintenance and repair as well as supportability costs [23]. Any damage should be detectable through inspection, and repaired so the structure is again capable of sustaining the DUL [24]. Inspection at well-defined intervals is therefore a critical criterion. This is graphically represented in Figure 4.

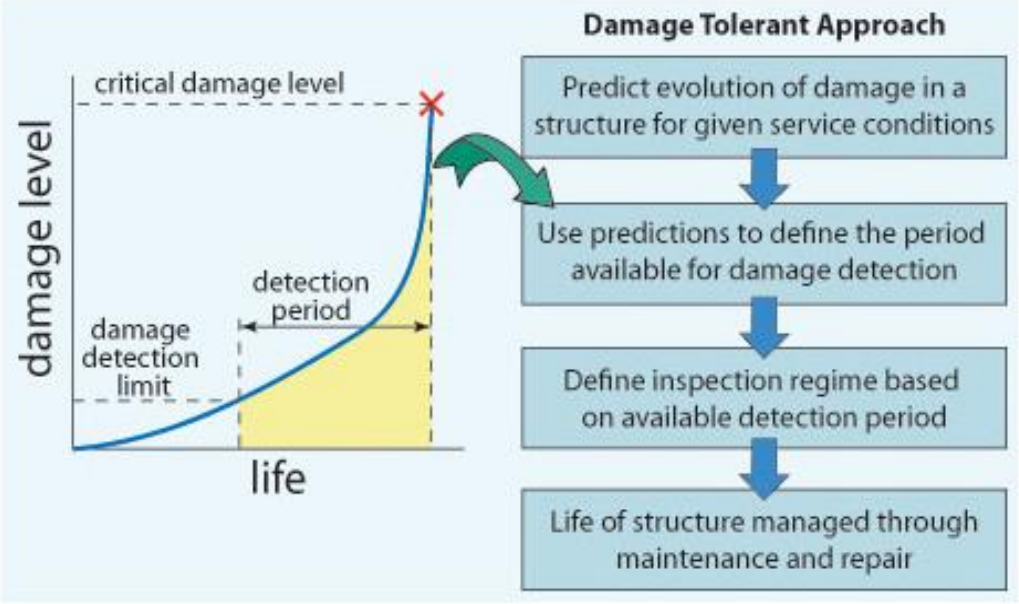

Figure 4: Damage tolerant design principle [9]

Damage tolerance designs must therefore consider three distinct, equally important, aspects: Residual strength (Allowable damage), Damage growth, and Damage detection (Inspection) [2,18,24]. Damage types and severity may be categorised against expected service loads. Figure 5 illustrates the damage categorisation process, additional details can be found in [3,22,25]. Figure 6 demonstrates how this approach compares the requirements of residual load bearing capacity to various categories of composite damage and how each damage type should be addressed.

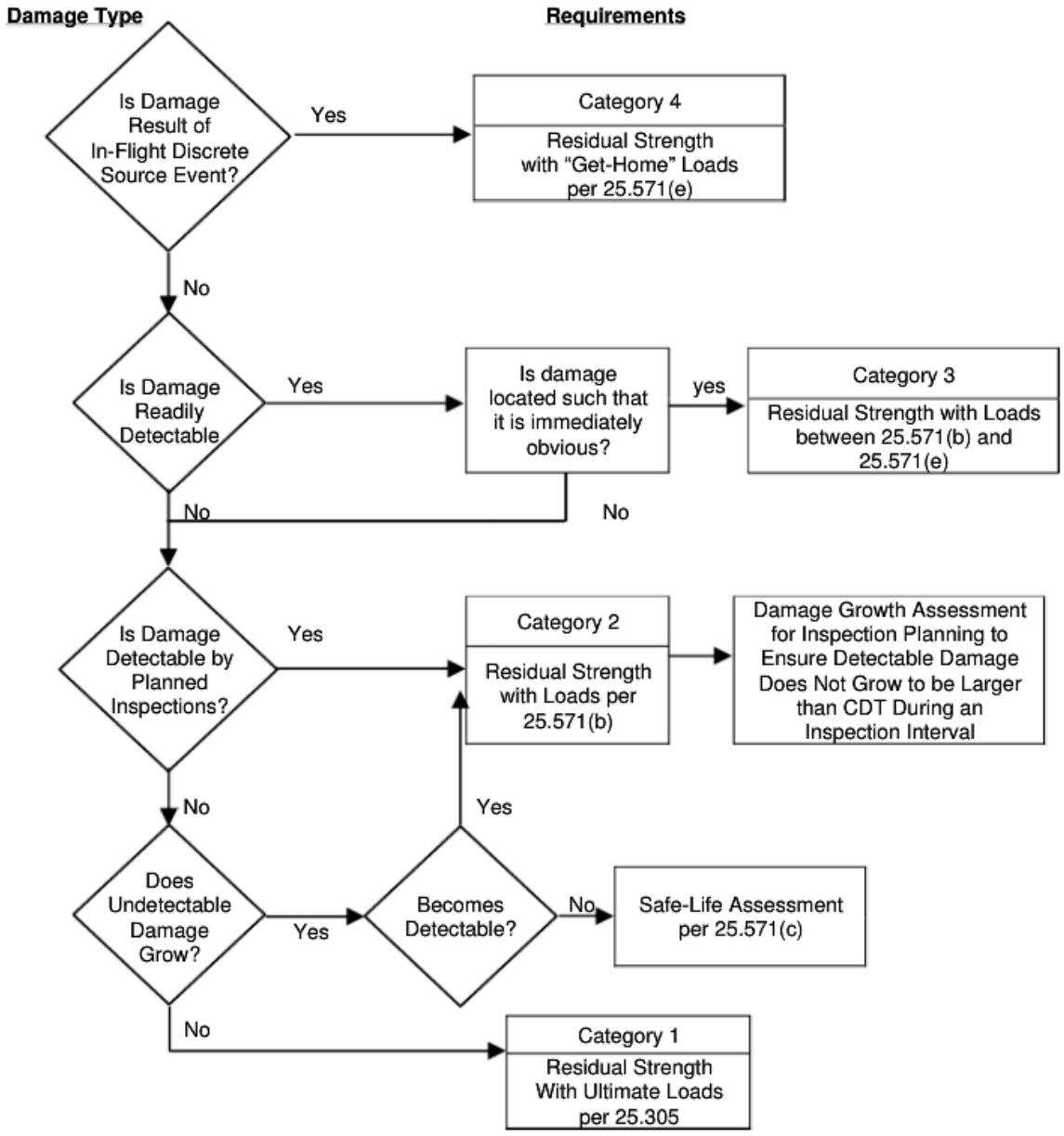

Figure 5: Composite damage categorisation process [26]

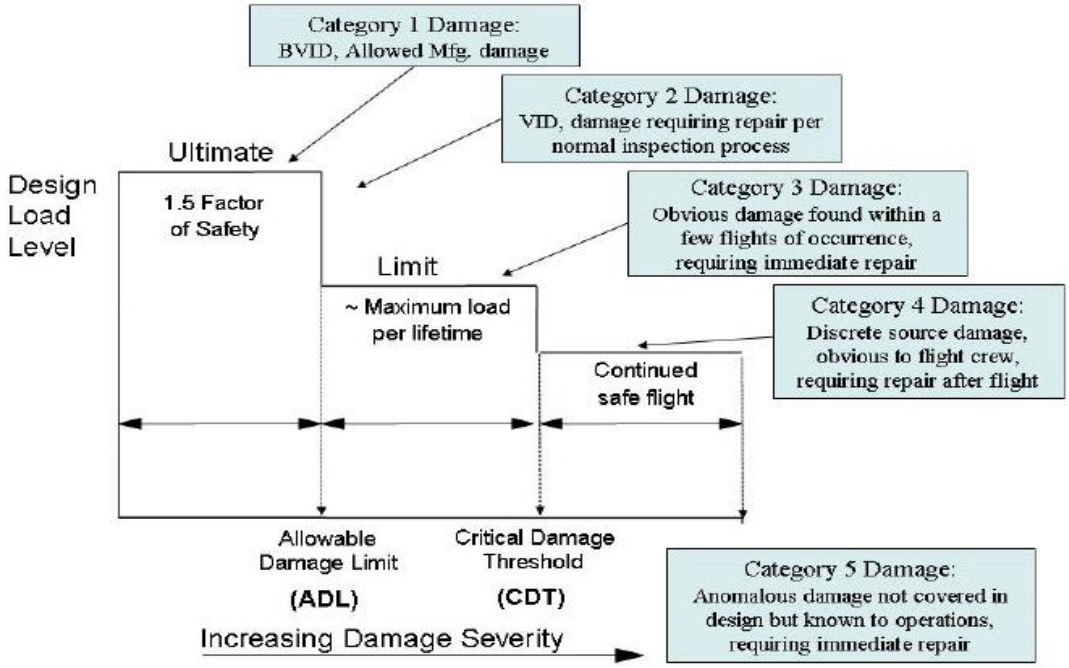

Figure 6: Categories of structural damage and the requirements of damage tolerant composite airframes [3]

To ensure damage is appropriately identified critical damage must be of a size that will be detected with a high degree of probability [14]. A good understanding of the structures residual strength and damage growth is therefore required. As damage must be easily identified it is important that damage tolerant structures are designed with a strong emphasis on accessibility and inspectability.

Accidental/discrete impact damage is the principle concern for both design and operation of damage tolerant composite structures [26,27]. This is due to difficulties identifying such damage – Barely Visible Impact Damage (BVID) – and the subsequent compressive strength. To compensate composite structures are generally designed to carry DUL with impact damage up to that which can be easily and reliably identified. As a result these structures are highly oversized in their undamaged condition. Inspection periods are determined using a semi-probabilistic approach, the probability that failure will occur determined by combining the probability of existing damage with the probability of experiencing a load greater than the strength of the damaged structure. The occurrence of such an unsafe event must be demonstrated as 'extremely improbable', i.e. less than 10^{-9} per flight hour. This is shown in Figure 7 and must be applied to all composite principle structural

elements (PSE) that are susceptible to low velocity impact events. Similar considerations may be applied to bonded structure which has the ability to be reliably inspected and which is capable of sustaining some damage without catastrophically failing. A description of how this is applied and illustrated in Figure 7 is presented below.

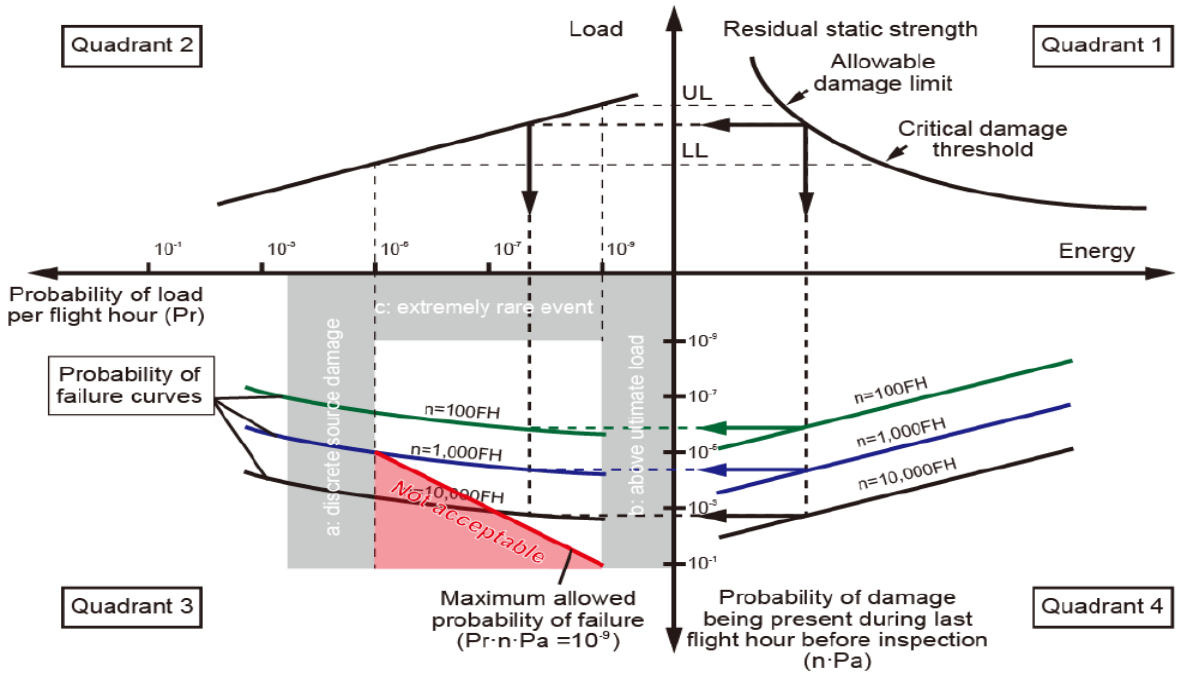

Figure 7: Probabilistic approach for determining inspection intervals of composite primary structure vulnerable to impact events [26]

The BVID energy or damage/disbond size in the case of a damage tolerant adhesive bond is set at a high level to ensure damage is identified; i.e. assumed probability of detection of 1.0. The probability of there being at least one accidental damage site being present in the structure at the end of an inspection interval can therefore be written as below (Equation 5), with the approximate equivalency being the case when n·Pa < 0.1.

$$1 - (1 - P_a)^n \approx n \cdot P_a$$

Equation 5

The probability of failure can then be written as:

$$P_f = P_r \cdot n \cdot P_a$$

Equation 6

Where P_f = Probability of failure

P_a = Probability of accidental damage per flight hour

n = Inspection interval in flight hours

P_r = probability of the occurrence of a flight load (e.g. as a result of a gust) of sufficient intensity when combined with the accidental damage of probability P_a would lead to catastrophic failure

Quadrant 1 in Figure 7 in the instance of impact shows the relationship between the energy of impact and the structures residual strength. Similar consideration may be made regarding adhesive bonds which due to potential issues/influences such as manufacturing induced defects or environmental degradation are reduced in strength. Quadrant 2 show applied loads and the probability such static loads are likely to occur using a log-linear scale. On the figure shown this probability distribution varies uniformly on a log-linear basis with a probability of 10^{-5} and 10^{-9} that DLL and DUL will occur respectively. In the instance the of the original source Quadrant 4 addresses the impact threat via the use of a probability distribution for impact energy and in particular that an event of this magnitude has occurred during the last flight of the inspection interval and is calculated using Equation 5. In the case of bonded structure this may instead represent the probability that although all actions have been made to ensure the bond is manufactured to the appropriate standard the joint strength has reduced to a lower level either as a result of degradation resulting from manufacturing errors or due to discrete damage events. Quadrant 3 addresses the probability of structural failure; the relationship for each scenario (impact energy, inspection interval, residual strength) established using Equation 6, the maximum allowable probability of failure defined as $Pr \cdot n \cdot Pa = 10^{-9}$. This is only required when loads are between limit and ultimate load as damage events reducing load bearing capabilities below this capability (greater than Category 3, Figure 6) are required to be obvious to flight crews and repaired before the next flight (‘get home capability required’). There is no requirement to identify damage that does not reduce the performance of the structure to below ultimate load capability (shaded area ‘b’ in Figure 7 – also see Category 1 damage Figure 6). Extremely improbable events ($< 10^{-9}$) are also not considered (shaded area ‘c’). The inspection interval is therefore determined by these boundaries, an acceptable

damage tolerance established for a specific inspection interval when the entire probability of failure curve is within this region. Figure 7 also shows that as the inspection interval increases the probability of failure curve in quadrant 3 moves downwards. In the example shown the maximum acceptable inspection interval is 1000 flight hours [26]. This however also reveals (further discussion in section 2.4 and Figure 13) that as inspection times are reduced greater damage growth rates and/or reduced residual strengths may be present without compromising current airworthiness demands. This therefore potentially allows less reliance on oversized/engineered structure. Benefits could therefore be significant in structure or adhesive bonds which can continue to operate with a degree of damage whist being either continuously of frequently inspected via in-situ SHM.

The damage detection threshold may be dependent on the characteristics of the structure as well as what maintenance and inspection procedures are used [18]. Figure 8 reveals how the earlier identification of damage via the use of NDI can allow the structure to be repaired earlier, thus maintaining a greater residual strength than if using purely visual detection techniques.

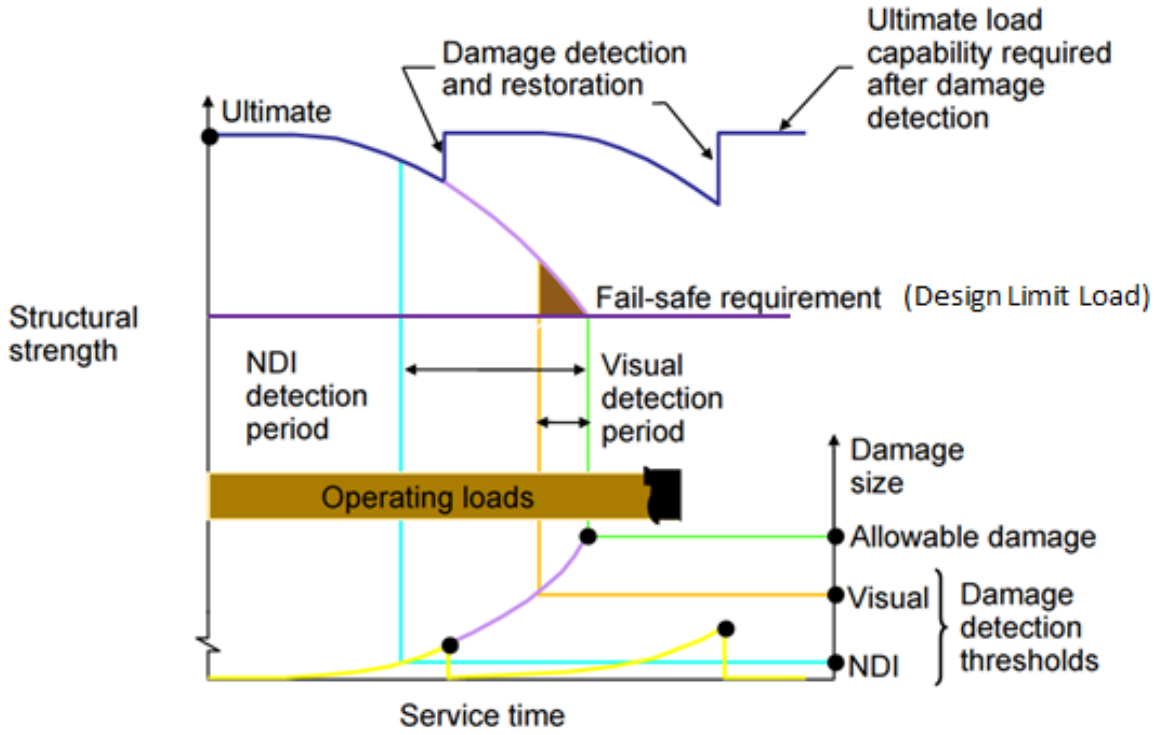

Figure 8: Strength requirements for damage tolerant structures [18]

Three approaches to ensure damage-tolerance in composite structures are defined in the FAA Advisory circular 'AC 20-107B – Composite aircraft structures' [3]. These are the:

- 'Arrested growth approach' which limits damage size either mechanically or ensures possible growth is terminated before becoming critical. Associated with appropriate inspections.

- 'No-growth approach', requires that with defined flaws present the structure can continue to function without adverse growth for the life of the structure [although it is also a requirement that any damage that reduces the strength to below DUL levels must still be identified and repaired – Figure 10]

- 'Slow growth approach', this must demonstrate that the structure, containing defined flaws, can endure appropriate repeated loading with slow, stable and predictable flaw growth, either for the life of the structure or beyond inspection intervals associated with suitable damage detection

Figure 9 illustrates how composite aerospace structure may be operated under each approach.

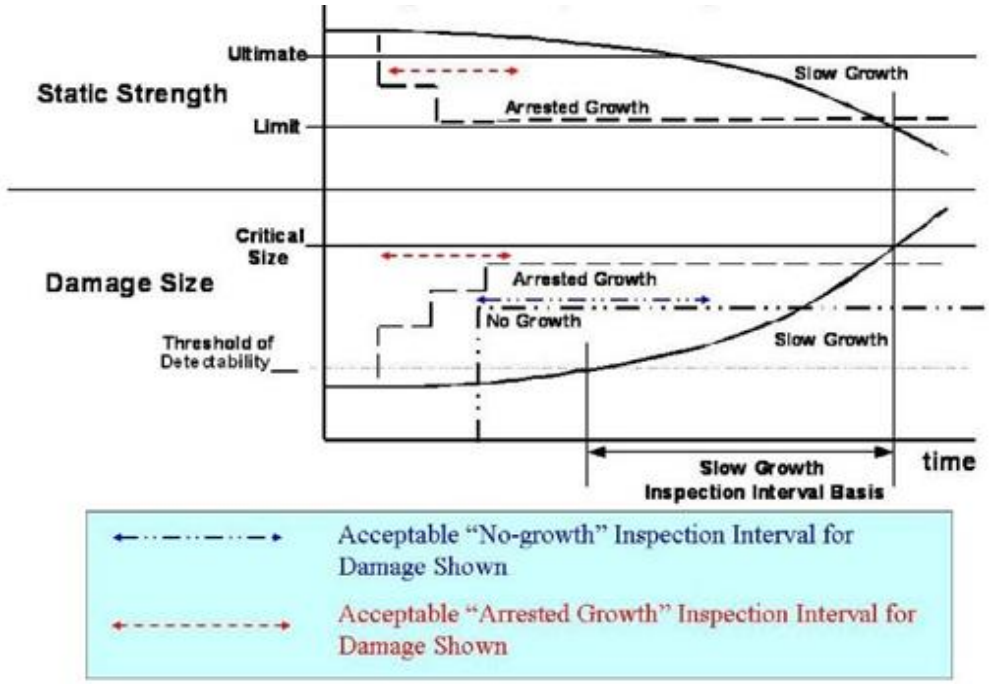

Figure 9: Residual strength and damage size relationships for 'No-growth', 'Slow-growth', and 'Arrested-growth' approaches to composite structural damage [3]

Traditionally due to inspection difficulties and rapid damage growth associated with composites composite airframe manufacturers have employed the 'no-growth' approach for non-visible damage [28]. Additionally under limit load conditions any visible damage will not grow to a critical size over two inspection intervals [29].

Subcomponents of critical composite structure must be tested under repeated loads (considering environmental factors) to establish damage susceptibility and validate appropriate no-growth behaviour. Such information assists in determining inspection intervals (and may as a result influence final sizing of the component) using approaches such as those described in Figure 7. This ensures the residual strength is not reduced to less than DUL capability for an period less than that acceptable for a typical slow growth scenario [3] (Figure 10).

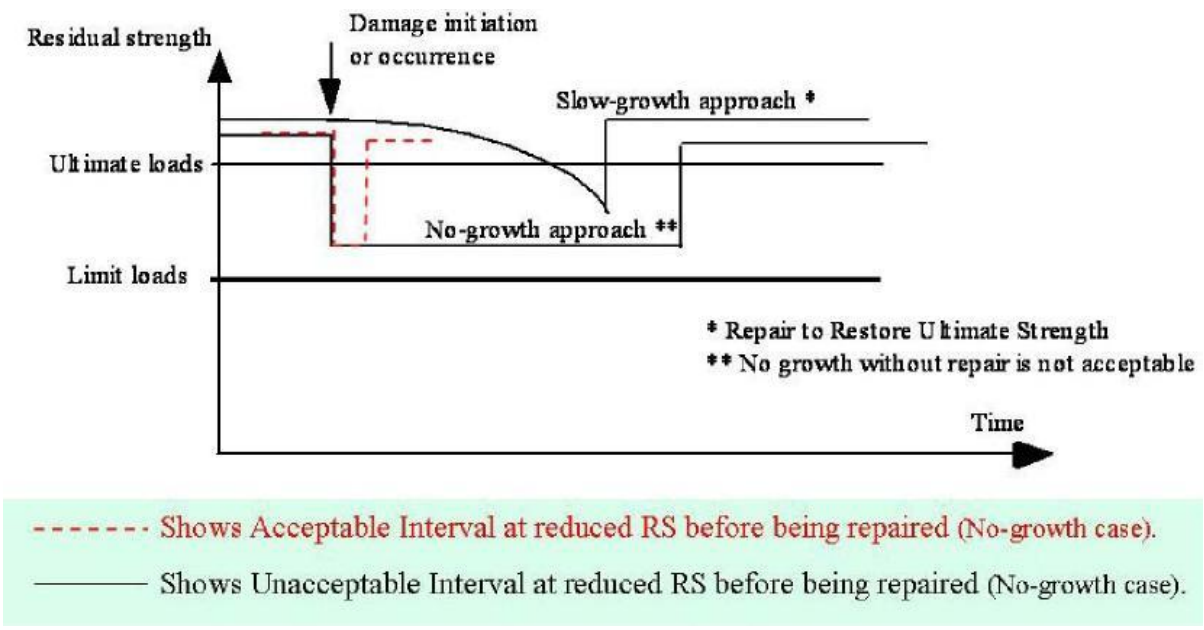

Figure 10: Schematic diagram of residual strength illustrating that significant accidental damage with "no-growth" should not be left in the structure without repair for a long time [3]

Note similar allowable times below DUL for slow-growth and acceptable no-growth cases

2.2.3.1 Damage Tolerant Evaluation

Steps that may be used in establishing a damage tolerant design are summarised below [2,30]:

- Identification of the structural components to be evaluated for damage tolerance

- Determine what possible damage could exist in each component.
- Ascertain the size and type of damage that may be undetectable by both the initial manufacturing quality inspection processes and subsequent in service inspections. This defines the design allowable limit values.
- Assume that damage at the size of the detection threshold is present at the most critical location of each fracture critical component.
- Calculate the required residual strength of the structure with undetectable damage at the required design limit load (this may be required to be 1.2x the design limit load [14]).
- Determine at what rate undetectable damage may grow during the service life of the structure and the point when damage becomes critical for design limit loads. This defines the critical damage threshold.
- Validation that the damage tolerant design objectives have been fulfilled through a process of analysis and/or structural tests.
- Produce an in service inspection program which includes methods and inspection intervals sufficient to detect damage before the strength is reduced to the critical damage threshold so the structure can be repaired therefore restoring the structure to its original strength.

The FAA [2] also recommends the following design approaches should be considered when designing damage tolerant structure:

- The use of multiple load paths and crack stoppers to ensure adequate residual strength and control crack growth (essentially ‘fail-safe’ structure)
- The use of appropriate materials and stress levels to ensure a slow, controlled rate of damage propagation after the formation of a crack or other damage, combined with high residual structural strength
- The arrangement of design details to ensure any failure in any critical structural component can be detected, with a high degree of probability, before the components strength has reduced to levels below that required to sustain the specified loading conditions, allowing timely repair or replacement of the damaged element.

2.3 Structural Health Monitoring: Technologies, Methods and Techniques

Various definitions of SHM are often stated depending on the party using such technologies. The 'SAE international, Aerospace Recommended Practice, Guidelines for Implementation of Structural Health Monitoring on Fixed Wing Aircraft' defines SHM as '… the process of acquiring and analysing data from on-board sensors to determine the condition of a structure' [4]. This can be in the form of: Scheduled SHM (S-SHM) interrogated at fixed scheduled inspection intervals, or Automated SHM (A-SHM) which constantly monitors the structure and provides information to maintenance personnel when an action is required. In-depth details of recommendations and requirements of SHM within aerospace structures are provided in the SAE document quoted as well as the Maintenance Steering Group 'MSG-3 maintenance program development' document [1,4]. Non-Destructive Inspection (NDI) describes a wide range approaches which like SHM can be used to evaluate a structures condition without damaging the structure. NDI is frequently used as part of inspection programs of aerospace components. Some NDI methods, e.g. ultrasonics, have been adapted for use within SHM systems. Unlike SHM, NDI systems cannot be permanently included on in-service structures due to limitations including bulk or the methods in how these methods are used. NDI may therefore only be used as part of scheduled inspections. Access to some structural components may also be limited. As how composite structural design may benefit from the inclusion of in-situ monitoring is investigated only SHM methods are considered within this work.

SHM data may be used for operational monitoring, i.e. flight hours, load exceedance or environmental monitoring, and/or for damage detection/monitoring. Within MSG-3 [1] damage is categorised into three forms; that of Environmental Damage (ED), Accidental Damage (AD), and Fatigue Damage (FD). Within this document damage sources, inspection requirements and intervals, structural maintenance program development procedures as well as ratings of these damage types are considered. The inclusion of SHM, particularly with any considered changes to structural design, may influence future development of such requirements and recommendations. The implementation of any SHM inspection approach will need to consider the nature,

causes and possible locations of these damage types. Information gained via SHM may either be used to complement any current inspection program or, if inspection requirements can be achieved, form an alternative approach to inspection [4]. SHM systems/sensors may be ‘active’ the system acting as signal producing actuators as well as sensors or ‘passive’ with sensors only detecting signals from external sources. Systems may also be either ‘online’ with all equipment on-board or ‘offline’ where only sensors are permanently in-situ and ground bases equipment is used to interrogate these ideally during scheduled inspections. Although significant benefits are often speculated no SHM systems are considered for contemporary transport aircraft [31].

Various approaches of SHM are currently under development, to various levels of technical readiness, by various international industrial organisations and academic institutions. Figure 11 attempts to correlate the most appropriate types of SHM with specific forms of composite damage based on reports presented in the literature. The coloured scoring system presented was a subjective appraisal based on the number of sources which made reference to the technologies with reference to specific composite damage types. Scores were given to each source dependent on the relevance and level of detail ranging from the simple acknowledgment that an approach may identify certain damage types, through partial details of the methods and measurand used, up to reports or investigations providing in-depth detail into the capabilities and mechanisms of the method. After a summation of awarded scores each cell was appropriately coloured. Green indicates the greatest correlation between the specific SHM approach and the particular damage type followed by yellow, orange and finally red as the quantity and quality of published work respectively reduces. Where no association between the SHM approach and a particular damage type could be identified the relevant cell remains grey in colour.

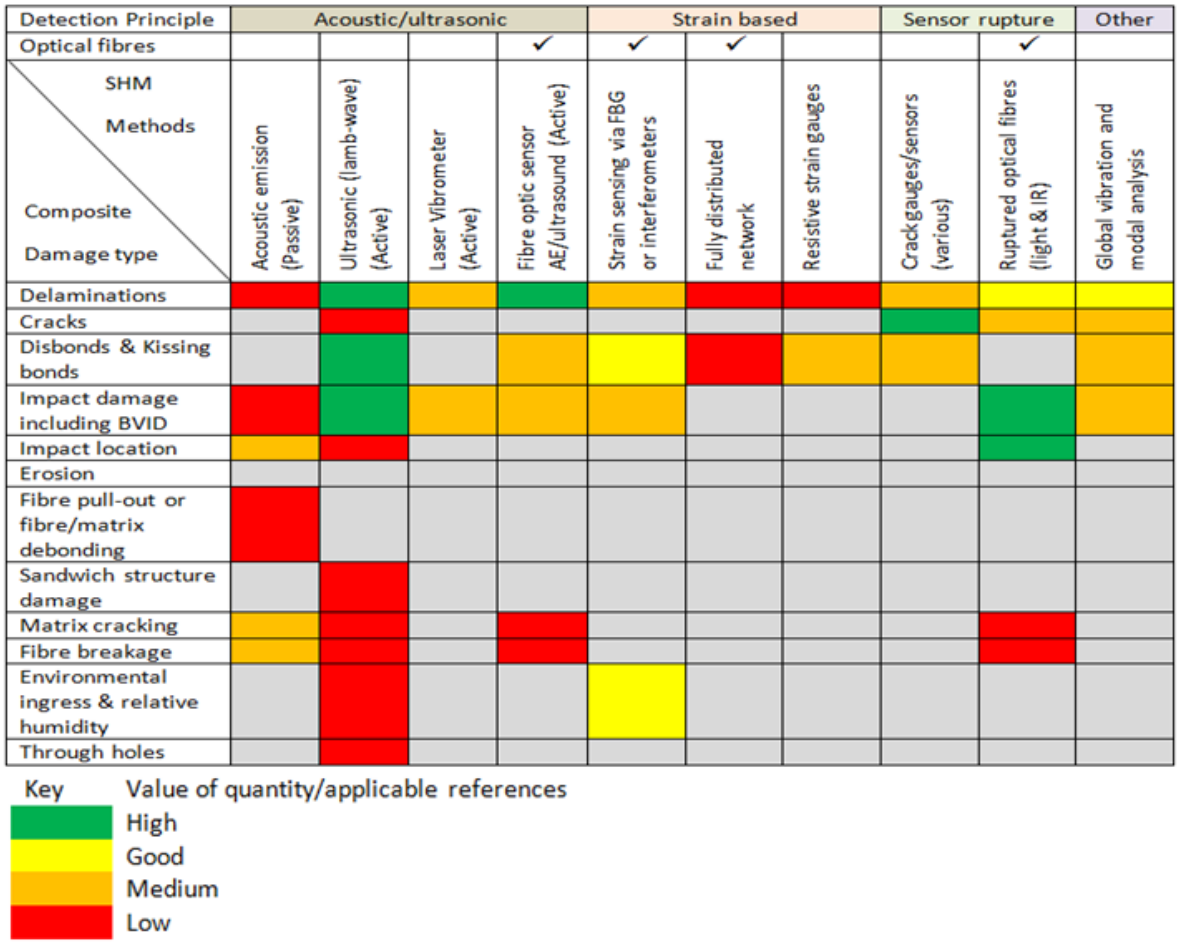

Figure 11: Relative quantity and applicability matrix of sources investigated for selected SHM methods/technologies

A description of each major principle is presented below:

2.3.1 Passive acoustic method – Acoustic Emission

Table 1: Sensing capabilities of passive acoustic based SHM techniques

Damage source types monitored	• Accidental damage • Fatigue damage
Major damage types	• Delamination • Impact damage – potentially inc BVID • Matric cracking • Fibre breakage
Detection principle	• Direct via emission from damage • Indirect via analysis of impact event
Sensing measurand	• Acoustic/ultrasonic stress wave

The term Acoustic Emission (AE) describes both an inspection technique as well as the measurand used to identify damage. Acoustic emissions themselves are elastic waves produced by the sudden release of energy [32] The AE method uses sensors to 'listen' for such signals produced either by structural damage (fracture) or external influences. The proportion of how much of this energy is released as elastic waves is dependent on the nature of the source, how localised the event is and the time period in which the energy release takes place [33]. Typically frequencies up to 1Mz are monitored. Detected signals are analysed to determine the nature and location of damage. Signal characteristics such as amplitude, duration, rise time and energy as well as other parameters such as ring down rate, count rate and total count may be used to identify damage characteristic [34]. Links between each damage type and AE energy values have been observed, although these can be difficult to define [35]. The AE frequency spectrum may also be analysed as different damage types may produces AE's with different frequency contents [36]. Fibre breakage, matrix cracking and delaminations can all produce AE signals [31,36,37]. AE can suffer from a low signal to noise ratio [38]. Although AE can be a comparatively simple process in isotropic materials, composite structures or structures with complex geometries may introduce additional difficulties [39]. In plate-like structures AE systems can also monitor different Lamb-wave modes.

Figure 11 reveals AE is ideally suited for detecting events which produce rapid releases of energy such as fibre breaks or crack growth or for identifying impact locations and with further analysis severity. AE however does not easily allow damage sizing to be directly made, however a novel approach by Gagar et al [40] does provide reasonable estimates of crack lengths in metallic structures. Grondal et al [41] have shown acoustic responses increased proportionally with impact energy and that energy levels could be successfully linked to events that did, or did not, cause damage identifiable via conventional NDT approaches. Staszewski et al [39] explored the use of a genetic algorithm (GA) optimisation, used with a modified multilateration process, to position low velocity, low energy impacts on complex geometry constructed from various materials.

2.3.2 Active-ultrasonic techniques

Table 2: Sensing capabilities of active ultrasonic based SHM techniques

Damage source types monitored	• Accidental damage
Major damage types	• Delamination • Cracks • Disbonds • Impact damage – potentially inc BVID • Fibre breakage • Matrix cracking
Detection principle	• Direct compared with ultrasonic NDI methods, i.e.: • Pitch-catch • Pitch-echo
Sensing measurand	• Ultrasonic properties, i.e. Lamb waves

Active-ultrasonic methods physically generate stress (elastic) waves within the structure to identify defects or damage by analysing wave reflection and/or scattering or changes in wave velocity. Piezoelectric transducers (PZTs) are commonly used both as actuators and sensors, although other technologies, e.g. micro-electro-mechanical systems (MEMS), have been researched [42,43]. Sensor/actuator arrays may be used however these usually require extensive wiring as well as a power supply (power generation using the PZTs themselves has been investigated [44]). Both these characteristics are undesirable in aircraft structures [37]; even so great interest in this approach is evident. Advances in actuation and sensing elements have allowed cracks ≈5mm to be identified [31]. PZTs may be surface mounted or embedded in composite structures. Some research has revealed embedded PZTs can act as stress raisers [45]. Similar devices to PZTs known as Inter-digital transducers (IDTs) which consist of an array of electrode 'fingers' have also been researched [46,47]. Optical fibres have been used as vibration/stress wave sensors [37,48] and It has been suggested that such sensors can be more effective in detecting damage than PZTs [49-52]. A variety of methods using fibre Bragg gratings (FBGs) – strain sensors incorporated into optical fibres – have been included within active acoustic systems as sensors to detect delaminations, secondary bond failure and impact damage with composites [50,53,54].

Active systems allow the structure to be interrogated on multiple occasions, enabling ambiguous signals to be reanalysed. Elastic waves can propagate over comparatively large distances allowing large areas to be monitored. They may also provide some through thickness interrogation which may be useful when monitoring composite laminates [55]. Active acoustic systems commonly utilise 'Lamb-waves', ultrasonic waves guided by the surfaces of thin walled structures [34][56]. Lamb waves can exploit the natural waveguide geometry of most aerospace geometries, such as skin to spar structures [57] as well as those found in adhesive bond-lines, both of uniform [58] and tapered thickness [59].

Two approaches are used with active ultra-acoustic systems, pulse echo and pitch catch. The pulse-echo approach excites the structure with a narrow band tone burst via an actuator. A sensor at the same location (possibly the same device) 'listens' for 'echoes' of the transmitted pulse, a method analogous to radar. This approach can generate maps of echo returns with no need for any undamaged structure baseline. The pitch-catch approach uses a network of transducers/sensors. Each transducer transmits a signal which is received by the other sensors in the network. Some methods may compare received signals undamaged structure baseline values. Differences are analysed to determine the location and severity of any damage present [46,56,57,60-62]. Pattern recognition techniques are used to classify the damage and estimate its severity [63]. Composite laminates may introduce further complexity into using the approach. As the elastic modulus of composites is direction dependent so too is the phase velocity of ultrasonic Lamb waves, the higher phase velocities being parallel to the reinforcement fibres [53,55,62]. Ultrasonic waves are also significantly attenuated by the resin matrix.

Active ultra-acoustic methods have been used in composite materials research to identify delaminations and cracks/cracking [45,55,60,61] including matrix cracking and fibre breaks [61] as well as to identify and locate Barely Visible Impact (BVID) events [41,46,55,60]. Evidence of the identifying secondary bond failure [41,60] as well as sandwich structure skin/core disbonding [57,61] has also been published.

A commercial/research acousto-ultrasonic SHM system consisting of a standard or customised 'SMART layer®' sensor arrays and 'ScanGenie®' diagnostic systems is

produced by ‘Acellent Technologies’. Reports and conference papers released by the manufactures claim this system can potentially be used to monitor in-service condition (damage) of structure, including delaminations, BVID, and bonding issues, as well as recording environmental conditions, characterising material degradation and in-situ monitoring of certain composite manufacturing processes [64-66]. Qing et al [67] have shown SMART layers can be embedded using the Resin Transfer Moulding (RTM) process. Further studies have also investigated the identification of adhesive disbonds and ‘kissing bonds’ [68]. As with other baseline acoustic systems factors including temperature or loading variation or poor coupling between the structure and transducer [38] may cause measured signals to ‘drift’ over time from the initially measured baseline.

2.3.3 Strain-based approaches

Table 3: Sensing capabilities of strain based SHM techniques

Damage source types monitored	• Accidental damage • Fatigue damage • Environmental Deterioration
Major damage types	• Delamination • Disbonds • Impact damage – potentially inc BVID
Detection principle	• Load path change
Sensing measurand	• Quasi-static strain

Strain based SHM techniques monitor strain distributions of the structure resulting from in-service loads. If the structure is subjected to damage, the strain distribution within the structure will change and be detected via the SHM system [37]. Strain measuring devices can be extremely sensitive and therefore provide significant structural information; however changes in measurable strain as a result of damage may only be present in close proximity to the damage event. As such strain sensors are limited in the range they can examine [69] and are therefore best suited to monitoring structural ‘hotspots’ [29]. Strain, by definition, is also direction dependent; this must therefore be considered when positioning strain sensors. For most sensor types it is also essential that an adequate bond between the sensor and structure is maintained.

Strain based methods may also be employed for usage/loads monitoring. Strain gauges are routinely used as a form a structural monitoring in military aircraft programs. Currently these are not directly used to identify damage but as a fleet management tool for assessing fatigue life consumption of safe-life airframes. An example of this is the Eurofighter Typhoon aircraft which uses this approach both on full scale major aircraft fatigue tests (MAFT) as well as in in-service airframes so these can be monitored relative to the qualification tests [15]. Other strain based systems may have the potential to monitor temperature [70] or even relative moisture values [49,71]. The primary technologies for in-situ strain monitoring sensors are those based on electrical strain gauges or technologies based on optical fibres.

Resistance strain gauges

Invented in the late 1930's Resistance Strain Gauges (RSGs) have been used in many engineering applications and with many materials. RSGs are available in a variety of forms and sizes. Strain gauges are adhered directly to the surface of the structure to be interrogated and are of small thickness but exhibit a high sensitivity. They can be used in relatively high temperature or pressure conditions [34,72]. Via an adhesive bond the gauge experiences an equal strain to the surface it is bonded to. As a consequence of structural strain the conductive material within the 'gauge length' both marginally lengthens and as a result of the Poisson effect becomes narrower increasing the gauges electrical resistance. Negative (compressive) strain reduces the gauges resistance. As the change in resistance is directly proportional to the applied strain this is used, via a Wheatstone bridge circuit, to calculate any change in strain in the monitored structure.

Individual strain gauges only provide strain information relative to their orientation. Any deviation from the direction of maximum strain will result in reduced values. To combat this effect two or more gauges at differing angles may be used at the same location (or in close proximity). When multiple gauges at different angles (rosettes) are used appropriate equations can be used to transform the strains experienced by the gauges to any other angle [73][74][75].

Although possible to use similar transform calculations to directly measure the principle *stresses* in isotropic materials (Hooke's law, details in [75]) this is not

possible with composite materials due to their anisotropic composition. If stress values are required these may be calculated through knowledge of the composites 'lay-up' and stress and strain relationships for each ply as described in textbooks such as [76]. This is generally not an issue as composite designs, unlike those of metals, are often more concerned with levels of strain rather than stress.

General issues associated with Resistance Strain Gauges [72]

- Strain values are averaged over the area covered by the grid. Therefore strain gauges notably larger than the peak strain region will indicate values lower than this peak value.
- Smaller strain gauges may resolve the problem above, however RSGs with gauge lengths less than ≈3mm may be susceptible to fatigue.
- Varying strain gauge types are available and should be considered for different test materials due issues including thermal expansion.
- RSGs only provide information for a small (almost point-like) area. Many may be required over a complex structure.

Issues associated with RSG's and composites [72]

- For woven fabrics the gauge should be large enough to cover changes in weave, i.e. warp/weft. Both directions may need to be considered (e.g. for standard woven fabric – 4 'cells').
- Preparation of surface and bonding issues. 'Sanding' surface in preparation for adhesion may introduce flaws into reinforcement which could potentially introduce local damage to the composite.
- The gauges must be insulated from 'conductive' carbon.

In addition to the issues above the strain gauges and the lead wires used to connect these may, dependent on the configuration used, be influenced by changes in temperature. Details of this consideration are included in section 5.4.2.

Optical fibre sensors

Optical fibre systems have been researched and used to monitor strain [38,49,77-82]. Adaptation of this technology has also been used to measure temperature, pressure, displacement and rotation, and ultrasound as well as many other physical attributes [49,50,71,79,83]. Optical fibre systems can exhibit multiplexing and

simultaneous sensing ability (multiple sensors along a single fibre), remote sensing, high flexibility, low propagation loss, high sensitivity and accuracy [84]. They also have a discreet cross sectional area (a typical polyamide-coated fibre diameter is 125μm and a total outside diameter – cladding – of approximately 250μm [31]), low production costs and an immunity to electromagnetic interference [79,85]. Additional wires are not required as the fibres act as both sensors and transfer the information; also no additional power source is required. Various sensor types have been designed to be used with and/or constructed from optical fibres including various configurations of interferometer, Fibre Bragg gratings (FBGs), and innovative new approaches such as the LUNA® distributed sensor system [82,86]. Many of these – including FBG's and the LUNA® system – only require a single ended connection [49]. This, in conjunction with their small diameter, makes them particularly suitable for embedment in either composite laminates or adhesive bond-lines. Research by Measures [87] has shown embedded optical fibres induce only a minimal detrimental effect and fibres with diameters <140μm introduce no measurable effect on the tensile strength or fatigue lives of tested carbon/epoxy specimens.

Many optical fibre systems feature discrete sensors positioned at locations along the fibres length. FBGs are amongst the most common sensor of this type. Although primarily used to monitor strain FBGs have also been used – possibly with the aid of additional coatings/features – to measure temperature [49,88] and moisture/humidity [49,71,83], both of which may influence performance of composite laminates [89] and adhesive joints [90,91]. Details on principles and fabrication of FBGs can be found in [42,49]. Minakuchi et al are developing crack arresters monitored by FBGs for use within the laminate/core interface of sandwich structures improving the damage tolerance of such structures [92,93]. Embedded FBGs have also been shown to identify BVID level impact events in composites [94] as well as identifying residual strains resulting from impact in fibre/metal composites (GLARE) [95].

Embedded FBGs have been investigated for monitoring strain within composite bonded joints [81]. Palaniappan et al [96] reported being able to track adhesive disbonds to an accuracy of 2mm using 'chirped' FBG sensors embedded in the adherends of GFRP single lap joints subjected to fatigue. Good results were also reported by de Silva et al [97], however this investigation highlighted placement of

optical fibres within a bond-line is far from trivial. An alternative approach is by monitoring the strains on the outer surface of the adherend at the joint overlap. This is known as the 'back-face strain technique', the disbond tracked by a progressive decrease in recorded strain as the disbond progresses. This approach has been used to identify progressive bond damage of single lap joints subjected to fatigue loading conditions both using RSGs [98-100] and surface mounted FBGs [97,101]. Other discrete sensors, generally in the form of interferometers, have been constructed. Such sensors – Fabry-Perot, Mach-Zehnder, Michelson, and Sagnac interferometers – are reviewed in terms of their application, operation and fabrication in [79] and with parametric sensors in [38].

Fully distributed systems, such as the system developed by Luna® technologies [102], which measure strain at multiple locations along an unmodified optical fibres length are also available. Such systems monitor Rayleigh, Ramen or Brillouin scattering of tuneable laser light resulting from random imperfections within the fibre [86][103]. Under research conditions the Luna® system has identified artificially induced disbonds of composite stiffeners/skins [82] and spar/skin disbonds on representative composite wing-box sections [78]. Herszberg et al [104] showed FBG sensors could show different responses (in agreement to FEA) to artificially induced delaminations compared to undamaged sections of GFRP.

2.3.4 Sensor rupture methods

Table 4: Sensing capabilities of sensor rupture based SHM techniques

Damage source types monitored	• Fatigue damage • Accidental damage
Major damage types	• Cracks • Delamination • Disbonds • Impact damage - potentially inc BVID
Detection principle	• Direct interaction with damage structure
Sensing measurand	• Physical crack growth

Various SHM systems which respond to rupture of the sensors have been investigated. Some approaches under investigation are summarised below:

Comparative Vacuum Monitoring (CVM) is a promising approach which is currently being trialled on long-term flight trials on actual commercial aircraft [105] as well as finding use in monitoring non-aerospace structures [105,106]. The sensor consists of a series of long, narrow galleries alternatively housing either the low vacuum or air at atmospheric pressure. The sensors are generally surface mounted, the surface of the test structure in effect forming part of the gallery wall. It is also suggested sensors may be embedded within components such as lap-joints or within laminates to identify delaminations [31]. The vacuum within the galleries is supplied via a stable vacuum source and the pressure within these galleries is monitored via the flow meter. If there is no damage the pressure with the galleries should remain constant. If, however, a crack/flaw forms at the bonded surface of the test object, air can flow from the atmospheric galleries to the vacuum galleries [37]. Commercial sensors claim to be able to detect defects as small as 250μm [107]. Minakuchi et al [69,108] has suggested a similar system which uses wide arrays of surface mounted air tight tapes bridging simple glass fibres (alternatively embedded glass capillaries are suggested). As the quality of vacuum is reduced due to fracture of the sensor galleries strain is imparted on the optical fibre which can be detected via FBGs.

Crack gauges and Surface mountable crack sensors (SMCS). These systems identify cracks/damage by the respective breaking or completion of electrical circuits. Like CVM these are used at recognised hot-spots. Unlike CVM such devices only provide a yes/no response and therefore cannot monitor damage growth. Issues can arise including electro-static build up and premature sensor failure [68,109-111]. Crack gauges are also available. Similar in construction to RSGs these consist of electrically isolated resistors or conductor tracks. A progressing crack in the underlying substrates will cause these features to fail and as a result change the resistance of the gauge [112].

Rupture of optical fibres. The failure of an embedded optical fibre can identify damage is present somewhere along the fibres length. Other methods which use the ‘escaped’ light from the point of rupture to locate damage in transparent composites have been investigated [77,87]. A similar system has been investigated for opaque (carbon) composites uses heat produced from escaping laser light [113].

2.3.5 Vibration based techniques

Table 5: Sensing capabilities of vibration based SHM techniques

Damage source types monitored	• Accidental damage
Major damage types	• Delamination • Cracks • Disbonds • Impact damage
Detection principle	• Response to changes in structural stiffness and mass
Sensing measurand	• Vibration model parameters, i.e. frequencies, mode shape and modal damping

Structures natural (modal) frequencies, damping ratios and modal shapes can be used to assess structural health [104,114,115]. Model vibration responses of damaged structure can be compared to characteristics of undamaged structure and/or finite element analysis (FEA) based models [116]. Methods include 'impulse response' (actively exciting the structure) and 'random decrement' (in-service stimuli). Other vibration related techniques, including electro-mechanical impedance, respond to local structural stiffness [117-120]. Global based techniques may be insensitive to the early stages of damage.

2.3.6 Other monitoring methodologies

Other novel approaches to structural monitoring have been investigated, however these are either at the earliest stages of development or not suitable for composite aerospace SHM application.

Micro-wave antenna. A comparatively new method which identifies disturbances in electromagnetic field parameters resulting from the presence of water [31].

Capacitance disbonding detection technique. A proposed technique for identifying disbonds by considering conductive CFRP components separated by insulating adhesives to be acting as capacitors [121].

Mode shape and the Gapped smoothing damage detection method. Analysing irregularities in loaded structure curvature to locate and assess the severity of damage [115,116].

Electrical resistance monitoring of structural carbon fibre. The direct monitoring of damage or strain changes by monitoring the electrical resistance of the carbon reinforcement fibres. Currently only used in the laboratory [122,123].

2.4 Application of Structural Health Monitoring within Composite Structural Design

SHM literature frequently suggests the greatest potential benefits in future aircraft (or other applications) may be achieved by including SHM as a fundamental consideration of the structures design and operation, particularly if composite materials are used. Section 2.2 recognises damage tolerant principles require composite structures to be optimised in regards to weight, manufacturing, maintenance and supportability costs. It also requires that residual strength, damage growth and damage detection forms part of the design. Although SHM systems provide a method for inspection in order to fulfil these requirements, and therefore enable the benefits often quoted, the application of SHM as part of the structures design must be considered. A design approach, based on SHM for damage tolerance could largely reduce/eliminate the current reliance on oversized or additional structure. Certain SHM technologies are well suited to identifying BVID type damage (Figure 11) a major consideration in the sizing of composite components. The inclusion of such technology may allow structure to be sized in accordance to levels of impact damage currently not reliably detectable. It is also identified some techniques are suitable for disbond detection and could therefore reduce uncertainty associated with in-service bonded structure. The reduced reliance on features including mechanical fasteners to account for such uncertainties, or less conservative designs potentially allowing a degree of damage growth as oppose to current no-growth philosophies may allow more efficient damage tolerant structure to be realised. Alternatively, bonded joints/repairs may be designed with reduced redundancy to account for uncertainties associated with the actual bond quality as a result of manufacture or in-service degradation e.g.

exposure to moisture. Such approaches would allow structure to be manufactured and operated with reduced weight/mass whilst maintaining appropriate levels of airworthiness allowing benefits such as reduced operation costs (fuel) or increased performance to be realised on top of maintenance benefits (Personnel Communication).

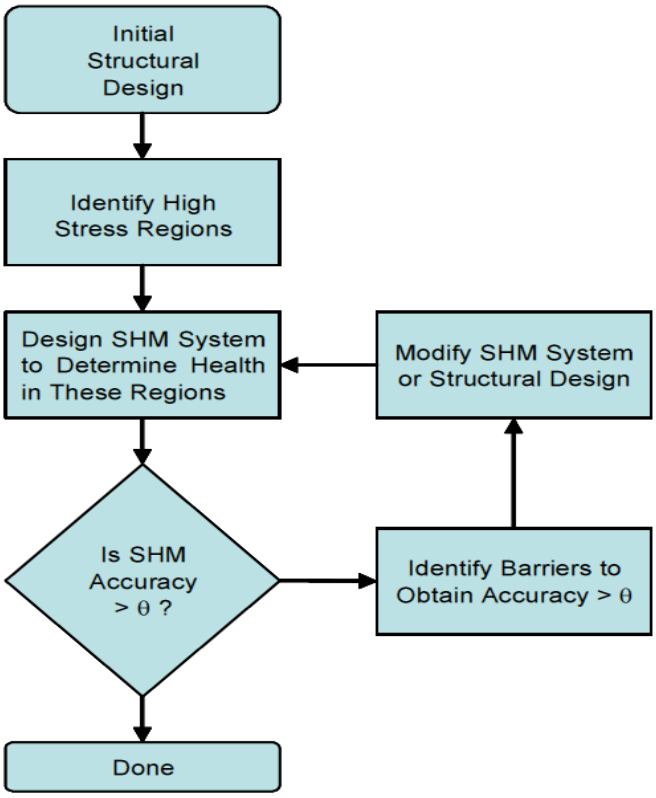

Figure 12: Potential design process incorporating SHM [124]

Recognition of the potential benefits of SHM assisted/enabled design, such as reductions in structural mass or more efficient in-service operation/maintenance programs, using SHM the methods discussed frequently cited. In almost all cases however no actual novel solutions to achieve this goal are presented [29,37,84,124-129]. In addition (again with no proposed solutions) it has been recognised that designing the structure so damage can be easily sensed via SHM will not only significantly improve the performance of the monitoring system but may also allow optimisation of both the number and placement of on-line sensors [124]. As such a simple process for developing SHM incorporated has been proposed (Figure 12), the symbol θ refers to an arbitrary value of SHM accuracy selected to ensure the effectiveness of the system.

Schmidt and colleagues [8,130,130-133] recognise the design criteria of the current dimensioning philosophy (in these cases for metallic aerospace structures however similar comparisons can be made to composites) are residual strength, crack [damage] growth and a large damage capability. Damage tolerance requires cracks (in the case of metals) grow only up to a critical length over two inspection periods. As metallic crack growth is a function of stress this can be used to ensure the structure is appropriately sized. Much of the load however is taken by internal stringers and frames, however as these cannot be visually inspected it must be assumed these do not contribute and the entire load is taken by the skin, increasing the calculated crack growth. It is proposed that by monitoring the stringers/frames via SHM their actual condition could be known therefore the current conservative approach would not be required as the inclusion of the stringer/frames contribution could be considered. Higher stresses could therefore be permitted for the same acceptable crack growth rate which, for identical loading, results in lighter structure.

A comparable SHM enabled design approach for composites has been proposed. Minakuchi et al [27] have developed an 'ultra-lightweight' composite stiffened panel philosophy based on a SHM and rapid repair system which demonstrates how lighter SHM enabled design may be operated (in this instance considering impact damage). It is proposed 'light-weight' aircraft composite skins are monitored via SHM to detect impact events. If detected a temporary repair is made with a rapid-cure CFRP patch – designed for rapid use at the airport gate – before the next flight for safe continued operation. During the next scheduled maintenance the damage is analysed via NDI and if required a scarf repair undertaken to restore the skin to full strength. Based on the impact damage tolerance design illustrated in Figure 7 the concept considers that when thick and thin structures are impacted with equal energies the thinner structures residual strength is generally lower than that of the thicker structure. As a result the strength curve in quadrant 1 of the 'damage tolerance / Inspection interval' moves downwards (Figure 13).

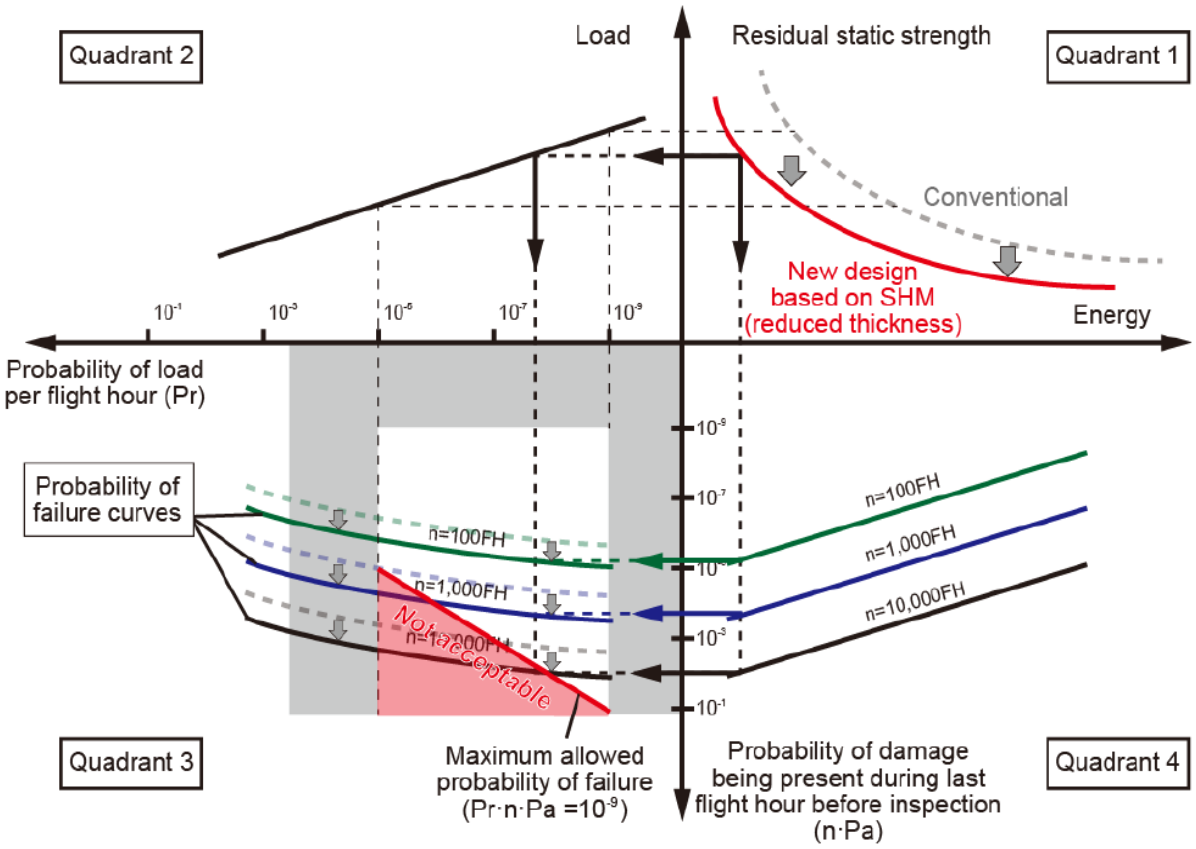

Figure 13: Failure probability of ultra-lightweight structure [27]

In response the curves in quadrants 4 and 3 also move downwards resulting in a shorter acceptable inspection interval (in this example <1000 flight hours). If the SHM system 'inspects' the structure after each flight – resulting in an inspection period in the region of ≈10hours – the required safety measurements are still achieved. It is then proposed the rapid repair system is used to recover the strength with minimum disruption to operation. An issue lies in that even if the appropriate inspection interval can be met as large non-economical repairs may be required and the required 'get home capabilities' may also not be available. As such this proposed concept relies on the strength recovery made by the rapid repair system. If the strength reclaimed is higher than the DUL capability and therefore greater than the requirements of conventional structure containing BVID such 'ultra-lightweight skins could be operated at least as safely as conventional structure. Tests performed on representative CFRP stiffened panels revealed adequate strength could be recovered in these cases.

MacConnell [126,127] also identifies that if smaller levels of damage can be identified components could be designed using higher assumed material properties (improved design allowables) resulting in lighter, more efficient structure. MacConnell considers using Integrated Systems Health Management (ISHM), of which SHM is a constituent part, along with diagnostic and prognostics on other systems including controls, power, avionic and propulsion. It is claimed that weight savings up to 20% could be achieved however again no physical engineering solutions are put forward. It is also suggested damage levels beyond the identification capabilities of the monitoring system (i.e. that required to support DUL) becomes less relevant as the capabilities of the monitoring system increase. It may therefore be possible to reduce the DUL value from 1.5xDLL to for example 1.25xDLL providing further weight benefits

A development team at Bombardier Aerospace [128] recognise the benefits of considering SHM for use with design. Their suggested approach however is to use SHM systems to validate models and predictions used in the development of novel composite aircraft fuselage designs such as bonded composite-sandwich oval shaped cabins and any associated detail changes as oppose to developing designs only made possible through SHM.

2.5 Summary/Discussion

This chapter has reviewed literature on the current philosophies used in aerospace design and SHM methods and techniques with a focus on composite structures. The final section has reviewed literature which considers the bringing together of SHM and structural design such that SHM is an intrinsic design parameter potentially resulting in benefits such as reductions in structural mass or benefits regarding in-service operation.

Previous research has almost exclusively concentrated on the development of monitoring sensors and diagnostic tools with little consideration of adapting the structure to be monitored. Although occasionally recognised that structure which allows damage to be easily sensed will aid SHM no experimentally verified engineering solutions which combine the application of SHM and structural design have been identified. Tests and results reported are all either performed on simple

plates or on structure representative of contemporary design and construction. Although commented that SHM may aid design little recognition that the structure under scrutiny must inherently behave in a manner akin to damage-tolerant operation – i.e. required residual strength, appropriate damage propagation and reliable damage detection – has been recognised within current literature. Monitoring a structure using SHM only has value when sign of damage can be detected such that maintenance can be performed in a timely manner i.e. while the structure still has sufficient integrity to be airworthy and ideally still exceeds limit load capability. The issue with some composite designs is that failure can occur with little or no warning. A prime example is the case of kissing bonds; joints which appear sound using both visual and NDI methods but actually exhibit strengths lower than expected by their design. In such cases there is no benefit from the use of SHM. The challenge for bringing together SHM and composite structural design is therefore to bring damage-tolerant type behaviour to the composite structure either by changing the structure design to be amenable to monitoring, by using SHM to help prognoses conditions under which sudden failure will occur or by using a combination of the above.

It has been highlighted by Herszberg et al [37] and Scott et al [29] that if SHM enabled designs are considered with reduced sections / higher allowable stress or strain values changes in failure modes, which may be less well understood, may occur. This may be the case with composite structures as, for example, unlike metals there is no stress relief via yielding. Also ‘fatigue’ is not currently considered a major issue due to limitations placed on allowable strains on composite aerospace structures (no damage growth approach). This may need to be examined if higher stress/strain allowables are considered. Although SHM may be capable of monitoring ‘composite fatigue’ once damage initiates its progression is generally rapid making a ‘slow-growth’ damage tolerant approach in monolithic composite structure impractical [14]. In addition thickness reduction of some composite structures, such as aircraft skins (which are already ‘thin’), may be limited by additional factors required of laminate construction as unlike metals laminates may not simply be made thinner without the removal of individual plies (unless, thinner material plies are available). This ‘black metal’ approach cannot always be

achieved, particularly in thinner constructions which contain few plies to begin with as issues such as directional load bearing capacity and considerations such as tension/bend/twist coupling affects or bearing strengths, which are lay-up dependent, must also be considered when designing structural laminates.

Bonded repairs (as per joints), even those made in ideal circumstances, are highly scrutinised due to uncertainties associated with their actual performance. Any temporary patch, such as that for use with the proposed ultra-lightweight composite skin proposed by Minakuchi et al (Section 2.4) must be perfectly reliable (or possibly monitored via SHM) to be viable. It may be possible for any existing sensors to continue to monitor the region after temporary or permanent repair (as is still essential), however if the included SHM system is also damaged this will need to be repaired/replaced. This, along with a required system diagnostic, may reduce the effectiveness of the quick turnaround suggested. Like any SHM enabled feature if the monitoring system cannot be repaired or replaced the full structure/sensor array must be substituted.

It has been recognised that design and operation of critical aerospace structure reliant on active systems is likely to raise concerns even with structural designers [126]. Comparisons can however be made to aerodynamically unstable military aircraft which are entirely dependent on digital systems and many aircraft, including many civil airliners, which now commonly rely on active load alleviation control to aid pilots.

It may be required that to initially introduce SHM enabled design into actual critical structure approaches may need to be understandable to general aerospace designers, operators and engineering non-specialists responsible for acceptance/certification of new developments. It may be partially for such reasons that CVM is currently at the highest technology readiness level (TRL) – TRL 7+ – of any current SHM system (details in [4]) rather than methods which heavily rely on more ‘abstract’ factors such as probabilistic algorithms or complex diagnostic approaches. Once acceptance of such a philosophy is accepted further gains may be achievable through the future introduction of more specialised approaches.

Figure 11 reveals many different SHM strategies may be potentially suitable for many issues associated with composite structures. Considering damage associated with impact and disbonding adhesive structure (identified in Chapter 3 as being the types of composite structural degradation with the greatest impact on structural design) active ultrasonic as well as strain sensing methods have in previous work shown the greatest potential for in-situ monitoring. Although active acoustic methods show significant promise the ability tailor such systems into a SHM considered structure or bond design is far from ideal. As the acoustic nature of such a structure is unlikely to be directly associated with the load transferring properties (the primary purpose the structure) some compromises may be present. At the very least two assessments of the structure, one of acoustic assessment in the presence of damage as well as the standard assessment of the structures load bearing capacity, will be required. In comparison strain not only forms a suitable means of monitoring but is the primary consideration when designing most composite laminates (rather than stress due to the different elastic moduli of the constituents) as well as in the design of adhesive bonds to aid analysis in the presence of plasticity (see Chapter 4). Strain is also directly linked to load transfer, particularly in the case of adhesively bonded joints. Strain measurement therefore provides a direct link to the structures condition with minimal requirement of the use of additional and complex diagnostic tools and methods used with other methods including active-ultrasonics.

It is evident little research has been conducted on the topic of SHM enabled design. When considered within the little literature this normally consists of general conceptual comments speculating potential benefits that may be realised using such an approach. There are few studies which demonstrate such designs with specific examples and experimental validation. This apparent gap in the literature forms the motivation for the research reported within this thesis. The issues identified within this review raise research questions required to be considered throughout research to enable SHM enabled design to become viable which in part also help identify structure and damage likely to benefit from and be suitable for the implementation of SHM enabled design. These factors are detailed in the following chapter.

3 Research Objectives

3.1 Section Introduction

The literature review revealed that although potential benefits may be made available via the inclusion of SHM, particularly within composite aerospace structures, no SHM systems (with the exceptions of CVM trials or strain based measuring of fatigue life consumption of safe-life aircraft) are currently used with civil/military aircraft. Although much research towards SHM has been conducted little work has been identified which considers adapting the structure itself to a) enhance and/or simplify the capabilities of the monitoring system (detection, location, severity, and prognosis), or b) to create more efficient structural designs by incorporating SHM as a design perimeter. It has been identified in the reviewed literature that more efficient composite structures can be designed, built and operated by using SHM as a fundamental consideration of structural design. Little work has been published however which attempts to combine the inclusion of in-situ monitoring with actual structural design features to increase the effectiveness of the monitoring system and to allow SHM enabled structure to be operated as part of an aerospace damage tolerant regime.

3.2 Composite Structural Design Features Identified to Benefit from Structural Health Monitoring

In an attempt to successfully produce effective structural designs which benefit from the consideration of in-situ monitoring as part of their design it is necessary to identify and select design features or operational issues likely to benefit from such an approach. The literature review revealed the composite damage types primarily associated with SHM research and development are delaminations, adhesive disbonds, and impact damage (Figure 11). All are major considerations within composite structural design and operation as each may significantly reduce structural performance. All however are intrinsically difficult to identify and categorise using standard damage tolerance practice (primarily using visual inspection [89]). As a result over-sized designs (as a result of larger design safety factors) and/or additional features are included to ensure adequate residual strength/stiffness remains in the presence of undetected damage. The removal of

such uncertainty with the aid of SHM will reduce the reliance on such additional features resulting in reduced mass and potentially aid both manufacturing and in-service operation. Delamination can form part of other more defined damage types, including impact damage, and is also similar in many aspects to adhesive disbonding. As a discrete damage type, not associated with a particular structural component or damage event, delamination alone has therefore been excluded from further targeted investigation.

3.2.1 Structural Joints

Table 6: Advantages and Disadvantages of Bonded and Bolted Joints (adapted from [134])

Advantages	Disadvantages
Bonded joints	
Low stress concentrations in adherends	Difficulty in bonding thick sections
Lightweight	Difficult to inspect [even after manufacture][135]
Stiff connection	Prone to environmental degradation
Excellent fatigue life	Sensitive to peel and cleavage stresses
No fretting problems	Cannot be disassembled
Smooth surface contour	High quality control required
Damage tolerant *	Potential for rapid, catastrophic failure [[136]]
Bolted Joints	
Easy to disassemble	Considerable stress concentration
No thickness limitations	Added weight of mechanical fasteners
Simple joint configuration	Composites have poor bearing properties***
Manufacturing and inspection straightforward	Metallic components are prone to fatigue
Environmentally insensitive**	Hole formation can damage composites
Insensitive to peel forces	Fretting a problem in metals
Potential for 'slow', bearing failure design ([137])	Shimming often required for composites

*See in text comment * below.

**The action of drilling may increase moisture ingress into composite adherends and if used with bonded/bolted structure additional means of ingress to the bond-line may also be introduced ([14]). If the composite adherends are carbon reinforced (likely in aerospace applications) the fastener materials or other solutions will also need to be considered due to galvanic corrosion issues.

***As a result inefficient lay-ups or ply build-ups around fasteners may be required resulting in additional mass and manufacturing/design demands (see Figure 32, section 4.7.4).

All complex engineering structures will likely contain joints, regardless of the choice of construction. Within composite structures, joints are generally formed via

mechanical fasteners (bolts, rivets etc), with adhesives, or by using a combination of these approaches. It is frequently recognised that in many cases joining composites purely via adhesive bonding presents advantages over the use of mechanical fasteners, although limitations do exist which must be considered [14,23,100,135]. Various advantages and disadvantages of bonded or bolted joints are summarised in Table 6. Many of the advantages associated with adhesively bonded structure result in a reduction in structural mass compared to mechanical joints. This design feature (as well as several others shown) makes the use of purely bonded structure highly desirable for use within aerospace type composite structures.

Although inspectability is a requirement in damage-tolerant airframes (section 2.2.3) it is inevitable some joints (e.g. internal stiffeners) may be physically inaccessible during most routine visual inspections. As such the structure must be designed (sizing, inspection intervals etc) as if non-inspectable components do not contribute to the structures integrity. Bonded structure has an additional issue that even if accessible the condition and therefore the strength of the bond can be difficult to assess (even at the point of manufacture – [3]) as although gaps in the bond may be identified via X-ray and ultrasonic NDI there is no current method which guarantees an apparent intact bond has sufficient load bearing capacity [135]. A well-known example is the 'kissing-bond' problem. Kissing bonds are 'zero volume' defects potentially resulting from poor surface preparation, the inclusion of moisture (possibly condensate), residual stress, contamination or other fabrication issues possibly resulting in poor or incomplete chemical (and/or potentially mechanical) bonding between the adhesive and adherend.

*Although bonded joints are frequently described as being 'damage tolerant' [14,134,138] in such cases this recognises that adhesive joints may sustain design loads even with regions of flaws/poor bonding within the bond-line (see section 4.5: 'Effects of flaws within the bond-line'). Once damage initiates however rapid catastrophic failure usually occurs [136] with little or no warning. This, combined with the inspection difficulties, does not allow damage-tolerance operation in an inspection/maintenance sense (section 2.2.3). Such behaviour prevents the use of purely adhesive bonding being used in primary structure resulting in additional design features included to ensure airworthiness. As a result, particularly in large

commercial transport class aircraft, mechanical fasteners are normally used with primary composite structure [135].

Acceptable means of compliance regarding the requirements of design, manufacturing and operation of structural bonds in composite aerospace structures is provided in AC 20-107B(7c) [3]. It states [139] (paragraph a.5.):

"*For any bonded joint the failure of which would result in the catastrophic loss of the airplane, the limit load capacity must be substantiated by one of the following methods*:

i. *The maximum disbonds of each bonded joint consistent to withstand the loads* [as described in [139] paragraph a.3.] *must be determined by analysis, tests, or both. Disbonds of each bond greater than this must be prevented by design features; or*

ii. *Proof testing must be conducted on each production article that will apply the critical design load to each critical bonded joint; or*

iii. *Repeatable and reliable non-destruction inspection techniques must be established that ensure the strength of each joint."*

It is recognised the above options may not supersede the requirements of qualified bonding process and stringent manufacturing quality control put in place to account for the inability of NDI to detect weak, or (due to environmental degradation) potentially weak bonds [14], resulting from inadequate quality of manufacturing. These requirements instead provide additional protection against unidentified/unforeseen problems that may occur despite these rigorous demands. Option *i* permits certain fail-safe methods and provides opportunities such as those currently used and described below. Option *ii* may not detect weak bonds which require time and exposure to degrade [140] (although this may be in part addressed via adequate demonstration that materials and processes have long-term environmental durability). Option *iii* currently cannot be exploited as no widely accepted form of NDI has been developed that can reliably detect weak bonds [3].

The usual approach to ensure the airworthiness of bonded structure is the inclusion of additional mechanical fasteners, both to restrict damage growth and prevent catastrophic failure. The performance of mechanical fasteners is easier to ascertain compared to adhesive bond-lines as well as being easier to visually inspect. Fasteners used with bonded structure (often referred to as 'anti-peel fasteners' or 'chicken-bolts') have been shown to arrest damage [141] or alternatively act as an alternative means of transferring the load in the event of adhesive bond-line failure [142]. Adhesive bonds are however stiffer than bolted joints when transferring shear loads, by an order of magnitude [136], and as such combining the two approaches provides no greater strength than a well-designed purely bonded joint [141] as the load in an undamaged joint is almost exclusively supported by the stiffer adhesive bond-line. If the bond-line fails the fasteners are available to support the structure [143]. Although it has been shown that fasteners in the immediate vicinity of damage may transfer some load and protect the adjacent adhesive bond each feature must however still be designed to independently transfer the full service load (DUL for the primary adhesive bond and a minimum of DLL for the mechanical fail-safe system if the component can be appropriately inspected or DUL if not). This method therefore introduces additional mass and manufacturing complexity but provides no increase in the design performance of the joint primarily acting in shear. In practice this results in joint being designed as if the adhesive joint is not present, i.e. it is assumed to provide no contribution to joint strength, the design being based on the less efficient mechanically fastened joint.

In addition to the increased mass resulting from the inclusion of two joining methods such an approach may be detrimental to the primary (adhesive) joining system. Fasteners are usually positioned at the ends of joint overlaps, the most critical region of an adhesive bond (see Chapter 4: Composite Joints). Drilling – a non-trivial process in composites [144] – may also damage the adherends/adhesive in these areas and unless carefully sealed may also allow detrimental environmental ingress, e.g. moisture, into the bond/adherend interface [14]. In addition, the use of thicker non-optimal lay-ups or local ply build-ups required to accommodate the fastener not only add mass but may increase peel loads (see Chapter 4: Composite Joints), a

'vicious circle' in design terms, which are detrimental to the adhesive bonds performance.

As well as additional fail-safe features, due to joints critical nature, multiple safety factors will be used during design, largely to account for the inherent material/structural uncertainty associated with such features. Table 7 provides an insight into values for partial design factors as recommended in the 'Guide to the structural use of adhesives' [145], a guide for structural (civil) engineers with no specialism in bonded joints.

Table 7: Recommended values for Partial Safety Factors (adapted from [134], original values from [145])

Joint Configuration	Design Factor
Adhesive Properties, γm1	1.5
Adhesive thickness, γm2	1.5
Long term loading, γm3	1.5
Environmental conditions, γm4	2.0
Fatigue (non-fail safe joints), γm5	
Periodic inspection, good access	2.0
Periodic inspection, poor access	2.5
No inspection/maintenance	3.0

It is stated that when designing an adhesive joint the adhesive properties should be divided by the combined design factor γm calculated by:

$$\gamma_m = \gamma_{m1}\gamma_{m2}\gamma_{m3}\gamma_{m4}\gamma_{m5}$$

Equation 7

In this source it is recommended the design factor γm should be no less than 4.0, although the above approach is for use in aiding the civil engineering sector where design, qualification and manufacture of joints may be conducted using less vigorous methods than those within the field of aerospace (and as such design factors are likely to differ). This however illustrates where additional gains may be made in regards to design enabled by SHM. Factors included for inspection, to account for environmental effects, and long term loading as well as uncertainties associated with the general condition and performance of the joint could be reduced or eliminated if inspection was enabled by appropriate monitoring. Design factors associated with the adhesive may also be reduced if the actual condition of the structure could be known. In short safety is maintained by reducing the uncertainty associated with the

performance of the joint rather than accounting for this uncertainty with the use of oversized structure.

It is evident current solutions used to account for uncertainties associated with purely bonded structure add additional mass, as well as other potential structural issues. Advantages may be viable if the reliance on additional features such as 'chicken-bolts' could be replaced via appropriate monitoring of structure designed to respond to degradation or damage so that such damage may be identified and repaired prior to unacceptable degradation in a manner similar to visual inspection on damage-tolerant metallic aircraft. Such an approach may allow operation of such structure whilst conforming to the requirements set in AC20-107B.

3.2.2 Barely Visible Impact Damage

As discussed (section 2.2.3) impact damage is a major concern for both design and operation of composite airframes and as such is the primary consideration when sizing/designing many composite components. This is due to the large number of damage sources, the potentially large reduction in physical properties (particularly compressive strength – >70% reduction with 60mm diameter impact damage) as well as the difficulties in reliably identifying such damage [89].

As discussed inspection is a critical foundation of damage-tolerance. As illustrated in Figure 6 composite structural damage can range from; Category 1 damage that will not be confidently identified and as such the structure must retain DUL, Category 2 where damage will be identified during normal inspection, Category 3 damage that is obvious and will be recognised within a few flights and DLL capability will be maintained, Category 4 where damage will be immediately obvious to flight crew but continued safe flight capability (normally 0.8 DLL), and Category 5 which is damage not considered by design which must be repaired immediately [3]. Although sophisticated NDI techniques may be used during detailed depot level checks most inspections currently assess the structure via visual assessment [89]. Although recognised as being subjective to each inspector (and dependent on additional factors including surface colour/finish and diameter/depth of any surface indentation [146]) Visual Impact Damage (VID) is normally described as that which is clearly visually identifiable from a distance of 1.5 meters under ambient light conditions

(Category 2 damage). BVID is defined as damage just under this threshold (Category 1 damage) [89]. Composite civil transport aircraft are therefore currently designed largely in consideration of this detection threshold, i.e. the transition between Category 1 and Category 2 damage [3].

SHM which can reliably identify, locate and classify composite impact damage may enable benefits, such as reductions in structural mass, to be made. Ambiguities regarding the BVID threshold could be eliminated, therefore permitting designs to be set to more defined limits. If smaller damage can be reliably detected some damage currently considered as BVID, may be re-categorised to VID. As VID need only support DLL as oppose to DUL, as is the case for BVID, lower residual strengths are required. As such, with the aid of SHM, lighter more efficient designs may be used whilst maintaining current levels of airworthiness (Figure 14). Continuous or frequent SHM enabled interrogation may also allow damage to be identified at reduced intervals, such as that proposed Minakuchi et al [27] (see section 2.4), or other changes to operation such as condition based maintenance to be potentially viable

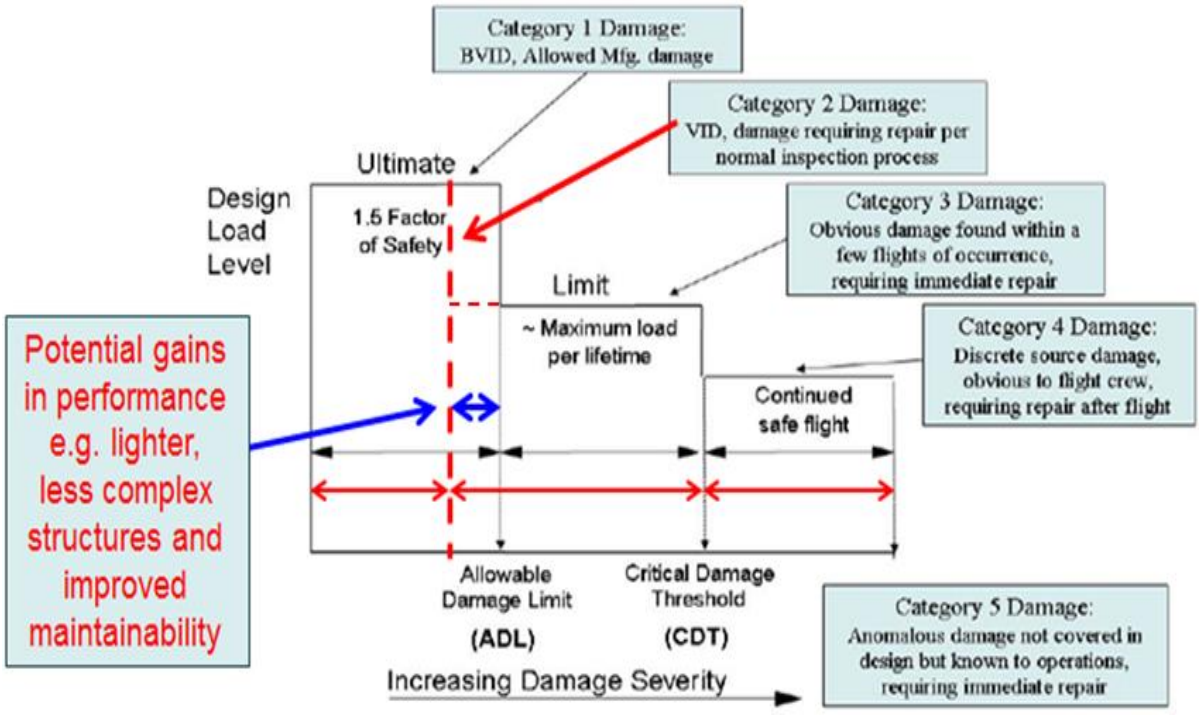

Figure 14: Influence of Improved Inspection Capability, made possible by SHM, on Damage Tolerant Design (adapted from [3])

3.3 Structure/SHM considered design and Justification for selecting adhesively bonded structure

As discussed few publications consider both the monitoring SHM technology and structure under scrutiny as a combined system. Obvious benefits are present if less reliance can be placed on additional structure currently used to account for uncertainty. With no definable indicators allowing initial damage to be identified, as well as appropriate slow or arrested damage-tolerant type damage growth, no potential gains may be achieved. If benefits are to be realised consideration must be made not only of the monitoring system but also the structure.

The case of bonded joint design has been selected due to the following reasons. The comparative low dimensionality, both in terms of structural form and loading direction, of bonded joints – when compared to plate-like surfaces susceptible to impact events – should aid both the structure/SHM design and analysis . Bonded components also contain considerable additional structure that could be removed if reliance on fail-safe fasteners is eliminated. In contrast impact susceptible composite skins cannot be simply ‘sized’ by adjusting their thickness (section 2.5). Further benefits to bonded joint design in many structures could also be achieved if design factors used to account for uncertainties associated with joint performance as a result of bond-line condition and prolonged service could be reduced if the minimum required condition could be assured. For example if a non-fail safe joint is manufactured using the partial safety factors as recommended in Table 7(Adhesive properties - $\gamma m1 = 1.5$, Adhesive thickness - $\gamma m2 = 1.5$, Long term loading - $\gamma m3 = 1.5$, Environmental conditions - $\gamma m4 = 2.0$, and there is no inspection/maintenance - $\gamma m5 = 3.0$) the resulting design factor is 20.25. This requires the joint is designed with over twenty times design strength. If such uncertainties could be removed by in-situ monitoring and considered design these partial design factors may be reduced to parity. If the joint, which is now inherently inspectable, is also given the partial design factor of a joint with good access this partial design factor may be reduced to 2 as recommended in Table 7. The result is a joint which only needs to be designed to transfer one tenth of the load required of the previously described design. Even compared to a joint with a design factor of 4, the minimum recommended by the institution of structural engineer’s [145], significant weight

savings may be achieved. As bond strength is largely related to bond width potential weight savings in the joint region may be as high as 50% if the joint bond width could simply be halved. Consideration such as included sensors or other features such as required overlap or potential additional design knock-down factors may however reduce this potential benefit.

Aerospace structures are usually designed (after consideration of material 'knock-down' factors and design allowables are applied to account for material variability and environmental effects [89]) to DUL capability, which is normally 1.5x DLL as discussed in section 2.2.3. These are in-effect the design factors used in aerospace designs. As previously discussed for purely bonded aerospace joints to comply with current legislation it is required at least DLL capacity must be substantiated by one of the methods highlighted on page 44. Currently purely bonded composite structure cannot fulfil these requirements and as such additional mass introducing features are required. The ability to allow bonded structure to be qualified and used without the need for such additional structure provides the greatest benefits.

To assess the viability of such SHM enabled bonded structure to be viable in the aerospace sector the following criteria will be considered:

- A minimum load capability (DLL) must be assured of the structure at manufacture with near 100% confidence
- In the event of performance degradation as a result of e.g. environmental ingress and partial damage that will occur due to overload of the degraded bond should not result in full catastrophic failure of the joint
- The damage described above should be positively identified with a degree of confidence approaching 100%. False damage indicators should be minimised, ideally to 0%.
- Regardless of the load at which damage is positively identified the joint should still have sufficient static load capacity allowing continued operation until repair (which may be performed immediately after the flight). This is equivalent to category 3 type damage (see Figure 5 & Figure 6) which is therefore required to have DLL static load capability. As the damage in this scenario could be inspected and positively identified after each flight as a

worst case scenario such damage may also be considered as category 4 and as such only 0.8xDLL capability is required. It is suggested that this allowance is only considered as a safety margin and ideally at least DLL capability should be provided by the joint when damage is identified.

- Well designed and fabricated joints will not fail under expected in-service loads by definition. Joint failures resulting from reduced strengths, possibly as a result of in-service degradation, therefore result from joints not acting as specified. Although cohesive failure is the preferred mode (but still unacceptable) in bonded joint design (see section 4.4) poor fabrication or contamination may result in adhesive failure which has a more significant influence on joint performance. Any system must therefore be capable of operating in the event of both failure modes but in particular the more problematic adhesive type failure.
- In the event of in-situ sensor failure the structure should be assessable via other methods and the sensor system repaired removing the requirement to replace the entire structure such as would be the case for a component that cannot be independently interrogated and/or the sensory system cannot be repaired/replaced.

3.4 Composite Bonded Joints Research Hypothesis and Questions

3.4.1 Composite bonded joints research hypothesis

‘Contemporary composite airframes use structural joints which are highly over-engineered to accommodate uncertainties associated with their condition and strength. Appropriate use of SHM, which includes considered design of the structure alongside the sensor type/placement strategy, will allow more efficient, lighter joint designs to be viable.’

3.4.2 Composite bonded joints research questions

To test the above hypothesis and in consideration of the criteria discussed in section 3.3 the following research questions were identified.

- How can SHM identify/monitor failure of adhesive bonds? Which methods and techniques are suited to providing easily interpreted responses to

damage initiation, with near 100% probability of detection, whist minimising false ‘no-fault-found’ responses? Which in-situ monitoring methods are best suited for use alongside aerospace structure considering operational and certification requirements?

- How can bonded structure be designed to complement the capabilities on the in-situ monitoring system and allow the requirements of the first research question and the previously identified criteria to be enabled? Can such a design in conjunction with appropriate operational and qualification procedure ensure adequate strength is present, ideally to DLL capability?

- How can bonded structure be designed to complement SHM; i.e. detectable, predictable and definable damage growth, potentially up to millimetre scale accuracy, aiding operation under an inspection based damage-tolerance regime?

3.5 Section Summary/Discussion

To be viable any SHM/structural system must respond appropriately both in terms of ease and probability of damage detection as well as ‘degrading’ in a damage-tolerant manner in the presence of damage. It has been recognised that the combination of both these vital factors can only be achieved if the structure and in-situ monitoring approach are regarded as a collective structure/SHM system. Although damage evolution is considered the structure should not be designed to deliberately fail, the pristine structure must be designed and manufactured to be both capable of carrying DUL and be durable just as that required of contemporary joints. The inclusion of any structure/SHM design instead provides an alternative approach to ensure appropriate airworthiness is maintained in the event of unidentified or unforeseen issues by means analogous to the requirements for adhesive bonding of primary composite airframe structure as stated in the advisory circular AC20-107B [3] without the requirement of additional structure.

Bonded composite joints have been identified as suitable structure in which to investigate such a concept, due to suitable structural topography and opportunities to remove significant structural mass as a result of implementing such an approach.

Although fatigue in bonded joints is commonly investigated this is not necessarily considered a major issue in service [136]. Any structural/SHM system however should still be capable of identifying/operating with such damage. Primary concerns however are related to rapid failures resulting from discrete damage events and lower than anticipated joint strength resulting from production quality control issues and/or progressive environmental degradation.

Uncertainty associated with actual structural condition and performance is a major issues linked with bonded structure. As such damage identification and appropriate damage growth characteristics must be evident even if the performance of the actual bond is lower than anticipated. Ideally any monitoring system which allows operation of bonded structure without additional structural features will need to robustly identify damage whilst at least limit load capability of the greater structure remains and with at least an equal confidence of identifying damage as would be expected if visually identifying damage on external surfaces. If however damage initiates at levels lower than expected, say between DUL and DLL (although such loads should not be experience during normal service), or potentially even lower than DLL due to degraded performance, the required residual strength (DLL) may still be available if the structure is designed such that the load bearing capacity (residual strength) is not immediately reduced as a result of damage initiation and partial damage. Alternatively the remaining load bearing capacity may be greater in the presence or partial damage than the load at which detectable damage initiates and can be positively detected. As such in the worst-case scenario, with damage initiating below DLL, sufficient 'get-home' capability may still exist if such non-diminishing behaviour is evident and structural loads above that which caused the damage can be avoided. This final scenario is obviously far from ideal and all steps should be taken to avoid this situation. A potential solution may be to proof test the component to acceptable load levels (as per option *ii* in AC20-107B) and use the structural/SHM considered design/behaviour to guard against failures resulting from in-service degradation.

4 Composite Joints

4.1 Section Introduction

It was recognised in Chapter 3 that adhesively bonded composite joints would be suitable structure to introduce a concept of structure/SHM considered design. To allow such designs to be developed an understanding of current design approaches is therefore required. An understanding of the mechanics of load transfer, as well as response to in service damage or manufacturing flaws allows design strategies that may promote appropriate damage response – as discussed in chapters 2 & 3 – to be proposed and tested.

This chapter scrutinises analytical and numeric approaches to joint design and analysis. General joint configurations are considered to identify suitable characteristics which may allow SHM enabled design to be viable. Failure modes as well as partial bond-line failures are discussed in part to identify the resulting in-service consequences but also to identify how potential issues may hinder or assist SHM enabled designs.

Although research is focused on SHM enabled bonded structure, comparisons with bolted joints were made. Design principles and guidelines for such structure are therefore also identified.

The use of SHM of adhesively bonded structure provides an alternative to structurally inefficient additional features used to account for uncertainty associated with the bond quality and condition. Reliable performance predictions can only be made if the exact condition and quality of the structure is known, i.e. no uncertainty exists. If this is the case – as is the ultimate goal of good manufacture, design and quality control – there is no requirement for either SHM or additional redundancy, as discussed in Chapter 2. As uncertainty is however present, practical design methods and structural concepts which promote suitable structural and sensing response regardless of these uncertainties (albeit with potentially lower ultimate load strengths) are attempted to be identified.

4.2 Bonded Structure

Design and analysis methods as well as configurations, considerations and issues associated with bonded structure are presented below. Why bonded current bonded structure is unsuitable for SHM is highlighted and strategies into how appropriate structure behaviour may lead to considered structural/SHM joint design are presented.

4.2.1 Joint configuration

The purpose of any joint is to transfer load from one component to another. Adhesively bonded joints should be designed with an ultimate strength higher than that of the adherends being joined (by 50% [147]) to avoid acting as a weak structural fuse. This philosophy is sensible as otherwise much of the greater structures capacity - not in the form of joints - would be wasted.

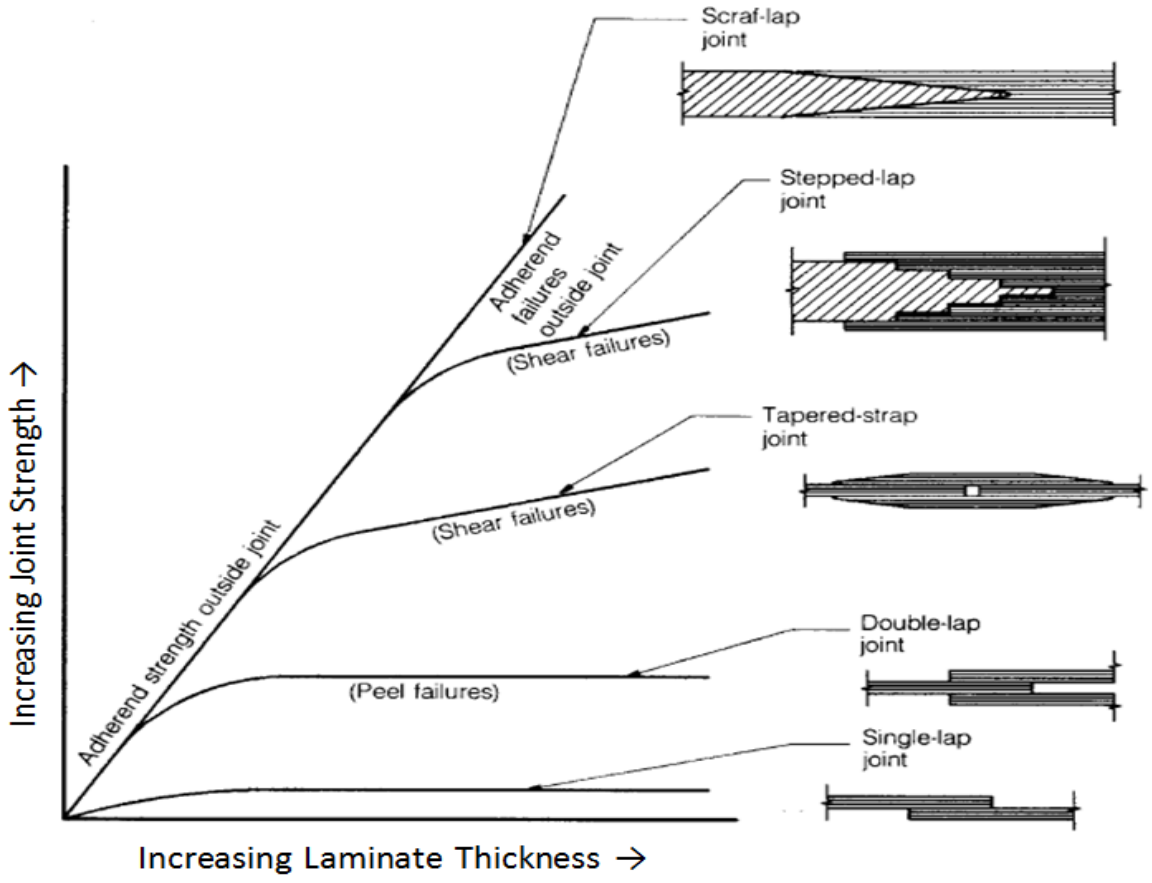

Figure 15: Bonded Joint Configuration strength Vs Increase in laminate thickness [23]

Joint strength is dependent not only on adhesive/adherend interface and adhesive qualities but also adherend properties and joint configuration. Various bonded joints design and manufacturing guidelines are presented [148][23]. A major consideration is that tension, peel or cleavage loading should be avoided as adhesives, and possibly to a greater extent the resin systems within laminated composites, are weak under such load cases (section 4.3.2.5). Bonded joint configurations, of various complexities, may be used which reduce such factors and increase load transfer via shear, a more effective load case for adhesives. Such designs may therefore be required if joining thicker and therefore stronger adherends (Figure 15).

Bonded joints are usually designed to hot/wet environmental conditions [135], generally the 'worst case' for both composites and adhesives. To reduce end peel effects various thickness tapering designs are suggested, including a 'reverse taper' with 'fillet', an alternative suggestion is the stiffening the adhesive ends [149]. Thickness tapers similar to that in Figure 15 with a 1 in 10 slope down to 0.51mm are commonly recommended [135] (0.25-0.75mm [137]). Thickness tapers are not considered in this study as in the event of damage propagation the effect of the taper would be lost. For similar reasons 'spew fillets' – adhesive squeezed from the joint during manufacture – which can provide relief against both peel and shear loads [149] are also not considered. This research considers SHM enabled design with double strap/lap joints due to their common application within aerospace and the comparative ease of analysis and manufacture compared to other configurations.

4.3 Design Approaches and Stress/Strain distributions

Below is a summary of the design and analysis procedures considered or used within this research.

4.3.1 Design Failure Criteria

During the design and analysis of bonded structure suitable criteria which predict failure within the adhesive (or adherend) must be defined. The most common are considered below.

4.3.1.1 Average Stress Method

This simple approach considers the average shear (or normal) bond stress (P/A). This is compared to average stress allowables established from test coupons [150]. Although historically used for bonding wooden aircraft – where uncertainty resulted in large bond areas – issues became apparent once accurate techniques to determine adhesive strength were established which resulted in less conservative bonding designs. Such issues where compounded when adhesives were used to join stronger materials [136]. This approach can only predict bond strengths if the structure has the same loading, joint geometry, material properties (both adhesive and adherends), and is under identical environmental conditions as that of the test coupons [150]. This is because the stress-strain distribution is not consistent across the bond-line and is influenced by the previously listed factors (see Figure 17 below). Use of such data with structure not identical to the test coupons can result in errors greater than a factor of 3 [150]. This method may be used to qualitatively compare the performance of several adhesives on identical coupons and is often quoted on adhesive data sheets as a 'property' in pascals. Although a test standard is typically attributed (ASTM D1002) no mention of the considerations discussed are usually included (although recognised within ASTM D1002). It may therefore be incorrectly inferred (as witnessed by the author) that this value may be used with any structure and simply scaled to provide strength values for any bond area.

4.3.1.2 Maximum Stress (or Strain) method

Methods which compare the maximum stresses or strains within the bond-line to the corresponding stress/strain values established from experimental tests (designed to eliminate non-uniform stress/strain distributions such as the thick adherend shear KGR-1 and KGR-2 extensometer tests [151]) are commonly used within industry. Comparisons may be made against the maximum normal, shear stresses (or strains) or von Mises stress values in the bond. Damage initiation (and therefore joint strength) is predicted when maximum values in the joint reach those established during testing. Improvements on the average stress approach are achieved by considering the variation in stress/strain throughout the bond-line. An advantage of this approach is that the structure being designed need not be of identical form of that of the test specimens [150].

Preliminary designs for simple joint geometries may be created using closed form equations approximating the behaviour of the adherends and adhesive. Further refinement or more complex joint geometries may be analysed with the aid of Finite Element Analysis (FEA). When using FEA issues may however occur in the form of stress singularities in regions of dissimilar materials or abrupt geometries. Such features could exhibit (theoretical) infinite stresses resulting in the predictive joint strength being zero. As values are however averaged over the size of FEA elements a practical joint failure criterion is explained by Penado and Dropek [150] and summarised below:

1. Ascertain the elastic moduli of the adhesive from bulk specimens; if non-linear (ductile/plastic) behaviour is evident appropriate stress-strain curves are required.
2. Determine the failure loads of simple test specimens, ensuring the strength of the 'singularity' at the damage initiation site(s) (material properties and local geometric changes) are as per the structure to be analysed.
3. Use FEA, in combination with the failure loads, to establish the stress or strain allowables in the test specimens. Element sizes in regions where steep gradients are expected, such as failure initiation sites, should be no larger than one third of the adhesive thickness.
4. Perform (linear or non-linear) FEA on the structure to be analysed comparing calculated stresses/strains to the allowables established in step 3. By comparing these values, in conjunction with applied loads, predicted failure loads can be established. It is essential the element size used at damage initiation sites are identical to those used to establish the stress/strain allowables in the test sample therefore ensuring identical comparisons are made as values are averaged over the volume of the elements.

4.3.1.3 Fracture mechanics Approaches

Various investigations have been made using fracture mechanics to determine the strength or failure criteria of adhesive joints [152-155]. Often such approaches determine the extension of existing cracks of a known size and location although the propagation of inherent imperfection and flaws may also be considered. Alternatively stress singularities which may occur between bonded dissimilar

materials have been used as a fracture criterion although it is recognised details used to calculate such values, such as sharp corners on adherends, may in reality differ to such assumptions (e.g. become more 'rounded') altering predictions [150].

Krieger [151] highlights concerns associated with using fracture mechanics based approaches with bonded joints in that rather than testing the propagation of a crack in a bulk sample the calculated energy required to grow a crack – i.e. the strain energy release rate 'G' – is based on double-cantilever beam (DCB) tests, even though fracture mechanics is based on monometallic or mono-plastic specimen properties not that of a construction. This concern is due to fracture mechanics stating that to stop crack progression it is required that there must be a plastic zone at the crack tip – which can be calculated using values of G – whilst the remainder of the material is within its elastic limit. When considered with a thin adhesive layer within a DCB or shear joint the plastic zone is however much larger than the bond-line thickness. As such this test does not fulfil the requirement of the approach. Krieger also highlights the formula used to establish G contains neither terms for the bond-line thickness or the tensile stress/strain adhesive properties. These factors cannot be ignored as, as Krieger states, such a test with different specimens exposed to variations in environmental exposure, with identical strain energy release rate values (G) can show a variation in tensile stress greater than 100%.

Fracture mechanics may also offer little benefit when joints degrade as a result of 'adhesive failure' (see section 4.4). Other influences associated with uncertainty, such as variation in adhesive quality within an in-service joint compared to an 'ideal' sample, may limit the application of fracture mechanics beyond assessment of strength and fatigue performance of non-problematic joints.

4.3.1.4 Reasons for considering Stress/strain approach and its application in considered Structure/SHM design.

Due to the issues discussed a SHM enabled design philosophy based primarily on critical levels of shear and/or 'peel' stresses-strains has been selected. Such approaches are already widely used in industry [150] and are therefore likely to be understood and accepted. Such a philosophy also allows the criteria for suitable design for loading and damage behaviour to be identical to that proposed for

monitoring, i.e. strain, therefore simplifying this synergistic approach at the design stage. Identification of stress and strain distributions within the structures geometry may allow suitable behaviour, both in terms of potential damage growth and monitoring, to be inherently tailored into the structures design regardless of the precise quality of failure mode of the joint (although at loads potentially lower than designed for pristine structure). Further design considerations, such as the inclusion of regions of minimum stress (section 4.3.2.4) within the joint to promote bond durability may also be simultaneously considered using such an approach.

4.3.2 Magnitude of Stresses and Strains in Adhesive Bonds

To consider a design approach based on critical stress and strain values an understanding of how these factors are influenced within the loaded structure, both in pristine and partially damage conditions, is required. Adhesive shear stresses and strains are not consistent across the length of an adhesive joint overlap, with greater shear stresses/strains found towards the ends due to the marginally elastic nature of the adherends. The majority of the joints shear transfer capability is taken by ‘plastic-zones’ in the adhesive where the adhesive shear stresses/strains plateau at a maximum. The remainder of the adhesive is subjected to shear via an elastic ‘trough’ region at the joints centre which is subjected to lower shear stress and strain and therefore contributes little to the loading capability. As such, increasing the joint overlap does little to improve the shear loading capability; however there are reasons for increasing the overlap length, at the cost of additional mass.

Analytical approaches which describe the stress and strain behaviour, including considerations applicable to practical design, are described below. As well as providing clues into how bonded structure may be adapted to allow SHM enabled design to be viable such methods allow preliminary designs to be produced and comparisons can be made against analyses made with the aid of FEA for modified geometries. Adaption of such approaches may also provide useful preliminary design tools for SHM enable bonded design.

4.3.2.1 Linear Elastic Analysis

The most simplistic analysis of lap based joints considers the adherends to be infinitely stiff and the adhesive to be subjected to shear loads only. This was the basis for the average stress approach (see section 4.3.1.3 above).

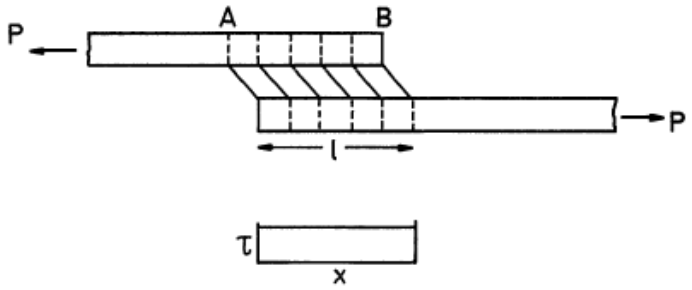

Figure 16: Exaggerated deformations in loaded single-lap joint with ridged adherends [149]

In reality the adherends will always be to some degree elastic. This behaviour is illustrated in Figure 17.

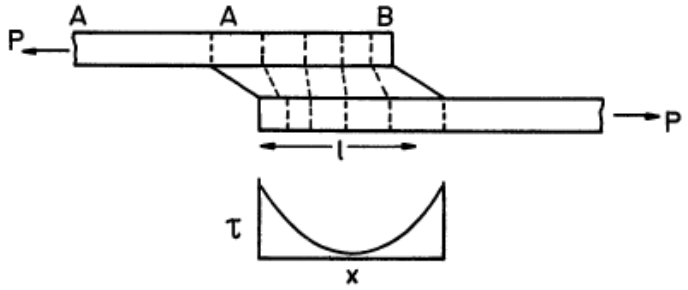

Figure 17: Exaggerated deformations in loaded single-lap joint with elastic adherends [149]

The upper adherend experiences a maximum tensile stress at position A which reduces to zero at B at the far end of the overlap, the adhesive 'sections' strained by progressively lower amounts over the overlap length. The lower adherend experiences similar deformation. Assuming ideal bonding between adhesive and adherends the result is a shear stress distribution which peaks at the overlap ends.

This effect (differential shear) was the basis of adhesive single lap joint analysis by Volkersen [156] (information gained via [147,149]). Volkersen's theory was adapted by de Brune [157] (information gained from [158,159]) for double lap joints. Although

these analyses only consider shear deformation of the adhesive and tensile deformation of the adherends they form the basis for later more refined analyses such as the work of Goland and Reissner [160] (Information gained from [137,147,149,158]) which include a bending moment factor to account for the rotation of single lap joints due to load path eccentricity. More recent work by Tsai, Oplinger and Morton [158] has extended these theories to include effects of shear within the adherends. Kim and Kedward [161] have also adapted the differential shear approach to account for specially varying in-plane shear stress resultants.

For a tension loaded lap joint a simple closed-for solution based on Volkersen's theory has been presented by Kim and Kedward [161] and shown below:

The governing equation is:

$$\frac{d^2\sigma_y^o}{dy^2} - \lambda_o^2\sigma_y^o + D_o = 0$$

Equation 8

Where $\lambda_o^2 = \frac{G_a}{t_a}\left(\frac{1}{E_y^o t_o} + \frac{1}{E_y^i t_i}\right)$ and $D_o = \frac{G_a}{t_a} \cdot \frac{N_y}{E_y^i\, t_i\, t_o}$

Equation 9 & Equation 10

The outer adherend tensile stress can be calculated for any position (y) along its length (2c), due to the load per unit width (N_y), by solving Equation 8.

$$\sigma_y^o = \frac{cosh\lambda_o y}{cosh\lambda_o c}\left(\frac{N_y}{2t_o} - \frac{D_o}{\lambda_o^2}\right) + \frac{sinh\lambda_o y}{sinh\lambda_o c}\frac{N_y}{2t_o} + \frac{D_o}{\lambda_o^2}$$

Equation 11

The adhesive shear stress at position y can calculated as follows

$$\left(\tau_{yz}^a\right)_{N_y} = t_o\frac{d\sigma_y^o}{dy} = t_o\lambda_o\left[\frac{sinh\lambda_o y}{cosh\lambda_o c}\left(\frac{N_y}{2t_o} - \frac{D_o}{\lambda_o^2}\right) + \frac{cosh\lambda_o y}{sinh\lambda_o c}\frac{N_y}{2t_o}\right]$$

Equation 12

The boundary conditions for lap-joints are:

$$\sigma_y^o = 0 \ at \ y = -c \quad \text{and} \quad \sigma_y^o = \frac{N_y}{t_o} \ at \ y = c$$

4.3.2.2 Elastic-Plastic Analysis and Hart-Smiths design approach

The approaches for analysing bond-line stresses discussed above all consider the behaviour of the adhesive to be elastic. It is however recognised that many modern adhesives may display non-linear plastic behaviour beyond the elastic yield point [149]. Hart-Smith modified Volkersen's work to include adhesive plasticity and thermal mismatch for single [162] and double [159] lap joints as well as work on stepped and scarfed bonded joints [163]. General considerations, particularly with composite materials, have also made up much of this extensive work [136,147,164]. This approach commonly forms the basis of preliminary design of bonded structure. Such considerations, with the aid of FEA for more 'non-standard' joints may be used to determine the applicability of each design and potentially the nature of its failure.

Hart-Smith highlighted that as applied load is increases the adhesive subjected to the highest shear loads – for lap/strap joints at the overlap ends – will begin to deform plastically. Due to ductile yielding the shear stress levels will plateau in these regions, an effect not considered within linear-elastic analysis. The adhesive will however still continue to deform until failure initiates as a result of shear *strain* (see Figure 18). In the case illustrated damage is equally likely to initiate at either end of the joint overlap, however such a configuration provides the greatest potential strength for this configuration. The joint is considered to be 'balanced', for a double lap joint this is defined as:

$$Ei \cdot ti(total) = Eo \cdot to(total)$$

Equation 13

Where Ei & ti are the tensile modulus and thickness of the inner (plate) adherend respectfully and Eo & to(total) are the modulus and combined thickness of the outer (strap) adherends.

Figure 19 illustrates how the increase in bond overlap affects the bond-line shear stress distribution. Hart-Smiths analysis predicts the regions where the adhesive will experience plastic deformation up to a characteristic length (C). For a 'balanced' joint this is has the length (l - d)/2 and is given in non-dimension form as [147]:

$$\frac{\lambda(l-d)}{2} = \sqrt{2\left(\frac{\gamma_p}{\gamma_e}\right)} = Constant$$

Equation 14

This value is independent of overlap length. The maximum adhesive shear stress/strains are identical for all overlap lengths for similar adhesives and adherends. As these values largely define the joints failure load only minor strength gains are made by increasing the overlap past this 'fully plastic' overlap length (note: other considerations are discussed in section 4.3.2.4).

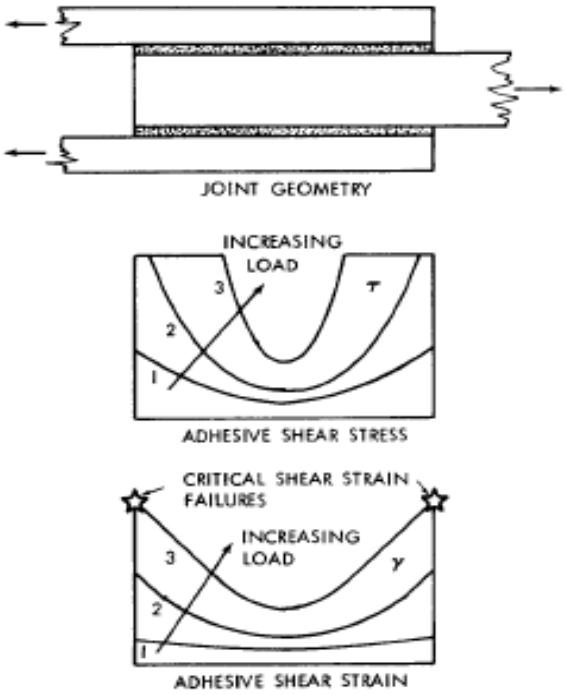

Figure 18: Adhesive shear stress and strain within a balenced double-lap joint subjected to increasing tensile loads [147]

The 'plateau' strengths for balanced double lap joints are defined characterised by the relationship below [147]:

$$\frac{\tau_{av}}{\tau_p}\left(\frac{\lambda l}{2}\right) = \sqrt{1+2\left(\frac{\gamma_p}{\gamma_e}\right)}$$

Equation 15

Where the exponent of elastic shear decay (λ) as defined by Volkerson (Equation 9) for single lap joints subjected to pure shear and therefore for double lap joints as a result of symmetry through the inner adherend (plate) is defined as:

$$\lambda^2 = \frac{G}{t_a}\left[\frac{1}{E_1 t_1} + \frac{1}{E_2 t_2}\right]$$

Equation 16

It is more convenient to consider the entire joint and use the full dimensions of the adherends ($t_i = 2t_o$). It is therefore more common to use the form shown below when considering double lap joints

$$\lambda^2 = \frac{G}{t_a}\left[\frac{1}{E_o t_o} + \frac{2}{E_i t_i}\right]$$

Equation 17

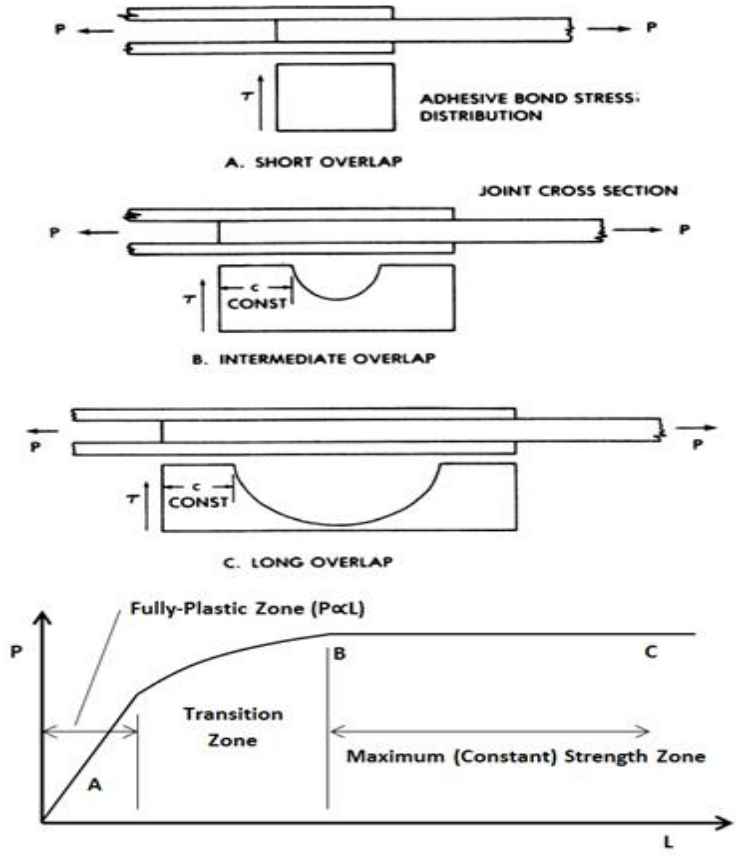

Figure 19: Influence of lap length on bond shear stress and joint strength [147]

$\lambda \cdot l$ in Equation 15 is used to form a non-dimensional joint overlap so that $\tau_{av} \cdot l$ is proportional to joint strength. Rearrangement of Equation 15 produces the explicit expression for the maximum transferable shear load P. As the double lap joint contains two bond-lines the strength is determined by $2\tau_{av}l$.

$$P = 2\tau_{av}l = \sqrt{4t_a\tau_p\left(\frac{1}{2}\gamma_e + \gamma_p\right)4E_o t_o}$$

Equation 18

Hart-Smith determined the joints adhesive shear strength is proportional to the area under the adhesives shear stress/strain curve. The precise nature of this curve is unimportant as long as the area remains unchanged. To simplify analysis the equation component $\tau_p(\frac{1}{2}\gamma_e + \gamma_p)$ refers to the area under a simplified shear stress-strain curve such as that shown in Figure 34. The product of this with t_a converts this to shear strain energy per unit area of bond.

The influence of the adherend extensional stiffness $E_o t_o$ can be seen to raise the potential shear strength of the bond. This raise in potential strength however is not as rapid as the increase in adherend strength resulting from this increase in thickness [147]. As a result, to ensure the joint does not become a structural weak-link, more sophisticated joint designs are required for thicker structures (Figure 15).

4.3.2.3 Unbalanced Joints

The above analysis describes 'balanced' joints. Predictions of the same form have been produced for use with un-balanced joints; i.e. the sum adherend product of E & t on one side of the joint <u>are not</u> equal to that on the other side. If a stiffness imbalance is present a greater part of the adhesive shear is experienced at the more compliant end of the overlap, as per Figure 20. As the critical shear strain is reached at a lower load than for that of a balanced joint the resulting is a weaker joint. To achieve the maximum possible bond strength adherend imbalances such as this should be minimised as potentially half the joint is wasted [136,159]

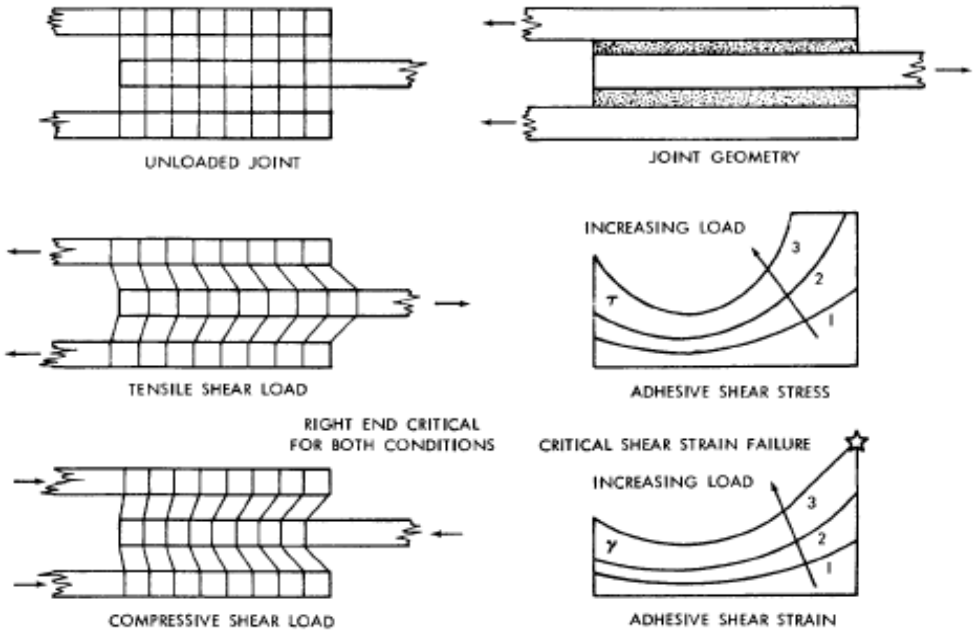

Figure 20: Deformations and adhesive shear stress/strains in unbalanced bonded joints [159]

In such a configuration damage will however initiate at a known location, the more compliant end of the joint. Modifications to Equation 18 allow the maximum possible shear load per unit width (P) to be established by considering the lower value of the following equations [159].

$$P = \sqrt{2\tau_p t_a \left(\frac{\gamma_e}{2} + \gamma_p\right) 4E_s t_s \left(1 + \frac{2E_s t_s}{E_p t_p}\right)}$$

Equation 19

$$P = \sqrt{2\tau_p t_a \left(\frac{\gamma_e}{2} + \gamma_p\right) 2E_p t_p \left(1 + \frac{E_p t_p}{2E_s t_s}\right)}$$

Equation 20

Similar effects as seen with stiffness unbalanced joints may be seen if adherends with dissimilar coefficients of thermal expansion are joined. This is due to residual deformations in the adhesive as a result of the curing process. Within this research identical materials are being joined, as such thermal mismatch is not considered. Further details regarding the consequences of joining such dissimilar materials are presented in [159].

4.3.2.4 Minimum Shear Stress Consideration

Although joint strength was recognised to not significantly rise as overlap length increased (Figure 19) Hart-Smiths design concept states a practical in-service joint should have an overlap greater than the minimum theoretical requirement. Firstly this provides some protection against damage or manufacturing flaws that if minimum overlaps were used would result in near instantaneous joint failure (see section 4.5). Secondly Figure 21 shows how the minimum shear stress/strain values in joints with short overlaps are almost at the same level as the maximum values, whereas the minimum values in longer overlap joints can be controlled by appropriate adjustment of the overlap length [137].

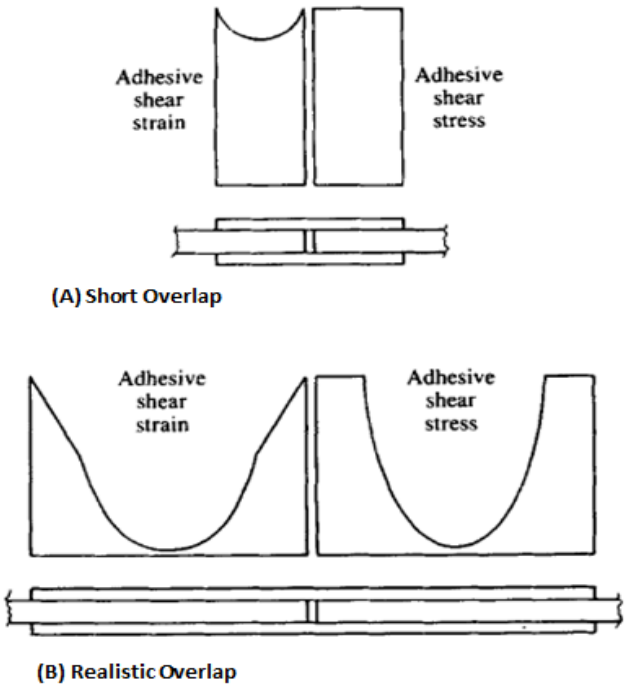

Figure 21: Non-uniform stresses in bonded joints [136]

Short overlap adhesive joints are as a result sensitive to creep rupture both from steady and cyclic loads. Whist creep does occur at the high stress regions of longer overlaps this cannot accumulate as the stiff adherends return the adhesive to its original position when the load is relaxed [137]. H-S therefore states the bond overlap should therefore be designed with consideration of the minimum stress at the middle of the joint [164]. During the PABST (Primary Adhesive Bonded Structure Technology) program [165] the minimum shear stress was defined as 10% of the

maximum, and this has been adopted in H-S's recommendations [136,137,164]. The distribution of shear, and calculations to determine these features for double lap/strap joints, are shown on Figure 22, although a similar approach may be made using FEA. The inclusion of this low shear-stress trough however does not prevent all damage resulting from ductile yielding. It is therefore recommended the adhesive should not deform plastically during normal operational loads (≤DLL) and the additional capability enabled by plastic deformation used to account for DUL cases [137,141,151]. For in-service joint design it is necessary to perform appropriate analysis at each load case. Such considerations may still be required for novel SHM enabled designs.

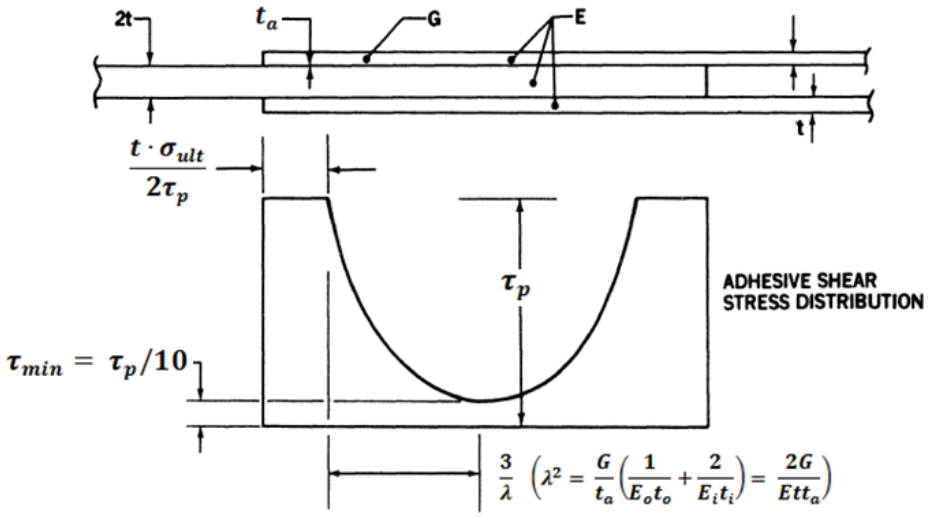

Figure 22: Shear stress considerations for design of (balanced) double lap/strap joints) [164]

4.3.2.5 Normal/Peel Loads

Adhesives, and laminated adherends, are potentially susceptible to peel loads, i.e. those normal to the adherends. Peel failures may occur within the bond-line or within the adherends, usually between the first two plies adjacent to the bond. Similar to shear, peel loads are not consistent across the bond-line and will be greatest at the overlap ends. This results from eccentric loading for unsupported single lap joints (Figure 23), or and/or bending moments in double lap/strap joints (Figure 24) [149]. Only tensile normal peel loads are a cause for concern.

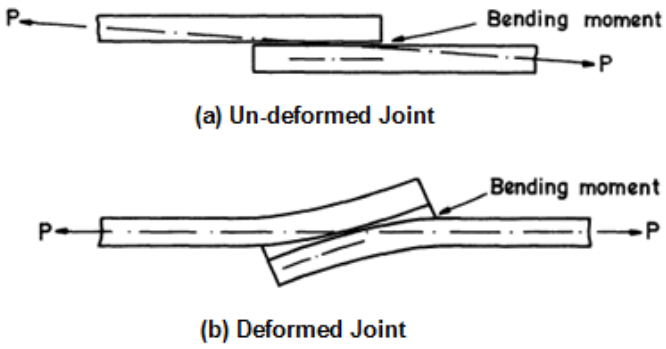

Figure 23: Induced peel forces resulting from eccentric loading in unsupported single lap joints [149]

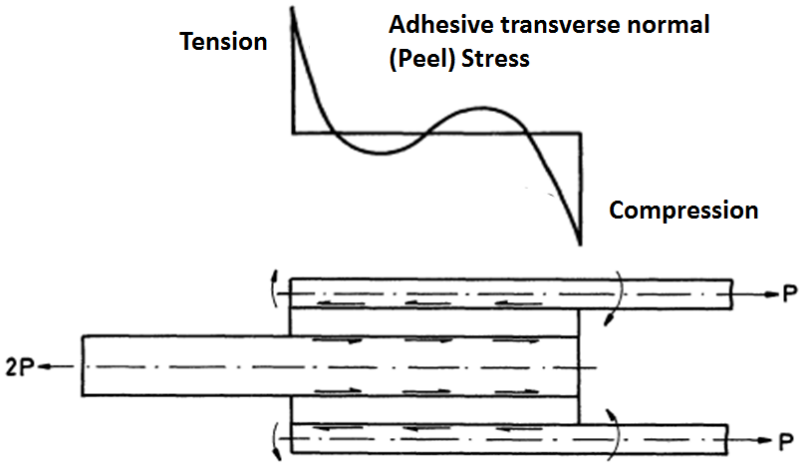

Figure 24: Bending moments induced in the outer adherends of double lap joints [149]

Increases in overlap length can to some extent reduce peel loads [147,166-168], particularly in single lap type joints. Tapering the adherend thickness (ply 'drop-offs') at the overlap ends in various forms (as well as thickening the adhesive and/or including an adhesive fillet in these regions) [147,149,166] has been shown to reduce peel loads and is commonly used in aerospace joints. As both approaches will change the local stiffness of the adherends (E·t) – modifying the bond-line shear stress/strain distribution – previous bond-line shear analysis may need to be amended. Investigations within this research are currently limited to constant thickness adherends/adhesives, however further developments aided with FEA should be possible which include such features. The presence of 'spew fillets' (adhesive squeezed from the joint ends) can also influence both the local magnitude

and distribution of s stresses/strains (a reduction in magnitude and a shift outwards as the size of the spew is increased [149,150]). Spew fillets are not considered within this work as if controllable damage propagation is achieved the spew fillet will only benefit the joint prior to damage initiation.

Linear analytical methods for predicting max peel loads have been proposed [147], however the use of such closed form equations may be difficult when considering non-linear material properties [149][135], particularly if non-standard configurations are considered. As such comparisons are made using FEA in this work.

4.4 Failure Modes: Causes and Implications

Adhesive joints should always be designed to be stronger than the structure being joined to avoid rapid, catastrophic, 'unzipping' of a joint acting as a weak-link fuse a result of a local; defect [135,147]. To do otherwise would make little sense as any structures strength is determined by the weakest point in the load path therefore the majority of the structure – not joint – would be over-engineered.

This research focuses on adhesive 'secondary bonding'; the joining of two (or more) fully cured composite components using an additional adhesive. Other methods include co-bonding (the joining of a cured and uncured composite part, possibly with an additional adhesive) and co-curing (the joining of two un-cured components via the resin used for the matrix system to effectively produce a single part). Secondary bonding may present the most practical option for many joining applications, however as joining is produced as a result of adhesion (as is potentially one part of a co-bonded joint) some issues may arise which may be less prevalent in the co-curing process which utilises chemical cross-linking.

Various forms of structural failure may be associated with bonded joints.

- Structural failure outside the bond over-lap
  As the adhesive bond should be stronger than the structure being joined this is the desirable structural failure mode related to well designed and manufactured joints.
- Failure within the joint over-lap
  This may take several forms:

- Cohesive Failure

Fracture within the adhesive layer characterised by adhesive being present on both adherends after fracture. Cohesion failure is normally a result of shear however peel or a combination of both may result in such failure. As this failure can be associated with the full strength of the adhesive such failures are generally the result of poor joint design, however high levels of adhesive porosity may also contribute to cohesive failure [140,169].

- Adhesive Failure

Adhesive failure (occasionally referred to as adhesion failure) occurs at the adhesive/adherend interface and may be caused by contamination or insufficiently chemically active surface reducing the strength of adhesion. Such failure may also occur if the adhesive has cured before formation of the bond [140,169]. Although factors such as operating loads, adhesive-creep and fatigue may contribute to the ultimate failure of the bond adhesive type failure within service is always the direct result of issues introduced during manufacture [140]

- ‘Inter-lamina’ or ‘fibre-tear’ failure

Failure may occur within the laminate matrix, often at the ply adjacent to the bond-line. Many bonding resins are stronger than those used as laminate matrix systems, as such failure may occur in the laminate prior to adhesive failure as a result of ‘peel’ loads. Such failures should be minimised by due consideration at the design stage (see section 4.3.2.5)

- Potential for mixture of failure modes

Failure may occur as a result of a mix of the above failure modes.

Other issues include:

- Disbonds

Areas may exist within the bond-line with no connection or the adherend and adhesive due to massive contaminations or gaps in the adhesive layer [170] (see section 4.5).

- Impact

  Damage resulting from impact can occur both during manufacture and in-service potentially damaging the adherends and potentially the adhesive bond [170].

Failures resulting from poor structural design - i.e. most cohesive and inter-lamina type failures - should not be the primary concern for SHM systems or SHM enabled designs. In these cases each component and material is performing in a consistent manner, therefore deficiencies should be identifiable as part of the design and 'building-block' testing principle used within aerospace development. Disbonds and impact damage resulting from manufacture should – within the limits of the detection – be identifiable via NDI [170] during production inspection. Fatigue failure (which contrary to common belief not the usual form of adhesive bond failure [136,140]) only occurs when joining thick adherends under high load and therefore can potentially be eliminated by suitable design. If such failure does occur it will propagate within the adhesive, in the plane of the carrier cloth in the case of film adhesives [140]

Problematic forms of structural degradation are those in the form of adhesive failures (as a result of poor surface preparation or moisture in the adhesive [135]) and potentially some cohesive failures caused by high levels of porosity resulting from exposure to high humidity prior to cure [140]. This is because the structure is degraded to an unknown level compared to the un-degraded design and NDI methods are unable to detect weak bonds resulting from such mechanisms due to the lack of a detectable interface [140,170]. Although such issues are the result of poor manufacturing and quality control – and should therefore be eliminated by the rigorous implementation of good practice – the uncertainty associated with their potential presence, and therefore structural performance, remains. This currently necessitates the inclusion of additional features and over engineered structure as discussed in Chapter 3 – Research Objectives. It is these cases, as a more efficient alternative to such additional features, where SHM enabled design may provide the greatest value.

4.5 Effects of Flaws within the Bond-line

Part of the extensive work conducted by Hart-Smith investigated the effects of local defects, resulting in partial disbonds, within lap joints [171,172]. Recognition of such effects on shear distribution within the adhesive bond-line will assist the formulation of strategies both in regards to joint design and sensing strategies. The loads in the cases published can be seen, due to the absence of 'plastic plateaus', to be lower than that required to strain the adhesive above its elastic limit at the joint ends.

Figure 25 reveals the shear stress distribution of a pristine joint. The larger than expected region of low strain (resulting from the overlap length) is present due to the joint being sized for hot/wet conditions, although this feature also aids bond-line durability in the presence of local disbonds.

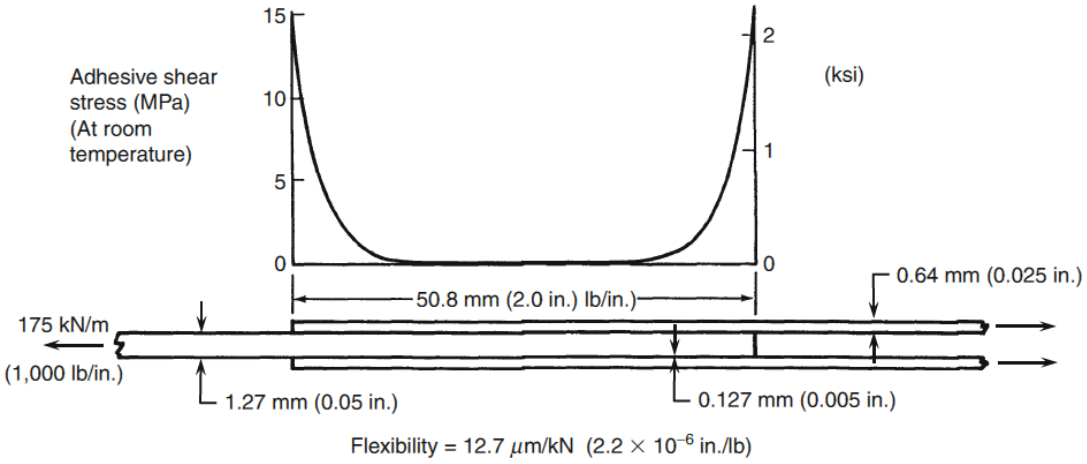

Figure 25: Adhesive shear stress distribution for bonded double lap joint with no defects/disbonds [172]

Figure 26 illustrates the calculated bond-line shear stress when a local disbond is close to the edge of the overlap. The shear load previously transferred via this region is now taken by the adhesive adjacent to the disbond. Little significant increase in peek shear-stress (and as no plastic deformation is present in this case a similar distribution in shear-strain) is present. The joints capacity is therefore largely unaffected. This highlights the robust nature of adhesive bonds to local flaws, although this capacity may be lost if the adhesive adjacent to the disbond is also close to failure [172].

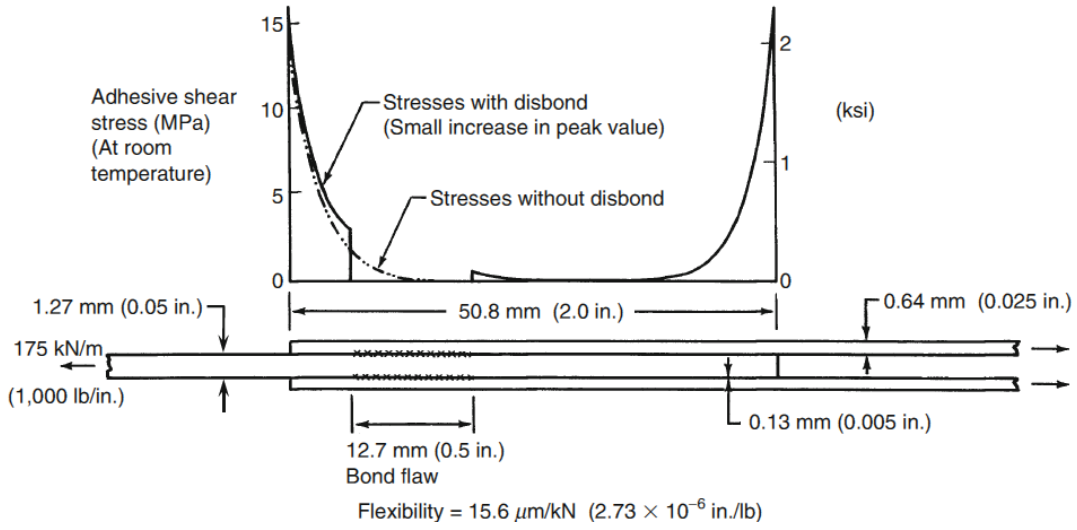

Figure 26: Adhesive shear stress redistribution resulting from a local flaw/dis-bond *near* the edge of the joint overlap [172]

The same size disbond is considered at the edge of the overlap in Figure 27. The peak magnitude of shear-stress calculated is again unaffected, the peak instead moving to the edge of the disbond (effectively the new overlap end).

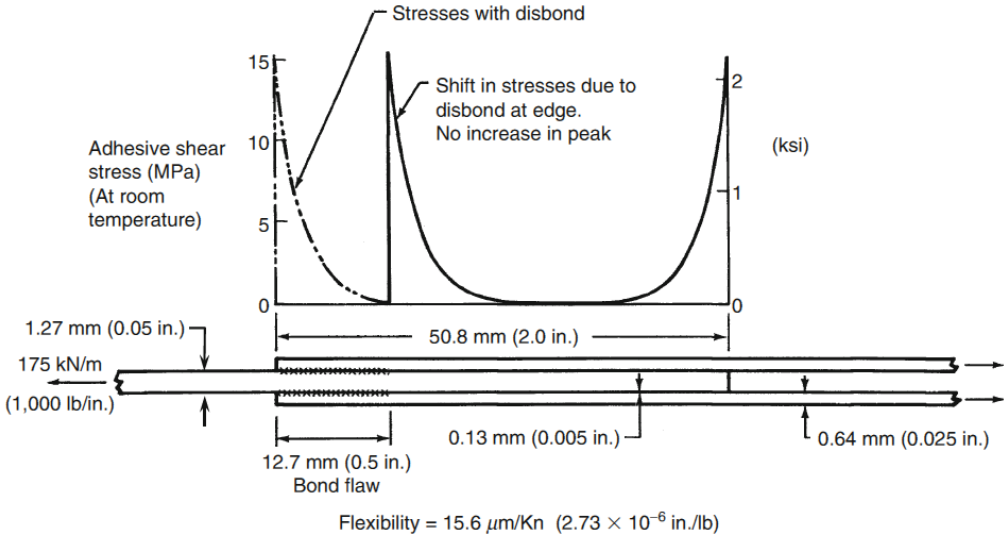

Figure 27: Adhesive shear stress redistribution resulting from a local flaw/dis-bond *at* the edge of the joint overlap [172]

Figure 28 shows how a defect/disbond at the centre of the overlap affects the shear stress distribution. As little or no load would be transferred in this region, even in a pristine joint, the peak stresses are largely unaffected [172].

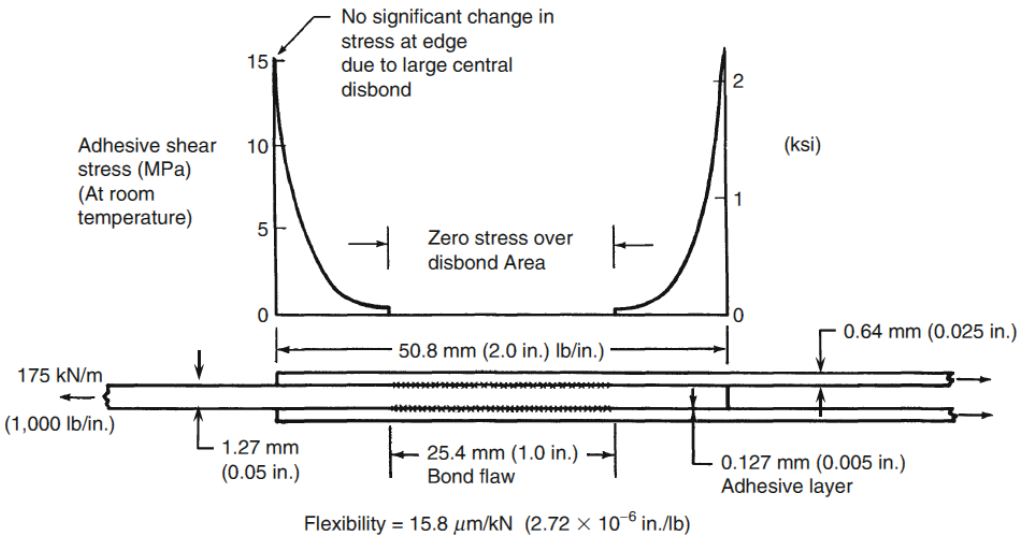

Figure 28: Adhesive shear stress redistribution resulting from a local flaw/dis-bond at the *centre* of the joint overlap [172]

Hart-Smith's work showed that well designed bonded joints inherently possess a high tolerance to large local defects/disbonds.

The calculated values published within the work illustrated in Figure 25 - Figure 28 are all with the linear region of the adhesive, therefore simplifying the analysis. In the presence of adhesive plastic deformation, due to exceedance of DLLs, other effects of local flaws may become apparent. Even if no disbond is present at the overlap edge when as plastic regions form and grow the curved sides of the elastic trough will progress into the overlap (as seen in Figure 22). Interaction may then occur with any flaw deeper within the overlap. A similar effect may be observed if the disbond is closer to the overlap edge than that considered on Figure 26. This would displace a higher region of shear stress, possibly resulting in overload and failure of the small outer portion of adhesive resulting in the disbond 'evolving' to a configuration similar to that in Figure 27. Whilst the central disbond (Figure 28) has little effect on performance its presence would compromise the ability to tolerate further damage. In the event of damage progressing from an overlap end upon interacting with the central disbond the effective bond-line length would be rapidly reduced to an extreme version of that seen in Figure 27. This much reduced bond may not be sufficient to maintain the operating load and will at least certainly possess much less tolerance to additional damage or creep rupture.

Note the above only concerns shear loads. Peel loads also influence bond strength and may distribute differently with such damage. FEA is used within this work to consider both distributions. Bond-line failure may occur as a resultant of these loads. Various studies have considered failure criterion such as 'von Mises' to account for this, however as such criterion are based on stress values it would seem difficult to interpret such data in regions beyond the adhesives elastic limit. Therefore to account for such strain resultants the maximum strains are considered during FEA study of the bond-line.

It is commonly observed that once adhesive failure initiates joint failure frequently follows almost instantaneously (see Chapter 3 & Chapter 6). Consideration of the above distributions, aided with FEA, will be made at each stage and described in appropriate subsequent sections, in an attempt to tailor behaviour more appropriate to SHM enabled design.

4.6 Adhesives

Although structural adhesives are available in several forms film adhesives are the preferred choice for bonding large areas as these can produce more uniform bond-lines, including bond-line thickness, and are easier to contain during heated cure [135].

Ductile adhesives are preferred to brittle adhesives [135] as their plastic nature provides greater ultimate strength (area under the shear stress-strain curve) and toughness. They may however be limited in higher temperature environments and as such brittle adhesive may need to be used at a sacrifice of ultimate strength [137]. Joint designs should be made considering the adhesive properties at the 'worst' environmental conditions expected in service, usually 'hot-wet' conditions.

When designing using analytical approaches adhesive properties are usually required in the form of adhesives shear stress-strain curves which may be simplified for use with relevant equations as per Figure 34. As previously discussed data gained from standard lap shear tests does not provide adequate design data due to the non-uniform shear stress distribution along the bonds overlap length resulting from the lack of adherend stiffness in such tests. To reduce such factors values may

be gained via the ‘thick adherend test’ (ASTM D 3983-81) which assumes the thick, stiff adherends should result in uniform and accurate shear stress/strain values across the entire overlap up to ultimate failure [151]. Some issues may however remain including deformation of the adherends [149]. To overcome this an accurate extensometer (KGR-1) and method was developed by Krieger which accurately determines the bond-line shear in thick adherend tests and includes a correction factor used to account for any deformation. The three points used to define the curve are the linear limit (LL), knee (KN) and ultimate load/ strength (UL). When using FEA bulk tensile stiffness values are used.

4.7 Bolted Structure

Although this research focuses on SHM enabled design of bonded structure initial comparisons were made to mechanically fastened (bolted) joints of similar configuration designed to a comparable load bearing capacity.

4.7.1 Bolted Joint Design Guidelines

Five ‘rules-of-thumb’ when designing bolted composite joints are recommended by Kassapoglou [89]. These are summarised below. Similar guidelines are also included in the MIL 17 Composite Materials Handbook, Volume 3’ [135,135]. Further recommendations are presented in [23] and [173].

- *Fastener rule 1.* To minimise fastener bending maintain a skin-thickness/fastener diameter ratio <1/3.
- *Fastener rule 2 (countersunk fasteners).* To avoid the fastener pulling through the skin during out of phase loading maintain a skin-thickness/to countersunk depth >2/3.
- *Fastener rule 3.* To improve load transfer around fasteners in bolted joints ensure a minimum of 40% of fibres are orientated at ±45° relative to the applied axial load. Similar considerations are presented by Hart-Smith (section 4.7.4, Figure 32).
- Fastener rule 4. To avoid loading interactions and increased stress concentrations, fasteners should be spaced at least 4-5 times the fastener diameter apart. This guideline does not however account for other considerations such as inter-fastener buckling. Specific requirements of

design may supersede this guideline. Over-spacing however will not maximise the strength of the joint/laminate.

- *Fastener rule 5.* The distance between a fastener and the edge of the part should be at least 2.5 x the fastener diameter + 1.3mm. This should minimise edge effects (at this distance the load distribution approaches that of a fastener in an infinite plate).

4.7.2 Load (on fastener) distributions

Aluminium alloys and other ductile metals have the ability to redistribute stresses through local yielding [14]. If a series of fasteners is used the result is the equal distribution of load experienced by the fasteners (Figure 29). Such yielding cannot occur in CFRPs due to the high stiffness and absence of plastic deformation of the reinforcement fibres. This results in an uneven load distribution. As the unevenly distributed load is higher at the outer fittings this can intensify problems associated with poor bearing strength in these regions. Joint strengths and load distributions on double lap bolted joints were calculated using the model developed by Tate and Rosenfeld [174] in this research aided by the design software CoDA (details presented in the CoDA user's manual [175])

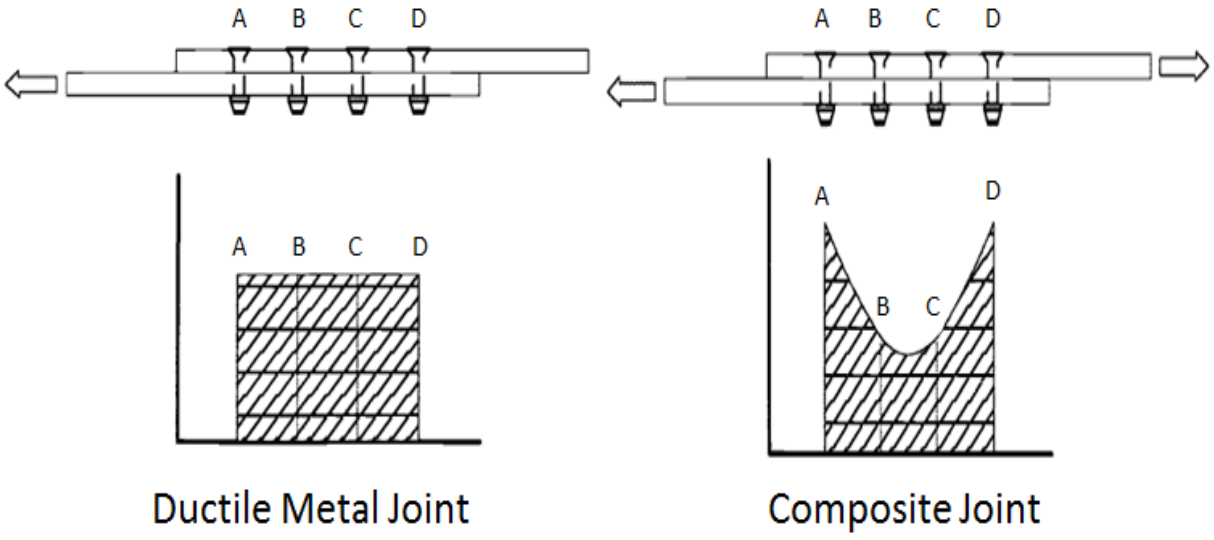

Figure 29: Load distribution behaviour of metallic and composite bolted joints [14]

The above behaviour should be taken into consideration when designing bolted joints. For example, optimal single row joints have only approximately ¾ of the strength of an ideal four row joint due to the higher bearing stress experienced by the

critical outer fasters in the single row joint [135,176]. This effect is compounded if the joint is unbalanced (see section 4.3.2.3) in a manner equivalent to bonded structure. In this case fastener at the more compliant end of the joint will experienced the greatest load, and will as a result become the point of failure at lower joint strengths than for similar balanced joints [14,136]. Well-designed bolted joints can only just exceed half the strength of the un-notched laminate due to stress concentrations [135].

4.7.3 Bolted joint failure modes

Composite bolted joints may fail in a variety of modes as shown in Figure 30 below.

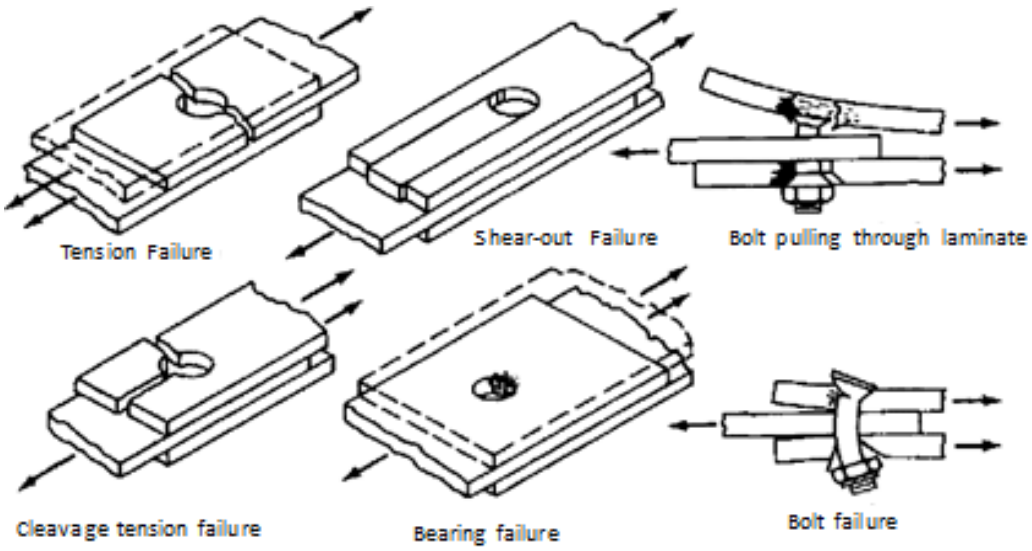

Figure 30: Main failure modes in mechanically fastened composites [137]

Tension failures are often an acceptable failure mode although bearing failure is often preferred due to the slow non-catastrophic nature of this mode [14,137]. Figure 31 illustrates the relationship between strengths of fastened joints in ductile metals, brittle materials and fibre reinforced composites. Bearing failures are identified by the linear regions on the ductile metal and fibrous composite curves. The generalised curve for fibrous composites assumes a laminate suitable for use with mechanical fasteners has been selected. The failure mechanisms for bolted laminated composites are largely dependent on the laminate 'lay-up'; i.e. the orientations of the reinforcing fibres. This is discussed in section 4.7.4.

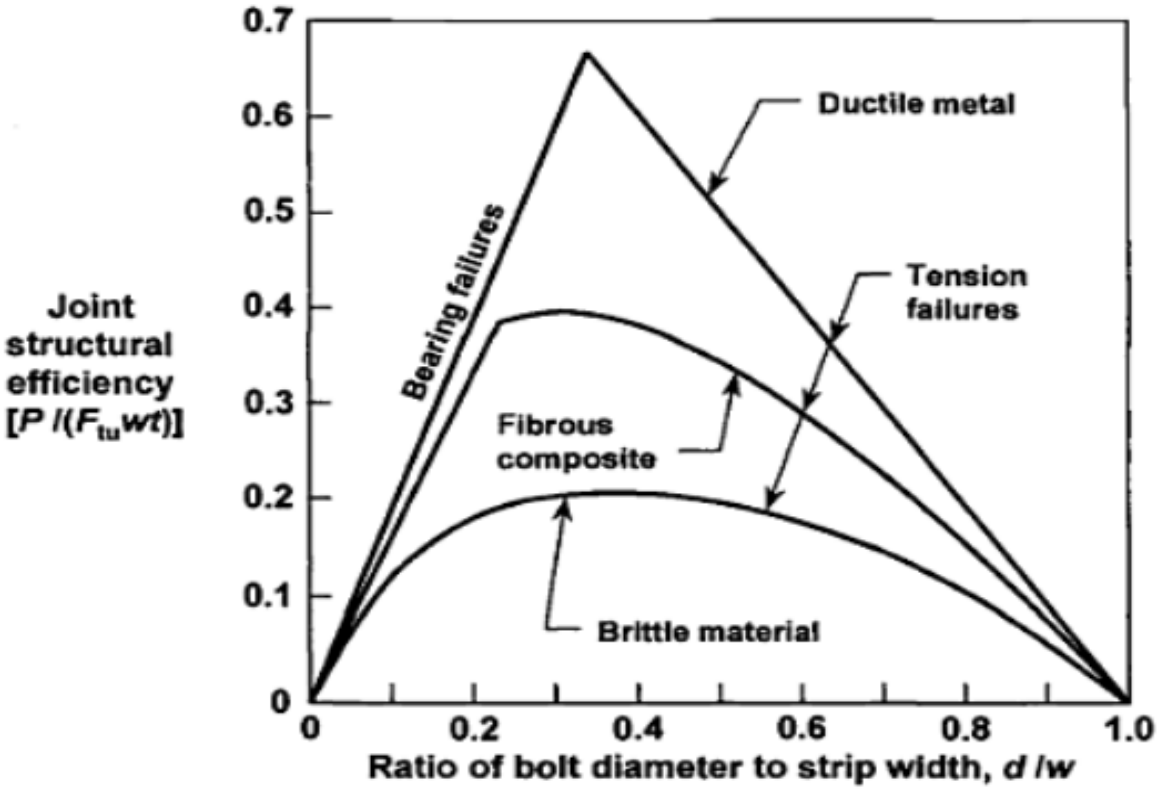

Figure 31: Relative efficiencies of bolted joints in ductile, fibrous composite and brittle materials [38]

4.7.4 Laminate Lay-ups for bolted joints

Composites have relatively low bearing strengths and are notch sensitive under the loading conditions associated with mechanical fasteners (i.e. bearing load). To account for this a variety of ply orientations, usually in the form of a quasi-isotropic laminate, must be used in the region of fasteners. This ensures at least some 0° fibres are available to support the load regardless of load direction [14] as well as assisting the transfer of load around the fastener [89]. As these lay-ups are less efficient at supporting the primary loads than specifically tailored laminates additional plies may be required to provide the required strength. Appropriate lay-up patterns are described by Figure 32.

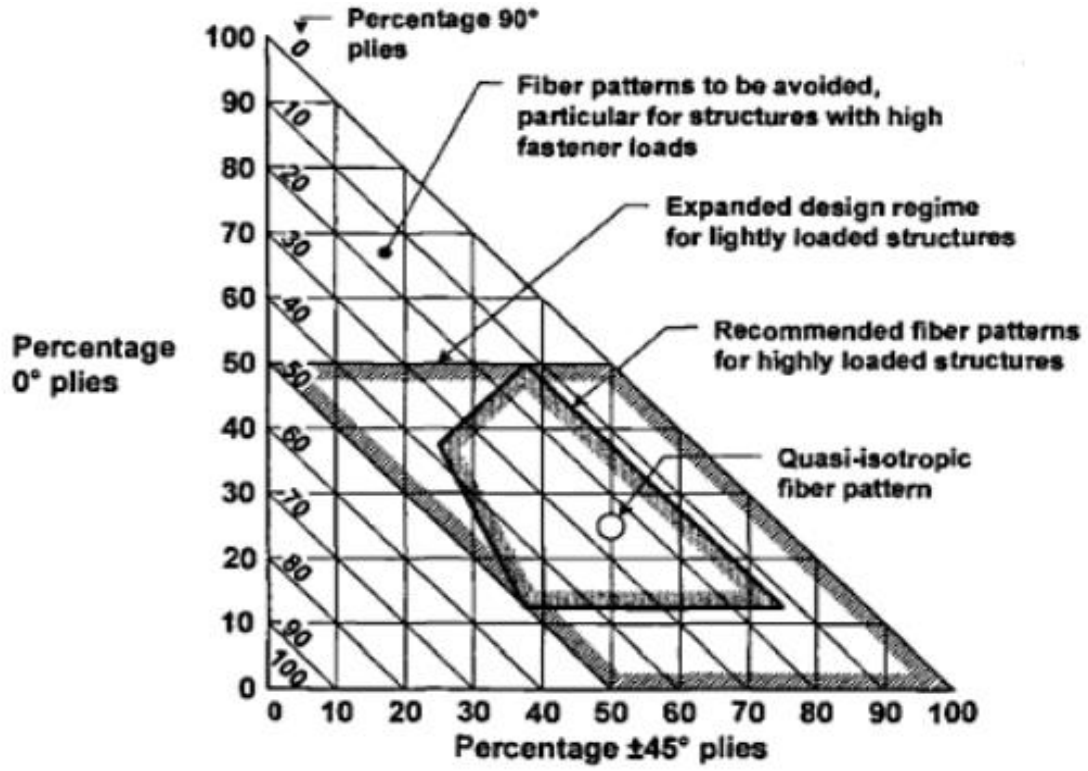

Figure 32: Selection of lay-up for composite laminates and recommendations for their use with mechanical fasteners [176]

4.7.5 Bolted Joints General

Mechanical fasteners may be used at the ends of bonded joints to reduce peel stresses. Fasteners may also be utilised as 'jigging aids' to assist component alignment or to apply pressure to adhesively bonded joints during manufacture, however their inclusion will always increase both weight and complexity as well as introducing potential sites for moisture ingress. As composite bonded joints are by an order of magnitude stiffer than bolted joints [136,141] each is independent and the bolt will only take the load once the adhesive has failed. As such each must be designed to be capable of independently supporting the appropriate load, i.e. DUL for the adhesive and DLL or DUL dependent on requirements for the fail-safe fastener. Such considerations, e.g. resulting increases in laminate thickness, may be detrimental to the primary adhesive bond.

4.8 Section Summary/Discussion

Well designed and manufactured joints should be stronger than the structure outside the joint overlap. If this could be guaranteed there would be no requirement for either SHM or the inclusion of fail-safe features such as mechanical fasteners. Such measures are however required due to uncertainties associated with manufacturing defects or in service degradation due to environmental ingress, cyclic loading, and overloading or discrete damage events. Within this work sample designs and fabrication processes are however used which ensure failure occurs within the joint boundaries as is the case for potentially problematic bonded structure. This not only simulates problematic structure but also to ensures the scrutinised feature is tested.

As damage propagation is usually observed to be rapid in continuous bonded structure it is necessary to engineer a SHM enabled joint in such a fashion to ensure growth is either truly slow or 'quasi-slow' as a result of damage arresting features so in the event of damage positive and timely identification can be made allowing appropriate actions to be undertaken. An SHM enabled joint however should not be designed to simply fail progressively over the structures life-span but to ensure airworthiness by eliminating any uncertainty just as contemporary joints which contain additional fasteners are not produced so the adhesive will fail. Bonded joints are stiffer by an order of magnitude compared to fasteners [136,141] and therefore if used together each works independently, the bolted joint only coming into play as a result of adhesive failure. Fasteners are in part actually used due to being easier to visually inspect than the adhesive bond-lines. SHM enabled joint design may therefore perform a similar role with the exclusion of detrimental features associated with fasteners.

Closed form or continuum mechanics approaches of determining the stress/strain distributions are limited to the 'basic-standard' joint configurations for which they were formed. They also only present a generalised impression of the experienced load distributions and are further limited by simplifications included to make them suitable as preliminary design aids. They can, however, be used as a 'sanity check' when using more general numeric approaches (FEA). More importantly by analysing the responses they provide - as has been the approach of Hart-Smith - the general

‘character’ of each design can be understood, and as such requirements as well as behaviour in response to damage hypothesised. By using such insight designs can be proposed and investigated using FEA prior to physical testing.

Many of the design considerations examined consider the stress, or more precisely the strain, experienced within the joint. Designing considering strain is a standard approach when designing composite structured in general due to the significantly different stiffness properties within the components of composite laminates. This, as well as strain monitoring being a good potential candidate for structural monitoring, would assist when simultaneously designing a complete composite structural system which includes SHM. Experimental work and appropriate analysis of composite joints used to consider such an approach within this research are discussed in the next chapter.

5 Experimental Methodology

5.1 Section Introduction

As previously identified in Chapter 4, section 4.3.1.4 an in-situ monitoring approach which considers strain responses would be ideally suited to complement common methods of composite structure and joint design which also consider strain. The commonality of these approaches would aid the simultaneous design of both the structure, including the necessary structural response in the presence of disbonds, as well as the associated sensing array used to identify said damage. Strain monitoring has been used within proposed structural monitoring systems by identifying changes in the load path (see Chapter 2, section 2.3.3). Although able to monitor disbonds in controlled fatigue cases this capability is not able to be utilised in actual structure due to the rapid catastrophic failure which follows damage initiation in realistic load cases (see Chapter 3; section 3.2.1 & Chapter 4, section 4.2). The considered synergistic approach may be able to address such issues making 'SHM enabled structural joints' a viable alternative to inelegant and inefficient contemporary solutions. This Chapter details the experimental processes – both numeric (FEA) and physical – used. Figure 33 below outlines the general iterative experimental approach used in this investigation.

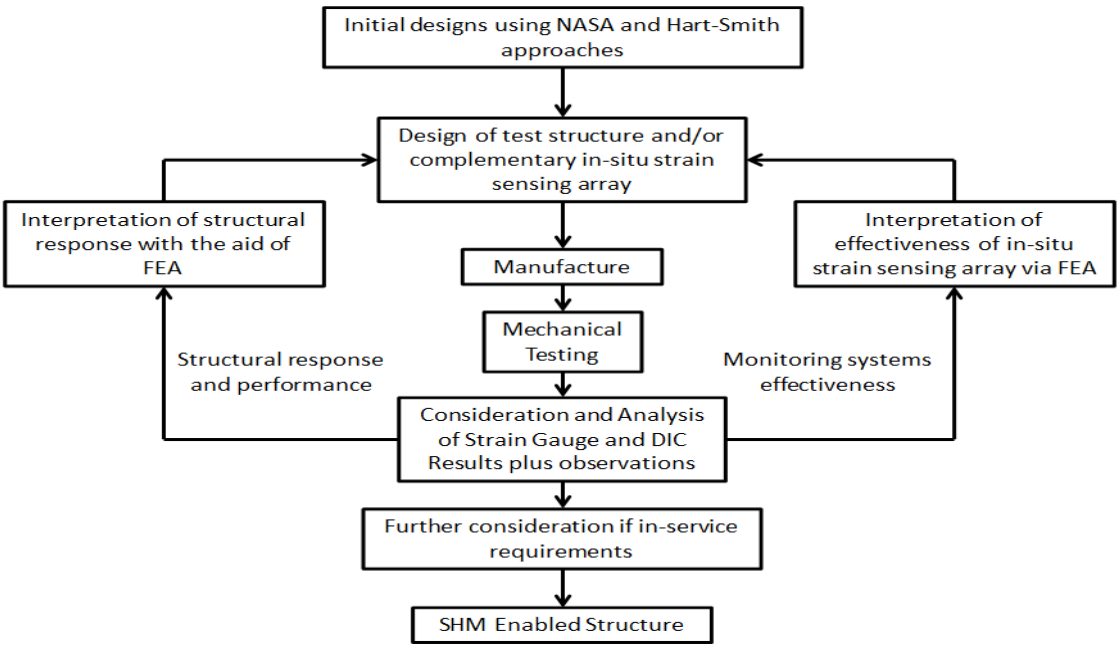

Figure 33: Iterative experimental investigation process

Although this investigation primarily investigated the development of SHM enabled bonded structure comparisons were made against similarly sized and configured bolted joints designed to similar load bearing capacities. Comparisons in performance in terms of variability and reliability of load bearing capacity, as well as failure modes could therefore be assessed.

5.2 Test Structure Design, Analysis and Modelling

A summary or the methods used to design and size preliminary tests as well as material properties used in these procedures are included below. The general approach to FEA used with both these initial tests and further designs is also discussed. Structural dimensions, experimental results and post testing analysis specific design iterations are included in subsequent relevant chapters.

5.2.1 Selection of general joint geometry: Double strap configuration.

Test specimens were designed and fabricated in the form of double strap joints. This configuration was used for initial contemporary type joint designs (both bonded and bolted) due to its relative ease of design and manufacture. Such designs are less prone to multiple failure modes such as peel compared to more simple single lap joints and therefore offer more desirable characteristic for use in service and are easier to analyse. Often in-service bonds which appear to be in the form of a single lap joint are located within the structure so any rotation producing additional peel loads is constrained. In such cases this structure may therefore be considered as one half of a double strap joint.

Adaption of the joint geometry to enable appropriate behaviour in the onset and presence of damage is also based on the double strap configuration due to the advantages stated above. Future developments based on this thesis may consider more complex bonded joint configurations (e.g. scarf or stepped-lap) for potential use joining thicker adherends.

5.2.2 Design and properties of laminate used in test specimens

To allow initial comparisons between standard adhesively bonded double lap/strap joints and comparative bolted structure within initial tests identical adherends were

used for both joint types. To aid manufacture identical laminates were also used for the inner and outer joint adherends (plates and straps respectively). As a result the joints were unbalanced (see section 4.3.2.3). Although weaker than balanced joints analysis can still be performed and the location of damage initiation can be predicted. To allow the laminate to be used with bolted structure a quasi-isotropic layup was selected (see Chapter 4: Figure 32). Bonded designs containing no fasteners may exploit more specifically tailored fibre directed layups resulting in fewer plies for similar performance therefore reducing both weight and the influence of peel loads. $\pm$45° plies are commonly used on the outer surfaces of aerospace laminate as plies orientated in this manner are more resilient to impact events (fibres subjected to lower levels of stress-strain than those directly aligned with the principle load). Although this orientation is well suited to bonding, laminates were initially selected with outer plies orientated at 0° to the load, therefore presenting the best surface for adhesive/adherend shear load transfer [23].

Joint plates and straps were fabricated from T800 (Carbon fibre) / M21 (Epoxy) 'pre-preg'. The following layup was used (angles relative to the joint loading direction). This produced quasi-isotropic, balanced, symmetric laminates $\approx$4.2mm thick (16 plies).

[0, 45, 90, -45, 0, 45, 90, -45]s

Laminate elastic properties were initially calculated using the 'cured unidirectional pre-preg properties' (M21/35%/268/T800s) quoted in the Hexcel HexPly® product data sheet for a single ply [177]. Laminate analysis (macro-mechanics, principles detailed in [76]) was used to determine the properties of the complete laminate based on the ply properties quoted aided by the composite design analysis software CoDA. The in-plane modulus and shear modulus values were initially calculated as 64.29 and 24.45GPa respectively. Tensile tests were performed to determine the manufactured laminates actual tensile elastic modulus using the test rig detailed in section 5.4.1 and strain gauges as detailed in section 5.4.2 using recorded loads and strain and the tensile modulus was calculated (E = Force / (Cross-section area x Strain)) revealing an actual tensile modulus of 52.0GPa. To compensate for this disparity individual ply tensile modulus values were reduced from those quoted and

laminate analysis (again aided by CoDA) was repeated until the calculated modulus values of the entire laminate matched that calculated from the tests described. The amended laminate properties calculated, as presented in Table 8, were used in further analysis and design of the bonded and bolted designs. 1 = the direction of the material in the applied load, 2 = the transverse direction & 3 = the laminate through thickness direction.

Table 8: Elastic properties of the composite adherends used in design and analysis

E1 (MPa)	E2 (MPa)	E3 (MPa)	v12	v13	v23	G12 (MPa)	G13 (MPa)	G23 (MPa)
52500	52500	8500	0.3146	0.1274	0.1274	20040	3333	3333

When used with FEA these properties produced highly comparable surface strains to those measured by surface mounted strain gauges and DIC during physical tests. Laminate tensile and compressive strengths were also required for the design of the bolted joints (Table 9). These were calculated using the Tsai-Wu criterion. The Tsai-Wu criterion was developed for and commonly used for determining the strength of antistrophic composite materials which in addition may exhibit different tensile and compressive strengths. The criterion can be tailored to account for various material symmetries and multi axial stresses. Extended details of the method can be found in [89,178,179]. The formulation used in the software CoDA is considered suitable for orthotropic laminates (relatively thin structure) subjected to plane stress (through thickness stress components not considered) [175]. Strength values presented in Table 9 therefore represent the strengths in the direction the laminate will be loaded, however due to the quasi-isotropic nature of the laminate these values should be near identical in all in-plane directions.

Table 9: Laminate Strength Properties (Tsai-Wu Criterion)

Tensile Strength	Compressive Strength	Shear Strength
997(MPa)	719 (MPa)	308 (MPa)

5.2.3 Adhesive used and physical properties

Cytec FM® 94 epoxy film adhesive was used due to its relevance as a modern, composites compatible, aerospace adhesive. This contained a 0.25mm polyester carrier which aided material handling and helped define the bond-line thickness. Material properties used for design and analysis were established from both manufactures datasheets and previously published work [180]. Although recognised that operational temperature and environmental conditions must be considered in real structures in this analysis only room temperature dry properties were considered.

5.2.3.1 Data for NASA simplified procedures for designing adhesively bonded composite joints

Adhesive property data used for the simplified NASA was taken directly from the appropriate data sheet. Issues as discussed in Chapter 4 exist when considering adhesive shear strengths quoted in pascals as these values are based on specific test conditions and are highly dependent on joint geometry and adherend properties. Peel strength in terms of pascals was unavailable so an identical ratio between this and the quoted shear strength was used as appeared on the example set within the NASA documentation. These factors highlight the fact this approach is only of use for initial general sizing of bonded joints. Material values used are in Table 10 below.

Table 10: Adhesive properties used with NASA simplified procedures for designing adhesive joints

Shear Modulus G #	Shear Strength #	Normal/Peel Strength ##	Thickness
823 MPa	46.6 MPa	55.6 MPa	0.25mm

Data from Cytec Technical data sheet – FM 94 Adhesive Film, Rev.01 Sept 2015. KGR-1 thick adherend test.

Data from above calculated using the identical ratio between the shear and normal/peel strength given on NASA procedures example to extrapolate normal/peel value from shear property.

5.2.3.2 Data used for elastic-plastic bonded joint strength analysis (Hart-Smith approach)

The data below (Table 11) represents points on the 'real' FM-94 adhesive shear stress-strain curve produced by a Krieger thick adherend test as discussed in Chapter 4, section 4.6. When using the Hart-Smith approach the values are amended to that of a simplified curve (Figure 34 – dotted line), with an equal area under the curves, to establish the ultimate potential joint strength (Table 12). To calculate the performance up to the structural DLL the true values are used (up to the linear limit or knee in the original curve). Hart-Smith approach calculations can be performed in the software CoDA for standard double-strap joints.

Table 11: FM 94 adhesive shear properties established from KGR-1 thick adherend test

Linear Limit (LL)			Knee (KN)		Ultimate Failure (UL)	
τ	γ	G	τ	γ	τ	γ
19.5	0.0237	823	32.0	0.0738	48.2	1.1934

τ = Shear stress (MPa), γ = Shear strain, G = Shear Modulus (MPa). Values at 24℃.

Data from Cytec Technical data sheet – FM 94 Adhesive Film, Rev.01 Sept 2015. KGR-1 thick adherend test.

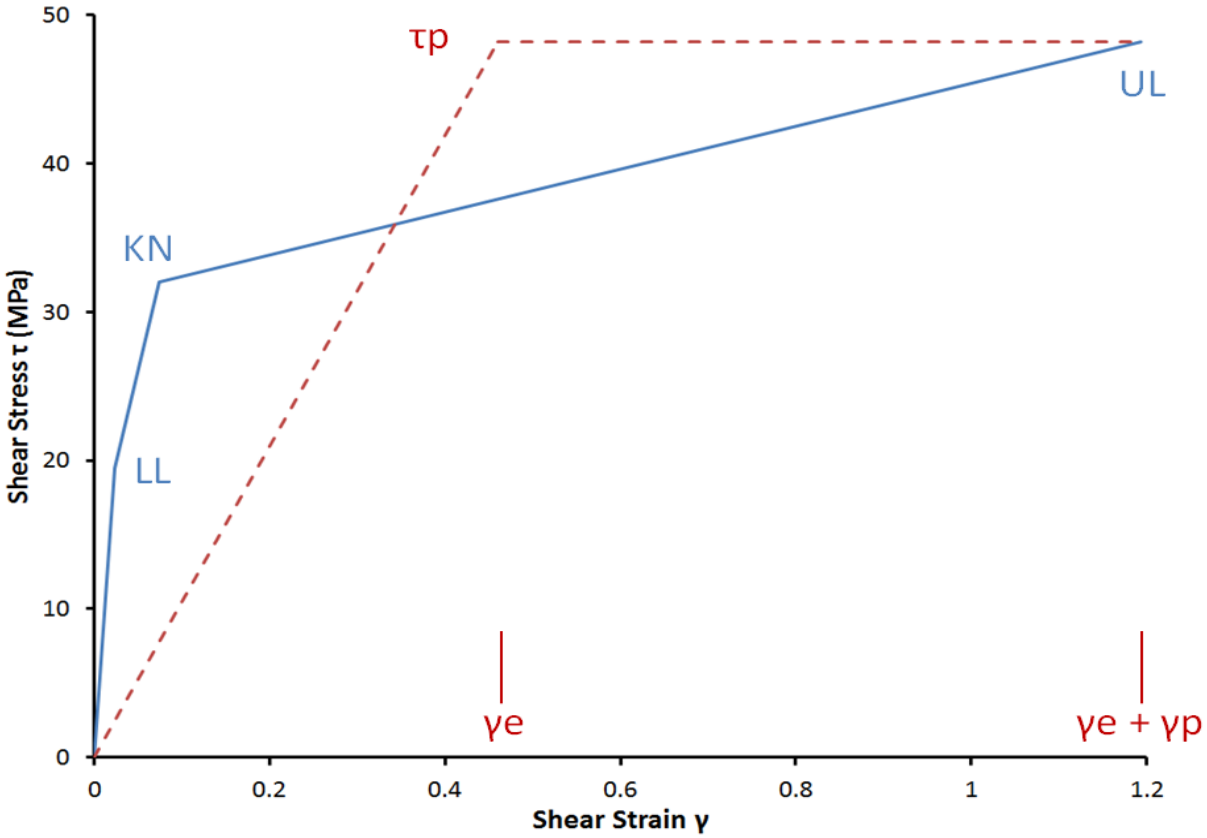

Figure 34: FM-94 Adhesive Shear Stress/Strain curve established by KGR-1 test (Blue) and the equivilent Elastic-Plastic Model (Red)

Table 12: FM 94 adhesive 'Elastic-Plastic Model' shear properties

Plastic Shear stress τp	Elastic Shear strain γe	Plastic Shear strain γp
48.2 MPa	0.461 m/m	0.733 m/m

5.2.3.3 Adhesive data used with Finite Element Analysis

The FM-94 adhesive was modelled as an elastic-plastic material within the FEA package Abaqus. Bulk tensile properties are input, the software calculates the shear characteristic of the material from these values. The engineering stress-strain curve for FM-94 was published within [180] and presented below (Figure 35).

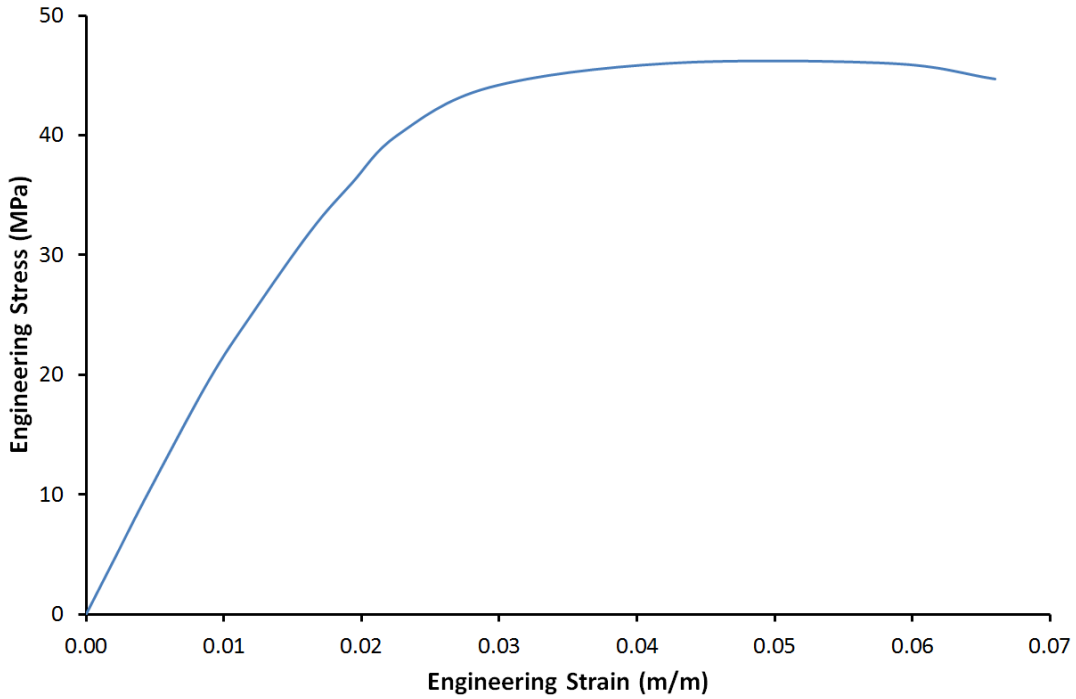

Figure 35: FM-94 (Engineering) Stress-Strain Curve

Abaqus requires the mechanical properties of elastic-plastic isotropic materials to be entered as true stress and true plastic strain [181]. The modulus of elasticity defines the elastic slope prior to plastic strain. The engineering stress is converted to true stress using the following equation.

$$\sigma_{true} = \sigma_{eng}\left(1 + \varepsilon_{eng}\right)$$

Equation 21

The engineering strain is converted to true strain using:

$$\varepsilon_{true} = ln\left(1 + \varepsilon_{eng}\right)$$

Equation 22

The true elastic strain is then subtracted from the true total strain to find the true plastic strain:

$$\varepsilon_{plastic} = \varepsilon_{true} - \frac{\sigma_{true}}{E}$$

Equation 23

Table 13: FM-94 adhesive material property data

Data from Figure 34		Property input data for FEA		
Engineering Stress (MPa)	**Engineering Strain**	**Elastic Properties**	**True Yield Stress (MPa)**	**True Plastic Strain**
0	0.0000	E = 2220 (MPa)	N/A	N/A
5	0.0022	v = 0.33 *	N/A	N/A
10	0.0044		N/A	N/A
19.5	0.0089		19.5	Linear Limit 0
25	0.0120		25.3	0.000533886
32	0.0163		32.5216	0.001521412
36	0.0193		36.6948	0.002589411
40	0.0226		40.904	0.003925946
44	0.0293		45.2892	0.008481483
46	0.0422		47.9412	0.019741972
46	0.0584		48.6864	0.034830817

The Poisson's ratio * of FM-94 is rarely stated in publications and when cited is inconsistent. The value above has been calculated considering the Young's Modulus value above and using the relationship for isotropic materials E = 2G(1+v). As Abaqus uses this to calculate the shear modulus (G) an appropriate value for v (0.33) was selected to ensure G = 823MPa as per the KGR-1 results (Table 11). Parallel FEA tests were performed with a poisson ratio of 0.38 as quoted on an on-line site (resulting in a reduced shear modulus value of 8.4MPa). Although minor differences in magnitude where shear/peel strain values peaked were observed (≤5%) across the bond-line away from such peaks values were very close or identical. Surface strains were indistinguishable.

5.2.4 NASA Simplified preliminary joint design procedures

Initial samples, as investigated in Chapter 6, were sized using NASA's simplified procedures for the preliminary design of composite adhesively bonded [167], and bolted joints [182]. The bolted joint designs also considered the guidelines highlighted in Chapter 4, section 4.7. Joint designs, initially based on equal expected loading capacity and specimen width, were made based on the predicted performance of two rows of 6mm bolts per 25mm width of joint within the selected laminate (Appendix A1). Bonded joints based on the criteria of average shear stress (short overlap – Appendix A2), peek shear stress (medium overlap – Appendix A3) and peel effects (long overlap – Appendix A4) were produced using this simplified approach for initial investigation, comparison and analysis. These procedures use

simple, streamlined calculations to size joints at the most preliminary stage of joint design. This provided a straightforward approach to form and size initial designs. Comparisons were also made with standard preliminary design approaches which consider the 'un-balanced' nature of the joints produced. No considerations of adhesive non-linearity or minimum stresses are considered using this approach.

5.2.5 CoDA – Component and Composite Design Analysis

CoDA is a commercially available software package used for composite laminate analysis as well as preliminary design of composite structures including double lap bonded and bolted joints. This was used as a comparative tool for preliminary joint design as well as acting as a convenient platform for computing the performance of the laminate adherends. Bolted joint analysis (double-strap configuration) is based on the model developed by Tate and Rosenfeld [174] with relevant details presented in the CoDA user's manual [175]. Bonded joint analysis uses Hart-Smiths elastic-plastic model as previously discussed (Chapter 4, section 4.3.2.2).

5.3 Representative Test Structure: FEA – Response to variable loads and damage

5.3.1 Finite Element Analysis

The Finite Element Analysis (FEA) software Abaqus was used to investigate potential non-standard joint designs which could not be produced using analytical design tools. Shear and peel stress and strain distributions within proposed adhesive designs were interrogated in an attempt to modify the failure characteristics of the joint. The same models were used to both to aid surface strain sensor placement (RSGs – section 5.4.2 below) and analyse responses from these sensors as well as global surface strains (section 5.4.3 below) recorded during physical tests.

Two approaches were initially investigated to model the laminates used in the test joints. Due to the nature of laminated composite materials consideration must be made of the potentially different stiffness, shear and poisson effects in each orthogonal direction. The first approach considered the laminates as bulk material but containing different properties dependent on the orthogonal direction within the material. Designated as 'engineering constraints' within Abaqus the material as a

whole was given the properties shown in Laminate elastic properties were initially calculated using the ‘cured unidirectional pre-preg properties’ (M21/35%/268/T800s) quoted in the Hexcel HexPly® product data sheet for a single ply [177]. Laminate analysis (macro-mechanics, principles detailed in [76]) was used to determine the properties of the complete laminate based on the ply properties quoted aided by the composite design analysis software CoDA. The in-plane modulus and shear modulus values were initially calculated as 64.29 and 24.45GPa respectively. Tensile tests were performed to determine the manufactured laminates actual tensile elastic modulus using the test rig detailed in section 5.4.1 and strain gauges as detailed in section 5.4.2 using recorded loads and strain and the tensile modulus was calculated (E = Force / (Cross-section area x Strain)) revealing an actual tensile modulus of 52.0GPa. To compensate for this disparity individual ply tensile modulus values were reduced from those quoted and laminate analysis (again aided by CoDA) was repeated until the calculated modulus values of the entire laminate matched that calculated from the tests described. The amended laminate properties calculated, as presented in Table 8, were used in further analysis and design of the bonded and bolted designs. 1 = the direction of the material in the applied load, 2 = the transverse direction & 3 = the laminate through thickness direction. This method is relatively simple to implement however this approach may result in minor differences in the laminates flexural stiffness. In laminated composites this property is not only a function of the stiffness and orientation of the plies within the laminate but also of their position within the stacking sequence and therefore distance from the neutral axis. For the laminate used, largely as a result of the placement of 0° plies at the adherends outer surfaces, the actual flexural modulus in the X-direction (i.e. the loading direction) was calculated via laminate analysis (CoDA) to be 68.9GPa. For bulk materials the flexural modulus is usually considered to be equivalent to the tensile modulus. The tensile modulus (in plane) of the laminate was 52.5GPa, as such the material modelled using this engineering-constraints approach will be less stiff in bending than the material used in physical specimens. As an alternative the composite materials were modelled as laminates. To allow all the potential benefits of 3-dimensional analysis to be possible the geometries of each modelled component were partitioned, each partition representing a single

lamina (16 plies in each laminate). Engineering constraint values were calculated for a single uni-directional ply. These properties were applied to each partitioned section in the orientation of the specific lamina in the physical material ensuring the differences in flexural properties were captured by the model.

Figure 36 below compares the two approaches by generating E11 strains on the centreline of the joint strap surface from the outer 'strap-end' (distance = 0) into the overlap. Minor differences are present although comparatively small. A marginal increase in surface strain is present in the laminate model compared to the more convenient to use engineering constraints approach. The compressive region (negative strain) seen close to the strap-end, produced as a result of slight bending of the straps due to bending moments as per Chapter 4; Figure 24, is also less pronounced in the laminate model due to this materials increased resistance to bending. The modelled laminate approach may also be also useful to identify any affects resulting from bend/twist coupling that may be present in most laminates including the lay-up used. The slight differences present appear relatively consistent for joint designs and degrees of damage once initiated. As such, if using an analysis approach such as the 'practical joint failure criterion' approach summarised in Chapter 4; section 4.3.1.2., differences such as these may not significantly affect analyses of the structure.

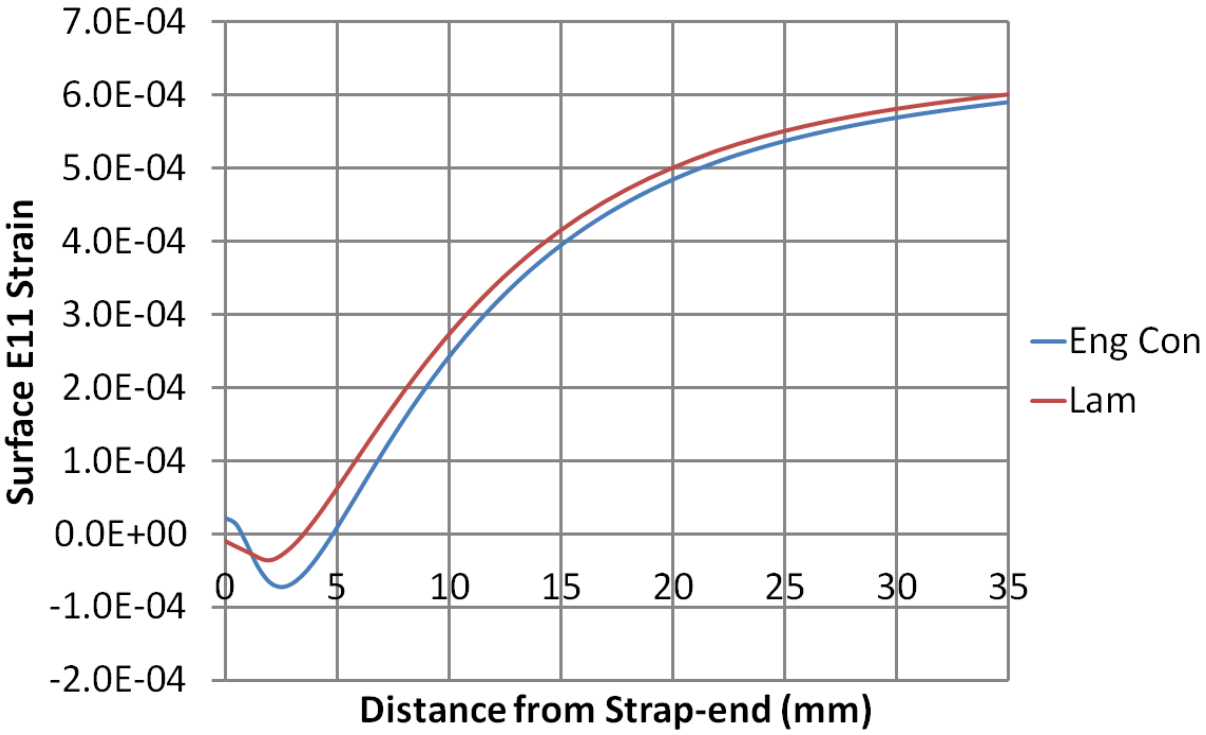

Figure 36: Comparison of FEA predicted E11 surface strains using the 'Engineering Constraints' and 'Laminate' modelling approaches on geometry of the standard bonded double strap 'Peel' design (Chapter 6) subjected to a 10kN load.

The laminate model required greater element numbers to account for both the partitioned structure and the necessity to model the entire joint due to no lines of symmetry due to ply orientations being present. As only marginal benefits in using the laminated approach were identified instead the 'engineering constraints' approach was primarily used with considerations of the above factors taken. This aided modelling and more effectively used available computer resource.

Using the engineering constraints approach, in cases where disbond lengths in each of the double strap joints two bond-lines where considered to be of equal length, only one quarter (symmetry in the horizontal and vertical planes) of the end of each double strap joint being investigated needed to be modelled. If differences in disbond length were considered half of the end of the joint (both bond-lines) under scrutiny needed to be modelled. The omitted end simply performs a convenient means of applying load when physically testing. In FEA the joint end performing this role, as well as any sections 'removed' due to symmetry, were replaced by suitable boundary conditions. A similar approach was recently used by Canal et al [81] in a

study investigating strain distributions within the bond-lines of lap joints using FBGs. Good agreement between measured strains and those presented by FEA were found, as such influence from this work has been adopted.

As per the method adopted by Canal et al, perfect bonding is assumed with no account taken for bond failure. This not only simplifies the modelling process but also allows analysis of the stress and strain distributions over a range of applied loads. As the actual condition and failure criteria of problematic joints are unknown an approach which considers a range of loads is required. Damage is therefore simulated by the removal of appropriate adhesive material from successive FEA models. No account for stress concentrations resulting from sharp crack tips is made due to the large plastic yielding capability of the adhesive. Spew fillets – adhesive that is squeezed from the edge of the bond – which are known to provide a degree of both shear and peel stress relief [150,183] are not included as their effect is lost once damage has initiated and propagates. Like Canal et al C3D20 elements (20 node cubic 3-dimensional elements) are used within Abaqus. Although computationally expensive these are used to retain parity. In addition such element are more able to translate rotation than lower order elements and may therefore provide improved insight into peel affects resulting from adherend bending at the overlap ends. Although analysis of both the bond-line and the strain response to bond-line damage at the surface are primarily investigated along the joints centre-line the use of 3-dimentional elements allows joint designs with structural variation along the overlaps length and stain values at any location, including through thickness, to be analysed. This could not be achieved using 2D FEA.

Unlike Canal's investigation the adhesive in this analysis was modelled using elastic-plastic properties (Table 11) to identify and account for behaviour after plastic yield. Although the mentioned study increased the mesh (and therefore element) density in the region of an embedded optical fibre under investigation within this current study the bond-line is modelled three elements thick the minimum recommended by Penado and Dropek [150]. Mesh density was however tailored in regions containing high stress and strain gradients, i.e. where the bond-line and/or adherend terminated. This ensures peek values are not lost by values being averaged over the element length. The mesh size at these sites and the rate which this evolved to

the global element size remained constant in all models to ensure parity as required by the ‘practical failure criterion’ approach described in Chapter 4, section 4.3.1.2.

5.3.1.1 Mesh size and distribution.

As described in the joint design approach ‘practical failure criterion’ values of FEA determined strain to comparable damage may be made providing the element size remains unchanged between the ‘control model’ and any subsequent FEA designs. As calculated values presented are averaged over the volume of the element more ‘accurate’ values should be produced with smaller element sizes and therefore higher mesh densities, particularly in regions containing high stress-strain gradients. This is particularly important in bonded joints as the regions with the greatest stress-strain gradients are likely to be at the ends of the joint overlaps where disbonds are likely to develop. Decreasing the element size, particularly in 3D models, increases element numbers and to a greater degree the computational time, as such a compromise therefore must be made. In addition element aspect ratios should be kept below 10:1, although < 4:1 is recommended by [150] (Abaqus will allow up to 20:1 but this is not recommended).

Below are four examples of meshes which helped to define the mesh strategy used within this analysis. The model geometry presented (one quarter of physical specimen end of interest) is that of the tapered specimen described in Chapter 7, although the same distribution was used for all simulations presented. As primary analysis considers values along the joints length this dimension influences the change in element size. The number of elements across the modelled joint width is however also quoted. Element size is quoted as the ‘seeding’ sizes used to generate the mesh (which the generated meshes match well) to which elements of the modelled structure are sized. The sizes are quoted without dimensions, however they relates to the units selected to model the geometry which was in mm.

Three load cases were performed for each element test model – 10, 20 & 30kN loading – which relates to states of purely elastic, early onset of plastic deformation at joint ends, and developed plastic deformation of the adhesive bond-line respectfully. Below are various meshing strategies which were considered for use in this study. A model with a high mesh density (model 105) and the recommended

minimum of three elements through the bond-line thickness is initially shown. Other examples with different mesh densities and different numbers of elements through the bond-line are presented for comparison (Figure 37 - Figure 41). Shear and peel strains along the centreline of the adhesive bond are then compared (Figure 42 - Figure 45). Times to solve each model are also presented, both for the calculation of all three load cases as well as for each individual case. Where a minor discrepancy exists between the summation of the individual cases and the total times (8-25 seconds) this is due to the initial start-up of the job submission process. The computer used to perform these simulations used an Intel® Core™ i5-3470 CPU @ 3.20GHz processor (4 cores) with 12GB of ram using a 64 bit operating system. Within the Abaqus software the use of three multiple processors was selected and the multiprocessing mode 'threads' was used. All models presented use the 'taper' geometry considered in Chapter 7.

Model 105 – High density mesh. Control model for comparison

- Element seeding size and strategy
  - Graduated from 0.1 at the strap end to 1 over 70mm. Global size 1. 1.5 at model ends.
  - Total number of elements: 50434
    - 3 elements through adhesive thickness
    - 43 elements across strap width
- Computational time
  - Total: 8 hours 14 minutes 57 seconds
  - 10kN loading: 13 minutes 55 seconds
  - 20kN loading: 26 minutes 35 seconds
  - 30kN loading: 7 hours 34 minutes 1 second

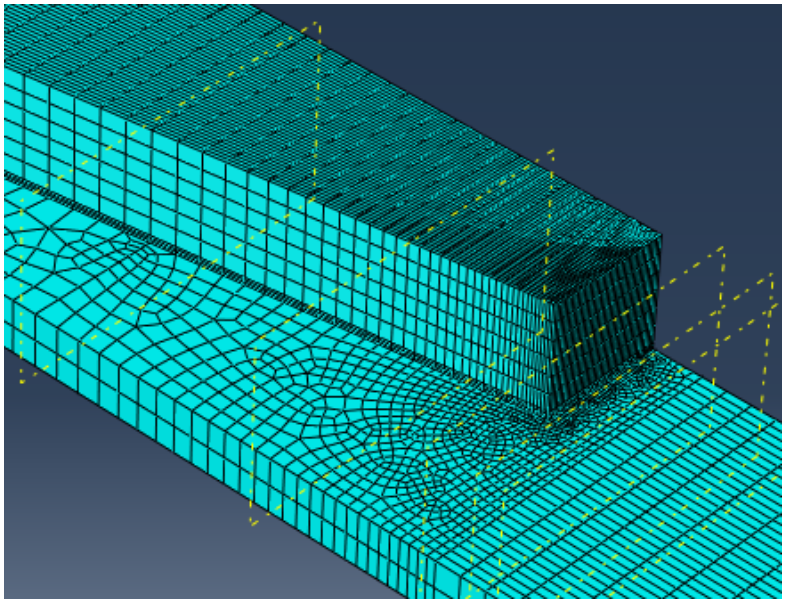

Figure 37: Mesh at strap-end of Model 105 – High density mesh comparison model

Model 63 – Low element density

- Element seeding size and strategy
  - 1 over first 10mm of strap. Remaining global size 1.5
  - Total number of elements: 5869
    - 1 element through adhesive thickness
    - 13 elements across strap width
- Computational time
  - Total: 4 minutes 27 seconds
  - 10kN loading: 17 seconds
  - 20kN loading: 18 seconds
  - 30kN loading: 3 minutes 55 seconds

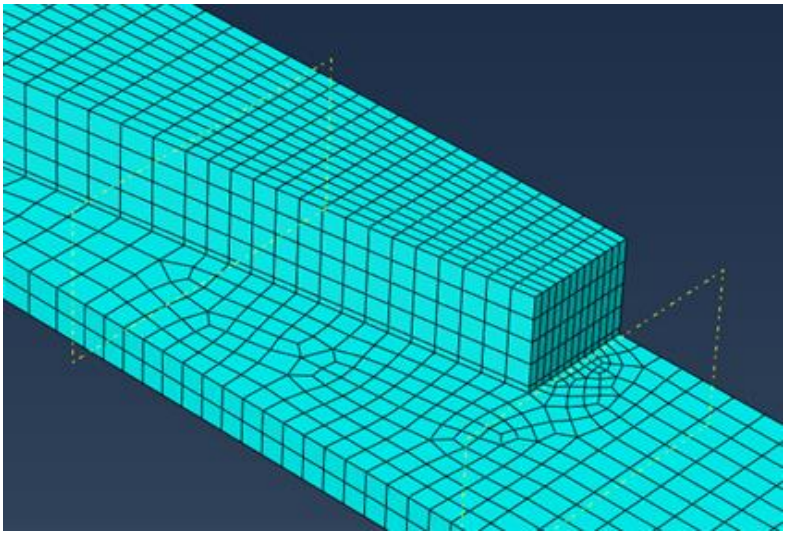

Figure 38: Mesh at strap-end of Model 63 – Simplistic low mesh density model

Model 63B – Low/medium element density

- Element seeding size and strategy
  - Graduated from 0.5 at the strap end to 1.5 over 10mm. Remaining global size 1.5
  - Total number of elements: 9889
    - 2 elements through adhesive thickness
    - 13 elements across strap width
- Computational time
  - Total: 9 minutes 51 seconds
  - 10kN loading: 33 seconds
  - 20kN loading: 38 seconds
  - 30kN loading: 8 minutes 30 seconds

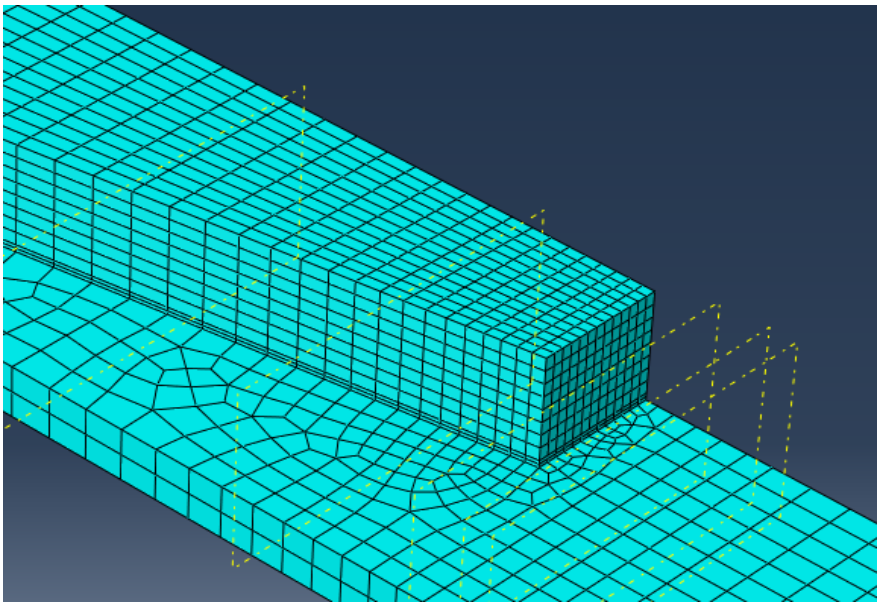

Figure 39: Mesh at strap-end of Model 63B – Low/medium mesh density model

Model 63C –Medium element density

- Element seeding size and strategy
  - Graduated from 0.2 at the strap end to 1.5 over 10mm. Remaining global size 1.5
  - Total number of elements: 12293
    - 2 elements through adhesive thickness
    - 15 elements across strap width
- Computational time
  - Total: 12 minutes 38 seconds
  - 10kN loading: 44 seconds
  - 20kN loading: 52 seconds
  - 30kN loading 10 minutes 50 seconds

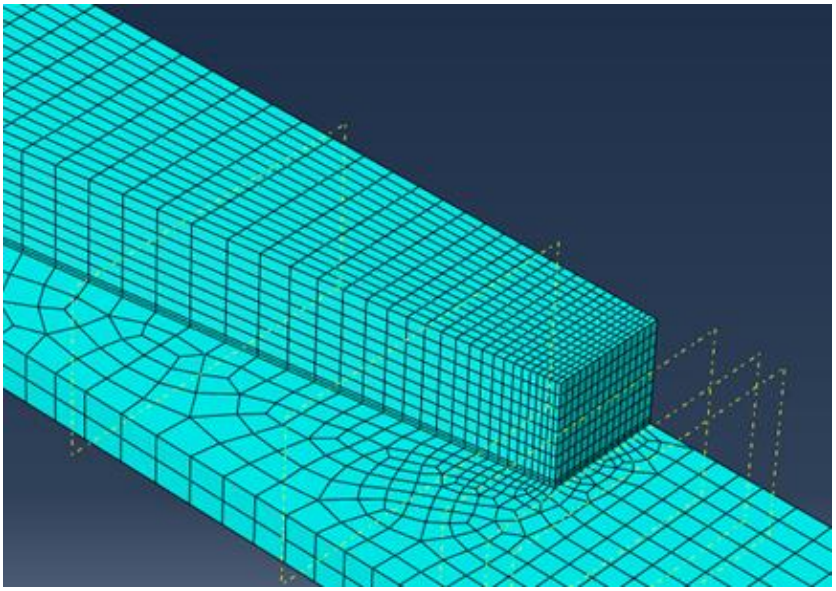

Figure 40: Mesh at strap-end of Model 63C – Medium mesh density model

Model 63D –Medium/high element density

- Element seeding size and strategy
  - Graduated from 0.1 at the strap end to 1 over 10mm. Global size 1. 1.5 at model ends.
  - Total number of elements: 19526
    - 3 elements through adhesive thickness
    - 17 elements across strap width
- Computational time
  - Total: 25 minutes 31 seconds
  - 10kN loading: 1 minute 19 seconds
  - 20kN loading: 2 minutes 15 seconds
  - 30kN loading: 21 minutes 42 seconds

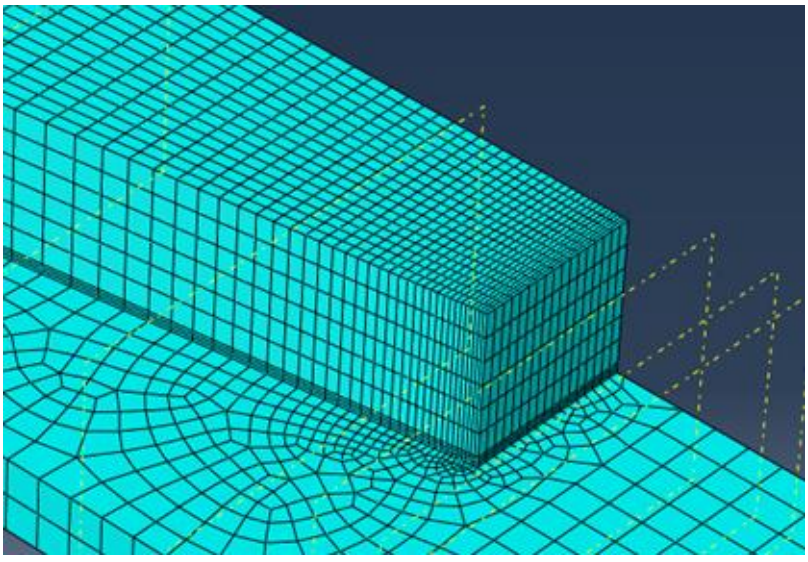

Figure 41: Mesh at strap-end of Model 63D – Medium/high mesh density model

To assess the mesh quality against the high density ‘model 105’ comparisons of calculated shear and peel strains along the bond-line mid-plane centreline of the 70mm overlap where made, these factors being likely to form the basis of later analysis. Figure 42 & Figure 43 show close agreement over the majority of the bond for each approach for both shear strains and through thickness peel strains.

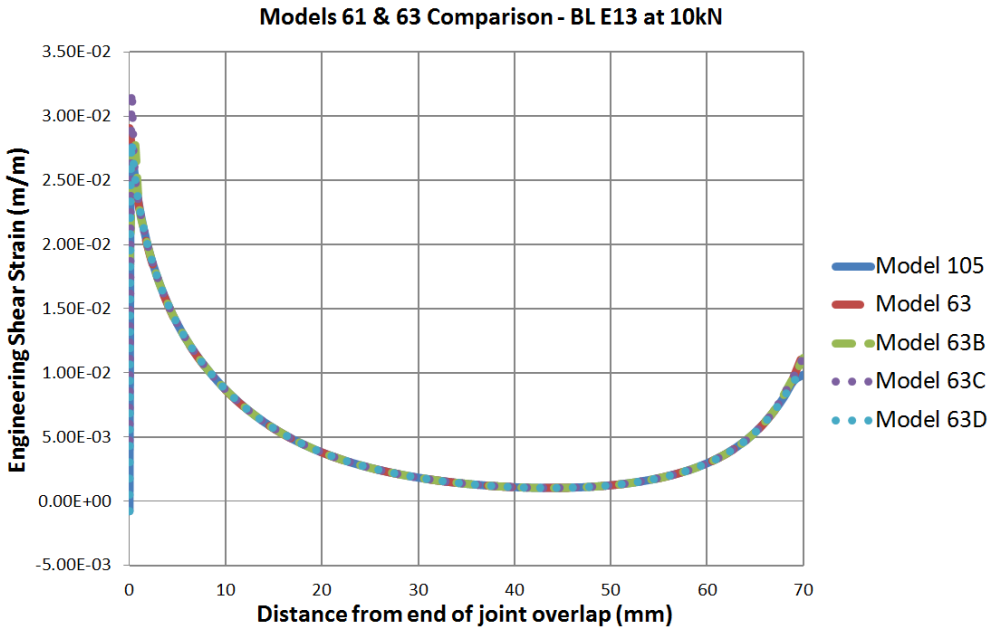

Figure 42: Comparison of FEA shear strains within the adhesive (10kN Loading)

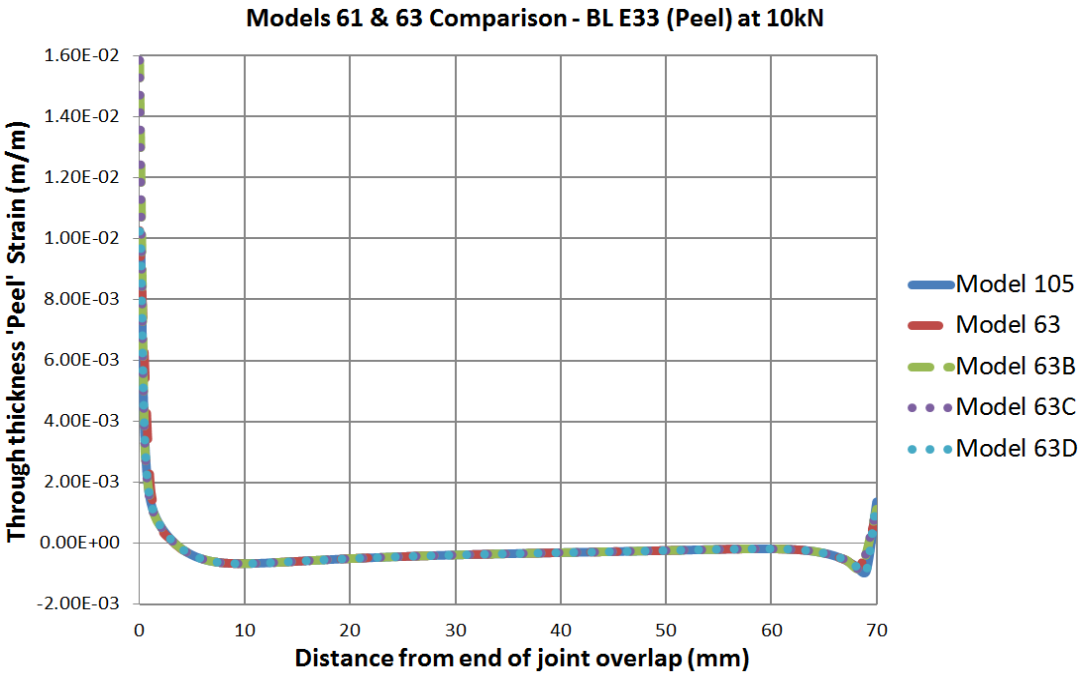

Figure 43: Comparison of FEA 'Peel' strains within the adhesive (10kN Loading)

Some disparity can be seen however at the overlap ends, particularly at the outside end of the strap (marked as distance = 0). This is also the region of greatest strain magnitude and the location likely to initiate a disbond event. As such this is also the region of increased mesh density. Figure 44 & Figure 45 detail this region.

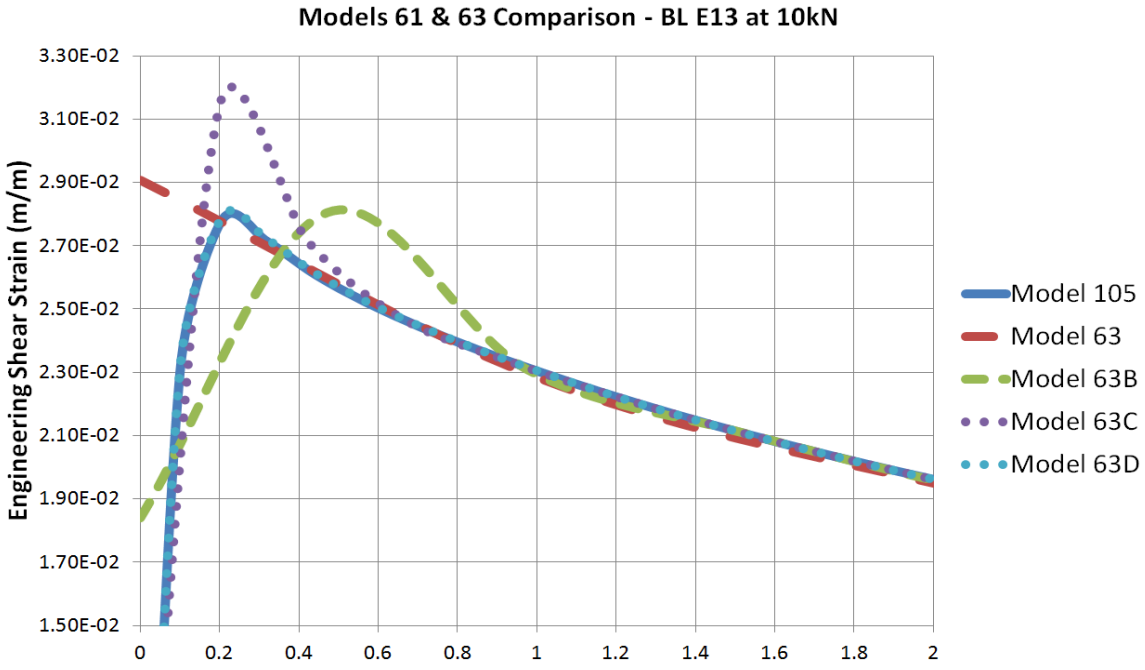

Figure 44: Comparison of FEA shear strains at the overlap end (10kN Loading)

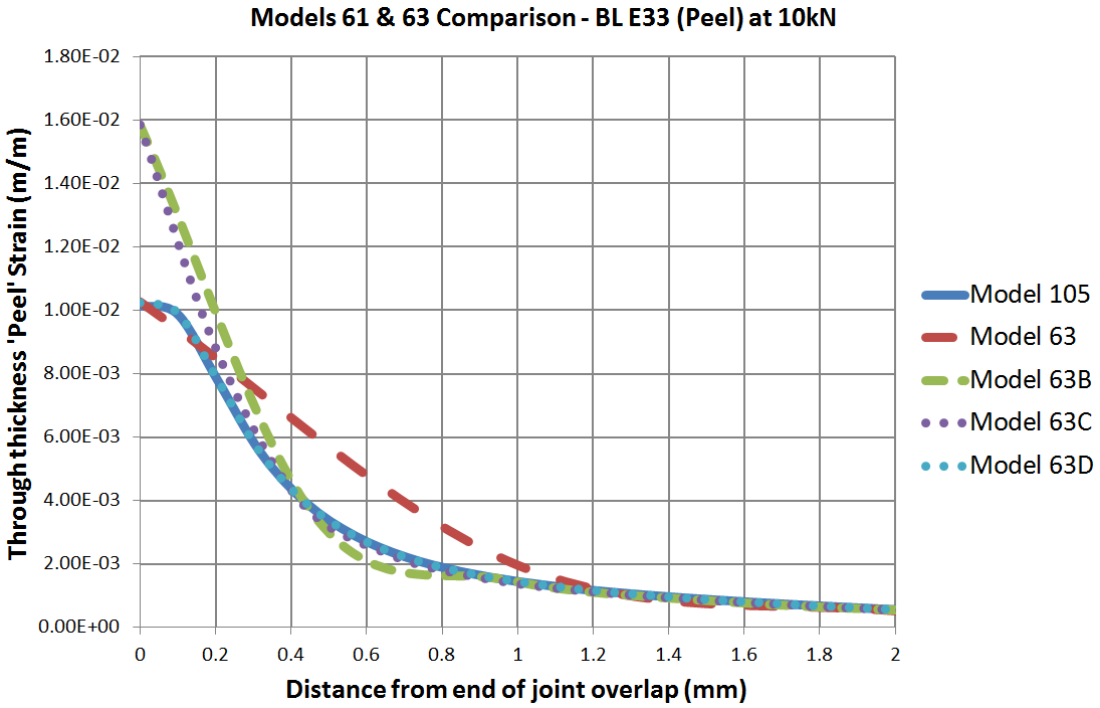

Figure 45: Comparison of FEA 'peel' strains at the overlap end (10kN Loading)

Although significant variation only occurs within the first mm of overlap ‘Model 63D’ almost perfectly matched the results produced by the ‘over defined’ FEA model 105. Unlike the other models these both contained three elements through the thickness of the adhesive (the minimum recommended by Penado and Dopek [150]). As comparisons are made of the adhesive bond-line this is likely to be a significant factor. To ensure the mesh used was effective a further convergence study was performed. The models investigated contained various numbers of elements in total but all included three elements through the bond-line thickness.

As discussed section ‘4.3 Design Approaches and Stress/Strain distributions’, and as part of the ‘practical failure criterion’ method of joint design, the primary feature of interest to determine bond failure is the peek value of shear and/or peel strain. Also of interest is the relative distribution of strains throughout the bond-line to aid the investigation of slow damage growth or arrested damage growth strategies. As seen in the previous study (Figure 37 – Figure 45) the strain values calculated by the different meshes are practically identical over the majority of the overlap length. In the cases of the models with three elements in the bond-line the peak strain values also appear at the same location (<0.01mm difference). The global strain distributions as well as the location of the peak strains calculated in the additional convergence study presented below were seen to fall within these perimeters. As such the variables used and presented in this convergence test were the number of elements in each model (independent variable) and the maximum strain value (dependent variable).

5.3.1.2 FEA mesh convergence study

Models with similar configuration meshes, all with three elements through the bond-line thickness, were produced with various mesh densities. Models produced contain total element numbers ranging from 5168 elements to 50434 elements (model 105 – Figure 37). Maximum shear strain values were plotted against these element numbers to determine which mesh was practically most suitable for use within this research in terms of computational power / time against ‘accuracy’. Values are shown for 10, 20 and 30kN loading scenarios which correspond to purely elastic, transient and developed plastic behaviour of the adhesive towards the strap

end where the maximum shear strain values are present. As element numbers are increased (greater element density) values produced should converge towards a stable value with no further increase in accuracy. As such further increasing the element density provides little or no further benefit at the price of addition computation resource / time. The purpose of the convergence test is therefore to not only ensure the model is stable but to select an efficient meshing strategy

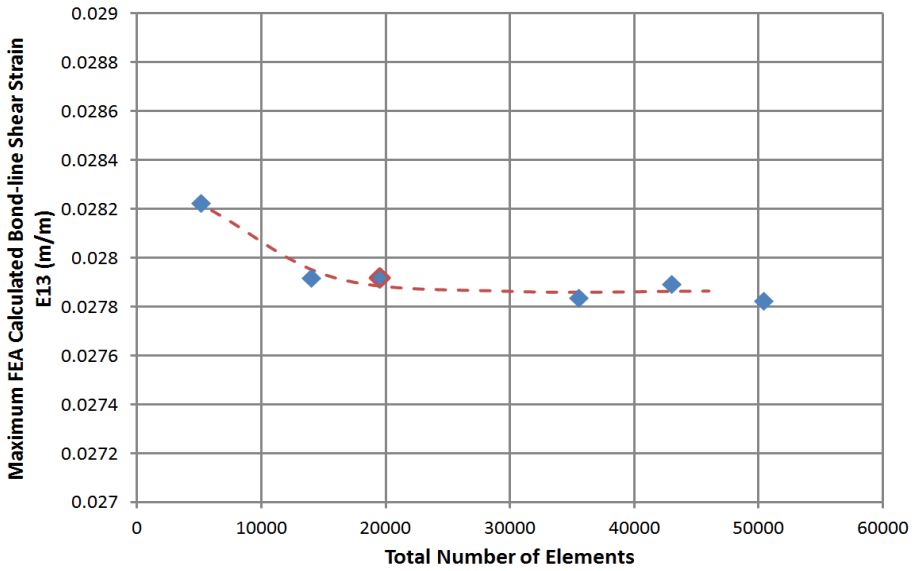

Figure 46: Maximum FEA calculated bond-line shear-strain values Vs total number of elements in each FEA model when subjected to 10kN tensile loading.

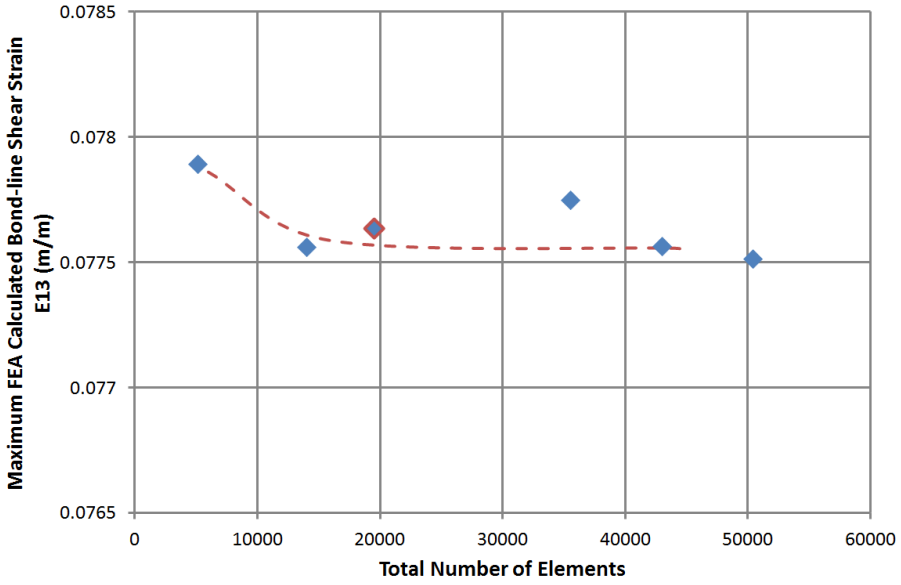

Figure 47: Maximum FEA calculated bond-line shear-strain values Vs total number of elements in each FEA model when subjected to 20kN tensile loading.

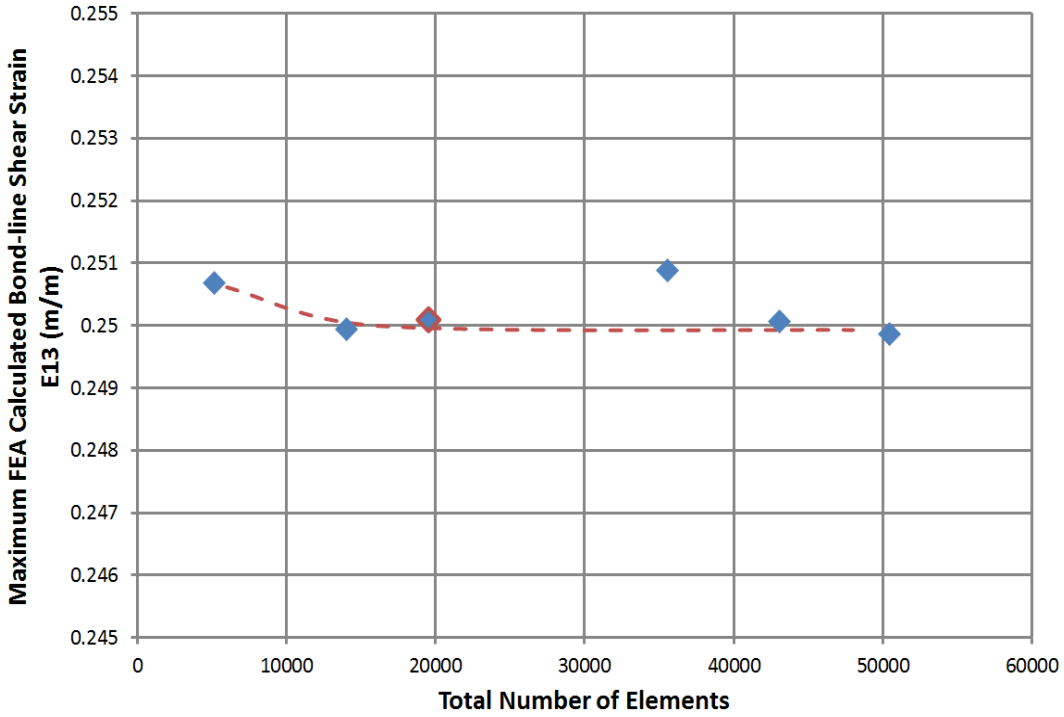

Figure 48: Maximum FEA calculated bond-line shear-strain values Vs total number of elements in each FEA model when subjected to 30kN tensile loading.

Figure 46, Figure 47 & Figure 48 show values rapidly converge (red dotted line) by the time the models contain ≈20000 elements in all three load cases shown. The variation shown from the converged value highlighted by the red line by the models is believed to be due to numerical instabilities common within FEA models at these levels. The greatest difference appears to be in the model containing 35549 elements particularly when subjected to 20 and 30kN loads. The percentage difference between these values and the proposed converged value is <0.4% in both cases, within the range that may be expected of numerical instability and certainly within the variability that may be expected in real bonded structure. Other cases can be seen to show error significantly lower than this value.

From these convergence curves the meshing strategy which contained 19526 elements (model 63D – Figure 41) was selected for use in this research (red bordered marker on Figure 46, Figure 47 & Figure 48). In each load case percentage errors compared to the converged value at 10, 20 and 30kN were 0.19%, 0.11% & 0.07% respectively. This meshing density was therefore chosen as values were near identical to more densely meshed models however solution times were

much lower than for more complex models; see models 105 and 63D details above. Such considerations will be of more reliance for designs containing bond-line partitions (see Chapter 8) where identical increases in mesh density as that used at the strap edge in the study above will be required at all adhesive terminations along the joint overlap edge to satisfy the requirements of the 'practical failure criterion' method of joint design.

5.4 Experimental Tests / Data Acquisition

Below is a brief description of the equipment and methods used to physically analyse the test specimens, - both in ultimate performance and in response to the onset of a disbond - and the capabilities of the strain based monitoring system to identify and monitor potential damage.

5.4.1 Tensile Testing

Test specimens were subjected to tensile loading until failure. Tests were performed using an Instron 6025-5500R test frame. Quasi-static tensile loads were applied to the test specimens via displacement control at a rate of 0.5mm per minute. Loads were recorded with a 100kN load cell.

As identified in Chapter 4 bond-line damage is likely to initiate at the ends of the bond. Due to the unbalanced joint design resulting from using identical laminates for both the joint plates and straps damage initiation is further limited to the bond regions at the outer ends of the joint straps (Chapter 4; section 4.3.2.3).

To minimise the likelihood of damage initiating at the end of the test specimens where surface strain monitoring methods are not primarily focused the straps at the unmonitored end of the joint are additionally clamped, as shown in Figure 51.

5.4.2 Discrete Surface Strain Measurement – Strain Gauge Arrays

RSGs were used to accurately monitor surface strains in locations preselected by analysing FEA predictions, similar to the 'back-face strain technique' discussed in Chapter 2; section 2.3.3. The RSGs not only attempt to monitor the structure as part of testing but represent sensors which may be used in a potential in-situ monitoring system. Some RSGs were located to check and potentially amend adherend

laminate properties previously calculated, such data could then be used in future FEA models. Strains were calculated via a quarter bridge circuit and values recorded by the programmable software LabVIEW. TML BFLA-2-5 gauges were used. These are specifically designed for use with use with carbon composite materials. Each gauge had a relatively short gauge length of 2mm. This allowed strains to be accurately monitored in regions where significant strain gradients were present. RSGs were mounted using cyanoacrylate adhesive with care to ensure the connecting wires were insulated from the semi-conductive carbon. Prior to bonding the surface was sanded, removing the rough epoxy rich surface produced by the textured peel-ply, to reveal a smooth surface suitable for bonding. Gauge locations for each stage of testing are detailed in Chapters 6, 7 and 8.

As the strain gauges were used in conjunction with a ¼ bridge array (two wire connection) no additional strain gauge was used for temperature compensation. The gauges used have a thermal output apparent strain (ε app) equal to the equation below (strain gauge data sheet):

$$\varepsilon \text{ app} = -7.59 \times 10^{1} + 5.11 \times T^{1} - 7.03 \times 10^{-2} \times T^{2} + 2.29 \times 10^{-4} \times T^{3} + 6.28 \times 10^{-9} \times T^{4} \quad (\mu \text{ m/m})$$

Tolerance: ± 0.85 [(μ m/m)/^{o}C], T : Temperature (^{o}C)

Equation 24

The Quasi-static tests performed in this research individually took <30 minutes to perform. As such minimal (< 1^{o}C) temperature variation occurred during each test. Over the course of a year the temperature variation within the laboratory is less than 10^{o}C (within 17 to 27^{o}C). At these extremes the gauges used would provide apparent strain values of -14.3 and 11.5 micro strains restively.

Apparent strain values can also be influenced by the temperature variation experienced by the lead wires on 2 wire systems. The thermal output of the lead wires (εL) can be calculated by the equation below (strain gauge data sheet).

$$\varepsilon L = \frac{r \cdot L \cdot \alpha \cdot \Delta T}{K\,(R + r \cdot L)}$$

Equation 25

Where: ε_L = thermal output of lead wires

r = total resistance per meter of lead wires (Ω/m)

L = length of lead wires (m)

α = temperature of coefficient of resistance of lead wires (copper wire = 3.9×10^{-3} / ^oC)

ΔT = temperature variation

K = gauge factor

R = gauge resistance

The wires used were 1.5m in length with a resistance of 0.34Ω per meter. The RSGs had a gauge factor and resistance of 2.1 and 120Ω respectively. As such in the unlikely event attest was performed over the extrema range of laboratory temperatures proposed ($\Delta T = 10^oC$) the influence of the wires would be 92.4 micro strains (92.4×10^{-6}). Again even including the additional potential apparent strain error introduced by the gauges themselves this error is insignificant compared to the strain values measured (at least one order of magnitude lower and generally 2-3 orders lower than values recorded showing significant damage events – see Chapters 6 - 9). In reality the temperature changes over the course of the tests would be much smaller and there for errors would be significantly reduced from those calculated. For a 1^o temperature change over the course of an individual test the potential error introduced by the wires would be 7.9 micro strains. RSGs readings could also be compared to and validated against the other means of analysing the structure, i.e. digital image correlation (see below) data also gained during testing as well as outputs from FEA simulations, to assess if any drift from resulting from thermal effects or any other influences is present.

RSGs were used within this analysis due to their relative ease of use. These may also find approval for use in actual applications as this technology is already certified for use in aerospace structures. Identical results would however be expected if other surface stain measuring sensors, such as those based on optical fibres which may present additional benefits as discussed in Chapter 2; section 2.3.3.

5.4.3 Global Surface Strain Measurement – Digital Image Correlation

While RSGs monitor surface strains in discrete locations, Digital Image Correlation (DIC) is used to monitor global surface strains and displacements. Details regarding the theoretical basis and application of the DIC method can be found in [184]. DIC monitors randomly distributed visual markers by capturing and recording digital images of the specimen surface. The relative change in displacement between these markers as a result of deformation of the inspected structure can be analysed during post processing and as such surface strains calculated. The surface visual markers within this test are in the form of a speckle pattern a method commonly used in such analysis. This is produced by initially preparing the surface with a thin layer of white primer and then spraying a randomly distributed series of black dots onto this surface. An example of this surface finish can be seen in Figure 51. To enable the entire region of interest of the test specimens to be analysed, and to prevent the DIC speckle pattern being concealed by the surface mounted RSGs and their associated wires, the DIC and RSG systems are used to monitor opposite faces of the test structure.

To perform this examination a Dantec Dynamics DIC system (TU-4XB), as well as post processing software (Istra 4D), was used. Images were captured with two Prosilica EC1600 two megapixel digital cameras. Digital images were captured at a rate of 120 frames per minute. The position of these cameras relative to the test specimen is included on the schematic shown in Figure 49.

5.4.4 Combined System

To allow outputs from the tensile test frame/load cell, in-situ surface mounted strain gauges and the DIC system the three systems were linked allowing loading values measured by the load cell to be recorded by all three systems. During analysis of data the load values recorded by each system were used as a reference to link data with specific damage events. A schematic of the entire test array is shown below in Figure 49.

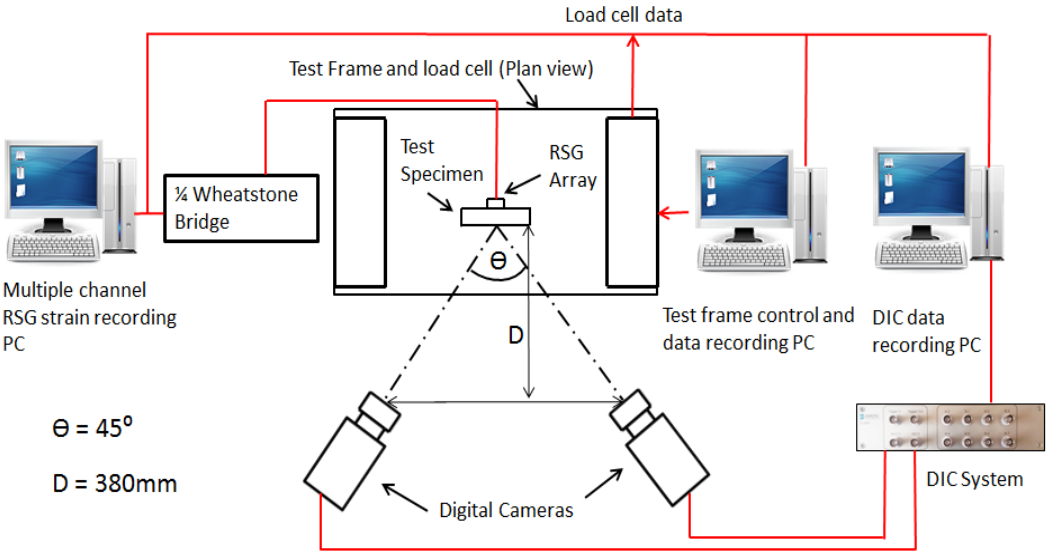

Figure 49: Schematic of the experimental test equipment including digital camera locations relative to test specimen speckled surface.

Figure 50: Load frame and digital cameras used for DIC

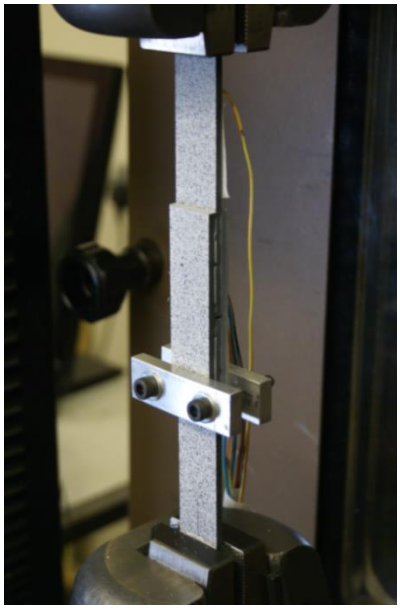

Figure 51: Specimen (standard configuration) located in the test frame

Figure 50 shows the test frame and the digital cameras used to monitor the test specimens surface strains via DIC. Figure 51 shows a test specimen in the load frame. The speckle pattern used by DIC can be seen on the near face. Wires associated with the surface mounted RSGs mounted on the far face can be seen.

The metallic clamp ensures damage initiation does not occur at the unmonitored end of the joint overlap.

5.5 Test specimen manufacture

Test specimens were fabricated to designs detailed in Chapters 6, 7 and 8.

5.5.1 Pre-preg composite laminate

Adherend material was manufactured using T800/M21 carbon fibre epoxy pre-preg with the lay-up and final properties as described in section 5.2.2 above. Laminates were cured using an autoclave as per the manufactures specifications in the M21 resin data sheet [177]. Due to the toughening agents present within the M21 epoxy matrix material the laminates were cut to the required dimensions using abrasive waterjet machining [185]. As previously discussed identical lay-ups were used in all components of all joint designs investigated.

5.5.2 Fabrication of bolted specimens

Joint components used for mechanically fastened test specimens were jigged to ensure accurate positioning of bolt holes. Holes were drilled using a carbide twist drill bit running at 300RPM and an additional layer of material clamped to the back-face to avoid break-out splitting of the laminate. Joint components were joined using Unbrako M6 x 45 socket cap screw bolts with washers either side of the joint. These formed a tight but not interference fit. These bolts provided a structural performance comparable with fasteners used in aerospace applications (stiffness, shear strength etc) and their dimensions ensured no part of the bearing laminate was in contact with the threaded section of bolt. As the preliminary design methods used to size these joints do not consider friction effects resulting from highly torqued fasteners, and as such effects cannot always be guaranteed over time in composite due to wear and creep, fastener were tightened to 5Nm the lowest torque that could be repeated using a small torque wretch.

5.5.3 Fabrication of adhesively bonded specimens

Bonded specimens were assembled within a jig to assure good positioning of each structural component. Peel ply was removed immediately prior to applying the FM-

94 film adhesive. This approach is often used when bonding composites as it has been proposed that a surface free of contaminants and with a good texture for bonding may be produced. Concerns regarding this simple approach are present, particularly when used in critical applications such as aerospace [186-189]. This approach was however used due to its ease of use and consistency. A minor amendment in this process was used in preparation of the tapered-partitioned specimens where an attempt was made to remove resin-rich peeks from the textured surface produced by the peel ply. Further comments on the effects of this are included in Chapter 8. Once assembled the joints were placed within an oven to cure the adhesive at the standard cure cycle (temperature ramp rate = 2°C per minute, held at 121°C for 60minutes) [190]. Pressure was applied to the bond under cure via a 5.86kg steel block placed on the joint overlap.

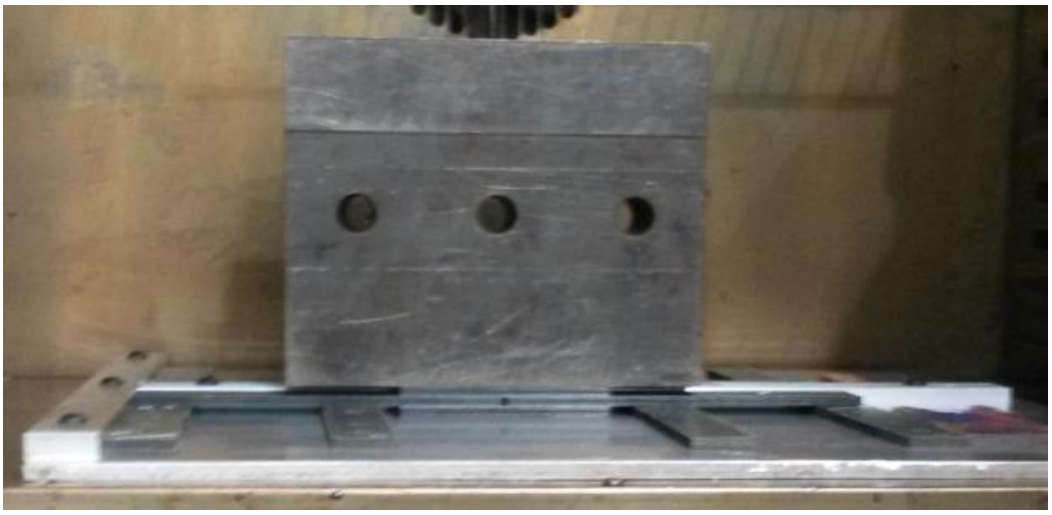

Figure 52: Adhesive joint, located on manufacturing jig and loaded with steel weight within the curing oven.

After fabrication of the joint metallic tabs were adhered at the ends of the joint plates using Araldite 420 paste adhesive. This allowed the specimens to be clamped within the test frame without damaging the laminates in and potentially initiating failure away from the monitored joint. The same procedure was also included on the bolted specimens.

5.6 Section Summary/Discussion

Commonly used composite joint design and analysis approaches have been selected to enable both initial preliminary joint designs to be produced and concepts allowing bonded structure to be enabled by in-situ sensing to be examined. Materials and sensing methods have been chosen which are currently certified for aerospace use. Double-strap configuration joints have been selected as this design eliminates direct load eccentricity resulting in joint twisting. Not only are these effects considered and ideally removed in actual structural design, this configuration allows shear, peel or bearing effects to be more easily analysed than the more complexed mixed modes resulting from apparently simpler single-lap configurations.

The use of discrete in-situ RSGs, global DIC and FEA allow each approach to validate the others. Data gained from these methods can be used to not only develop the structure but consider the structures degradation and appropriate in-situ sensor placement, as would be used in service, in later design iterations.

Physical testing takes the form of quasi-static loading. Although controlled via displacement control (0.5mm/minute) tensile loads will increase until total failure of the joints. Unlike previous studies which have 'grown' disbonds using controlled fatigue cycles this approach ensures any strategy used to retard damage growth can achieve this at elevated loads and provide insight into the structures remaining potential strength once/if damage is identified. This also allows a range of loads to be applied, important as problematic joints are those which are weaker than expected in design and as such their precise condition is unknown. Such designs are also expected to perform well if subjected to fatigue loading.

The next three chapters are dedicated to using the methods above to analyse current standard structure, address the research questions raised in Chapter 3; Research Objectives and develop SHM enable bonded joints which, with their associated benefits, may be incorporated into aerospace structures and legislation.

6 Testing, Results and Analysis: Standard Double Strap Joints

6.1 Section Introduction

Initial tests were made on standard configuration composite joints to better understand joint design, fabrication issues, comparison of bonded joints with variation in over-lap length and to form comparisons against similar sized bolted joints (strength, reliability, weight etc.).

Adhesively bonded and bolted joints, calculated to fail at similar loads were produced using preliminary design methods. 'Double strap' type joints were selected to eliminate load eccentricities. Three lengths of bonded joint overlap were produced and tested based on simplified assumptions of average and maximum shear strains as well as those for peel loads. Comparisons in the actual performance and SHM capability of this variation could therefore be made and further analysis of structural behaviour assessed using more sophisticated methods.

Primary interest focused on defining and measuring bond-line damage as a result of increased quasi-static loading. Concurrent to this the capabilities of the in-situ (RSGs) and non-contact sensing equipment (DIC) were examined. Potential responses measured by these methods associated with damage precursors, disbond initiation and damage propagation were predicted and considered during analysis. Three iterations of RSG configuration were used with the bonded specimens in an attempt to capture such responses. If detectable such measurand and sensor placement may be used in the design of future SHM enabled structure. As damage-tolerance operation requires suitable residual structural strength to be present after damage is identified the presence of any such characteristics are also scrutinised.

6.2 Joint design

Adhesively bonded and mechanically fastened joint designs were initially designed to have comparable strength to allow comparisons in performance and weight. Initial designs were based on the NASA simplified procedures for designing adhesively bonded and bolted joints [167,182] with the addition of common calculations used to account for 'unbalanced' components and stress concentrations. As investigation

indicated bolted joint strength is defined (for selected adherend material and fastener size) by the number and configuration of bolts used (clamp-down forces not considered) this joining approach was initial used to design a representative joint. Bonded joints were then designed using method summarised below with the initial goal of matching the strength of the bolted structures.

6.2.1 Comparative Bolted Joint Design

Bolted joints were initially designed and sized with consideration of available testing facilities, standard and comparable joint geometry and typical aerospace drill sizes. A design featuring two bolts either side of the joint – designed to initially fail due to bearing failure – resulted in a predicted joint strength of 34kN. As no bolt clamp force was considered, and as this can reduce significantly over time due to material wear and creep, bolts were tightened to 5Nm (the lowest repeatable value using a torque wrench) reducing additional performance associated with friction. As discussed in Chapter 4: section 4.7.3-4 considerations in the laminate lay-up must be made to accommodate fasteners and ensure acceptable modes of failure. As such a 'quasi-isotropic', 16 ply, 4.2mm laminate was produced (details including material properties are included in Chapter 5: section 5.2.2). For ease of manufacture the joints plates and straps were constructed from the same laminate, all with identical material orientation.

The bolted joint design was initially based on NASA procedures for multi-bolt composite joints with consideration of the bolted joint design guidelines summarised in Chapter 4: section 4.7.1. It is recognised these procedures may not account for the variation in load transfer for multiple fasteners positioned in a row (as illustrated in Figure 29) and that this effect is enhanced by the 'un-balanced' nature of the joint. The most critical bolt can however be considered individually and a desirable initial failure mode (bearing failure) established. As such a realistic joint comprising of one row containing two bolts was selected as this minimises the load variation whilst still stabilising the joint against minor load eccentricities. 6mm diameter bolts promoted desirable bearing failure in this configuration.

Bolts were selected to ensure no thread was in contact with the laminate bearing surface. Large washers prevented crushing or the bolts potentially being pulled

through the joint straps. The program CoDA (see Chapter 5, section 5.2.5) which does account for load differences across bolts in a row for both balanced and un-balance joints was used as a comparator for both strength and predicted failure mode. Close predictions were made using each approach. Values are presented in Table 14, section 6.6.1. The peel ply was not removed from the joint surface of one specimen presenting a smoother, lower friction surface than that of the specimen with peal ply removed for comparison.

A design/manufacturing drawing for the bolted samples is in Appendix A1.

6.2.2 Bonded Joint Designs

Adhesively bonded joints of equal width, material, general configuration and initially anticipated strength (34kN) to that of the comparative bolted samples were produced. Designs were made using preliminary design methods from a similar source to that used to design the bolted structure (NASA simplified procedures for designing adhesively bonded joints – Chapter 5: section 5.2.4). Joint designs were produced which considered the average and maximum shear stress as well as peel loads using simplistic calculation methods resulting in joints with 15, 45 and 70mm overlaps respectfully. Strengths for these designs were compared to predictions using the Hart-Smith elastic-plastic approach via the software CoDA considering shear strain values at the adhesives linear limit, 'knee' and ultimate load for comparison. Values are presented in Table 15. The general-arrangement of these joints is shown in Figure 53 with the region of measured overlap highlighted. When quoted distances along the joint overlap are taken from the free end of this overlap. Detailed design/manufacturing drawings for the standard bonded joints are in Appendix A2-4.

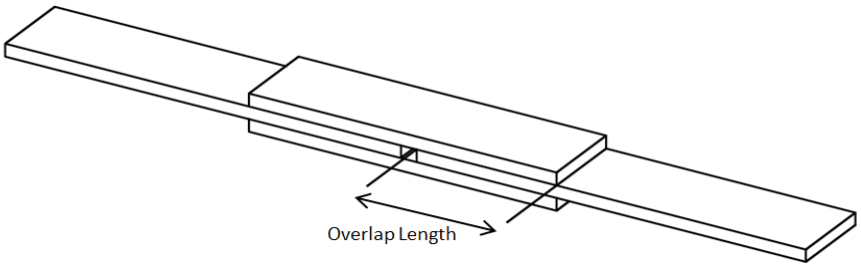

Figure 53: General arrangement of bonded double strap joint

6.3 Recap on damage initiation and probable damage growth

To initially propose strategies to interrogate the structure, particularly in regards to in-situ sensor placement, a recap into the expected behaviour of the structure, the initiation of damage and potential propagation is required. Consideration of such factors when interpreting structural responses may also aid analysis and potential amendments to future designs.

As discussed in Chapter 4: section 4.3.2 adhesive bond-line damage initiates as a result of reaching a critical level of shear strain. The location of the maximum shear strain value can be predicted (via shear stress) by considering Volkersen's and Hart-Smiths, as well as others, analyses. Complementary evaluation can be made via FEA to directly determine adhesive strain and account for non-linear effects resulting from plasticity. As the greatest values are seen at the overlap ends, particularly as the joint structure is unbalanced (Chapter 4, section 4.3.2.3), bond-line damage should initiate in these regions. Furthermore as damage initiates due to crossing the shear strain threshold the bond is effectively removed from this area. The region of peak shear strain therefore moves to the adjacent area of bond, which is effectively the new end of the overlap, and this section of adhesive becomes the site for continued failure. The peak shear strain will therefore track this damage front as per Chapter 4; Figure 27. As a result damage may be expected to start at the strap end and progress inwards until catastrophic failure occurs.

6.4 Surface Strain Predictions

By considering the anticipated behaviour discussed (section 6.3) simplistic FEA simulations using methods discussed in Chapters 5 was used to predict load induced surface strains and their response to various sizes of bond-line damage. Such information guides placement strategies of surface sensors as well as the analysis of the structures response captured from these sensors during physical experiments. DIC was used to produce global surface strain maps directly comparable with the FEA predictions both along the strap centre-line – as per Figure 54 – as well as the entire strap surface. As well as an additional validation method this approach helped to positively link the localised responses of the RSGs to the global predictions of the FEA.

Figure 54 illustrates FEA predictions of surface strains (E11) along the centre-line of the bonded straps of a 'Peel-70mm' sample containing disbonds of various lengths whilst subjected to a static 20kN tensile load. Strains can be seen to rapidly drop to zero (after a potential compressive strain) as the disbond progresses. This response should be identified by an appropriately positioned strain gauge. As per previous studies focusing on fatigue multiple sensors may therefore track damage as it propagates.

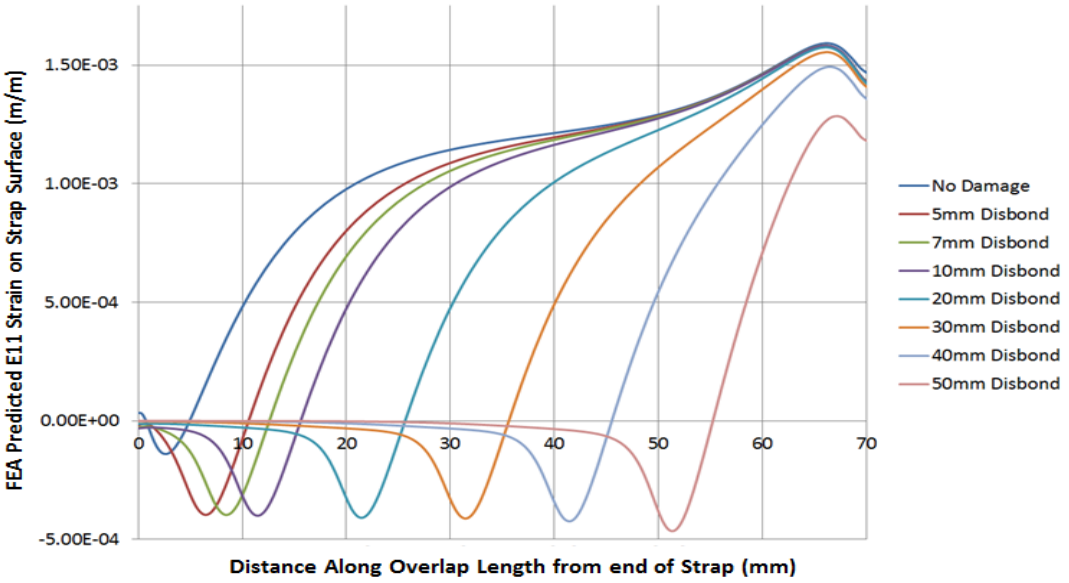

Figure 54: FEA prediction of surface strains on the strap surface centre-line of a 'Peel-70mm' specimen with various sizes of disbond (propagating 'inwards' from distance = 0) when subjected to a constant 20kN tensile load.

The compressive strain features (negative values) present on each strain curve in Figure 54, positioned at approximately the same distance from the over-lap length as the length of the associated disbond, are created by the 'free-end' of the strap bending away from the plate as a result of bending moments produced by the applied load and distance between the plate and strap (see Chapter 4, section 4.3.2.5). When modelled as a laminate (rather than using 'engineering constraints' as shown) the adherends a have a higher flexural-modulus resulting from the ply sequence. Due to this increased bending stiffness lower magnitude values of compressive strain may be presented if this modelling approach is used. As this 'laminate modelling' approach may better represent the bending behaviour the compressive values measured on test samples may be similarly less pronounced.

6.5 Surface Strain Gauge Array

Three general arrangements of surface mounted strain gauges were used during these initial tests. Each was designed in turn with consideration of predicted damage initiation and potential propagation as well as from lessons learned from testing using the previous array. The initial arrangement shown in Figure 55-A was designed to identify regions of interest in surface strain both near the region expected to experience the greatest adhesive shear and peel stress-strain (and therefore the region where damage was expected to initiate) across the full width of both the joint strap and plate. Additional gauges (G1 & G8) were placed away from regions expected to experience high strain gradients. These gauges allow a ready check that overall strain levels are as anticipated and in addition provide reference strain values against which the strain values closer to the bond edge can be compared. The isolated gauge on the joint plate (G1) also allowed the tensile modulus of the material used to construct the joints to be checked ensuring this significant factor was in agreement with values used to model the joints response. RSG arrangements B & C were designed to both identify damage initiation as well as to potentially track the initial disbond growth as this progressed across the initial overlap and therefore track under the staggered RSGs.

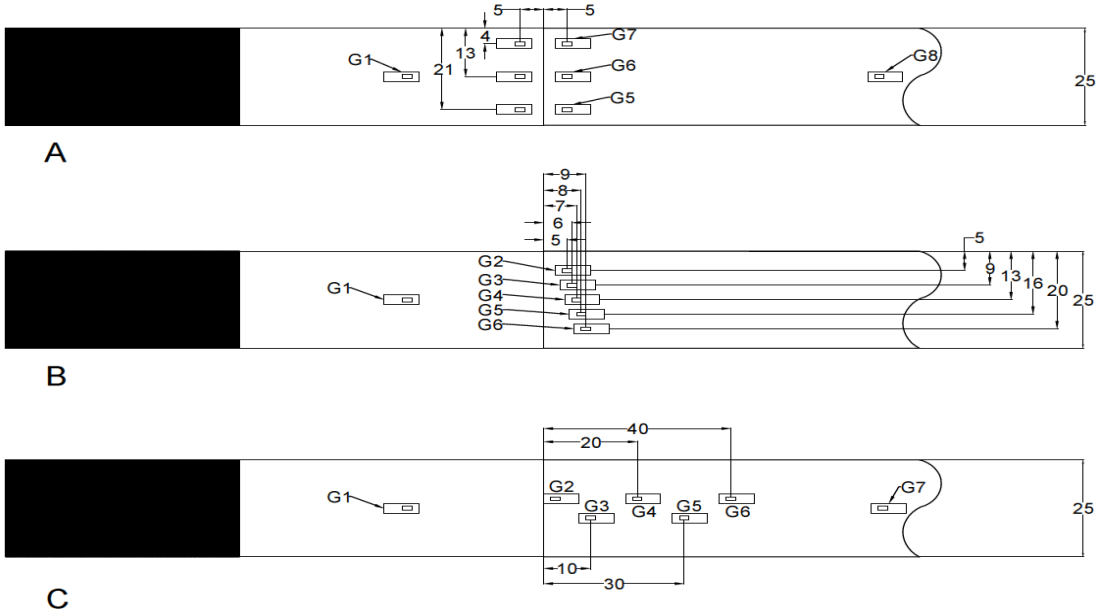

Figure 55: RSG positions used with standard double strap joints

6.6 Testing Results

Results and brief discussions regarding the testing of standard double strap joints are shown in this section. A brief overview of the bolted joint test results is made. The remainder and greater part focuses on the adhesively bonded samples

6.6.1 Bolted Joints

The bolted samples initially designed and tested for comparison in regards to structural mass, performance and reliability are presented in Table 14 below.

Table 14: Comparative Bolted Joints Test Summary

Comparative Bolted Joints	**Sample**	
Test	**Bolt: B1**	**Bolt: B2**
Note: Peel ply not removed from B2 to reduce friction between plates and straps		
Performance	**Value**	
Design strength - (kN): NASA, (Predicted strength: CoDA)	34 (33.3)	34 (33.3)
Predicted Failure mode: CoDA	Bearing of plate, row 1 (outer bolt)	Bearing of plate, row 1 (outer bolt)
Initial failure load (kN) - Observed	34	33
Initial failure mode - Observed	Bearing of plate, row 1 (outer bolt)	Bearing of plate, row 1 (outer bolt)
Ultimate strength (kN) - Observed	48	46
Ultimate failure mode - Observed	Net failure of plate, row 1 (outer bolt)	Net failure of plate, row 1 (outer bolt)

Table 14 reveals in the two cases tested both design approaches produced similar joint strength predictions both of which provided values similar to those observed during testing. The initial failure – bearing – was identified from a defined reduction in the gradient of the load/extension curve during testing validating the modelling approaches at least for these specimens.

6.6.2 Bonded Joints

Table 15 displays the design and predicted strengths of the standard (unbalanced) adhesively bonded joints used in this stage of the analysis. These joint designs, made using the 'NASA simplified procedures for designing adhesively bonded joints [167]', are designated 'Avg' for those based on the average shear stress (15mm overlap), 'Max' for those based on the estimate of the maximum shear stress *

(45mm overlap)., and 'Peel' based on simple calculations of peel loads based on adherend geometry (70mm overlap). Strength predictions made using the Hart-Smith approach, via the software CoDA, are also presented. These include the predicted maximum potential shear strength as well as values that may be considered for DLL based on adhesive limit loads (LL) and 'knee' (KN) shear stress-strain curve values.. Values calculated using the Hart-Smith approach were identical for all geometries tested. All predictions consider only the material properties of the adhesive and adherends and assume perfect bonding. As such only cohesive failure of the bond (or potentially interlaminar/fibre-tear failure of the adherends if peel forces result in failure of the laminated adherends in which the matrix material is weaker than the adhesive) or tensile failure of the structure outside the overlap is considered. Such assessment cannot predict the more problematic 'adhesive-failure' mode as the adhesion strength is not associated with material properties (and is largely affected by manufacturing quality and procedures) and may therefore be unknown.

* As discussed in Chapter 4, section 4.3.2 a more appropriate consideration may be shear strain, however as these simple procedures do not consider non-linear plastic behaviour the magnitudes of each are in parity

Table 15: Bonded sample design strengths (NASA) – with various design criteria – and comparison against the Hart-Smith elastic-plastic approach.

NASA Joint design strength considering:	
Average shear stress (15mm overlap)	34kN
Maximum shear stress (45mm overlap)	34kN
Peel stress (70mm overlap)	34kN
Maximum theoretical bond shear strength (H-S approach)	107.2kN **
Design Limit Load: adhesive shear Linear limit (H-S approach)	7.5kN
Design Limit Load: adhesive shear 'knee' values (H-S approach)	17.1kN

** This strength value is greater than that calculated for the tensile strength of the laminates being joined (104.5kN: Tsai-Wu criterion).

Table 16 summarises the ultimate failure loads of the 'standard' double strap samples and which RSG array was used with each. All samples can be seen to

have failed via ‘adhesive failure’ (also see section 6.6.5: visual inspection), as such the failure strengths are lower than those predicted by either the NASA or Hart-Smith (CoDA) approaches. As previously discussed this failure mode – the result of poor surface preparation and/or manufacturing quality – is the primary form of problematic damage to be found in in-service bonded structure. This is due to potentially significant and undeterminable reductions in strength when compared to the design performance as well as difficulties associated with the identification of such degrading characteristics. The percentage difference between the highest and lowest strength values of the 70mm overlap ‘Peel’ specimens was 47%. This in conjunction with the undesirable ‘adhesive’ failure mode highlights the difficulties in producing good quality, repeatable bonded structure even under laboratory conditions.

Table 16: Standard Bonded Double Strap Test Summary

Specimen Title	Specimen configuration and overlap	RSG Array type	DIC Available	Ultimate Strength (kN)	Failure Mode
Specimen-1	Avg – 15mm	A	X	13.57	Adhesive
Specimen-2	Max – 45mm	A	X	21.84	Adhesive
Specimen-3	Peel – 70mm	A	X	22.53	Adhesive
Specimen-4	Avg – 15mm	B	✓	13.8	Adhesive
Specimen-5	Max – 45mm	B	✓	20.4	Adhesive
Specimen-6	Peel – 70mm	B	✓	32.4	Adhesive
Specimen-7	Peel – 70mm	C	✓	20.87	Adhesive
Specimen-8	Peel – 70mm	C	✓	24.06	Adhesive
Specimen-9	Peel – 70mm	C	✓	22.92	Adhesive

6.6.3 Surface Strain Gauges

Plots of strains recorded by RSGs located on the joint straps which attempt to identify evidence of disbond precursors, initiation and propagation are presented below.

6.6.3.1 RSG Array A – Specimens 2 and 3

RSG array ‘A’ was used to monitor strains on the ‘plate’ near the region of expected damage initiation (G2, 3 & 4 – Figure 55A) and on the ‘strap’ where damage initiation was expected to occur (G5, 6 & 7). Strain gauges also interrogated the plate and

strap positioned in areas expected not to experience high variations in apparent strain or damage initiation (G1 & G8 respectively). In agreement with FEA predictions the gauges positioned away from the strap end, as well as those positioned on the plate, all recorded a linear response up-until the point of joint failure and not included in the main body of this report

Figure 56 shows strain verses load measured by the RSGs nearest the strap edge for specimens 2 and 3. As previously identified this is the region of most interest for detecting indications of damage. Due to initial technical problems with the strain recording equipment RSG data is unavailable for Specimen-1. Surface strains can be seen to increase linearly with increasing load; however a decrease is evident prior to failure, possibly due to disbond initiation or bending of the adherends.

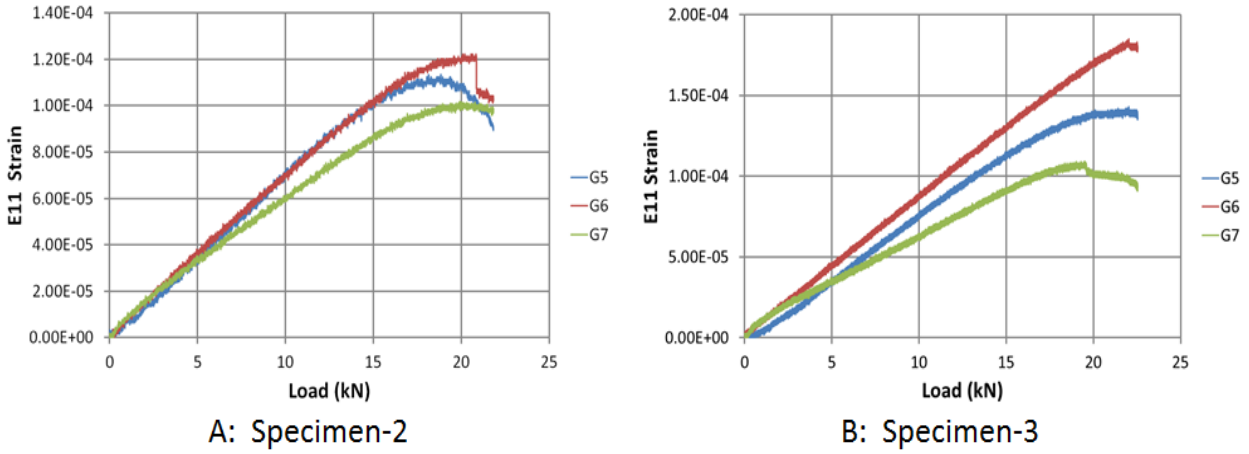

Figure 56: RSG response (Array type A) to increasing tensile load until catastrophic failure.

6.6.3.2 RSG Array B – Specimens 4, 5 and 6

Little useful information appeared to be provided by placing the RSGs on the plate or strap far from where damage should initiate (both from array-A measurements and assessment of FEA). Array type B therefore directly focused on the region at the strap end. The staggered array (Figure 55B) was conceived to both identify and potentially track initial disbond growth or other damage precursors. This array interrogated a region similar to that of array A but extended this marginally further into the joint overlap. As seen in Figure 54 surface strains close to the strap edge are very low. The placement of gauges deeper into the overlap, in this case up to

9mm, puts them at a location which initially experiences not only a greater strain value but as can be seen in Figure 54 where a high gradient in the change of strain over the joint length is present. Therefore in the presence of even a small disbond event these sensors should show a significant reduction in strain.

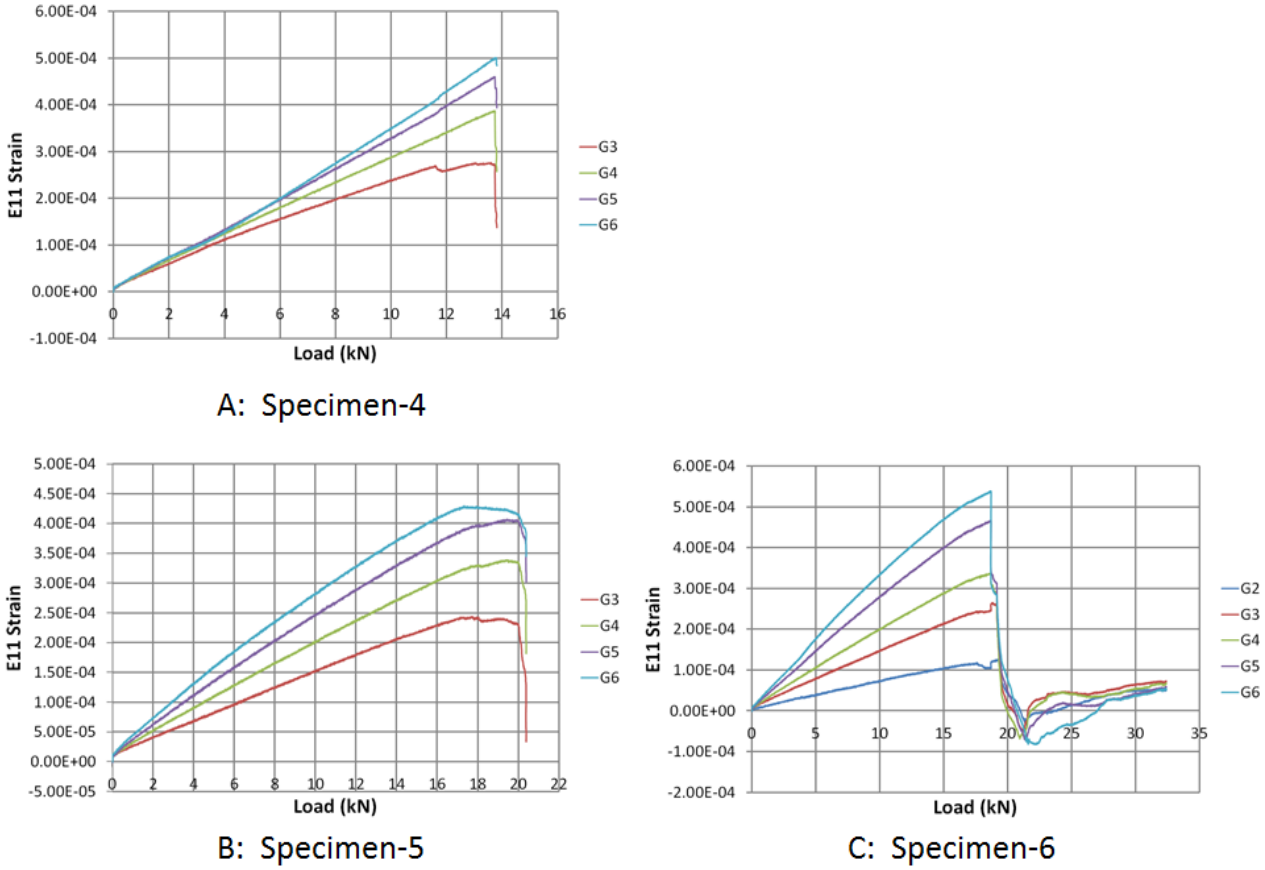

Figure 57: RSG response (Array type B) to increasing tensile load until catastrophic failure.

Figure 57 shows the strains recorded by the gauges positioned at the strap ends of specimens 4, 5 & 6 respectively (RSG array 'B', gauges G2-G6 Figure 55). Data for the gauge placed closest to the strap end (G2) is not available for specimens 4 & 5. For specimens 4 & 5 strains can be seen to increase near linearly with load until failure. Failure can be identified by the sharp discontinuity in the strain readings as seen at approximately 14, 20 and 32kN on Figure 57A, B & C respectively resulting from global strain relief as the specimen fails and no longer transfers load. Data from beyond the moment of failure has been omitted for clarity.

A small ‘event’ can be seen prior to the Specimen-4 reaching 12kN of load and a decrease in strain prior to failure on Specimen-5, similar to that observed on Specimens 2 & 3, is evident although strains per load are higher due to the RSGs placement further from the strap end. Specimen-6 reveals a different RSG response. Strains initially increase linearly with load; their magnitude and rate of increase rising as the position of the gauges from the strap end increases as expected. At approximately 17kN a dramatic reduction in strain is experience by all gauges. This response is characteristic of a disbond front rapidly passing beneath the positions of the RSGs. The joint continues to support an increasing load after this event until ultimate failure at approximately 32kN. In this instance three sequences of behaviour can be seen: 1. linear increase in strain on all gauges indicating an intact, load bearing bond, followed by 2. Pronounced reduction in strain levels at approximately 20kN indicating a loss of bond strength beneath the gauge positions, followed by 3. Continued load transfer and residual strength until ultimate failure at approximately 32.5 kN. This behaviour is characteristic of a progressive bond failure and a joint with some level of damage tolerance. As the dramatic strain drop occurs almost simultaneously across all sensors this suggests they are placed too close together to effectively track damage growth.

6.6.3.3 RSG Array C – Specimens 7, 8 and 9

Array C was designed to monitor further detail of disbond growth if similar apparent degradation as observed in Specimen-6 occurs. It was proposed the greater sensor spread may be better suited to monitor damage progression than the closely spaced sensors in array B. If such damage (i.e. non ‘near-instantaneous’ failure) was present a succession of rapid strain drops may be observed as a disbond progressed under the respective surface mounted gauges. Evidence gained via DIC of Specimen-6 which showed evidence of progressive disbond growth revealed major and measurable strain drops up to 30 and 40mm into the overlap respectively (see section 6.6.4 below). The sensors within array C were therefore spread over this region. As per array A additional surface sensors were placed away from regions of expected damage on both the plate and strap to check general values against FEA and for potential comparisons against strain responses in the damage region.

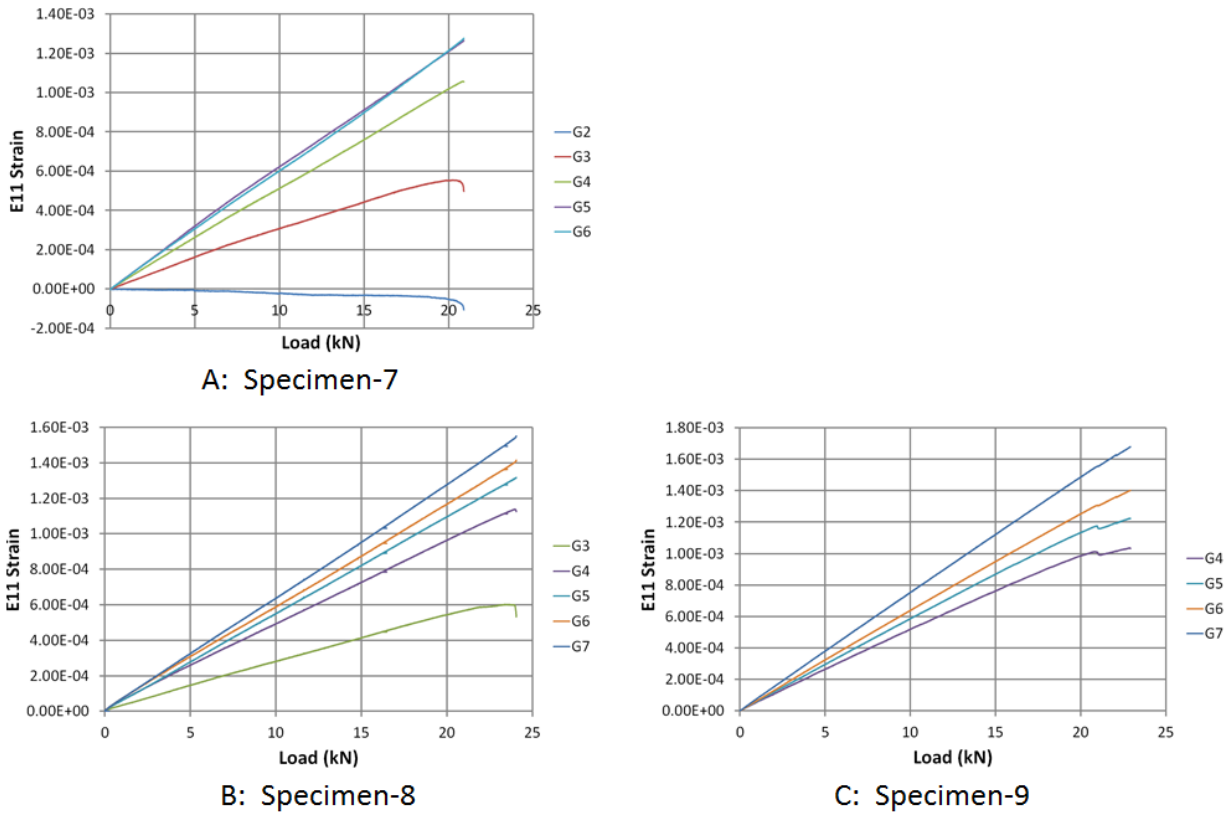

Figure 58: RSG array type C measured surface strain (E11) responses to increasing tensile load until catastrophic failure.

Figure 58 shows surface E11 strains on the joint strap recorded by RSGs in the 'Array C' formation; specimens 7, 8 & 9 respectively. Gauges G7 on Specimen-7, G2 on Specimen 8, and G2 & 3 on Specimen-9 are excluded due to equipment failure. In addition the gauge positioned closest to the strap edge (G2) on Specimen-7 reveals some unlikely behaviour (final 'drop-off' marginally increasing in compressive magnitude). This is however included to illustrate the very low strain close to the strap edge which may not assist monitoring. Gauge 7, located on the strap away from the expected damage initiation region, is included on the Specimen 8 and 9 plots (6B & 6C) for comparison. In each case surface strains can be seen to rise linearly as load increases with no (or at best extremely minimal and undefinable) features prior to catastrophic failure.

6.6.4 Digital Image Correlation

DIC was also used to monitor each specimen providing an additional independent form of surface strain measurement. This was used to further corroborate the RSG

measurements and FEA predictions as well as providing a 2-dimension visualisation of strains at all points on the specimen during mechanical testing. Due to technical difficulties DIC was not available for tests using RSG Array A.

Comparisons are shown between Specimen-5 ('Max' stress NASA design) – which via the strain gauges showed no damage indicators prior to failure – and Specimen-6 ('Peel' stress NASA design) which shows evidence of progressive growth using the surface strain gauge array type B. A further example of a Peel design type sample using the type C array is presented which showed no evidence of progressive failure either via the surface gauges or DIC. This response was near identical for the other samples in this set.

Figure 59 displays surface E11 strains measured via DIC along the centreline of Specimen-5 (45mm overlap).

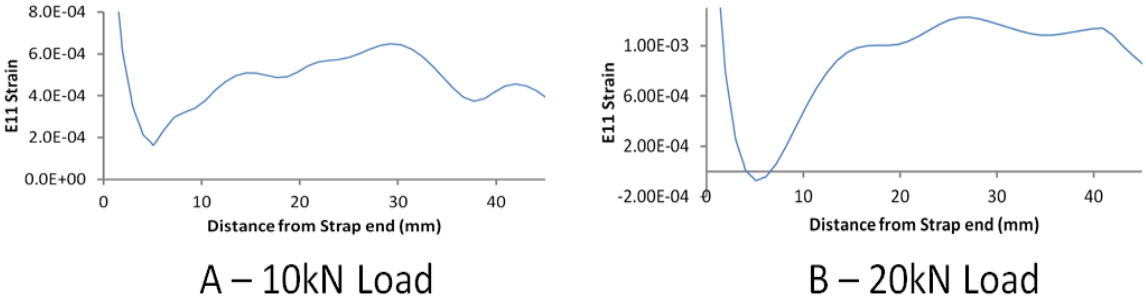

Figure 59: E11 surface strains measured via DIC along the strap centreline of Specimen-5 partially through tensile testing (A) and just prior to failure (B)

The DIC results presented show measured strains partially through loading (10kN) and just prior to failure (20kN). The characteristics of the curve remain unchanged with no evidence of a zero/slow strain region indicating a disbond propagating from the likely damage initiation (strap end: distance = 0). This suggests failure is rapid and catastrophic supporting the diagnosis formed from the RSG response.

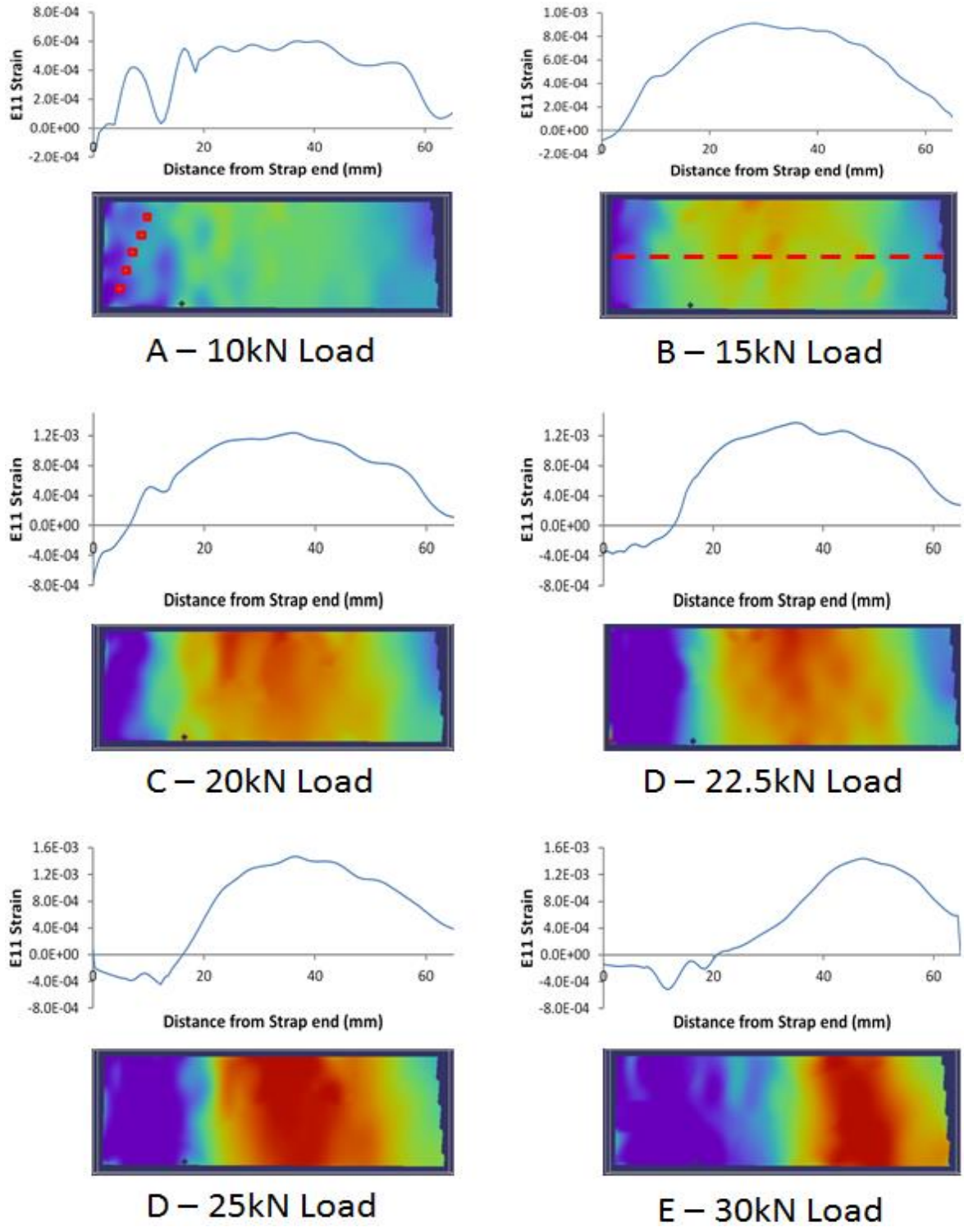

Figure 60: DIC measured E11 surface strains, at various tensile loads and degree of progressing disbond, along the centre-line (above) and globally (below), on the monitored strap of Specimen-6 (70mm overlap).

Figure 60 summarises the surface E11 strains recorded on the strap of Specimen-6 (70mm overlap) which exhibited a RSG response suggestive of progressive failure.

Figure 60A also shows the position of the RSGs mounted on the opposite strap-face and Figure 60B highlights the centreline presented in the graphs above the global 2D plots. A response similar to that predicted by FEA (Figure 54) associated with a disbond can be seen initiating between 15& 20kN and continuing to advance until catastrophic failure of the joint.

Figure 61 presents DIC monitored E11 surface strains on the strap centre-line of Specimen-9 (70mm overlap). The character of each curve remains unchanged as load increases up to failure (just subsequent to D-24kN), i.e.no progression of low surface strain indicative of a disbond, as seen in Specimen-6 (Figure 60), is present. This is in agreement with the diagnosis made via the surface mounted RSGs (Figure 58). Near identical characteristic behaviour was recorded via DIC for all 'Peel' design samples using RSG array C.

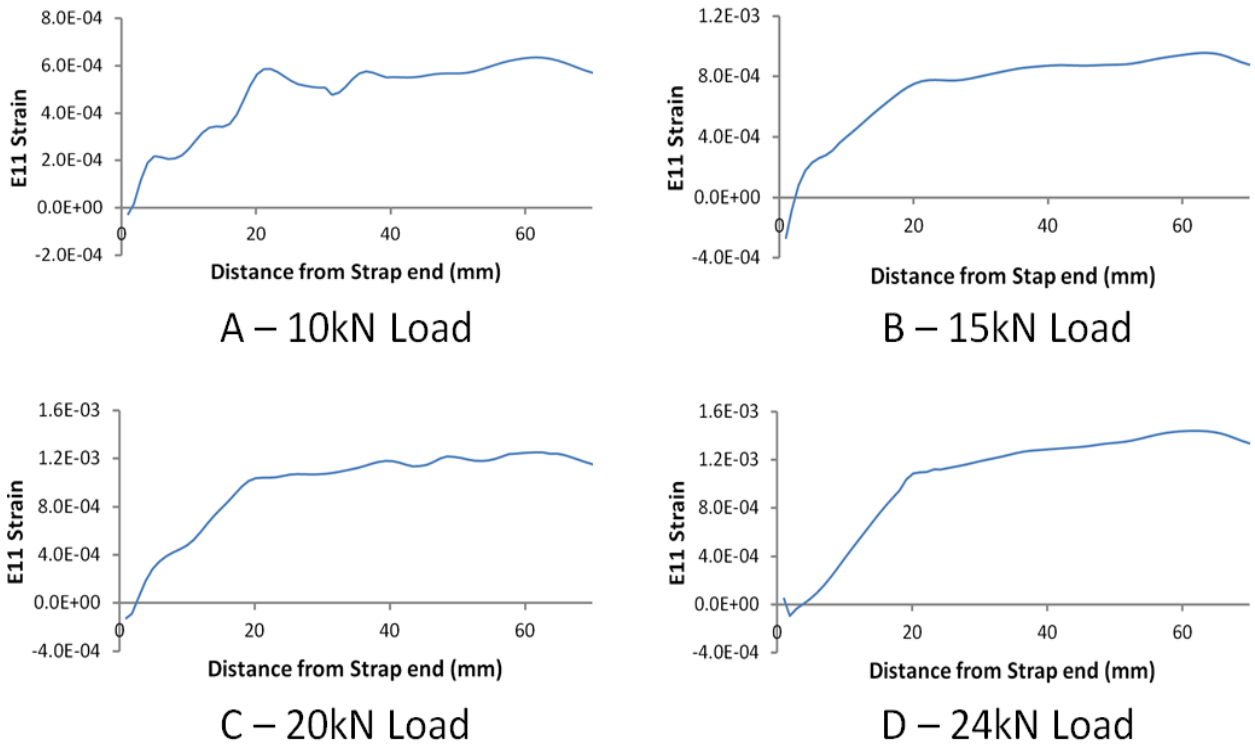

Figure 61: E11 surface strains along the strap centreline of Specimen-9 (70mm overlap) at various tensile loads during testing and just prior to joint failure (D)

6.6.5 Visual Inspection

Test specimens were visually examined after testing to failure to determine the bond failure modes. Photographs of the Standard specimens considered in this chapter post testing are presented below.

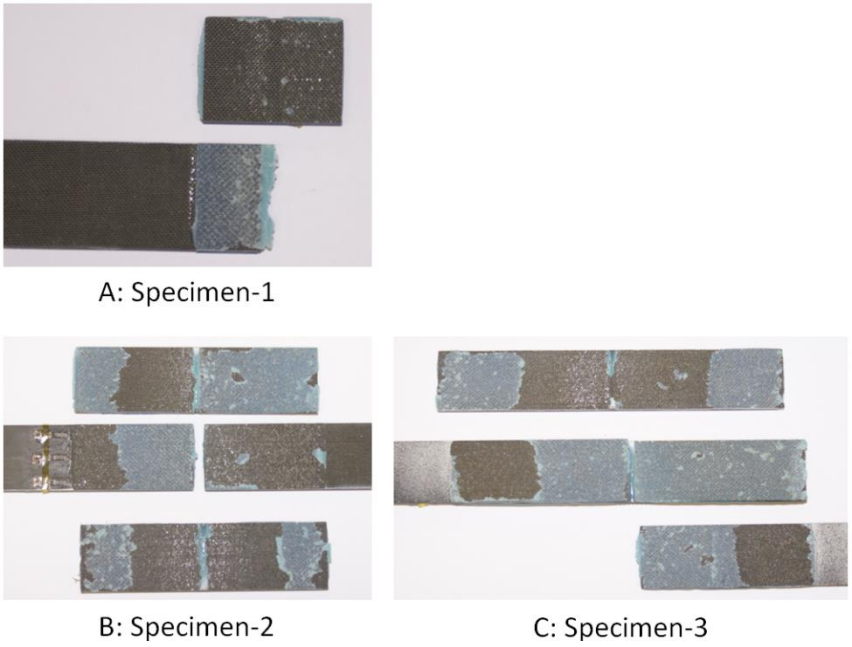

Figure 62: RSG Array-A Specimens. Bonded surfaces post testing.

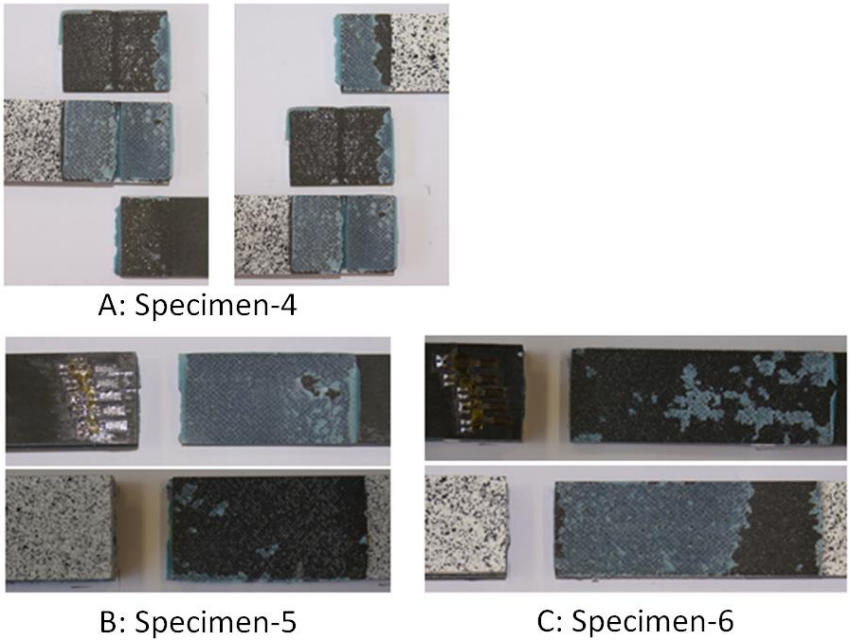

Figure 63: RSG Array B Specimens. Bonded surfaces post testing.

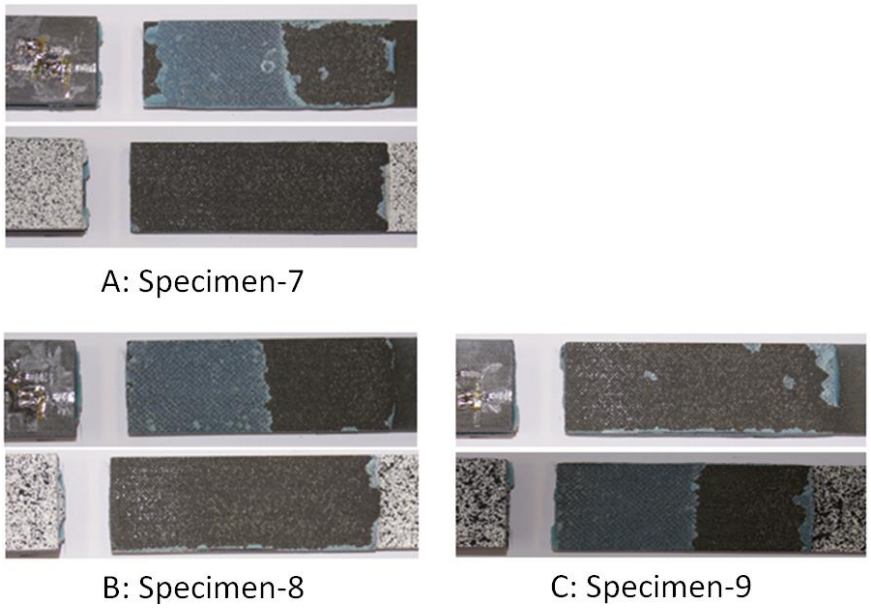

Figure 64: RSG Array C test samples. Adhesive surfaces post testing.

In all cases the failure mode has been identified as ‘adhesive failure’, i.e. failure at the adhesive/adherend interface, the classic characteristic of the adhesive cleanly separating from one adherend and remaining intact on the face of the opposing adherend [140,169]. Such failure is representative of problematic bonded structure. This failure type – a result of insufficient manufacturing quality or process [140] – results in joint strengths lower than those designed although possibly appearing identical to well fabricated structure even using NDI methods. The fact all specimens in these test failed in this manner despite being manufactured under well controlled manufacturing conditions highlights the difficulty of ensuring maximum strength is produced when fabricating bonded structure.

6.7 Section Summary/Discussion

6.7.1 General observations of sample failure observed via surface strain monitoring

These initial tests concur with previous investigations highlighting standard adhesive double strap joint designs when subjected to quasi-static tensile loading commonly fail both rapidly and catastrophically once damage initiates. In most cases little or no easily recognisable symptoms prior to failure, either visual or surface strain based, appear present. Symptoms that do appear (reductions in the rate of strain increase

and/or minor drops in strain per increase in subjected load) may be ambiguous and occur with little or no warning prior to failure. Hence, any form of joint monitoring based on surface strain measurement would be of little use because no advance warning of failure could be achieved hence ruling out any opportunity to perform maintenance or take any other action.

In these tests the only exception to the common behaviour discussed was that of Specimen-6. Both RSG and DIC data reveal a comparatively slow and controlled disbond initiating from the region of greatest shear and peel stresses-strains (at the strap end) which progressed into the overlap as load increased. Although the reason for this different behaviour is not understood the highly defined RSG response (and agreement with DIC), combined with the sample's ability to continue to transfer a significant increase in load after detection, i.e. residual strength (ultimate failure load ≈190% of damage detection load), is perfectly suited to SHM aided damage-tolerant operation. Surface strain based SHM enabled structural joints may therefore be viable if such behaviour in the event of damage initiation can be incorporated and guaranteed as part of the approach to structural design. This points the way to a design goal for damage tolerant, adhesive joints that can be engineered to fail in a progressive manner while allowing simultaneous monitoring via surface strain. This design goal will be explored in the next chapter.

6.7.2 Performance and predictive strength of bonded structure

Bolted Samples

The bolted samples tested proved to be reliable, failing at the design loads and in the desired non-catastrophic failure mode (bearing failure). The ultimate failure strength (via tension failure) could also be predicted. Bonded joints are still however heavier than potentially suitable purely bonded joints due to the inclusion of fasteners and their requirements of inefficient laminate lay-ups. Other issues such as fasteners potentially being sites for moisture ingress as well as tooling and tolerance requirements are also undesirable. In addition the joints in this study (which behaved in a manner representative of bolted composite structure) were only capable of transferring 1/3 of the surrounding structures potential load capacity. Currently however the disadvantages summarised are outweighed by the design

reliability shown relative to pure bonded structure for use in many critical applications.

Adhesively Bonded Specimens

The bonded specimens appeared less reliable with greater variation and possible reductions in strength resulting from difficult to identify manufacturing issues. Measured strengths compared to the surrounding structure being joined were again low, however compromises in the structure were made so identical laminates could be used for both bonded and bolted samples. Improvements in fabrication practice (surface preparation) and more appropriate laminates may have improved strength, and removed both bulk and mass.

Comparing the analytical predictions of adhesive bond strengths with FEA revealed some points of interest. Although the Hart-Smith approach predicts all overlaps tested to have the same strength (Ultimate and practical DLL) the FEA model shows undesirable near total plastic behaviour across the entire bond-line at 20kN loading for the 15mm overlap design. Even if this does not result in failure it is significantly lower than the ultimate strength of 107.2kN. Although unclear in many sources using the approach Hart-Smith does however suggest designs are made with minimum shear stresses no more than 10% of the plastic shear stress (Chapter 4: section 4.3.2.4) therefore determining a minimum overlap length.

Although the maximum potential strength could not be determined due to adhesive type failure estimates of the joints DLL can made by considering the outputs of the FEA models. As discussed in Chapter 4 it is recommended that during normal operational loading (below DLL) the adhesive should not deform plastically to prevent permanent damage [137,141,151]. The additional strength provided during plastic deformation should be available for DUL cases (generally 1.5xDLL capability). Figure 65 - Figure 68 show FEA shear-stress curves along the adhesive mid-plane centre-line of the longer ‘Peel’ specimens (70mm overlap) at various loads with corresponding screenshots highlighting adhesive regions subjected to plastic deformation. (Dark blue = zero plastic deformation. Red line shows centre-line plotted on shear stress curve).

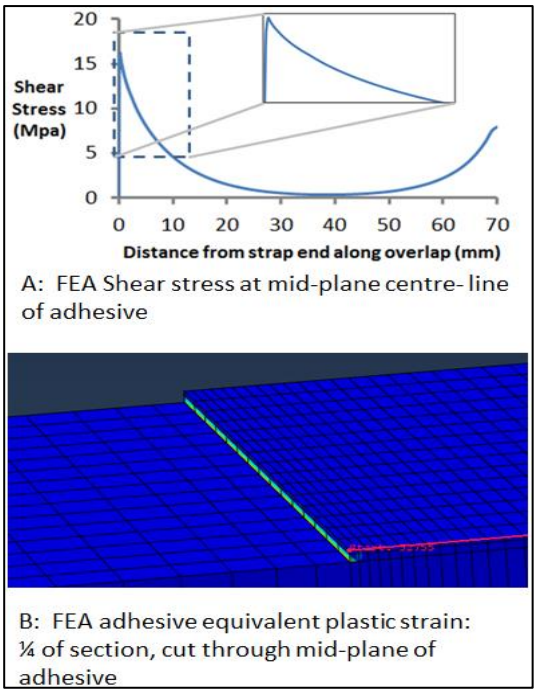

Figure 65: 10kN Loading; Zero/minimal Evidence of adhesive plastic behaviour

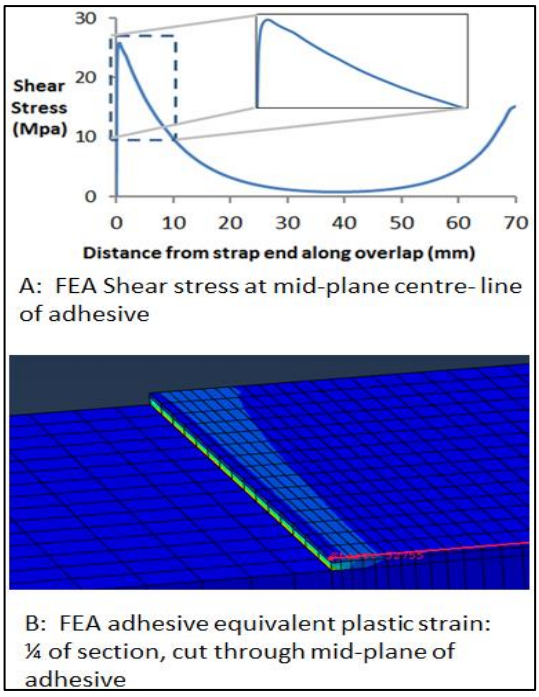

Figure 66: 20kN Loading; Evidence of onset of adhesive plastic behaviour

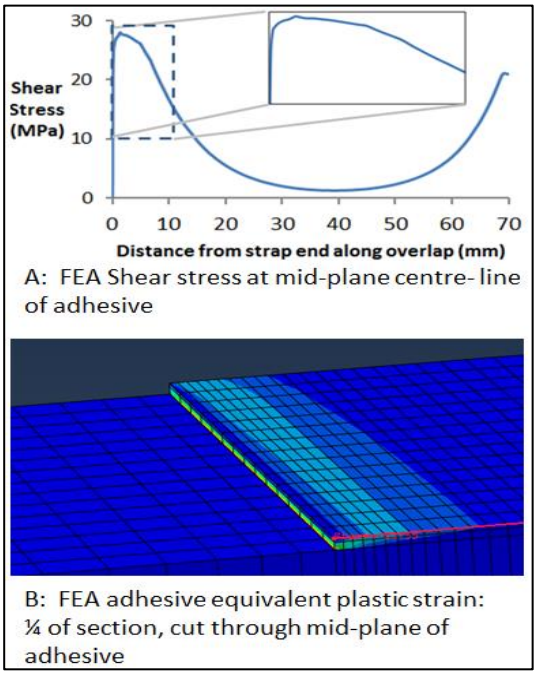

Figure 67: 30kN Loading; Defined adhesive plastic behaviour

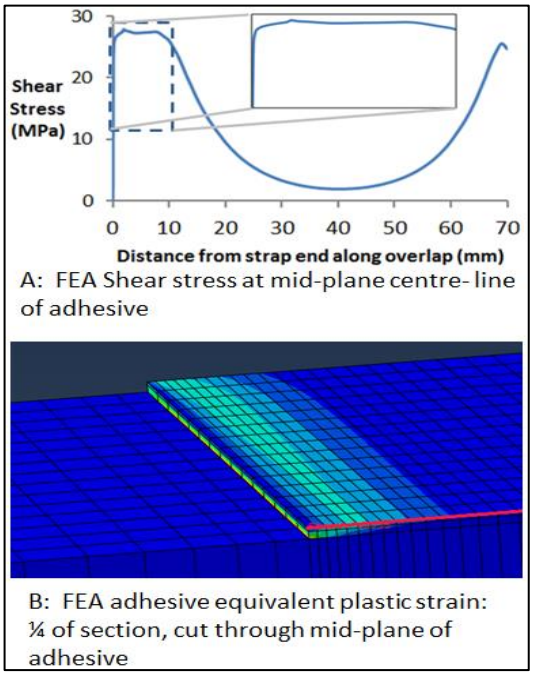

Figure 68: 40kN Loading; Progression of adhesive plastic behaviour

As load increases the ‘sharp edge’ of the adhesive shear-stress curve, characteristic of elastic behaviour, can be seen to ‘blunt’ and form the plateau characteristic of plastic deformation. The FEA ‘equivalent plastic strain’ plots – which consider plastic deformation in all orientations – concur. The high values present at the ‘corner’ of the adherend and adhesive should be considered with caution due to unrealistic stress raiser created by the sharp corner in the CAD geometry. If no plastic deformation is permitted the apparent DLL will therefore be <20kN, in the region of 17.1kN as predicted using the ‘knee’ values and the Hart-Smith approach (Table 15). Therefore the DUL for this structure will be ≈17.1 x 1.5 = DUL ≈ 25.7kN. Omitting the test cases for the short ‘Avg’ specimens (15mm overlap) failure of the samples tested (‘Max’ medium overlap 45mm and ‘Peel long overlap 70mm) ultimately failed between 20.4 & 32.4kN, close or exceeding the DUL even with the problematic adhesive failure mode.

6.7.3 Reasoning for rapid catastrophic failure based on the maximum stress-strain method

As discussed in Chapter 4 it is reasoned that bond-line damage initiates once a critical stress-strain threshold is exceeded at the bond-line at the strap end. The disbonds which initiate in this region effectively shorten the overlap, progressing into the joint. The region of peak stress/strain tracks this progression as illustrated in Figure 27, Chapter 4: section 4.5. As the joint is subjected to continuous loading, and over-lap length has little effect on stress/strain magnitudes at the joint end, the stress/strain experienced at this ‘new joint end’ remains above the critical value; assuming the bond quality remains similar. The process therefore continues resulting in rapid catastrophic failure. Figure 69 - Figure 72 present plots of FEA calculated shear and ‘peel’ stresses-strains at this peek location (at the bond-line mid-plane) as a simulated disbond progresses along a joint (70mm overlap) subjected to a constant 20kN tensile load. Effects of stress concentrations due to sharp crack tips are not considered due to both the plastic nature of the adhesive and the likelihood that problematic failure will occur at the adhesive/adherend interface.

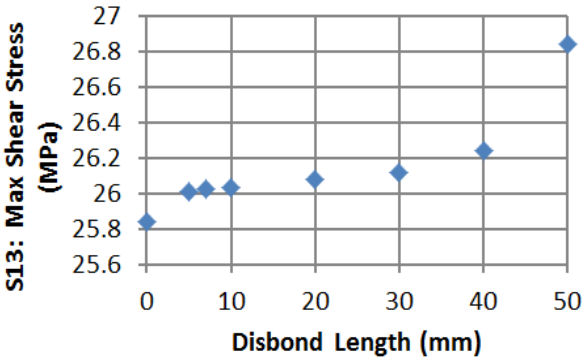

Figure 69: Maximum adhesive mid-plane shear stress values (FEA) at 20kN for various disbond lengths in the 70mm over-lap samples

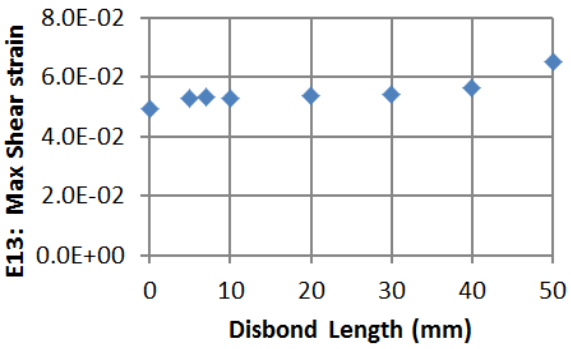

Figure 70: Maximum adhesive mid-plane shear strain values (FEA) at 20kN for various disbond lengths in the 70mm over-lap samples

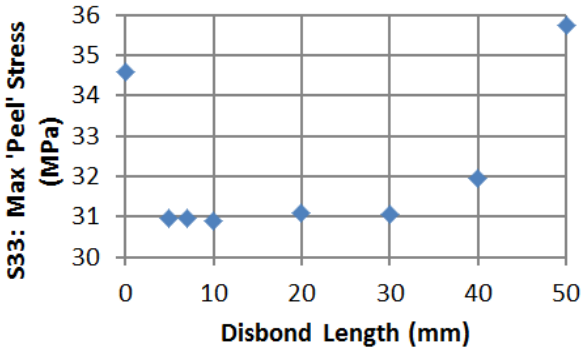

Figure 71: Maximum adhesive mid-plane 'Peel' stress values (FEA) at 20kN for various disbond lengths in the 70mm over-lap samples

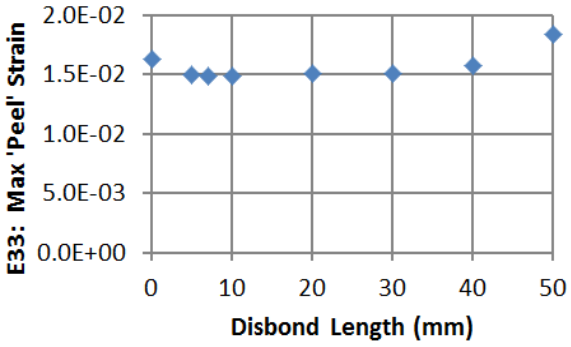

Figure 72: Maximum adhesive mid-plane 'Peel' strain values (FEA) at 20kN for various disbond lengths in the 70mm over-lap samples

Increasing levels of stress-strain as the disbond propagates can be observed. This reveals an effective weakening of the joint as if the stresses-strains are to be kept below the critical value the load transferred by the joint must be reduced. Although a degree of peel stress-strain relief is suggested as damage initiates (Figure 71 & Figure 72) as the disbond continues these values are also seen to increase.

As previously discussed the degraded strength of a problematic bond will be unknown. The shear and peel stress-strain distributions should therefore be considered for all potential damage thresholds. Similar FEA stress-strain plots for the 70mm overlap 'peel' sample at 10kN (purely elastic adhesive behaviour) and

30kN (established plastic behaviour at end of bond-line) loads are presented in Appendix B. Similar characteristic are observed for all loads.

6.7.4 Failure mode and the requirements of SHM enabled structure to account for 'adhesive' failure'

Visual examination revealed all samples within these initial tests failed as a result of 'adhesive failure' (see Figure 62 - Figure 64), a result of poor fabrication quality. Although unacceptable this failure mode presents the greatest issue for in-service bonded structure and is a major limitation on their widespread use in safety critical structures such as aircraft. Well-designed composite structure (qualified within the aerospace sector by comprehensive testing of materials, assemblies, components and structures using the 'building block' approach [3,14]) that is manufactured to the appropriate quality will not by definition fail under expected in-service conditions. Analysis of structure known to be perfectly manufactured will provide only minor benefits as such structure should behave as designed (in the case of bonded joints failure may be designed to occur outside the joint overlap – Chapter 4, section 4.4) and therefore should be unproblematic. Problematic bonded structure likely to benefit from SHM is that which, contrary to good design and manufacturing process, fails as a result of adhesive-failure and therefore at lower than that expected loads. Even with stringent production quality control measures the potential for such joints to be present forms the contemporary reasoning for the inclusion of additional structural features such as 'anti-peel fasteners' to prevent catastrophic failure.

Adhesive failure and therefore the presence of the poor adhesive-adherend interface in the specimens produced within the laboratory highlights the potential for such issues to be present. Although through additional experience, specialist facilities and stringent quality control measures within industry such issues may be minimised the absence of adhesive-failure promoting factors (contamination, moisture etc) are not be guaranteed. This, combined with difficulties identifying such degraded joints, even with the aid of sophisticated NDI techniques, results in an inherent uncertainty regarding the joint's condition resulting in the necessary inclusion of features such as additional fasteners to ensure airworthiness.

A usable SHM enabled structural joint design should be able to identify damage prior to ultimate failure (to allow damage-tolerant type operation) even if such disparity between design performance and actual strength exists (see Chapter 9, Application). A system must therefore be effective in the case of adhesive failure, although cohesive failure resulting from a major degradation in adhesive properties or even a potential ‘inter-laminar’ form of damage propagation should also be detectable and provide a similar response.

6.7.5 The development of SHM enabled structural bonded joints

Results from initial tests showed surface strain monitoring can identify adhesive bond-line damage initiation and propagation subjected to quasi-static loading providing the structure responds in an appropriate ‘slow-growth’ manner, as seen in the test structure Specimen-6. Such a response with the aid of monitoring may allow operation in a damage-tolerance type regime. Such a response is not common and was not observed on the other similarly designed and fabricated specimens. If SHM enable bonded joints are to be viable such behaviour must therefore be engineered into the structures design.

Considering the reasoning above (section 6.7.3) to promote a response suitable for monitoring and damage-tolerance operation – that which reliably emulates the slow growth and strain response observed in Specimen-6 – it is proposed either the joint strength must increase and/or the shear strain experienced (and potentially shear stress and peel loads) at the bond-line must decrease as a disbond progresses. This characteristic should ensure the stresses-strains do not remain at a locally critical level; therefore retarding damage growth and promoting the desired response providing the structure is not subjected to loads greater than when damage was initially identified. In the next chapter these goals are investigated in detail in an attempt to create repeatable, slow damage growth characteristics for adhesively bonded joints whilst exploiting such behaviour as part of a SHM enabled bonded joint design.

7 Testing, Results and Analysis: Novel Configuration Double Strap Joints

7.1 Section Introduction

The study included in Chapter 6 explored the potential for monitoring standard configuration bonded joints subjected to quasi-static loading using surface strain monitoring via in-situ sensors (strain gauges) as well as non-contact laboratory based DIC. It was shown this approach could both identify and track bond-line damage providing damage progressed at a rate slow enough to produce a measurable response prior to catastrophic failure. It also revealed if such behaviour is evident sufficient residual strength may remain to allow operation under a regime similar to that of aerospace damage-tolerant practice (see Chapter 2, section 2.2.3). Results from this study – as well as previous investigations – highlight such behaviour in bonded structure when subjected to quasi-static loading is not common and that ultimate failure commonly occurs almost spontaneously with little or no warning. One specimen did however exhibit the behaviour discussed. If this could be emulated and assured by considered structural design the prospect of useful structural monitoring and the potential benefits from such operation may be achieved.

In Chapter 6 it was proposed, based on the maximum stress/strain design and consideration of the changes in bond-line stresses as overlaps are reduced due to damage, that rapid disbonding may be thought to occur due to once the strength threshold of the bond has been passed the disbond progresses into the overlap. As the shear stress-strain at the new end of the overlap is equal to or greater than that (for a given load) of that which caused the previous section of bond to fail and assuming an equal quality of adhesive and adhesion is present in the new section of bond subjected to the peak loading this section also near instantaneously fails. This process repeats resulting in an unzipping of the entire bond. The ability to influence the distribution of the stresses-strains along the bond-line was considered. Factors such as unbalanced adherends (Chapter 4, section 4.3.2.3) may be used to ensure damage initiation occurs at predetermined locations. Bonded joint strength is also largely unaffected by overlap length (although still considered relevant – see Chapter

6; section 6.7.3) but does increase with width. It was therefore reasoned the magnitudes of stresses-strains experienced by the bond-line for a given tensile load could be tailored as the bond area changed due to damage. Based on this reasoning a novel form of joint design which aims to reduce the rate of damage growth whist providing opportunities for heath monitoring via surface mounted strain measurement is explored in this chapter. Such consideration led to the design and testing of new joints, in which the straps are tapered, i.e. the strap width reduces along the length of the overlap (see Figure 73 & Figure 80). This design ensures damage initiates at the strap end and as this propagates the effective width of the joint increases reducing the bond-line strain per unit load. Although such a design may show a reduction in the joints maximum potential initial performance (sections 7.2.1 and 7.6.3 below) allowance could be considered within the structures overall design.

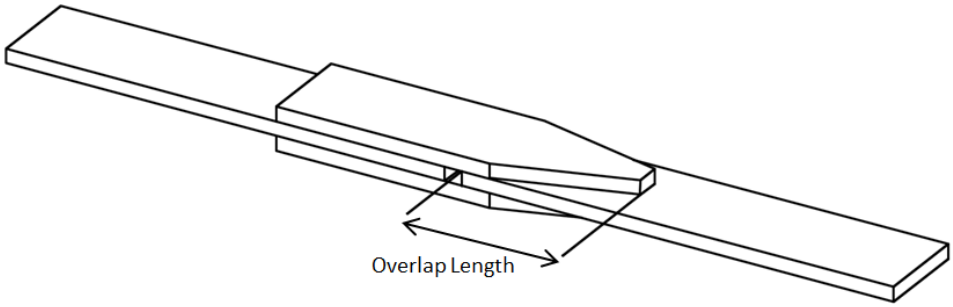

Figure 73: General arrangement of Tapered double strap joint

7.2 Bonded Joint Design

As joints used within this investigation were not for a specific application their design could be selected to aid manufacture and testing as well as comparison against previous tests. As such the construction was near identical to the specimens previously tested; standard test specimen width of 25mm and identical overlap length (70mm) as well as identical laminates used for both joint plates and straps. The only amendment was the inclusion of the taper on both straps at the side of the joint to be monitored. Detailed design/manufacturing drawings for the tapered joints are in Appendix A5.

Taper dimensions were chosen to aid analysis. Each strap width was tapered at an angle of ≈8.53° on each side. This produces not only a joint with a standard test specimen width of 25mm and strap end of 10mm but also results in a convenient increase in strap/bond width of 3mm for every 10mm loss of bond-line length. The degree of taper in real-world designs may be adjusted to balance the desirability of maximum potential strength with control over damage growth as well as other design constraints.

The capability of the design to inhibit catastrophic damage growth based on the reasoning of critical bond-line stress-strain values is considered in section 7.6.4 below.

7.2.1 FEA Predicted Effects of the taper design on the stress maximum stresses and strains experienced at the bond-line

FEA models of the tapered specimen geometry were interrogated to determine the relative damage initiation strengths compared to standard configurations. These were also used to determine if the reductions in stresses-strains associated with the concept to produce slow or retarded damage growth were present in this design.

Figure 74 - Figure 76 illustrate and compare maximum shear strain values present at the joint/disbond end, for the proposed tapered design (red markers) and the previously investigated standard double strap configuration (70mm overlap). This analysis only considered stresses and strains along the joint centre-line at the mid-plane of the adhesive bond. As per the previous analysis stress concentrations due to sharp crack tips are not considered due to the assumption of local plastic deformation of the adhesive and that problematic damage may occur at the adhesive adherend interface. It is recognised problematic adhesive type damage will in reality occur at the adhesive-adherend interface. As in the previous chapter maximum FEA calculated stress and strain values (which as per the standard strap joints appear at or very near the overlap end) are plotted for a constant, static load as simulated disbonds of various lengths are modelled.

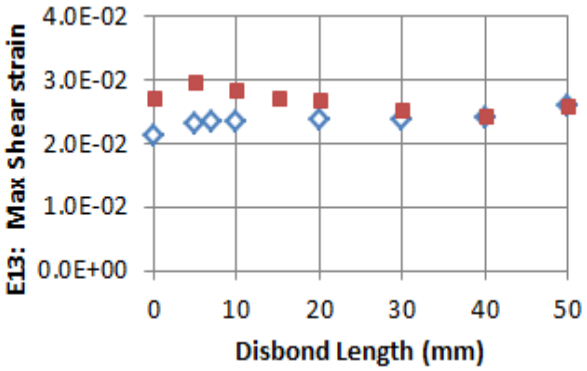

Figure 74: Maximum adhesive shear strain values (FEA) at 10kN for various disbond lengths in the Tapered (Red) and Standard 70mm (Blue) joints

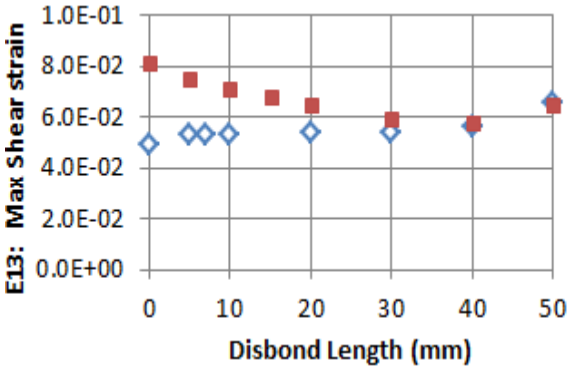

Figure 75: Maximum adhesive shear strain values (FEA) at 20kN for various disbond lengths in the Tapered (Red) and Standard 70mm (Blue) joints

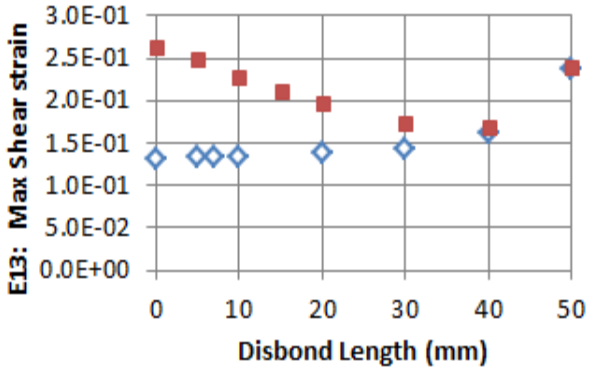

Figure 76: Maximum adhesive shear strain values (FEA) at 30kN for various disbond lengths in the Tapered (Red) and Standard 70mm (Blue) joints

The 10, 20 and 30kN loads shown relate to purely elastic, transient/early plastic and developed plastic behaviour in the adhesive respectively at the overlap or disbond edge (see section 7.6.3). It can be seen (with the exception of preliminary damage up to 5mm at 10kN) the shear-strain values decrease, for a given load, as the disbond length increases for the tapered geometry, unlike the standard geometry where values increase. It is proposed this should result in the bond strength increasing as the disbond propagates hence the resistance to further damage propagation should also increase. Shear strain values can however be seen to rise

even for the tapered geometry when the disbond length reaches approximately 40mm. This may therefore represent the limit to the slow damage growth region.

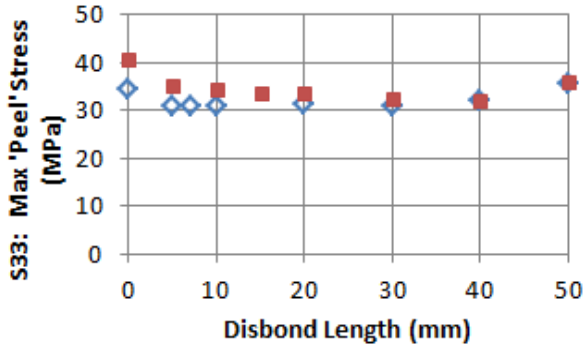

Figure 77: Maximum adhesive 'Peel' stress values (FEA) at 20kN for various disbond lengths in the Tapered (Red) and Standard 70mm (Blue) joints

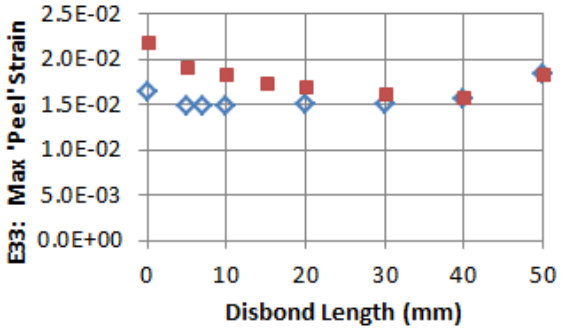

Figure 78: Maximum adhesive 'Peel' strain values (FEA) at 20kN for various disbond lengths in the Tapered (Red) and Standard 70mm (Blue) joints

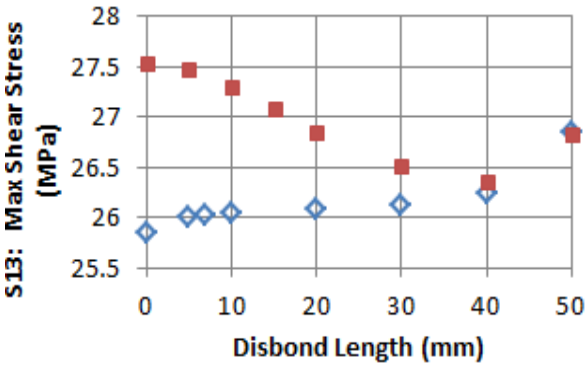

Figure 79: Maximum adhesive shear stress values (FEA) at 20kN for various disbond lengths in the Tapered (Red) and Standard 70mm (Blue) joints

Although excessive shear strain is often the primary consideration for bond-line failure (Chapter 4, section 4.3) this approach usually assumes perfect bonding between adhesive and adherends and therefore cohesive type failure. This approach must also assure the dominant load transfer through the bond is shear with through thickness normal/peel loads reduced by appropriate design considerations.

As the precise condition of the adhesive/adherend interface of joints that ultimately degrade by adhesive failure will be unknown as well as shear stresses maximum ‘peel’ stresses and strains were also considered as any of these, or a combination of these factors, may govern damage growth. Comparative plots for these factors are presented for a 20kN joint tensile load (Figure 77 - Figure 79).

The characteristic drop in magnitude can be observed for each proposed potential damage driving component. Again the minima values for the tapered configuration appear at 40mm from the strap end. Similar characteristics are seen for 10 and 30kN loading (Appendix C). A variation to these characteristics is seen on the stress plots – both in shear and peel – at 30kN loading where the values remain largely unchanged due to plastic deformation.

Study of Figure 74 - Figure 76 (Shear strain), as well as the other bond-line stress-strain componants, reveals a widening disparity of the maximun stress-strain values experienced at the bond-line between the undamaged-standard and undamaged-tapered geometries as the applied load increases. Although this appears to suggest the initial undamaged strength of the undamaged tapered joint reduces as load increases relative to the standard configuration investigation via FEA reveals this is not the case. To determine the magnitude of a strength knock-down factor compared to standard configuration simulated (FEA) tensile loads experienced by the undamaged-tapered design were reduced therefore lowering the maximum stress-strain levels calculated in the undamaged standard joints. Initial load reductions were based on the disparity of the values shown on the E13 plots (undamaged standard shear strain / undamaged Tapered shear strain: ≈78% at 10kN, ≈61% at 20kN and ≈50% at 30kN (Figure 74 - Figure 76). This approach produced maximum shear-strain values that were incorrect (not equivalent) for all but the 10kN fully elastic load case. This investigation was repeated using this knockdown (0.78) for all loads and compared to each stress-strain component. Results for each load and stress-strain component are presented in Table 17 below.

Table 17: Comparison of maximum bond-line stress & strain values (FEA) of the loaded Standard (70mm) joint and the Tapered geometry at 78% of the Standard joint loading

	Tensile load Standard joint	Applied load Taper joint		Tensile load Standard joint	Applied load Taper joint		Tensile load Standard joint	Applied load Taper joint	
	10kN	7.8kN		20kN	15.6kN		30kN	23.4kN	
Stress-Strain Componant	Max value Standard	Max value Tapered	% Difference	Max value Standard	Max value Tapered	% Difference	Max value Standard	Max value Tapered	% Difference
E13	0.02129	0.02068	2.90%	0.0495	0.04867	1.68%	0.13128	0.1366	3.98%
E33	0.00808	0.0084	3.90%	0.01634	0.01697	3.82%	0.02646	0.02847	7.29%
S13 (Mpa)	16.1877	15.7797	2.55%	25.843	25.7566	0.33%	27.9931	27.7821	0.76%
S33 (Mpa)	20.4606	21.2868	3.96%	34.5923	35.9633	3.89%	41.6601	42.0664	0.97%

The results shown in Table 17 reveal only minimal variation in maximum stress and strain values between the standard joint configuration and that experience by the tapered design in all cases. The difference in the 10kN E13 measurements (2.90%), from which the original knock-down factor of 78% was derived, is thought to be largely generated from rounding errors. This reveals the knock-down should be consistent for all loads.

The acknowledgement that the knock-down remains constant over the full range of operational loads allows the structure to be designed with an appropriate reduction in strength (from this analysis ≈78% of the standard joint) knowing in the event of degradation no additional deviation should be present through the potential load range, including that of DLL and DUL. Further investigation supports this hypothesis (section 7.6.4). If, with an extended study, parameters which influence the knockdown can be quantified (e.g. taper angle, overlap length, material thicknesses and properties etc.) such values can be used with existing design calculations to form useful preliminary design tools.

Although a reduction in the maximum potential and design strength may result from increases in maximum shear and peel stresses-strains for a given structural load these capabilities could be accounted for when designing the greater structure. With considered designs however similar structural loads may however be achieved as: *a*) as less reliance is required of supplementary structure (e.g. chicken fasteners and

their associated laminate build-ups) which does not provide additional loading capacity some structural mass and bulk could be reassigned from this role into additional load bearing SHM enabled bonded structure and/or *b*) as uncertainty associated with the structures condition is removed the reduction in design strengths due to design allowables associated with uncertainty may in whole or part be eliminated.

7.3 Surface Strain Gauge Array

The FEA predictions above have shown the desired reduction in stress/strain characteristics extend ≈40mm into the overlap of the test specimen geometry. If this concept proves to guide and control damage growth it highlights which area of the joint may benefit from monitoring. As such a strain gauge array was spread across and slightly beyond this region to monitor any progressive disbond. The gauges are designated as G1 (4mm), G2 (10mm) ….G6 (51mm).

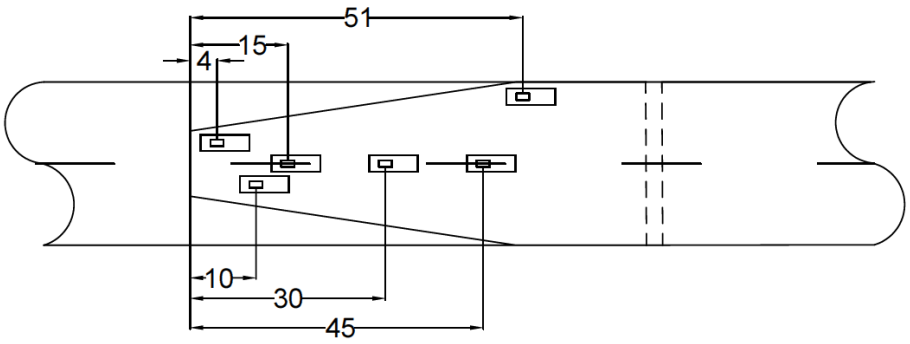

Figure 80: RSG positions used with the tapered geometry joints

Gauges G1 - G3 were staggered to both increase the sensor density at the overlap end. Gauge G6 was positioned at the ‘shoulder’ of the taper to potentially identify any damage which may be induced by the change in strap geometry.

7.4 Surface Strain Predictions

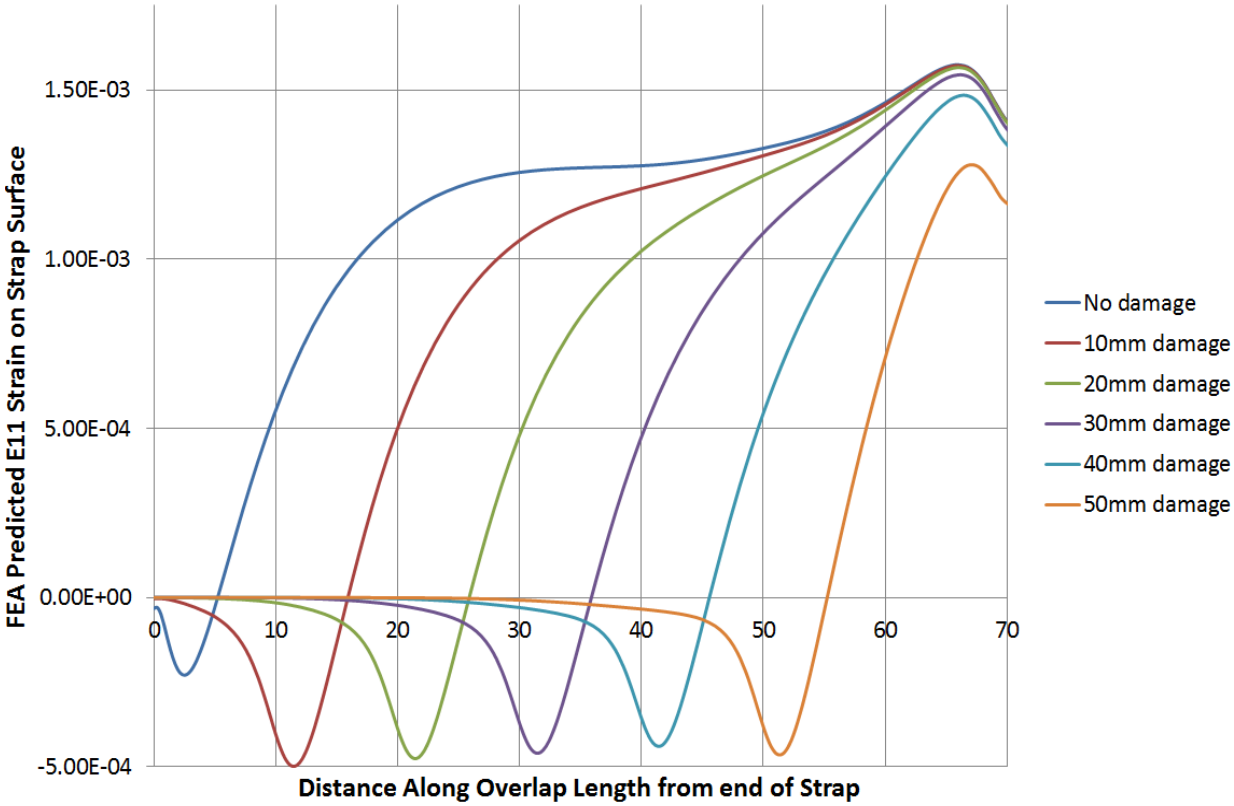

Figure 81: FEA prediction of surface strains on the strap surface centre-line of a 'Taper' specimen with various disbond lengths (propagating from distance = 0) when subjected to a constant 20kN tensile load.

Figure 81 shows the surface centre-line E11 strains that may be expected (FEA) as a disbond propagates into the overlap at a joint load of 20kN. As previously noted, due to the method used to model the adherends, the actual laminate may be marginally stiffer in bending. As such the compressive values caused by 'upward' bending of the free laminate ends may in reality be less pronounced.

The Taper design surface strain curves are similar to those predicted for conventional joints (Figure 54) although while significant overlap remains the plateau region is slightly 'flatter' and the strain drop is marginally more pronounced. Although minimal this change in character may slightly assist assessment by arrays of fixed sensors due to the more defined difference in strain values experienced as the disbond progresses relative to these sensors (see Figure 80 above).

7.5 Testing Results

The first observation of note is that all specimens failed in a 'slow damage growth' mode as predicted hence underlining the validity of the approach to design. This is in contrast to the standard non-tapered joints reported in the previous chapter most of which failed spontaneously with no slow damage growth behaviour.

Table 18 summarises the ultimate failure loads of the 'Tapered' test joints as well as the failure mode established by visual inspection after testing (section 7.5.3).

Table 18: Tapered specimens ultimate strength and failure mode

Specimen Title	Ultimate failure Load	Failure Mode
Taper -1	50.53kN	Adhesive with some Cohesive
Taper -2	47.60kN	Adhesive with some Cohesive
Taper -3	48.07kN	Adhesive with some Cohesive
Taper -4	30.58kN	Adhesive
Taper -5	27.49kN	Adhesive

Strength predictions are not included as no current design calculations exist for such joints. The length of undamaged overlap is however identical to the standard un-tapered specimens designed by the simplified NASA procedures to account for peel loads (70mm) investigated in Chapter 6.

7.5.1 Surface Strain Gauges

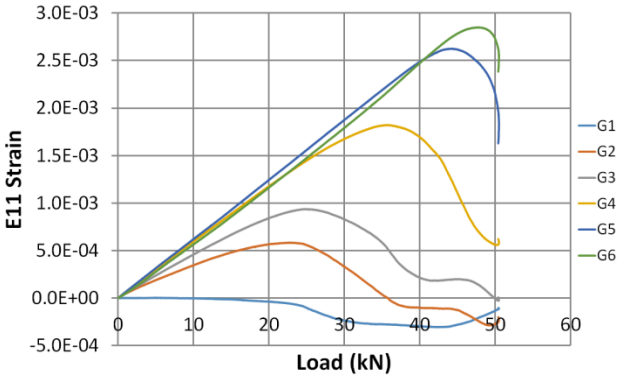

Figure 82: 'Taper-1' Surface Strains (RSG)

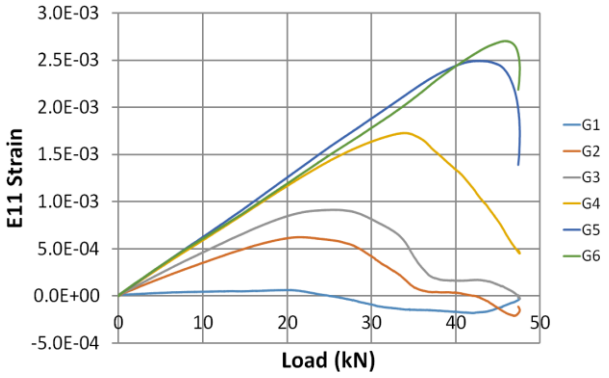

Figure 83: 'Taper-2' Surface Strains (RSG)

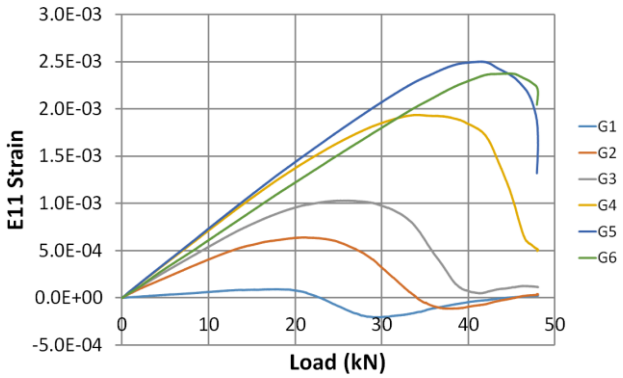

Figure 84: 'Taper-3' Surface Strains (RSG)

Figure 82 - Figure 84 present the E11 surface strain responses recorded by the in-situ sensors on the tapered specimens 1-3 respectively. Responses are highly comparable, both in magnitude as well as character, throughout loading until failure in each case. Strains can be seen to initially rise approximately linearly. Rates of strain increase (and eventually magnitude) per unit load are then seen to decrease by each RSG, starting with the gauge placed closest to the strap end (G1) and then sequentially by each gauge as its distance increases from the strap end. This response is what may be expected from a slow progressive disbond originating at the strap end and working inwards. Comparisons with DIC and FEA are shown in Figure 87.

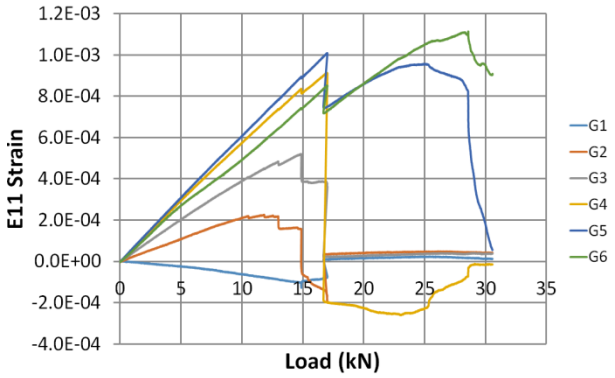

Figure 85: 'Taper-4' Surface Strains RSG

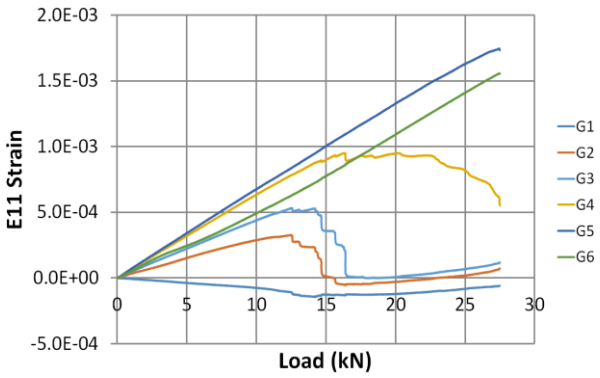

Figure 86: 'Taper-5' Surface Strains RSG

Figure 85 & Figure 86 show strain responses for the Taper 4 & 5 specimens which reveal more erratic responses to those shown for Taper specimens 1-3. Small to very large near instantaneous drops in measured strain are evident. The presence and magnitudes of these drops are again first experienced by the gauges closest to the strap end and followed in turn by the gauges further into the overlap. Strains values can be seen to eventually settle at zero strains (gauges G1-4 on Taper 4 and G1-3 on Taper 5). In addition to the difference in surface strain these specimens produce far more audible noise than the previous tests, particularly at loads corresponding to the 'jagged' strain reductions seen on the plots above. This strain response would be consistent with that of sections of bond failing (the size of failing section corresponding to the degree of rapid strain drop) and being temporally arrested until the increasing applied load continues the process until ultimate failure. Comparisons with DIC and FEA are shown in Figure 88 & Figure 89.

7.5.2 Digital Image Correlation

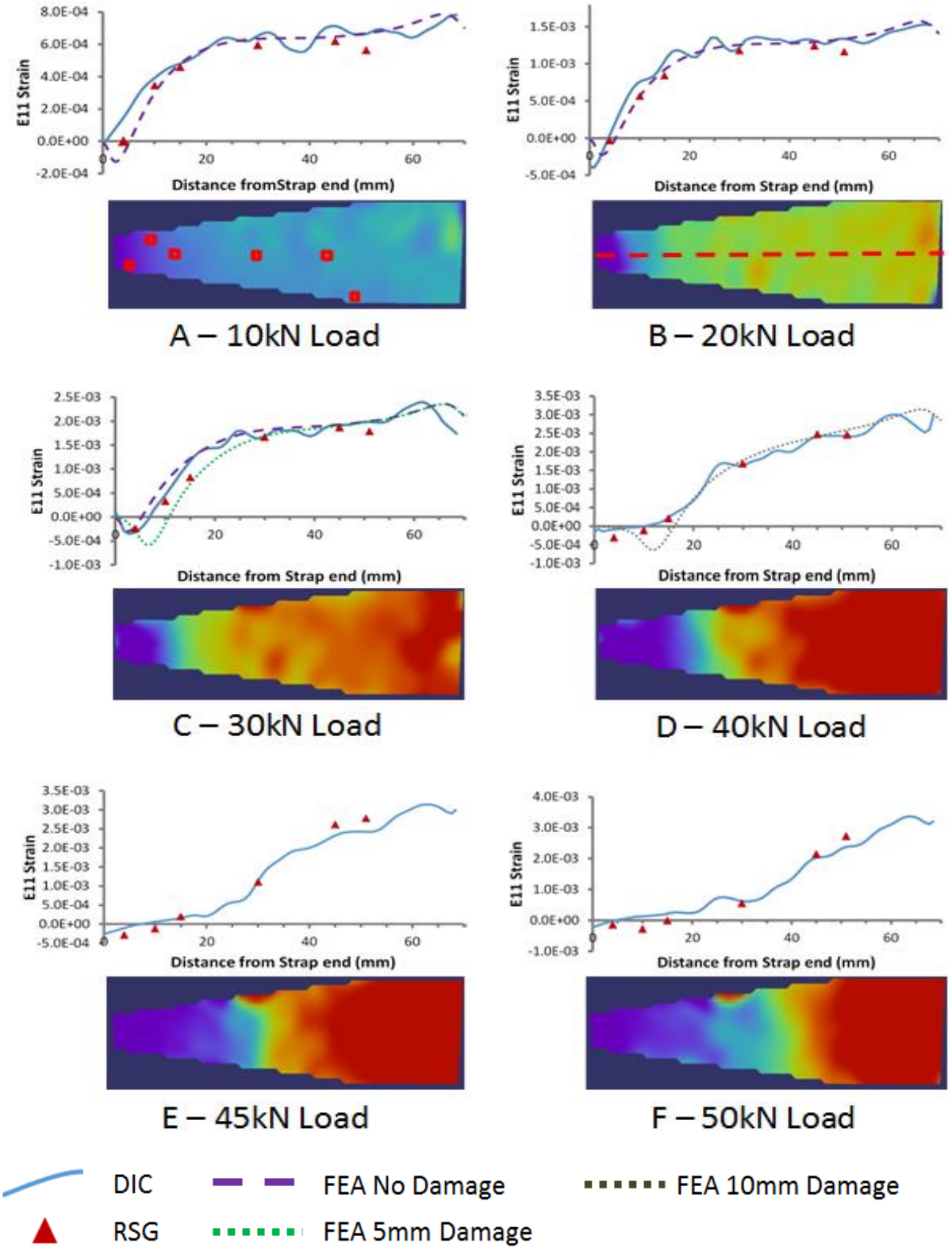

Figure 87: Surface strains at various tensile loads and degree of progressing disbond on the monitored strap of specimen 'Taper-1'.

Figure 87 summarises DIC recorded strains on the strap of specimen ‘Taper-1’. The position of the RSGs (opposite face) and the centreline presented in the corresponding graphs are highlighted in Figure 87A & B respectively. Strain gauge values are plotted for comparison; note the gauge positioned 51mm from the strap end is placed at the strap edge and as such provides a slightly lower strain response. FEA calculated surface strain curves at equivalent loads are included to attempt to match disbond lengths with strain responses. No FEA data is available for loads greater than 40kN due to convergence issues associated with localised high levels of adhesive strain.

A similar response to that observed in the ‘standard’ configuration (70mm overlap) Specimen-6 (see Chapter 6, Figure 60) which showed evidence of slow damage growth, is present. Evidence of damage (movement of the low strain ‘front’) starts at approximately 20kN loading (B). This corresponds to the reduction in the rate of strain increase experienced by the RSGs located towards the strap end (Figure 82). As in the standard joint Specimen-6 the low/zero strain front associated with a disbond can be seen to steadily progress until failure at 50.5kN. Consideration of each DIC step in succession (1656 in total from the start of loading until ultimate failure for Taper specimen 1) further reveals the slow even rate of progression of the low strain front until the moment of catastrophic failure. Near identical DIC responses were seen for each specimen that showed a smooth, progressive response from the RSG data and mixed mode adhesive/cohesive failure (Taper 1 – 3). DIC values are in close agreement with those from the RSGs in corresponding positions along the bond-line. FEA plots also produce similar results when the condition of the joint was known, i.e. disbond length = 0. FEA surface strain profiles are similar to those produced by experimental sensors although in each case a small degree of ambiguity is present, particularly at the region where the low strain associated with a disbond meets the rise in strain where the bond remains intact. This makes determining the precise disbond length difficult.

Figure 88 below shows centre-line DIC surface strain values for specimen ‘Taper-4’. The various selected loads presented were chosen due to significant strain responses recorded by the RSGs just prior to these loads (Figure 85).

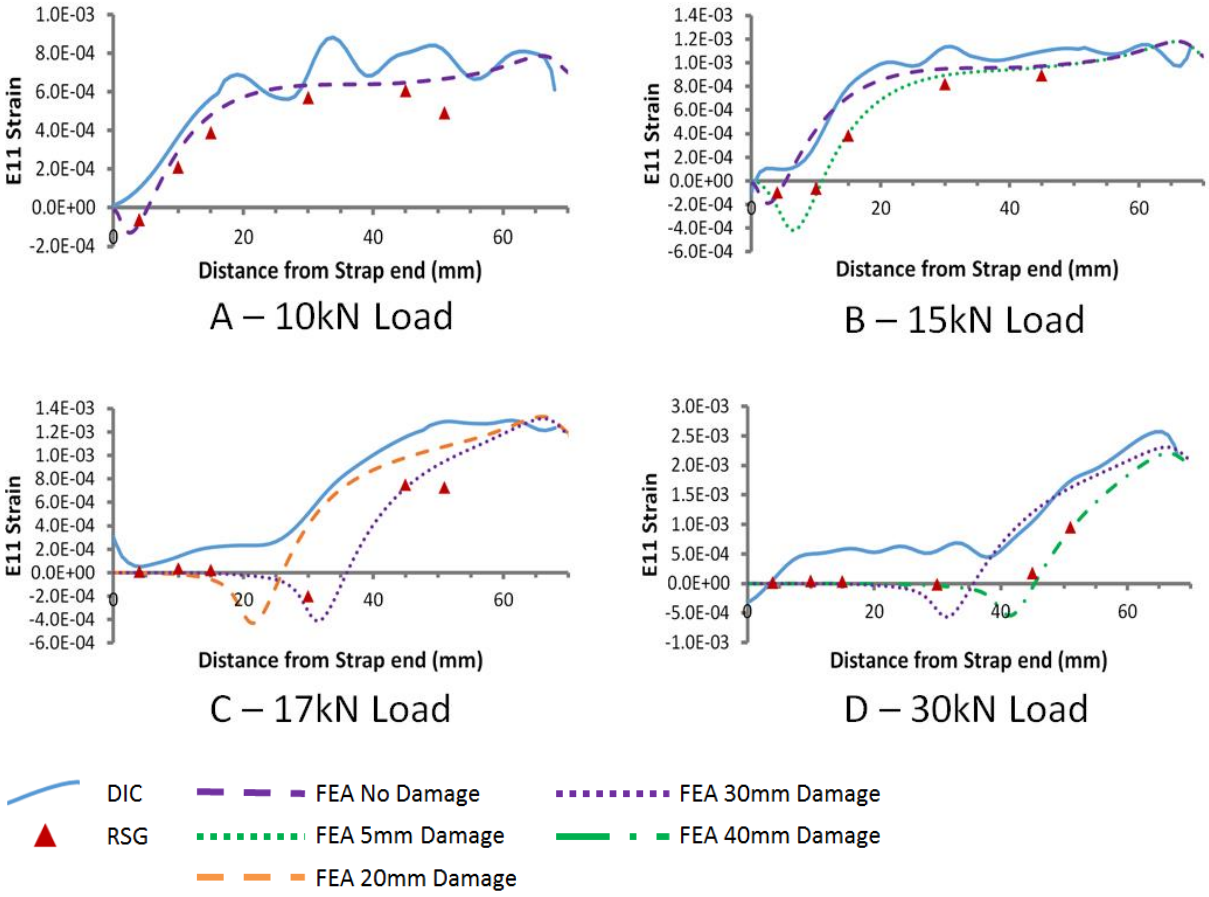

Figure 88: DIC measured E11 surface strains, at various tensile loads and degree of progressing disbond, along the centre-line on the strap of specimen 'Taper-4'

Figure 88A shows the DIC strap centre-line response prior to any non-linear response from the RSGs. Figure 88B is just after the first major drop in strain by several gauges, the most dramatic drop observed by gauge 2 (10mm). Figure 88C shows strains after a second major event observed by the in-situ sensors where strain drops are witnessed by the remaining RSGs, particularity gauge 3 (15mm) and gauge 4 (30mm) which rapidly fall to ≈0 strain. Figure 88D illustrates the DIC measures strains just prior to failure. Between C & D the remaining RSGs continue to suggest degradation, particularly gauge 5 (45mm) which at 30kN is reporting a strain value approaching zero. At the times when sudden strain drops are reported by the RSGs, particularly that by gauges 3 & 4 at approximately 17kN loading, a sudden progression of the low strain front is evident (in the case if the 17kN event a rapid movement of ≈20mm) from the DIC data.

Although both DIC and RSG responses suggest a progressing disbond there are disparities between numerical values reported by these approaches. The most prominent is an apparent positive shift is strain values reported via DIC. Not only is a shift relative to RSG values present but strain values also remain at a constant positive value where the bond-line appears to have failed and therefore no measurable strain should be present. This is clearest on Figure 88D where E11 strains plateau at ≈5.0 E-04 strain. The character of the DIC output is still useful to interpret the behaviour of the structure particularly when such considerations are recognised. If shifted 'downwards' values more closely concur with RSG values although some difference still remains. Potential reasons for such differences are speculated in Chapter 8 section 8.3.2. FEA curves attributed to upper and lower bound estimates of disbond length are been included on the DIC plots above.

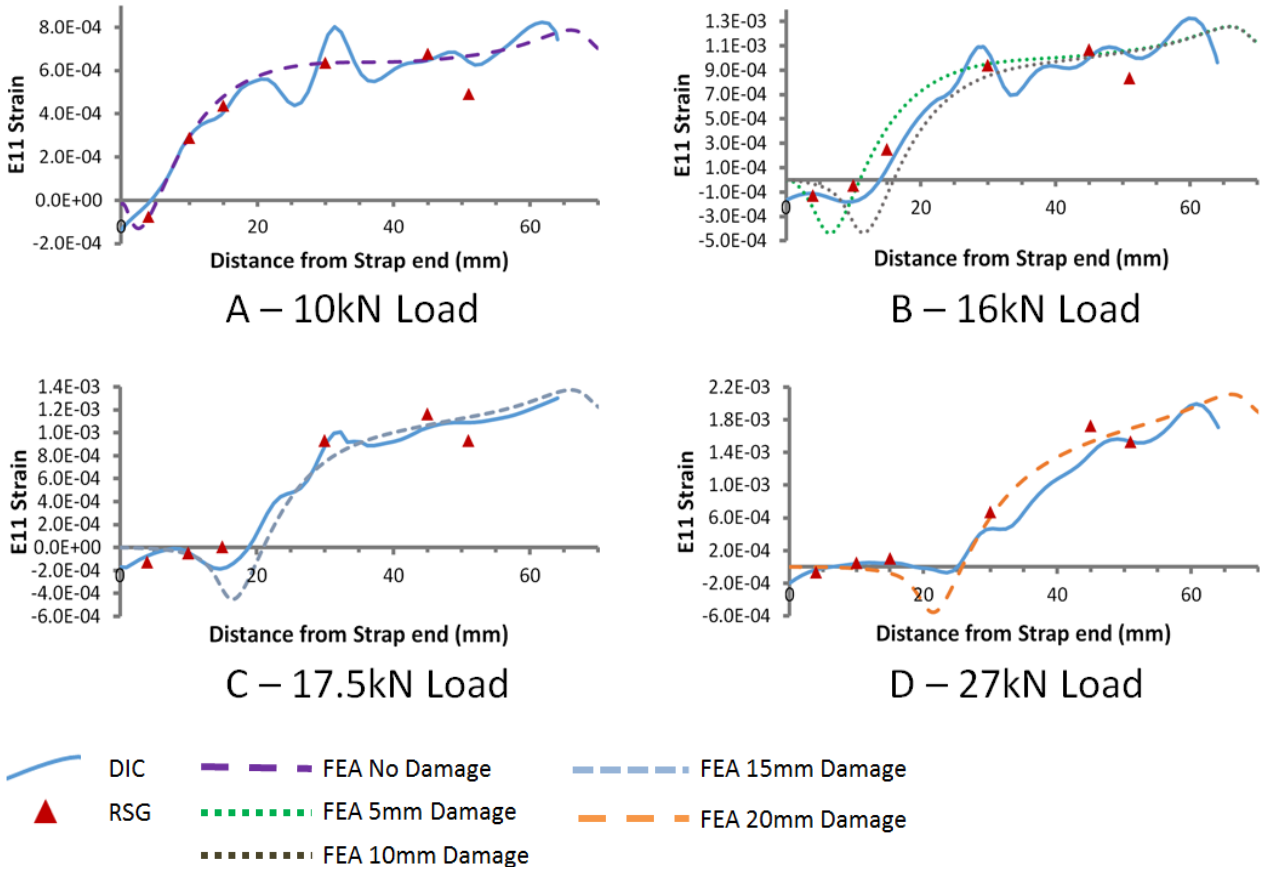

Figure 89: DIC measured E11 surface strains, at various tensile loads and degree of progressing disbond, along the centre-line on the strap of specimen 'Taper-5'

Figure 89 shows centre-line DIC strain values for specimen ‘Taper-5’. The various load cases presented were chosen due to significant responses recorded by the RSGs just prior to these loads (Figure 86). Figure 89B & C are the surface strains immediately after gauges 2 (10mm) and 3 (15mm) fail to zero strain (after a period of erratic strain reduction) respectively. Figure 89D shows the DIC recorded strain just prior to ultimate failure and after further signs of degradation by gauge 4 (30mm); although RSG values (G4-6) in this case do not reduce to zero prior to failure.

The rate of progression of the low strain front associated with damage again appears linked to the rate of fall in strain measured by the RSGs. As per the Tapered specimen 4 vertical drops in RSG measured strain occur as near instantaneous shifts in the low strain front are observed via DIC. The length of these sudden shifts associated with disbond growth are related to the magnitude of strain drop experienced by the RSGs relative to their position to the advancing disbond, i.e. the closer the RSG position to the disbond the larger the sudden drop in strain for a given sudden increase in disbond length.

A good correlation between DIC and RSG values, as well as the strain profile produced by FEA, is evident. It is however still difficult to determine the exact disbond length (within $\pm$5mm). Unlike the DIC results from specimen Taper-4 (Figure 88) which appeared to show a positive DIC strain output values in this test more closely match those provided by the strain gauges and show values close to zero once the advancing disbond has passed.

7.5.3 Visual Inspection

The tapered specimens were visually examined post testing to determine the failure modes. In each instance the joint plate at the monitored end was pulled from the straps which both remained bonded to the opposing plate (non-tapered and clamped as per Chapter 5; Figure 51). The images below (Figure 90 & Figure 91) show the bond face of both sides of the pulled out strap.

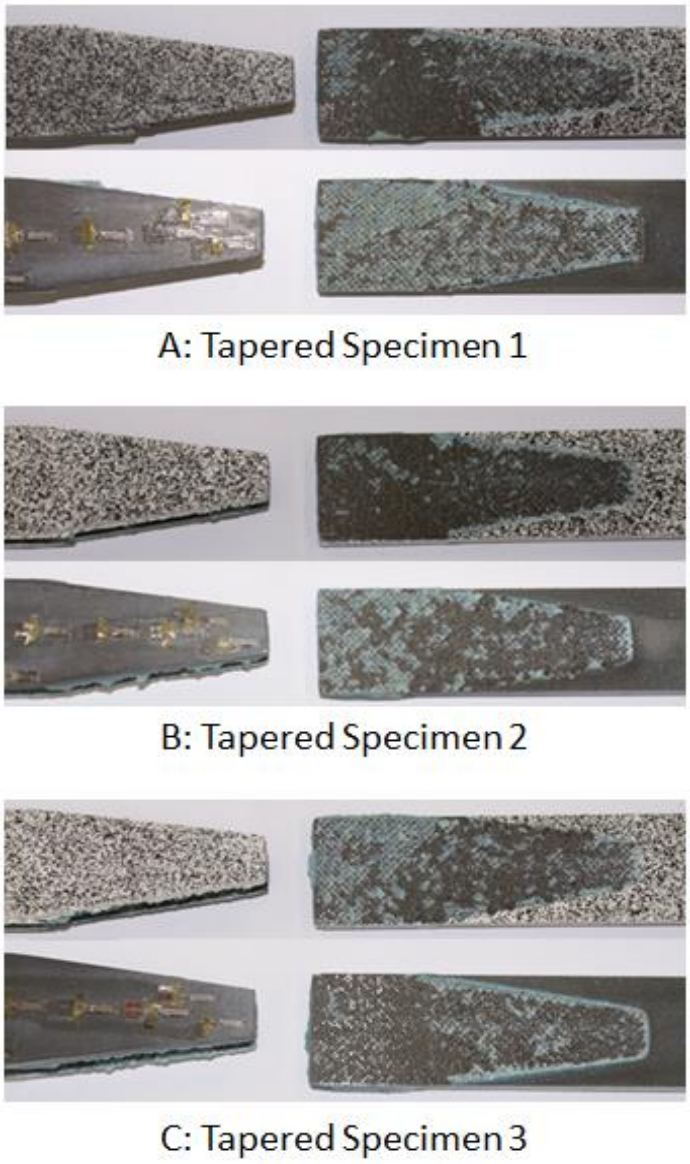

Figure 90: Visual inspection of the Tapered specimens which revealed a type slow, progressive surface strain response during tensile testing.

Tapered specimens 1-3 all exhibited a slow, progressive RSG response (Figure 82 - Figure 84). Further interrogation using DIC revealed a stable progression of the low/zero surface strain-front associated with an advancing disbond (Figure 87). Visual inspection revealed features associated primarily with adhesive type failure (large areas where the adhesive remains largely undamaged and is present on a single surface), however unlike previous tests evidence of cohesive failure (damage to the adhesive material itself) is also present. This is therefore defined as mixed adhesive/cohesive failure.

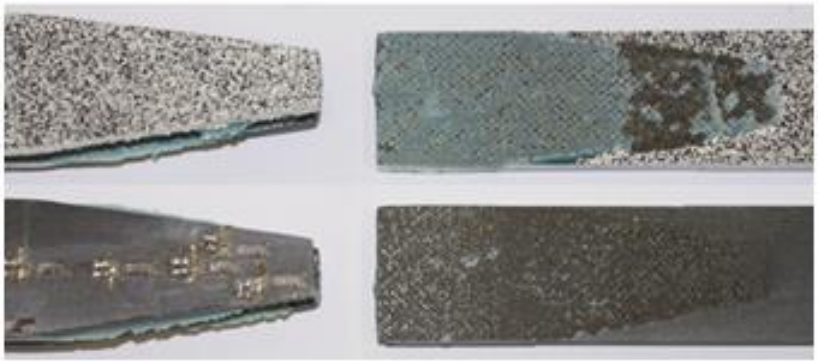

A: Tapered Specimen 4

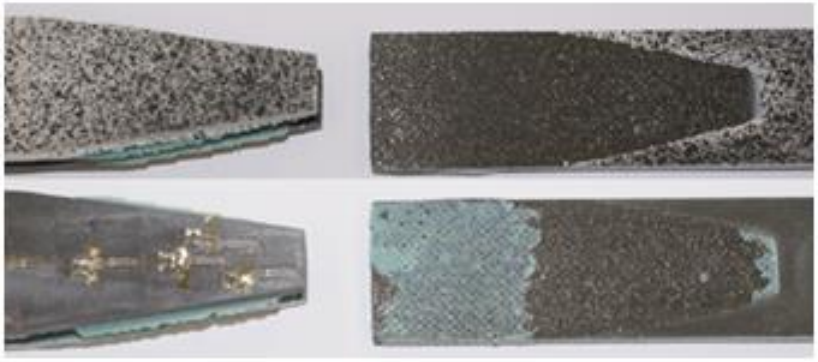

B: Tapered Specimen 5

Figure 91: Visual inspection of the Tapered specimens which revealed a rapid/arrested surface strain response during tensile testing.

Tapered specimens 4 & 5 presented erratic RSG responses with DIC revealing occasional rapid 'jumps' in the low surface strain front indicating rapid but temporarily arrested disbonds. These appeared to range from small millimetre scale events up to rapid disbonds up to approximately 20mm in length (Figure 88B to C). Post testing visual inspection revealed classic evidence of adhesive failure (Figure 91).

7.6 Section Summary/Discussion

7.6.1 Designed slow damage growth and compatibility of the SHM enabled design to damage tolerant operation

Chapter 6 identified that for SHM to enable more efficient bonded composite structure which is less reliant on additional fail-safe features to be viable, the opportunity to operate and manage such structure under a regime similar to that of damage-tolerance must be available. Structure which does not provide sufficient

time or residual properties to allow appropriate maintenance to be made cannot benefit from the inclusion of SHM. Tests on contemporary joint designs confirmed such degradation was uncommon with only a single specimen conforming to these requirements. The primary design goal within this chapter was to produce bonded structure that emulated this slow damage growth repeatedly, ideally regardless of the quality of the adhesive bond.

This goal has been achieved. The concept of 'strengthening' the joint as damage progresses has repeatedly produced the desired failure characteristics whilst providing an unambiguous response to damage via surface strain. Further comments are made in section 10.1 'Research discussion'. In addition when damage has been identified adequate residual properties have remained even though different failure modes and associated differences in joint quality and strength were observed.

Damage propagation was identified (RSGs and DIC) at loads of less than 50% of the joints ultimate capacity therefore offering ample residual strength for damage-tolerant operation. Surface sensors observed different characteristics for specimens which failed primarily via mixed mode adhesive/cohesive failure compared to those which failed via 'adhesive failure'. Both however provided adequate warning whilst significant residual strength remained, the tapered design retarding damage growth in each instance preventing catastrophic failure.

Areas of low or no adhesion associated with adhesive type failure bonds were identified by sudden shifts in a low surface strain front, these were however successfully arrested. It is recognised such a rapid disbond (region of low or zero adhesion) towards the later portion of the overlap may effectively shorten the region of controlled damage growth prior to catastrophic failure (e.g. specimen Taper 5). As such, as per damage-tolerant practice, damage should be repaired at the earliest convenient opportunity once identified. Even in this instance however damage initiation was identified at less than 50% of the joints ultimate failure load. Further considerations and potential approaches to allow implementation of this approach into aerospace structure are discussed in Chapter 9: Application.

7.6.2 Joint performance observations

The ultimate failure strengths of specimens Taper 1, 2 & 3 (50.5, 47.6 & 48.1kN respectfully) which produced smooth, progressive surface strain responses and via visual inspection showed a mixed adhesive/cohesive failure mode were approximately 168% of that of specimens Taper 4 & 5 (30.6 & 27.5kN) which failed showing classic visual indicators of adhesive failure. The tapered specimens generally performed better than the standard joints interrogated in chapter 6 with the exception of the 'slow damage growth' seen in the standard joint Specimen-6 which failed at 32.4kN (marginally greater than the tapered adhesive failures but lower than the mixed mode failure specimens above). This is likely due to improved manufacturing quality of the Taper batch. Even though different failure modes occurred, each influencing the static strength of the joint, identifiable damage and progressive damage growth was present.

7.6.3 Relative design strength and knock-down factors

Further interrogation of FEA models regarding the suggested knockdown factor against the standard full-width geometry were made by considering the transition from elastic to plastic behaviour of the adhesive. Figure 92 - Figure 95 illustrate the onset and progression of plastic strain within the adhesive bond-line at the strap end of the tapered specimens. Dark blue = zero plastic strain in each case. The figures show the onset of plastic deformation just prior to 15kN of loading. This therefore defines the DLL for this joint during standard operation. The estimated DLL of the standard joint, based on 'knee' values of the adhesive shear stress curve, the Hart-Smith approach and consideration of plasticity was 17.1kN. Considering the suggested knockdown this suggests a DLL for this configuration of 17.1 x 0.78 = 13.3kN with a corresponding DUL (DLL x 1.5) of 20kN. This shows good agreement with the FEA investigation. The elevated values seen at the corner or the adhesive-adherend interface should again be considered with caution due to unrealistic stress raisers created by the sharp corners in the CAD geometry. Even though the specimens in these tests all revealed evidence of adhesive type failure all showed evidence of damage initiation near or above the suggested DLL and ultimately failed at loads higher than the proposed structural DUL.

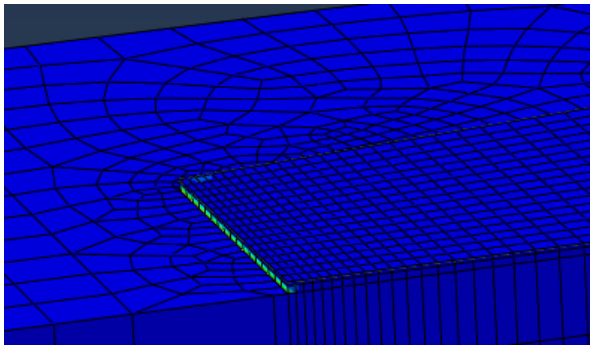

Figure 92: 10kN Loading; Zero/minimal evidence of adhesive plastic behaviour

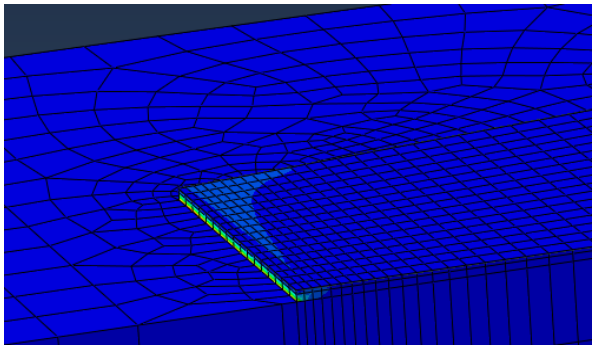

Figure 93: 15kN Loading; Evidence of onset of adhesive plastic behaviour

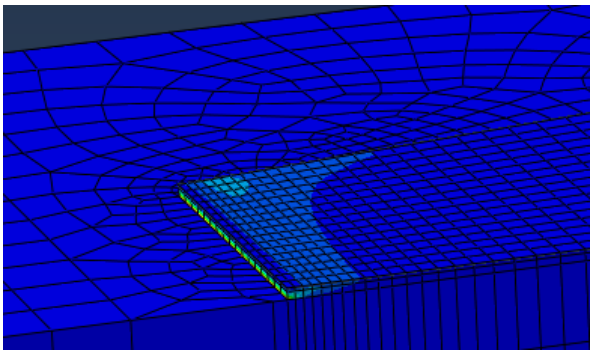

Figure 94: 20kN Loading; Defined adhesive plastic behaviour

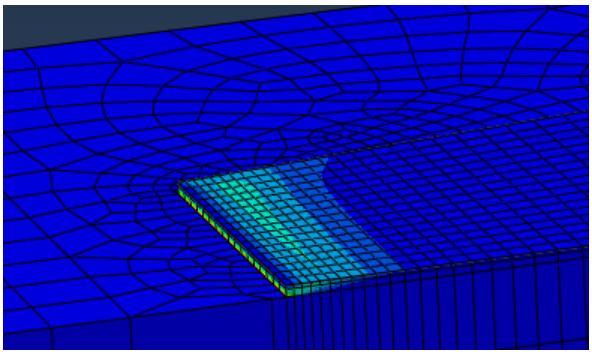

Figure 95: 30kN Loading; Progression of adhesive plastic behaviour

7.6.4 Comparison to Damage growth concept

Theorised strength increases based on the required increases in load to raise the shear strains to those experience at damage initiation as the disbond progresses (based on simple FEA) have been compared to the loads supported by the joints with estimated disbond lengths relative to the load estimated to have initiated damage. It appears the effective strength increase regulating damage propagation maybe more directly associated to the increase in effective strap width as the effective overlap shortens than the simplified adaptation of the maximum shear strain approach proposed. This may be due to the bond-line failing predominately at the adhesive/adherend interface rather than cohesively within the adhesive where the comparative shear strain values were measured. In addition the maximum strain

approach assumes a material property and may therefore be more suited to structural failure of the adhesive (cohesive failure) than that due to poor adhesion (adhesive failure). If this is the case the design approach is still sound as the effective rate of strength increase as disbond length increases is greater if the increase in width is the predominate consideration rather than the direct consideration of shear strain. If both damage progression models are relevant to different failure modes operation under an approach such as that discussed in 'Chapter 9; Application' may still be possible.

As previously discussed the load at damage initiation and the precise disbond length for a given load are difficult to establish from the data available. Exact disbond lengths are problematic to quantify due to difficulties in making direct observations. Comparisons of the surface strain monitoring methods and FEA predictions for surface strains at various disbond lengths have been made. If it is assumed that prior to the deviation of the linear surface strain response to increasing load (RSGs), and similarly the shift in the surface low strain front observed via DIC, that no damage has occurred a relative datum linking the surface strain to the bond-line length may be assumed. It is possible however the nature of this datum may be different for an undamaged joint and for one containing a disbond. Marginal differences between the DIC and RSG data are also evident. These may be related to the differences in disbond length on each of the double strap monitored by the different methods and/or the resolution of the monitoring approaches, most likely the non-contact DIC. In addition even though DIC images show a reasonably even and perpendicular disbond leading edge any deviation from this may make determining the precise disbond length more difficult. Either way highly accurate determination (within a range of several millimetres) of the disbond length cannot be made with the current data.

Accuracy to within such tolerances may not be required for SHM enabled designs to operate as long as damage can be positively identified whilst a guaranteed degree of residual strength remains however a better understanding of the response to specific damage will assist further development and design.

7.6.5 Continued development

It has been shown the proposed SHM enabled structural joint design can produce both measurand that can be linked to bond-line damage and the required damage growth characteristics required to make such monitoring meaningful, i.e. the ability to operate the structure within an inspection (via SHM) and maintenance regime.

Different, but recognisable behaviours have been shown for both mixed adhesive/cohesive bond-line failure and adhesive bond-line failure. The short but rapid disbonds observed on the specimens that failed with pure adhesive failure – although possibly undesirable in a structural sense – do provide highly recognisable responses suitable for monitoring and diagnostic purposes. Disbonds which appear to rapidly track over several millimetres and therefore produce significant drops in RSG measured strain are particularly recognisable. If such defined signals could be associated with known disbond sizes this could form part of a simple diagnostic method which may with other information be used to produce a useful structural diagnosis or alternatively aid analysis of data produced with the specimens used in this chapter.

The next stage of investigation attempts to deliberately include structural features and sensing which may allow damage sizes to be more positively defined by deliberately reproducing the responses discussed at known locations within the bond-line.

8 Testing, Results and Analysis: Partitioned Double Strap Joints

8.1 Section Introduction

The investigation made in chapter 7 revealed bonded composite joints can be designed to promote slow or arrested disbond growth and such growth may be identified by simple in-situ strain sensors while significant residual joint strength remains. Such behaviour may ultimately allow bonded structure in aerospace applications to be operated under a regime similar to that of damage tolerance, i.e. inspection (via SHM) and timely maintenance. Furthermore, by eliminating the uncertainty associated with such structures condition, the reliance on additional features (which add mass but provide no increase in operational performance) to ensure airworthiness may be reduced or eliminated allowing more efficient structures to be operated with no reduction in airworthiness.

The specimens tested and analysed in Chapter 7 revealed qualitative responses to damage growth. Although estimates regarding damage size were made, the exact disbond sizes are difficult to determine. Such information may not only aid analysis and design but if available with actual structure may provide easily identified and predetermined thresholds. Crossing such positive thresholds may trigger maintenance actions and eliminate 'no-fault-found' actions potentially resulting from more ambiguous responses. This chapter attempts to introduce features within the tapered strap design which promote highly defined responses, mimicking those associated with specimens that failed via adhesive failure in Chapter 7 (specimens Taper 4 & 5). The near instantaneous strain drops recorded by the in-situ RSGs (Chapter 7; Figure 85 & Figure 86) and the rapid shifts in the low strain region captured via DIC (Chapter 7; Figure 88 & Figure 89) are associated with rapid arrested disbonds progressing over short distances. If features could be included at known locations which display this characteristic in a controlled manner direct links between recorded surface strain responses and known disbond lengths may be made.

8.1.1 Structural Response to Damage with Bond-line Partitions

In order to test this concept joint designs which include strategically placed bond-line gaps or partitions were manufactured and tested in an attempt to promote unambiguous responses/signals as discussed above. It is proposed that as a growing disbond propagates into the joint from the strap-end it will encounter a partition. As a result the disbond length with effectively instantly increase by the length of the partition. The disbond may be fully or partially retarded by the bond beyond the partition; which should experience less stress and strain due to the marginally increased width provided by the taper. As seen in the non-partitioned tapered specimens that exhibited short, rapid disbond events such behaviour should result in rapid and significant drops in strain recorded by the surface mounted RSGs. If such strain drops are observed, and these can be associated with the deliberately placed partitions at known locations, improved estimates regarding the size of the disbond may be made. Such information may aid design and analysis of non-partitioned SHM enable joints or may potentially be included within in-service structure to aid diagnosis and potentially prognosis of bonded structure.

8.2 Bonded Joint Design

Consideration of the size and locations of bond-line partitions was required to ensure the structure could be manufactured in the facilities available (including RSG placement), appropriate responses to damage may be expected, and only minimal influence on the potential performance of the joint was introduced. Factors which may influence these issues are identified and addressed in this section.

Manufacture of the test specimens was identical to previous test structure with the addition of partitions within the bond-line. A minor amendment was a light sanding of the areas to be bonded in an attempt to remove high resin peaks resulting from the texture of the peal ply as this has been reported to potentially weaken the adhesive bond [135]. It was noticed however that this produced a white powder – epoxy powder – (the previous references does recognise the requirement for clean, non-contaminated surfaces). Although care was taken to eliminate this some remained potentially contaminating the bonding surface. Further comments regarding this and other potential manufacturing issues are included in section 8.2.6.3.

8.2.1 Adhesive partition design considerations

Identical tapered strap dimensions as those considered in the previous chapter were to be used in this investigation. The size and form of the bond-line partitions was determined by tests designed to identify issues associated with adhesive bridging the partition gaps as well as any other bonding issues. As such adherend material and dimensions was not required to be identical to the structural joint specimens and the specimens were not subjected to tensile loading.

8.2.1.1 Partition Investigation

Test specimens were produced using glass fibre reinforced plastic (GFRP). The transparent/translucent nature of this material allowed the influence of the included partitions on the flow of adhesive and any effects of non-wetted bond surfaces to be visually analysed. The similar matrix materials (epoxy) of the GFRP test specimens and the CFRP joints, as well as comparable surface finishes of the two materials, should influence the adhesive in an identical manner in each case.

To eliminate or reduce the partitions being ‘bridged’ by flowing adhesive (which may also remove adhesive from the bonded areas) a ‘filler’ material was used. Polytetrafluoroethylene (PTFE) tape was selected as this would not influence the bond, could be used at the temperatures required to cure the FM-94 adhesive and was convenient for use in manufacture (thickness, availability, ease of use). The PTFE used was in the form of adherent tape.

8.2.1.2 Bond-line Partition test Specimens

Tests were conducted on 25x100mm specimens bonded with FM-94 film adhesive, each containing three partitions 12.5mm wide. Figure 96-upper shows a photograph of a bond-line partition test specimen prior to curing the adhesive. The contrast between the adhesive and the partitions (in this instance containing PTFE tape) can be clearly seen. The boundaries between these regions are marked to help identify any flow of adhesive during curing. Figure 96-lower shows a schematic of the specimen, the hashed regions showing adhesive and the plain regions the partitions.

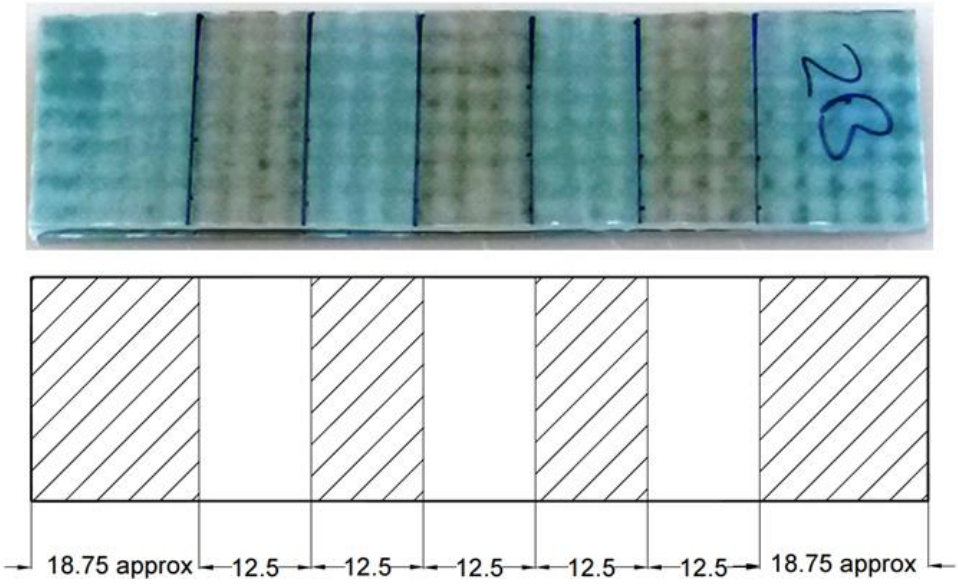

Figure 96: Bond-line partition test specimen

The PTFE tape had a measured thickness of 0.1mm and contained adhesive on one side. The FM-94 film adhesive contained a 0.25mm carrier film which may help determine the bond-line thickness; however inspection of previous specimens prior to destructive testing revealed cured bond-line thickness of approximately 0.3mm. Bond thicknesses of the partition specimens were measured after manufacture. The measured thickness of the uncured film adhesive was 0.28mm.

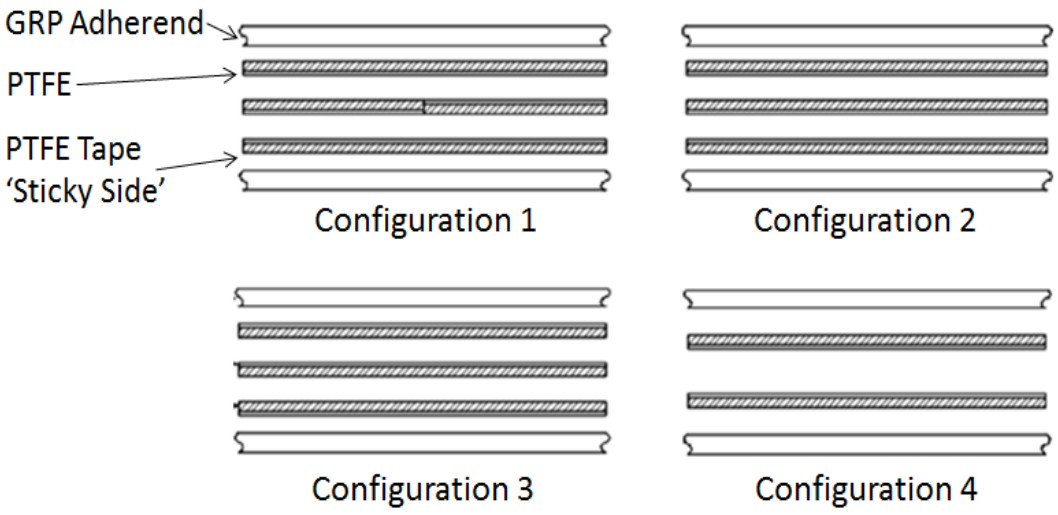

Figure 97: PTFE tape configurations (not to scale) used to fill the bond-line partitions

To assess any effects of PTFE thickness within the bond, as well as establishing if the adhesive surface of the PTFE tape influenced adhesive flow, configurations of

three (0.3mm nominal thickness) and two layers (0.2mm nominal thickness) of PTFE tape were assessed (Figure 97). In addition samples were also produced with no PTFE filler within the partition sections for comparison.

8.2.1.3 Partition investigation Test Results

Two specimens were produced for each partition type (three configurations containing three tapes, one with two tapes and a final 'configuration' containing no PTFE filler material). The specimens were designated as follows:

- AD-1A & AD-1B Configuration 1 (3 Layers)
- AD-2A & AD-2B Configuration 2 (3 Layers)
- AD-3A & AD-3B Configuration 3 (3 Layers)
- AD-4A & AD-4B Configuration 4 (2 Layers)
- AD-5A & AD-5B No PTFE filler

Photographic images from macroscopic inspections and comments on the effects of the various arrangements are presented below.

Filler configurations 1, 2 and 3 – 3 PTFE layers

Bond-line partition configurations 1, 2 & 3 are presented together as these each showed similar features when visually inspected.

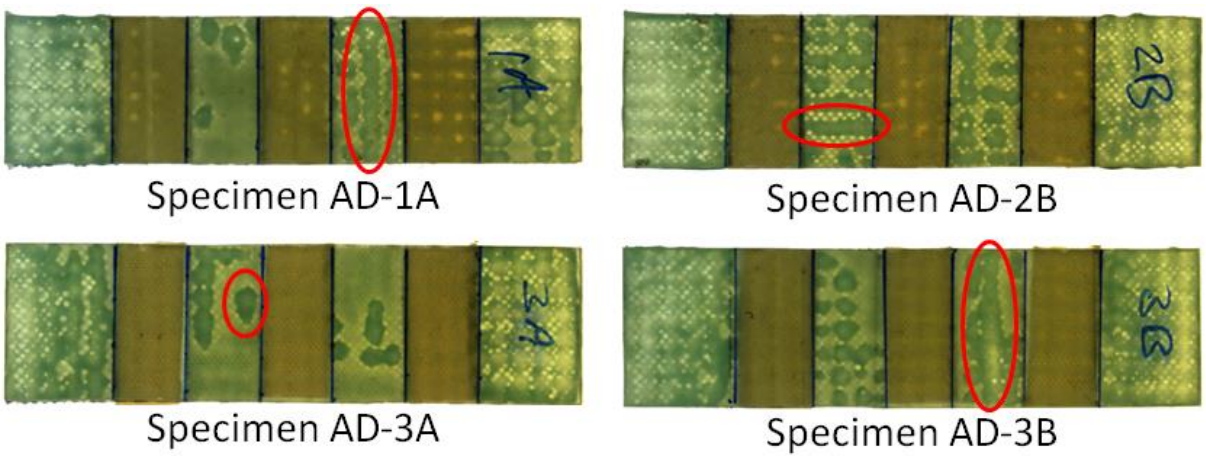

Figure 98: Selection of backlit images of specimens containing three layers of PTFE tape with some areas of successfully wetted bonded surface highlighted

Figure 98 shows a selection of the specimens containing three layers of PTFE tape. The darker PTFE partition sections appear reasonably uniform in colour, indicating

little or no progression of the flowing adhesive into these regions. The lighter, green sections are those containing adhesive. The backlit images above show darker regions – a small portion of which have been highlighted – which show areas where the adhesive has successfully wetted the adherend surface. The majority of the bonded regions (particularly the centre sections with partitions on either side) appear not to have bonded well. This may be a result of the thick (≈0.3mm) partition filler preventing appropriate pressure to be applied to these regions.

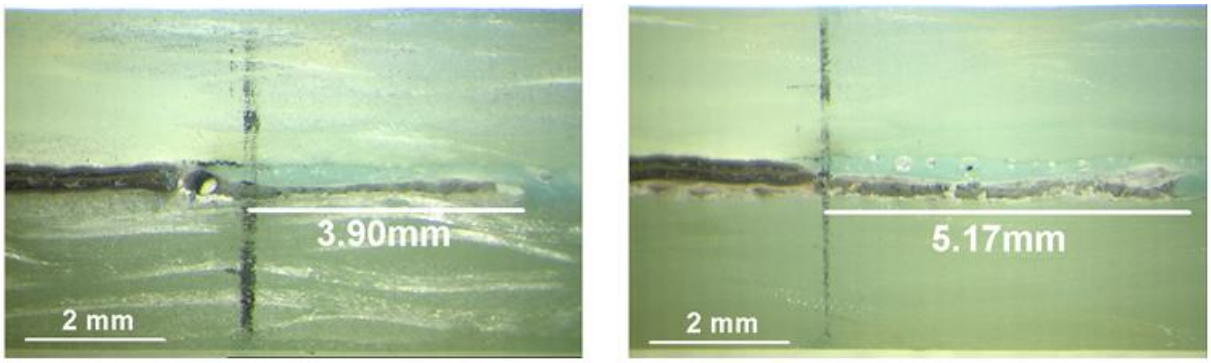

Figure 99: Side view of two partitions / adhesive sections at the centreline of bond-line partition specimen AD-3B.

To ensure analysis of the specimens via backlighting was correct several specimens were cut along their centreline so the bond-line could be observed directly. Findings were as expected. Figure 99 shows two regions of specimen AD-3B (configuration 3) where a PTFE filled partition (to the left of each image) borders an adhesive region. Large areas – 5.17mm on the right hand image, over half the width of the adhesive section – can be seen not to have bonded to one adherend surface.

Filler configurations 4 – 2 PTFE layers

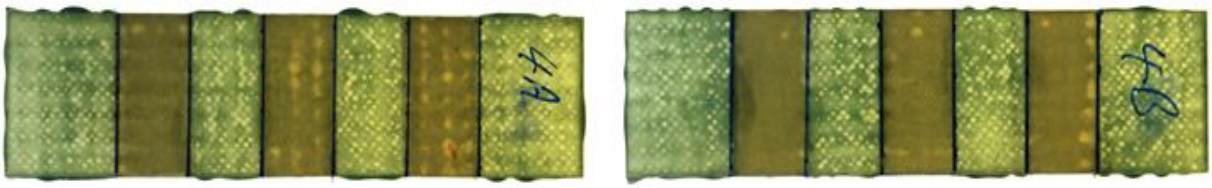

Figure 100: Backlit images of specimens containing two layers (0.2mm) of PTFE filler

Figure 100 presents backlit images of the specimens with partitions containing two PTFE layers (configuration 4). The bonded areas appear more consistent than in

those containing three layers of filler. Adhesive has also been squeezed from the sides of these sections. Both observations suggest the entire surface is in contact with the adhesive. No adhesive appears to have flowed into the partitioned areas.

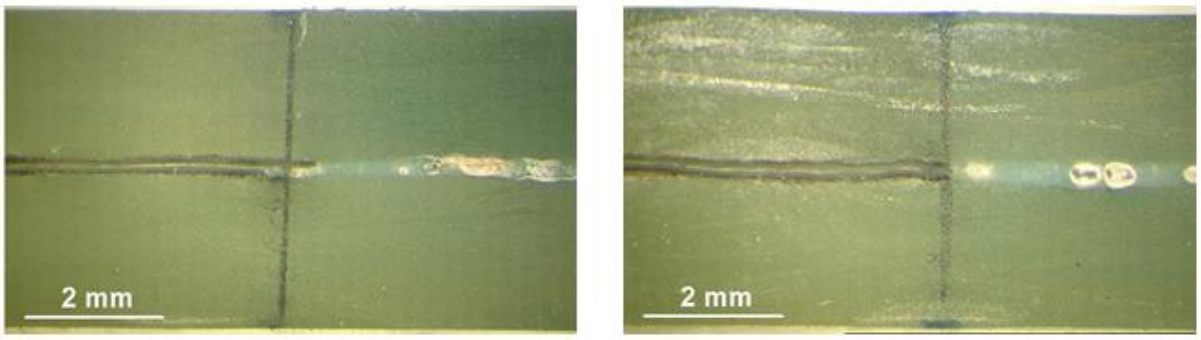

Figure 101: Side view of two partitions / adhesive interfaces at the centreline of bond-line partition specimens AD-4A (left) and AD-4B (right).

Figure 101 shows examples of the partition-adhesive interfaces at the centrelines of the specimens shown in Figure 100. A defined transition between the partition sections (left side of above images) to the bonded regions, with no adhesive flow into the partitions, is evident.

Control – no partition filler material

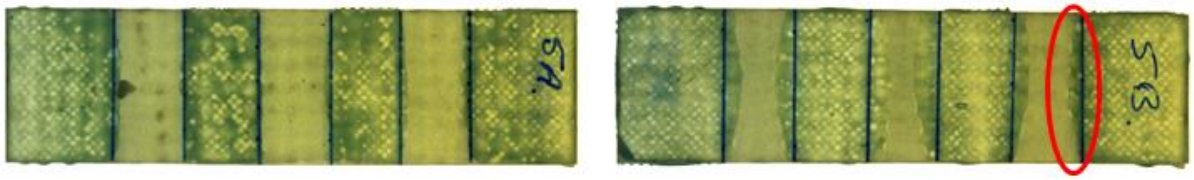

Figure 102: Backlit images of specimens containing no partition filler

Figure 102 shows backlit images of the specimens containing no PTFE filler in the partition sections. The contrast within the bonded sections appears relatively consistent and a small quantity of adhesive has again been squeezed from the sides of these sections. These observations again suggest the adhesive regions are fully wetted and potentially adhered. Adhesive flow into the partition areas can however been seen at each adhesive-partition interface. This is particularly evident in specimen AD-5B (Figure 102–Right) where an example is highlighted however adhesive flow can be seen in each control specimen.

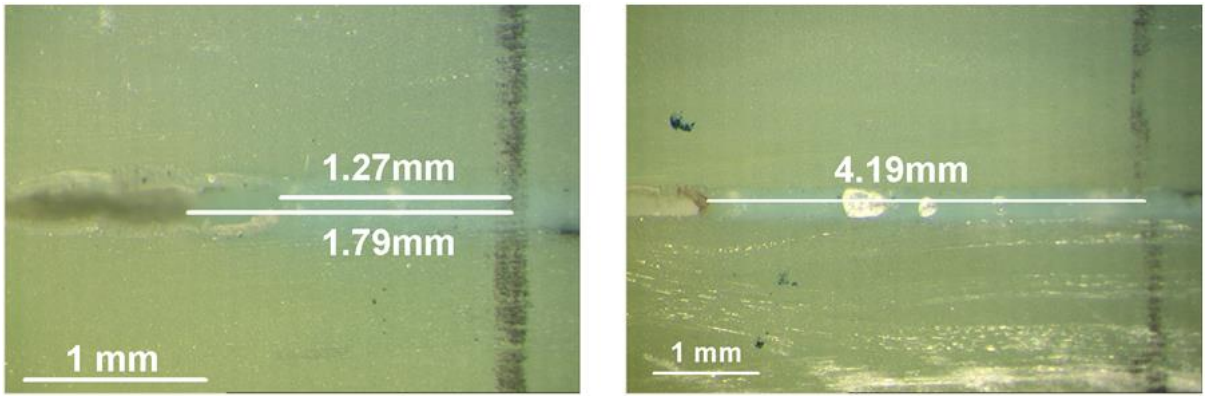

Figure 103: Side view of two partitions / adhesive interfaces at the centreline of bond-line partition specimens AD-5A (left) and AD-5B (right).

Figure 103 shows examples of the adhesive flow into the non-filled partitions left of the pencil lines in the images above. Significant flow can be seen particularly in AD-5B where a flow greater than 4mm can be seen. As such if similar flow progresses from the opposing side of the partitions the 10mm gaps used in these cases may be bridged.

8.2.1.4 Test summary/Discussion

The above test revealed that for use with the FM-94 film adhesive the inclusion of three layers of PTFE filler (0.3mm thickness) created bonding issues in the adjacent adhesive sections. This was likely due to the thickness of the PTFE being marginally greater than that of the uncured film adhesive and as such preventing sufficient pressure to be applied during curing. This approach was therefore unsuitable. The specimens with partitions containing no filler showed adhesive would naturally flow into the unfilled partitions and, particularly if the partition widths were reduced, may bridge these spaces. The specimens with two layers of PTFE showed no significant evidence of either the adhesive flowing into the partitioned sections or poor bonded regions due to the presence of the filler material. As such this configuration was used. The presence of the adhesive on the PTFE film appeared to have little influence of the effectiveness of the filled partitions.

Further visual examination of the bond-lines within all specimens revealed significant variation in bond-line thickness. Post-cured bond thicknesses from 0.16 to >0.5mm were measured highlighting the variability that may be expected when bonding

composite structures (associated with difficulties producing precise, flat surfaces). As bond-line thickness can affect joint performance such variability may influence the properties of in-service joints. The majority of bond thicknesses within these tests however were in the range of 0.24-0.3mm. Some small voids were also noted. Such voids may further influence bond performance.

Although the partitions in the partition investigation test specimens were 10mm wide maximise the available bonding surface and minimise the influence of the partitions on raising levels of localised stress-strain (see section 8.2.2) it is desirable to reduce this size. Ease of manufacture lead to a decision to make partitions 5mm wide. PTFE tape could be conveniently cut into appropriate strips by using the tacky surface to lightly adhere the tape to the edge of a clean 5mm thick metal plate allowing the tape to be accurately trimmed. The 5mm gaps in the adhesive should be adequate to prevent any adhesive bridging and also produce positive, identifiable surface strain responses when interacting with an advancing disbond.

8.2.2 FEA: Appropriate adhesive partition placement

As discussed in Chapter 4; section 4.5 large flaws or gaps within the bond-line may exist without significantly affecting the shear stress distribution within the adhesive. If however such gaps are present close to the joint edges – where stress-strain values rise to maximum values – values in the thin region between the gap and the joint edge may increase significantly. If partitions are to be included as part of in-service SHM enabled joints such factors must be considered to reduce any impact of including these features. FEA was used to investigate the influence of partitions on the maximum stresses and strains experienced at the joint end. The studies shown below consider a single 5mm partition at different locations along the bond-line. Although some influence may be introduced by the presence of a second partition as this will be positioned further within the overlap, and therefore in a region experiencing lower levels of stress-strain, any additional affect should be of low significance.

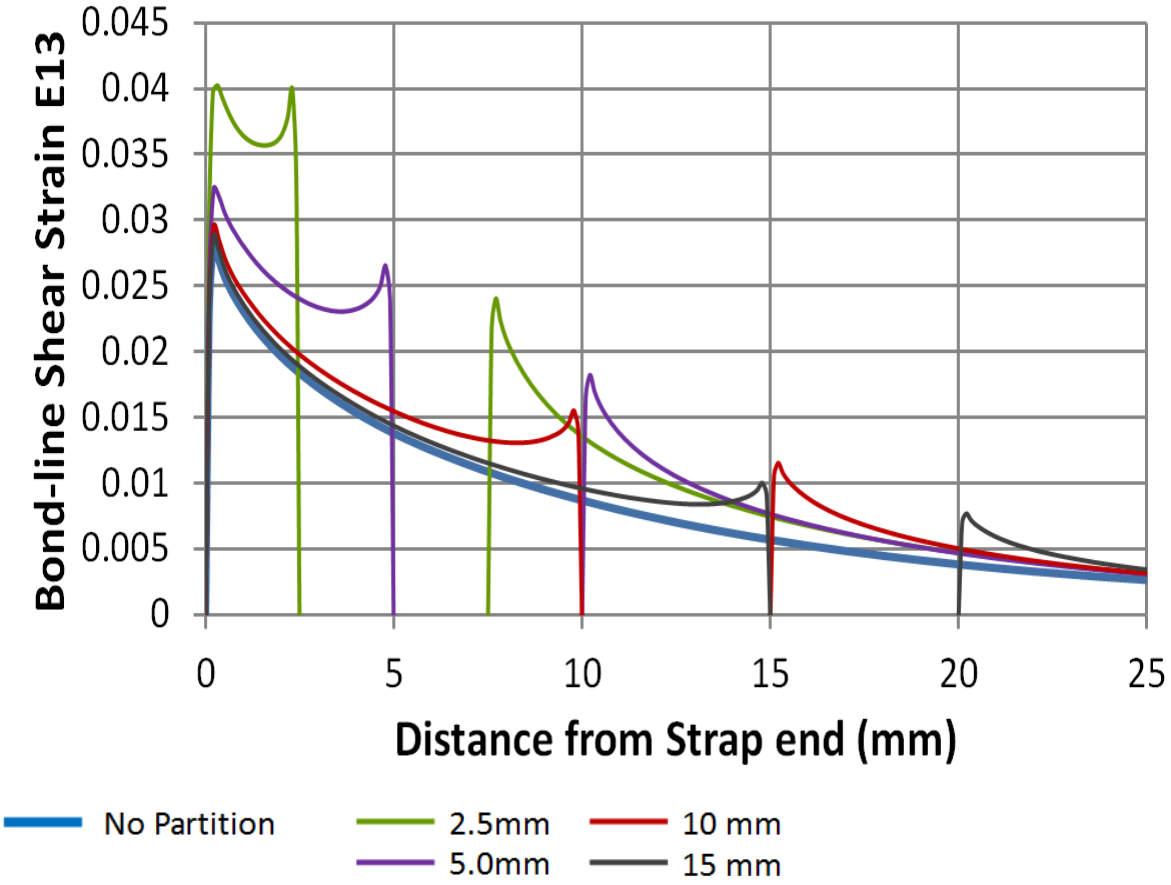

Figure 104: FEA Analysis: Influence on E13 shear strain in the adhesive by the presence of 5mm partitions at various locations within the bond-line at 10kN loading

Figure 104 compares the FEA calculated shear strain (E13) within the adhesive bond (centre-line mid-plane) for a tapered joint – subjected to 10kN loading – containing no partitions (Blue) against tapered joints containing 5mm wide bond-line partitions positioned at various locations within the bond. The measurements stated within the key describe the distance from the strap-end to the start of the relevant partition. At partition locations the strains in Figure 104 are seen to be zero.

The maximum strains (at. distance ≈ zero) are seen to only marginally increase when partitions are included well into the bond overlap. Those placed closer to the strap end can be seen to significantly increase the magnitude of peek shear strain.

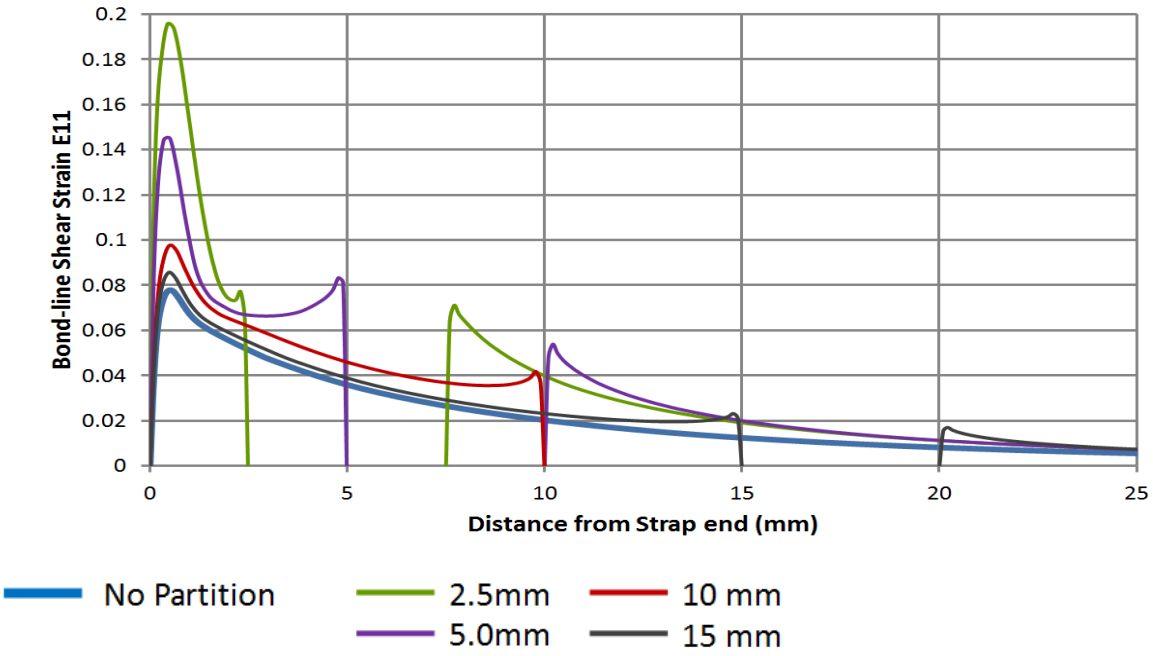

Figure 105: FEA Analysis: Influence on E13 shear strain in the adhesive by the presence of 5mm partitions at various locations within the bond-line at 20kN loading

Figure 105 shows bond shear strain at 20kN load (DUL for the tapered design). Although the influence is still low for partitions further into the overlap (e.g. 10 or 15mm from the strap end) closer partitions which displace greater levels of strain to their adjacent adhesive sections increase the maximum values considerably. The maximum E13 value calculated when a partition is included at 2.5mm from the strap end is more than double that for a joint containing no partitions.

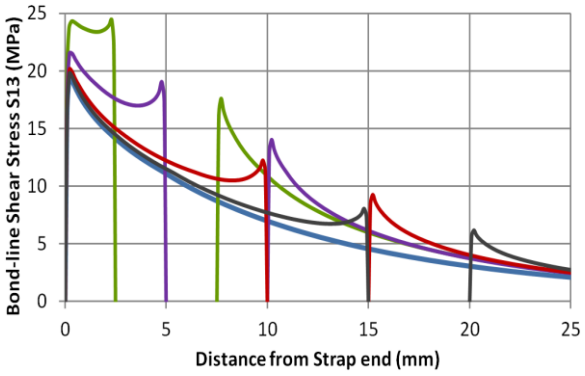

Figure 106: Bond-line shear stress with various partitions at 10kN load

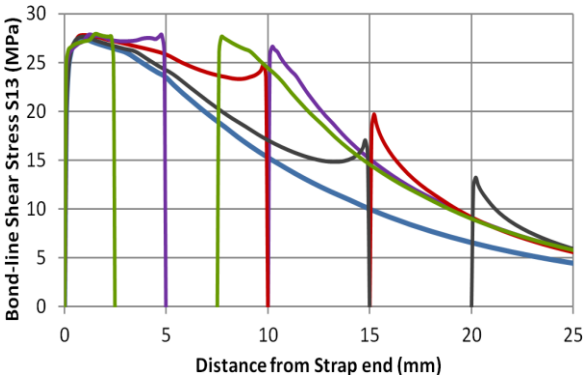

Figure 107: Bond-line shear stress with various partitions at 20kN load

Figure 106 & Figure 107 compare FEA calculated shear stresses at the mid-plane centreline of the bond-line with 5mm partitions placed at various locations subjected to 10 and 20kN loads respectively. The shear-stress distributions at 10kN appear similar to the shear-strain responses for the same load (Figure 104) as the adhesive is working within its elastic range (below DLL). Figure 107 – which displays the joints at DUL – reveals plateaued shear stress values within the first adhesive sections of the joints containing partitions 2.5 and 5mm from the strap end. This reveals plastic deformation and potential permanent damage. In the case of the partition placed 2.5mm from the strap end the shear-stress in the next adhesive section (starting at 7.5mm) is also elevated to the value required to cause plastic deformation. In the case of partition placement 10mm from the strap end (or further into the overlap) although shear-stress is raised over the first adhesive section only the adhesive towards the strap edge is deforming plastically and therefore subjected to permanent degradation, similar to that of the non-partitioned structure.

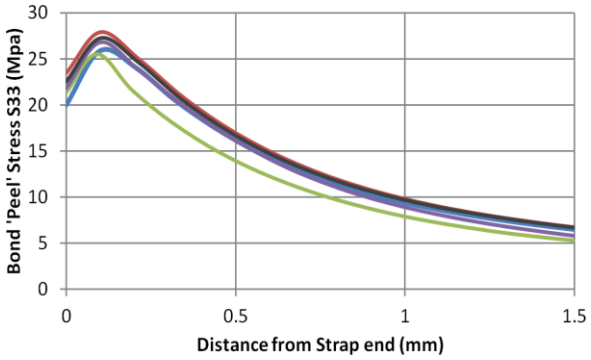

Figure 108: Bond-line 'Peel' stress with various partitions at 10kN load

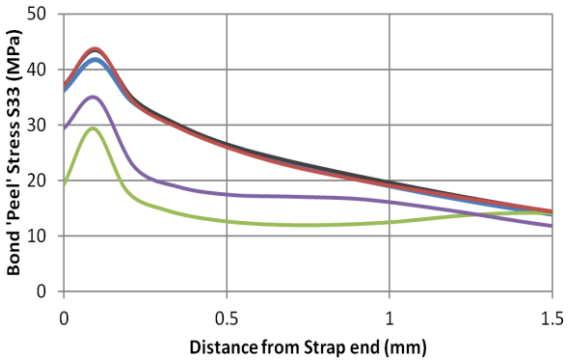

Figure 109: Bond-line 'Peel' stress with various partitions at 20kN load

Figure 108 & Figure 109 show the influence of the differing partition placements on peak adhesive peel stresses (centreline mid-plane within the first 1.5mm of the overlap) at 10 & 20kN respectively. Similar results can be seen for each partition configuration. Some shear-stress relief is however evident when partitions are placed close to the strap edge (i.e. 2.5 & 5mm) as the effects of peel are partially shared with the next adhesive section.

8.2.3 Partitioned Joint Design

By considering the investigations above 5mm partitions were selected separating both the strap ends and adjacent adhesive sections by 10mm. FEA suggested 5mm partitions at this position provide a reasonable compromise when compared to other configurations and the non-partitioned tapered design. Maximum shear-strain values are only marginally increased at expected normal operational loads (10kN - Figure 104). Shear-strains were increased by ≈20% compared to the non-partitioned geometry at the proposed DUL (20kN - Figure 105). Loading to this value however should not routinely occur and sufficient additional shear-strain capability should still be available, at least in non-degraded structure. This is due to the DUL value being based on 1.5x the load required to initiate plastic deformation of the adhesive not the adhesives maximum theoretical shear strain capability. In this configuration plastic deformation is not present across the entire first adhesive section at DUL meaning even if some permanent damage does occur due to overload (>DLL) the majority of the initial adhesive section should remain unaffected, as should the bond beyond this partition. Influence from through thickness (Peel) loading also appears comparable with the non-tapered design. These considerations should ensure critical strains are not simultaneously exceeded in adjacent bond sections, preventing a fast failure mechanism, as well as ensuring local strains are not significantly increased therefore lowering the joint design strength.

Two partitions were included in this investigation and are presented in Figure 110.

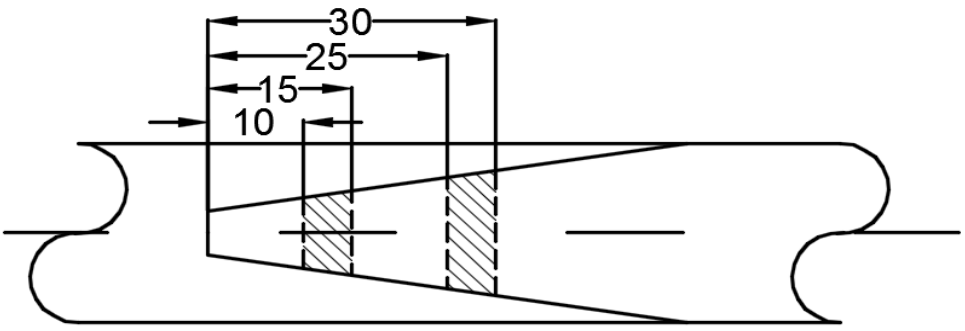

Figure 110: Location of the 5mm bond-line partitions within the tapered joint

Although these partitions are equally spaced the number, size and locations of partitions, may be tailored to suite the SHM enabled joints specific requirements.

8.2.4 FEA comparison of surface strain responses of partitioned and non-partitioned tapered joint specimens

Figure 111 plots FEA calculated surface E11 strain responses of tapered joints containing no partitions, a single 5mm partition the front edge located 10mm from the strap end, and with two partitions the second located 25mm from the strap edge as per Figure 110. Minor differences are present; however these are no larger than variabilities that may be expected when monitoring real structure. As such similar surface strain responses to damage are also likely regardless of the inclusion of partitions. As a result any data gained from tests including partitions may be comparable with previous studies of non-partitioned tapered test specimens.

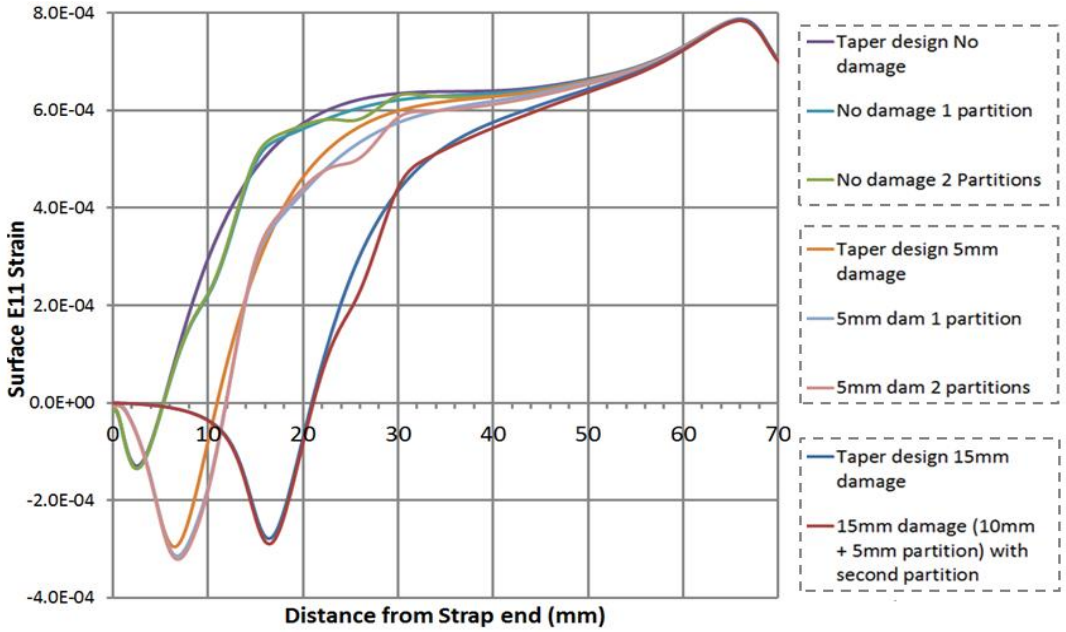

Figure 111: Comparison of FEA generated surface strain response (10kN Loading) of specimens containing zero, one or two bond-line partitions

8.2.5 Strain Gauge Array

Figure 112 shows the locations of the RSGs on the partitioned-tapered specimens. As in the previous study the gauges are designated numbers starting from the end of the overlap, i.e. G1 (9mm), G2 (16mm) …. G6 (65mm). The positions of Gauges G1-4 were selected so their entire gauge length (2mm) was above the edge of the adhesive sections adjacent to the bond partitions. It was reasoned this placement should provide strong responses as each adhesive section failed and the disbond

rapidly advanced the additional 5mm of the partition. Gauge G5 (40mm) is placed at the edge of the originally proposed limit of potential slow or arrested damage growth (Chapter 7). Gauge G6 (65mm) is in an area not expected to show any significant relative change in strain as disbonds initiate and progress. Strain values from this may be compared against those in the regions expected to show slow growth.

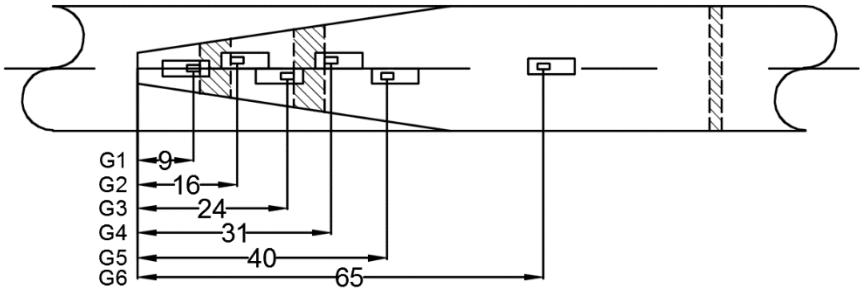

Figure 112: RSG positions used with the partitioned tapered geometry joints

8.2.6 Partitioned joint testing: Results

The partitioned joint specimens were tested in the same manner as the standard and tapered joints (Chapter 5; section 5.4). Data from these tests is presented below.

Table 19: Pre-testing visual inspection notes, ultimate failure loads and bond-line failure modes established by post-testing visual inspection of the Partition specimens

Specimen ID	Visual features/defects prior to testing	Ultimate Failure Load	Failure mode
Partition-1	End adhesive section on one side (DIC side) largely unbonded. Small area at corner appears bonded however light can be seen through the remainder of the section (plate side of adhesive) .	18.1kN	Adhesive Failure
Partition-2	Quality of adhesive section at nose on one side questionable. Region appears to be bonded but no evidence of 'spew' from this area.	20.45kN	Adhesive Failure
Partition-3	As Partition-2 but with visually better quality adhesive section at the strap end. Still no adhesive 'spew', however section appears more adequately 'filled to the edge' than in the case of Partition-2.	19.49kN	Adhesive Failure
Partition-4	Visually good sample	27.92kN	Adhesive Failure
Partition-5	Visually good sample	28.81kN	Adhesive Failure

8.2.6.1 Strain Gauge Array

Figure 113 - Figure 117 present surface E11 strain, recorded by the in-situ RSGs, on the partitioned-tapered specimens throughout the range of loads experienced.

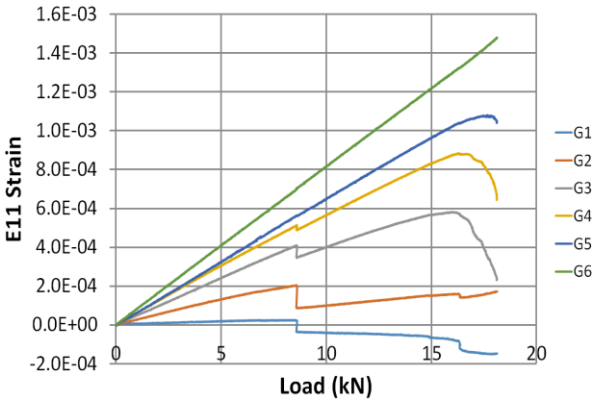

Figure 113: 'Partition-1' E11 Strains (RSG)

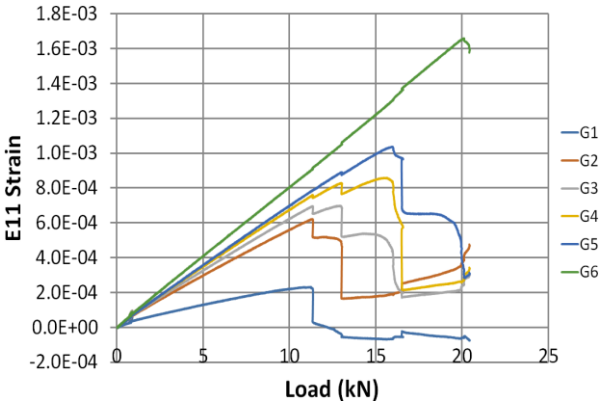

Figure 114: 'Partition-2' E11 Strains (RSG)

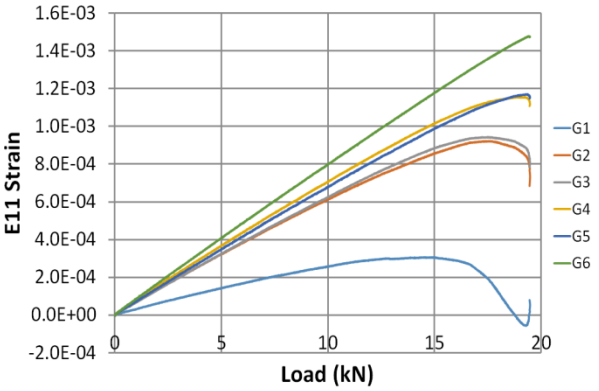

Figure 115: 'Partition-3' E11 Strains (RSG)

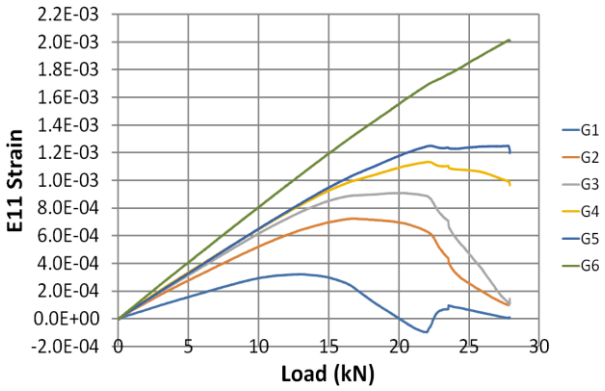

Figure 116: 'Partition-4' E11 Strains (RSG)

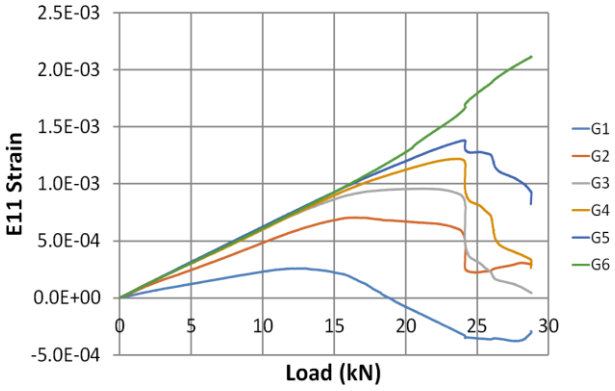

Figure 117: 'Partition-5' E11 Strains (RSG)

Specimen 'Partition-1' (Figure 113) shows a generally linear response indicating little or no damage growth for much of the test. A reduction in strain is reported by several RSGs from approximately 16kN loading until failure at 18.1kN, possibly as a result of slow bond-line damage growth. Prior to this event however a sudden

clearly definable drop in strain is reported by gauges 1-4 at ≈8.6kN. This rapid strain reduction is similar to events observed in the non-partitioned taper samples (Chapter 7) the cause attributed to short sections of rapid, but arrested disbond growth. The gauges closer the strap-end, and therefore presumably closer to the disbond event show a larger reduction in strain than those positioned further into the overlap.

Specimen 'Partition-2' (Figure 114) reveals a similar response to Partition-1 however similar rapid strain drops are reported at approximately 11.5, 13 and 16.5kN loads. Each of these events may again be attributed to periods of rapid, but arrested disbond growth. As per specimens Partiton-1 gauges which are likely to be closer to disbond events show greater strain drops during these rapid events. As three events can be seen and only two partitions are present at least one event must be linked to a disbond not associated with a partition. After a succession of partial failures gauges G2-G5 can be seen to 'plateau' in the region of 2E-4 strain. It is not clear if these are true strain values or an effect of strain-gauge damage as a result of the dynamic partial failures (see section 8.3.3 below). Analysis of RSG data after catastrophic failure show gauges G5 and G6 report zero strain. The remaining gauges report very large tensile or compressive values. At failure the in-situ gauges and the associated wiring was damaged to various degrees. This would explain the unrealistic strain values reported by the majority of sensors. It is unclear if the near zero strain values reported by gauges G5 and G6 are true values or a shift from the strains reported prior to ultimate failure as a result of dynamic failure.

Specimen Partition-3 (Figure 115) shows a similar response to that of Partition-1 however in this case no defined rapid strain drops are present. This suggests no instances of rapid but arrested disbonds occurred. This also implies there were no interactions between an advancing disbond and any of the bond-line partitions. The relatively slow, progressive reductions in strain shown by the RSGs, particularly those closer to the strap-end, may result from slow initial damage growth in the first adhesive section prior to full failure. In the absence of any evidence of interaction with a partition the disbond length appears to have been <10mm at the moment of catastrophic failure.

Specimens ‘Partition-4 & 5’ (Figure 116 & Figure 117) show RSG responses initially showing the linear strain vs load associated with no damage growth followed by a gradual decreasing in strain per unit load in sequence with the RSGs position relative to the strap end. More defined responses are also present in each case. This most prominent is on specimen 5 where an instantaneous strain drop is reported by several of the RSGs just prior to 25kN loading. Again the most dramatic strain drops are experience by the RSGs closest to the advancing disbond front. In a similar fashion to specimen Partition-2 the gauges present stain values which plateau in the region of ≈2.5E-4 strains once values reach a minimal value. In the case of Partition-5 two rapid events can be identified. Gauge G2 (9mm – just prior to the leading edge of the first adhesive partition) and possibly gauge G6 (16mm just after this adhesive partition) in Partiton-5 only show a single drop. Gauges G4 & 5 – which boarder the second adhesive partition – show only a partial drop in strain followed by a second partial drop at ≈26kN. This suggests the disbond front did not reach the second bond-line partition at this point of loading. A continued slow reduction in strain can be seen implying a continuing slow disbond prior to total failure. As no additional rapid strain drop is present this suggests the disbond had not grown to the second bond-line partition (25mm) in this interval.

8.2.6.2 DIC, RSGs and FEA comparisons

Below are comparative output plots – at specific load cases – of the experimental interrogation methods, i.e. non-contact DIC and in-situ RSGs, as well as FEA calculated surface strain curves used to estimate disbond lengths.

Specimen ‘Partition-1’

Figure 118 presents DIC and RSG data, as well as comparative FEA plots, for specimen Partition-1. The presented load cases were selected to aid analysis of features of interest seen on the RSG strain-load plot Figure 113. Prior to mechanical testing it was visually recognised only a small area of the adhesive section, closest to the strap end on the DIC side of the joint, had not successfully bonded. Backlight was visible through the un-bonded area. Further evidence of the extent of the unsuccessful bond can be seen in Figure 123A (lower) where surface contaminant is still present.

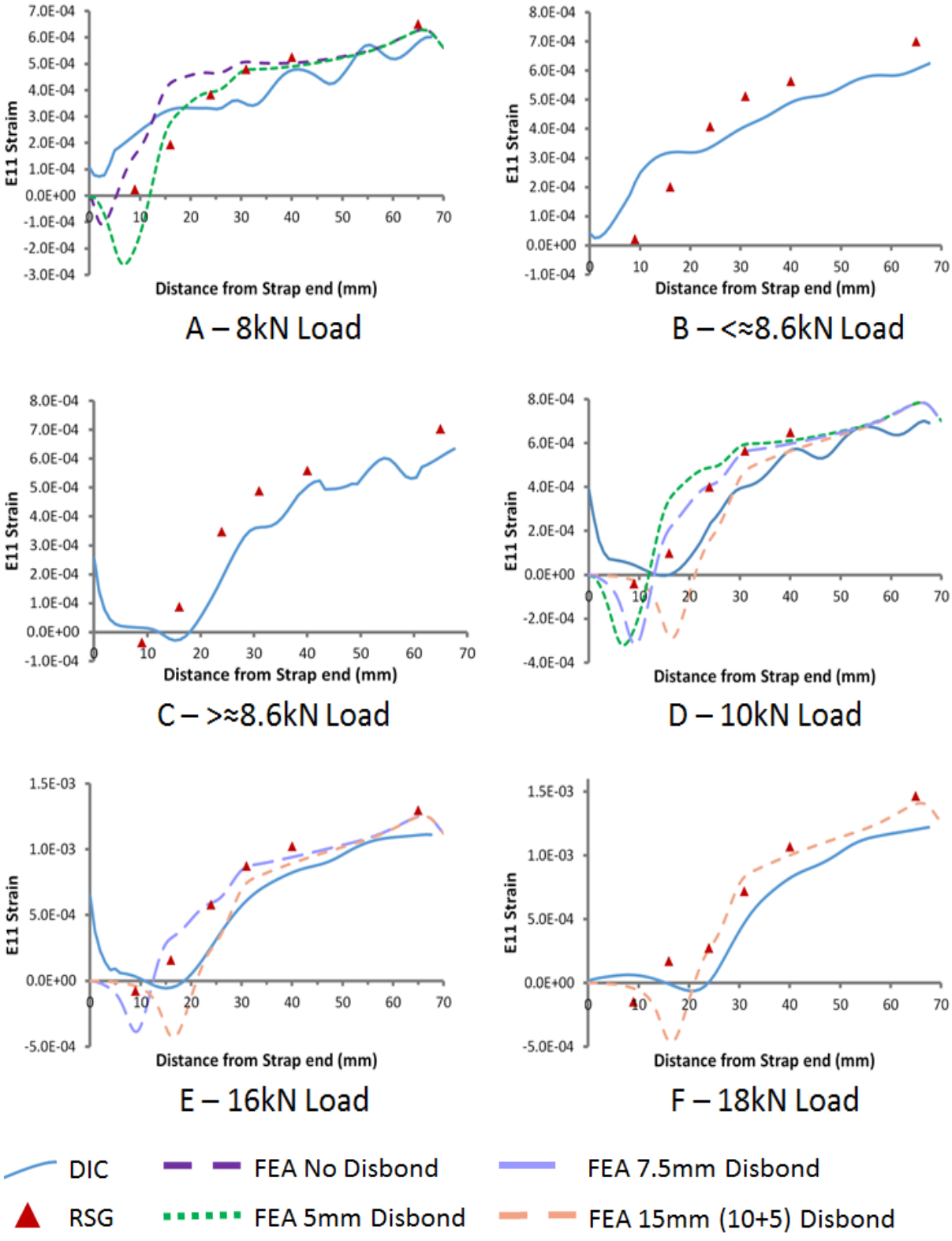

Figure 118: DIC measured E11 surface strains, at various tensile loads and degree of progressing disbond, along the centre-line on the strap of specimen 'Partition-1'

Initially (A) – prior to any deviation from the linear behaviour seen in Figure 113 – strain-gauge responses best fit FEA strain predictions of a 5mm disbond. Although the DIC shows a similar trend further into the joint overlap values appear elevated and difficult to interpret towards the strap-edge.

Figure 118B & C show the DIC and RSG results immediately prior to and after the sudden partial strain drop by RSGs 1-4 at ≈8.6kN loading evident in Figure 113. These figures are separated by a single DIC step and as such the event occurred in less than 0.1 seconds. Prior to (B) the distribution of RSG outputs are near identical (allowing for strain increases proportional to load) to those at 8kN. This suggests no further significant damage has occurred. After this rapid event (C) a shift in the DIC curve can be seen and strain values in RSGs 1-4 marginally fall (as per Figure 113) suggesting disbond growth. These distributions (compared to comparative FEA curves for similar disbond lengths) remain unchanged in the 10kN plot. Comparisons against FEA curves suggest the RSG data is showing a disbond approximately 7.5mm in length (3/4 of the first adhesive section). Comparisons against the DIC suggest a disbond of 15mm which equates to the first adhesive section (10mm) plus the first 5mm partition.

RSG and DIC distributions show no significant change up to 16kN (Figure 118E) again suggesting no further significant disbonding. From 16kN to ultimate failure at approximately 18kN a decrease in strain reported by the RSG can be seen in Figure 113. This is mirrored in the difference between Figure 118E & F where the RSGs suggest a disbond growth from approximately 7.5mm to 15mm; equivalent to the first adhesive section and partition. The curve fit is particularly good if the values of the gauges thought to be already positioned over a disbonded region and have settled at a non-zero but stable value as discussed in section 8.2.6.1. Further discussion regarding the non-zero strain values is included in section 8.3.3 below. The low strain front measured by DIC also appears to have progressed by ≈5mm in this interval.

Specimen 'Partition-2'

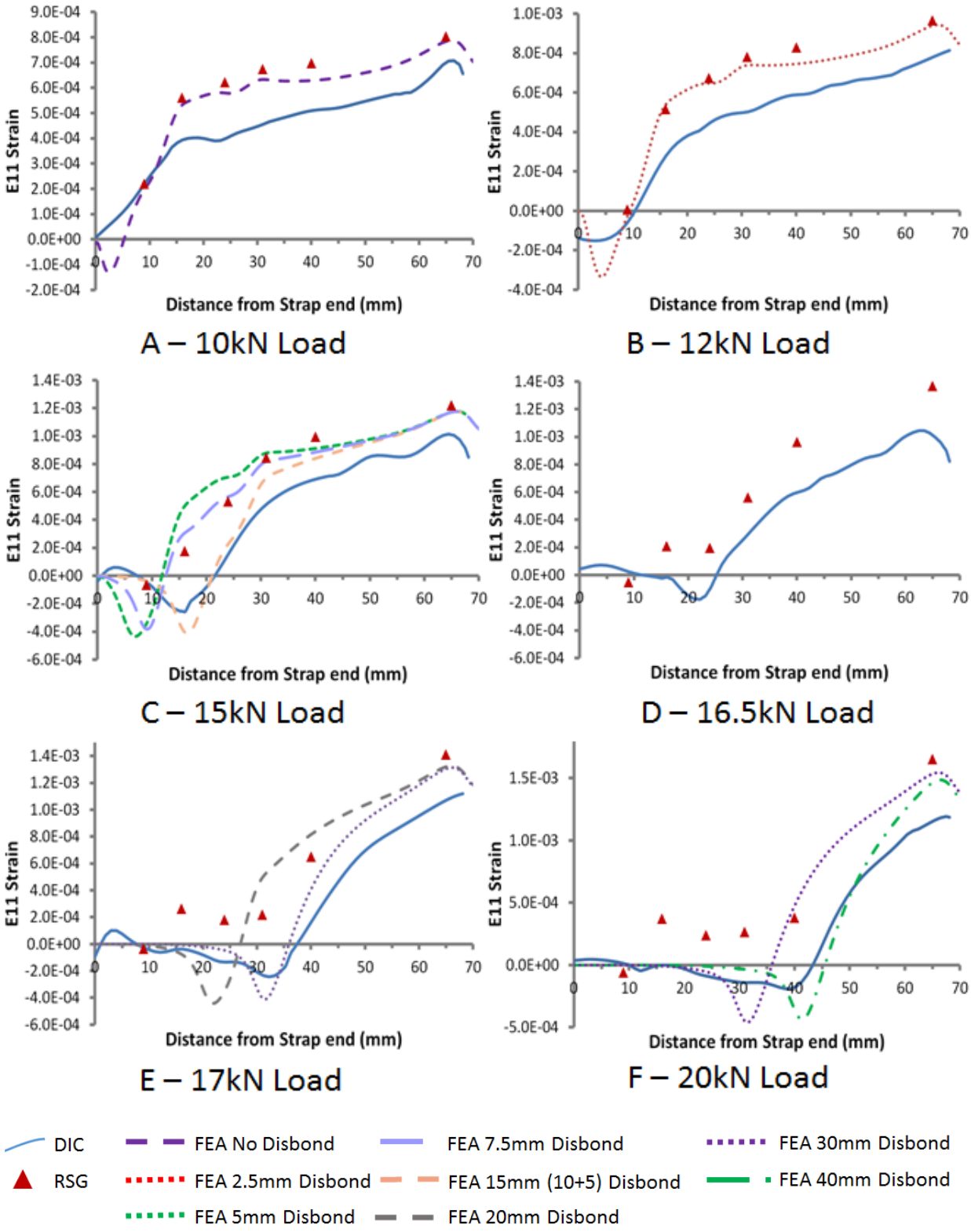

Figure 119: DIC measured E11 surface strains, at various tensile loads and degree of progressing disbond, along the centre-line on the strap of specimen 'Partition-2'

Figure 119 presents DIC and RSG data, as well as comparative FEA plots, for specimen Partition-2.

Prior to any deviation shown on the RSG strain vs Load plot (Figure 114) the RSG data in Figure 119A shows a close fit to the FEA curve associated with no damage. The character of the strain reported via DIC is similar to that reported by the RSGs however the magnitude of values appears lower over much of the joint overlap than that shown by the RSGs or predicted by FEA.

After the first near instantaneous strain drop evident on the RSG strain vs load curve (at ≈11.3kN) a shift in the low strain area is illustrated by both the RSGs and DIC. Figure 119B shows the RSGs values agree with FEA predicted strains associated with a 2.5mm disbond. A marginally larger shift may be apparent in the DIC data. The DIC strain magnitudes presented continue to be lower than shown or predicated by the RSGs or FEA.

A second, apparently larger, rapid drop in strain occurs on Figure 114 at ≈13kN. Figure 119C again reveals a shift in the low strain front both by the RSGs and DIC. Closer examination again reveals this rapid shift takes place within a single DIC step (<0.1 seconds). The strain gauges appear to show a disbond extending ≈7.5mm into the overlap. The DIC monitoring the specimens opposite face shows a response that may best fit FEA calculated strains associated with a disbond the length of the first adhesive section and partition (15mm).

A third larger near-instantaneous strain drop occurred at ≈16.5kN loading (Figure 114). This is immediately preceded by a period of rapid but not apparently instantaneous strain reduction reported by several of the RSGs (also Figure 119 C-D above). During this preliminary phase gauge G3 (positioned above the inner edge of the second adhesive section – Figure 112) reduces to almost the settled non-zero strain condition further discussed in discussed in Section 8.3.3. RSG G4, positioned above the edge of the final adhesive area after the second partition, experiences a significant strain reduction during this phase however values do not immediately reduce to zero or the settled non-zero condition. During the actual rapid event that follows gauge G4 does immediately drop to the non-zero strain condition. Simultaneously a dramatic, but not total, drop in strain is reported by gauge G5

placed further within the adhesive beyond the second partition. Surface strain shifts before and after this phase can be seen in Figure 119D-E. The distribution in the RSG values suggest the preliminary reduction in strain was at least in part associated with the final disbonding of the second adhesive section on the RSG side and the rapid event which followed was associated with the rapid increase in disbond length associated with the second adhesive-partition. The low strain front monitored via DIC also progressed approximately 5mm when the strain rapidly reduced. The best fit to FEA predicted surface strain is that associated with a 30m disbond which equates to failure up to and including the second adhesive partition.

Progressive damage continues, particularly from 19kN to the final moment of failure. Figure 119F presents RSG and DIC strain measurements at 20kN loading just prior to failure at 20.4kN. DIC suggests the disbond at this time was ≈40mm in length (10mm into the final region of adhesive). The low strain front measured by DIC continued to extend after the figure shown above. Immediately prior to total failure (20.4kN loading) this had progressed a further ≈7.5mm into the overlap.

The disbond length estimated from RSG data is harder to determine due to the limited number of RSGs in this region to fit the FEA curves. Gauge G5 reports strain at the non-zero strain condition. Study of shorter intervals between Figure 119F and total failure, as well as data presented on Figure 112, reveals a progressive reduction in strain presented by G5 up to the moment of failure revealing strain measurements – at least as relative readings – were recorded up to the moment of ultimate failure. The FEA curve fit presented in Figure 119F therefore includes the value shown. As the absolute strain value is potentially uncertain however (possibly between that presented and zero) precise placement of the comparative FEA curve cannot be made.

Throughout this entire data-set an apparent offset between the strain values presented by the RSGs and DIC is apparent. Further discussion regarding the possible causes and interpretation of this are made in section 8.3.3.

Specimen 'Partition-3'

The presented load cases were selected due to features of interest seen on the RSG strain-load plot Figure 115.

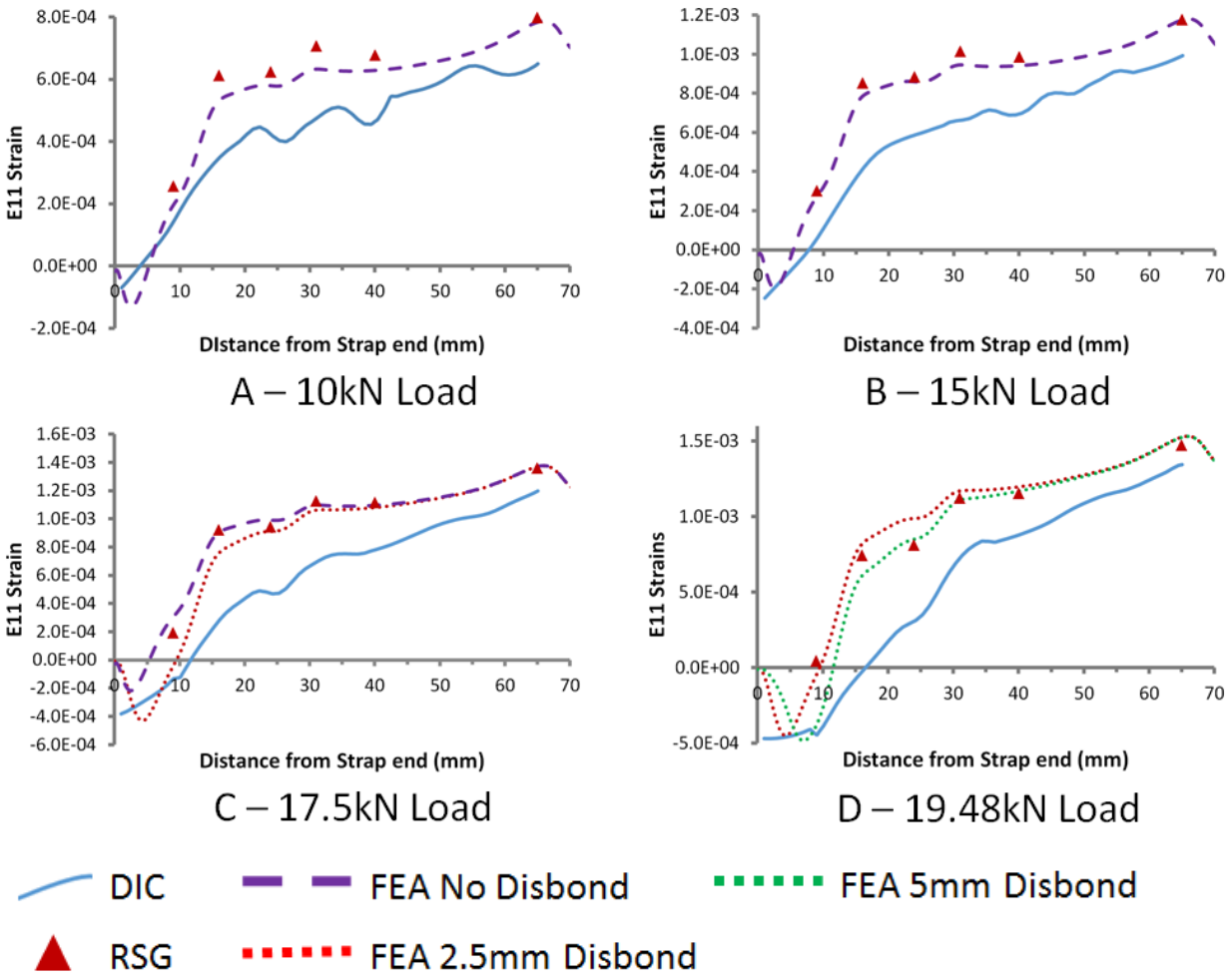

Figure 120: DIC measured E11 surface strains, at various tensile loads and degree of progressing disbond, along the centre-line on the strap of specimen 'Partition-3'

A similar strain offset as seen in the results of specimen Partition-2 appears present in the results. Further discussion regarding this feature is made in section 8.3.3.

No instant strain drops were apparent in Figure 115 although reductions in strain were recorded prior to failure, particularly by the RSGs closer to the strap end. Up to 10kN loading all RSG responses shown in Figure 115 were apparently linear with respect to applied load. Figure 120A shows RSG values are in good agreement with FEA surface strain predictions with no damage at this load. Similar to the Partition-2

results DIC values are lower than those presented by the RSGs or predicated by FEA. The general character of the response however shows similar features.

Figure 120B compares the DIC, RSG and FEA data once a defined deviation from the linear strain-load response was present in gauge G1. A close comparison between RSG results and the FEA prediction for no disbond is still present. A small degree of shift (possibly relating to a small disbond) relative to the FEA curve may be present however this is too small to confirm damage. A small amount of shift also appears present in the DIC data.

Figure 120C compares data at 17.5kN when deviation from the linear behaviour of RSGs G2&3 is seen. Again a small shift in the RSG distribution appears present. Compared to FEA predictions this shows a disbond shorter than 2.5mm. The DIC response also appears to marginally shirt inwards.

Figure 120D compares the data immediately prior to failure of the joint. Again a small perceivable shift in the RSG data is evident suggesting a disbond ≈2.5 – 5mm in length. Although the disbond is small gauge G1 reports zero strain. If undamaged this gauge should report ≈5.0E-04 strain at this load. The DIC curve again appears to shift inwards suggesting further, but still limited, disbond growth.

Specimen 'Partition-4'

The presented load cases presented below were selected due to features of interest seen on the RSG strain-load plot Figure 116. Good agreement between the RSG and DIC data is evident. Both interrogation methods closely match the FEA calculated curve relating to surface strain at this load when no disbond is present.

Figure 121B displays comparisons after most in-situ sensors have displayed some reduction in strain relative to applied load. At the 20kN load case presented the strain reported by gauge G1 has dropped to zero. Again a good agreement between the RSG and DIC data can be seen. Both distributions show good agreement with FEA surface strain predictions for a disbond length of 5mm (half the first adhesive section) at this load.

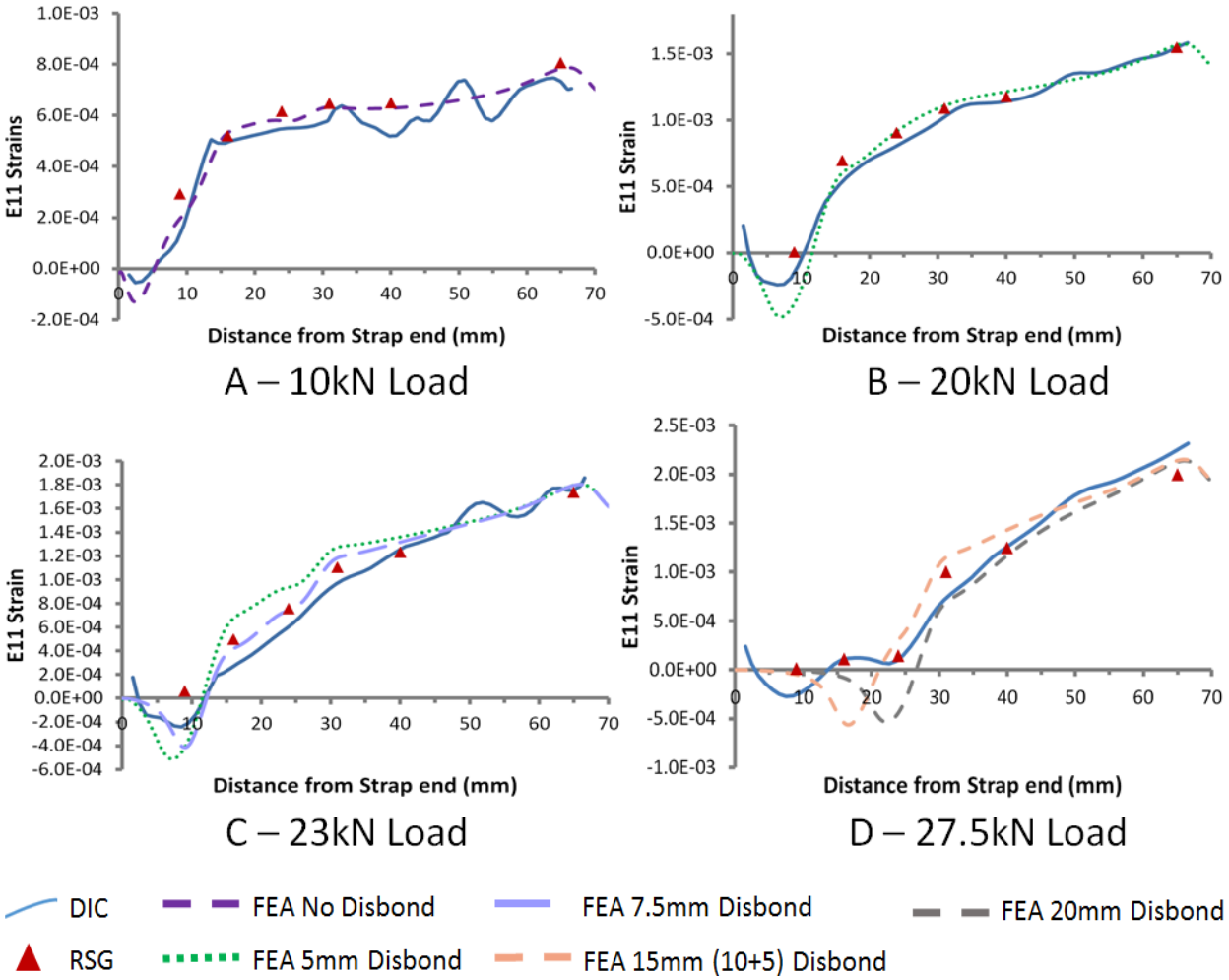

Figure 121: DIC measured E11 surface strains, at various tensile loads and degree of progressing disbond, along the centre-line on the strap of specimen 'Partition-4'

Figure 121C shows the RSG and DIC values shortly after a difference in the rate of change in strain vs load occurs; including a small increase in positive strain by G1 (Figure 116). RSG and DIC results are again in close agreement. This data concurs with FEA predictions of surface strain when a 7.5mm (3/4 of the first adhesive section) disbond is present at this load.

Figure 121D displays RSG and DIC data prior to ultimate failure. Examination of RSG and DIC data at short intervals between 23kN (Figure 121C) and ultimate failure suggest a slow, progressive increase in disbond length until the joint catastrophically fails just prior to 28kN loading. A different behaviour appears to occur in this degradation phase compared to other specimens or indeed the disbond growth up to this stage. RSG (primarily G2 & G3) and DIC strain values gradually

drop together over the region 15 to 25mm from the strap-end until the zero-strain plateau seen on the DIC curve in Figure 121D is totally formed. In other cases the low strain front is seen to progress directly from left to right in these plots. This behaviour also appears unusual as the disbond, estimated by comparison against FEA, appears to be in the range of 15 to 20mm in length. A disbond of this length must include the first bond-line partition however no evidence of an interaction is clearly apparent.

Specimen 'Partition-5'

The presented load cases were selected due to features of interest seen on the RSG strain-load plot Figure 117.

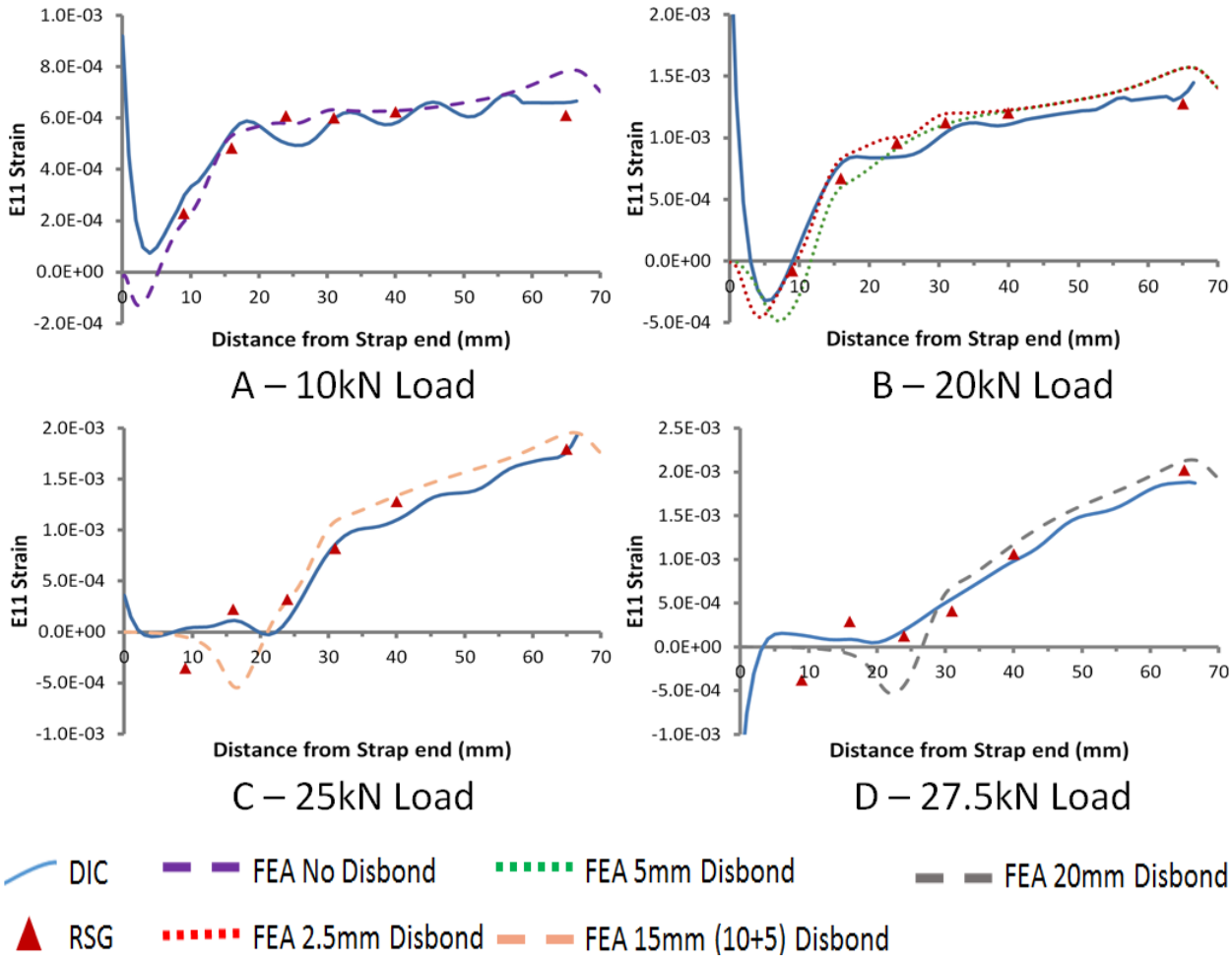

Figure 122: DIC measured E11 surface strains, at various tensile loads and degree of progressing disbond, along the centre-line on the strap of specimen 'Partition-5'

Figure 122A compares RSG and DIC data, as well as an overlay of FEA calculated surface strain to estimate disbond size, prior to deviation from the linear strain vs load relationship shown by any of the in-situ RSGs on Figure 117. A close agreement in strain values is presented by the RSGs and DIC although an unrealistic strain anomaly is shown by the DIC close to the strap end (towards and including distance = 0). The data from these methods closely match the strains calculated by FEA for the joint loaded at 10kN with no disbond present.

Figure 122B presents experimentally measured and FEA calculated surface strains after several of the RSGs deviated from the linear strain vs load behaviour (Figure 117) in a similar behaviour to that of specimen Partition-4. The greatest deviation is again seen in the gauges closest to the strap-end. Both RSG and DIC values suggest a disbond 2.5 – 5mm in length.

Figure 122C shows strain responses just after the major strain drop reported by the RSGs between 24 & 25kN loading. Up to this event strain distributions of both the RSGs and DIC remain largely unchanged from those presented at 20kN (Figure 122B) indicating little or no further disbond growth. After the event – which again took <0.1 seconds –strains were as in Figure 122C, indicating a 15mm disbond. This suggests the first adhesive section had failed and the associated disbond was arrested at the start (or very close to the start) of the second adhesive section, just after the first partition. Gauge G1, located just out-board of the first partition, reaches its lowest strain value as a result of this disbond (again at a non-zero value of ≈2.5E-4 strains as seen on several other specimens). The remaining gauges located further into the overlap all show a strain drop (again relative to their distance from the damage event) however all continue to show further strain reductions likely associated with further disbond propagation.

Figure 122D shows the surface strain just prior to ultimate failure. The total disbond length at this time appears to be just greater than 20mm. The pronounced drop in the strain distribution towards the zero/low strain region (as per the FEA curve on this plot) is not well defined in this DIC data. The disbond recorded by this method may therefore be approximately 15mm in length (unchanged from Figure 122C) or just greater than 30mm as suggested by the RSGs.

8.2.6.3 Post testing visual Inspection

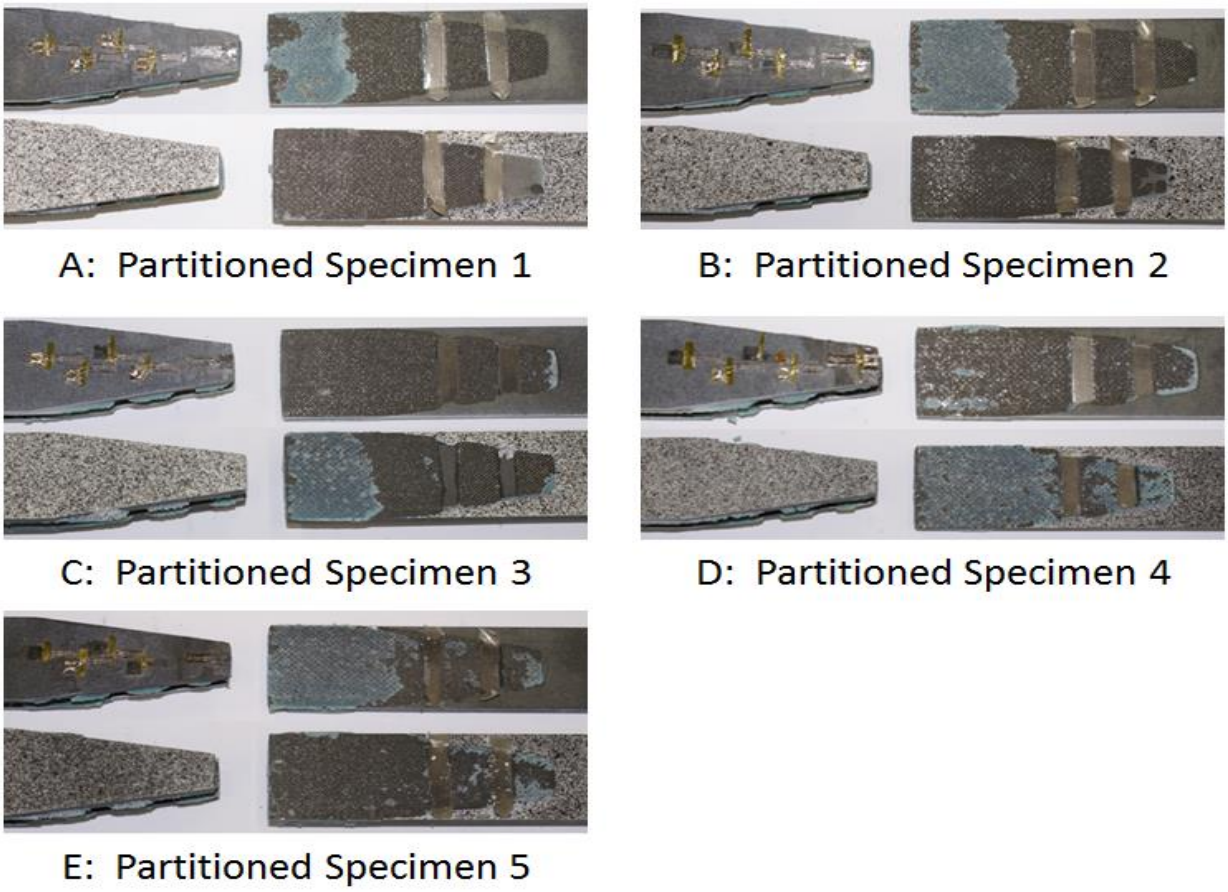

Figure 123: Visual Inspection of the Partitioned Tapered Specimens

Figure 123 shows the partitioned specimens bond surfaces after testing. As per the non-partitioned tapered specimens the plates at the monitored end of the joint were pulled from the straps which remained attached to the opposite plate.

All specimens show strong evidence of adhesive type failure. Specimens 4&5 do show small areas which show evidence of mixed adhesive-cohesive failure, however even in these areas most damage is at the adherend-adhesive interface, rather than in the adhesive itself, indicating predominant adhesive type failure.

Evidence of contamination resulting from the light sanding of the adherend surfaces prior to bonding can be seen. This action was undertaken in an attempt to remove high resin peaks formed by the surface finish of the peel ply. On the non-DIC face of the plates (Figure 123A upper) epoxy dust can be seen in contrast against where the surface has been ‘cleaned’ by the adhesive bond. Dust contamination can also be

seen at the location of the first adhesive segment on the DIC side of specimen 1 (Figure 122A lower). This adhesive section had been visually identified prior to destructive testing to have not successfully bonded to both adherends during manufacture. The darker area visible in Figure 122A at the lower, right hand corner of this poorly fabricated adhesive section shows where the small section of adhesive did make contact with each opposing adherend.

8.3 Section Summary/Discussion

8.3.1 Determination of disbond length aided by interactions with bond-line partitions

Evidence of interaction between advancing disbonds and the partitions included within the adhesive have been observed, supporting the design hypothesis. Spontaneous shifts in measured surface strains are in agreement with FEA predicted surface strain profiles associated with disbonds interacting with the bond-line partitions. Such disbond events generally appear to be fully or partially arrested when encountering the next adhesive section. These characteristics can be identified in specimens Partition-1, 2 & 5 (Figure 118, Figure 119 & Figure 122).

Specimen Partition-3 appears to fail catastrophically before the disbond has progressed far enough onto the overlap to encounter the first partition. Specimen Partition-4 presents a less defined strain response than expected as the disbond appears to Section 8.3.3 or possibly a disbond in which the damage front of not normal to the direction of growth. Even considering these issues the adhesive partitions have acted as markers linking strain responses to known damage sizes. As such – with consideration of factors identified in section 8.3.3 – the disbond length can be estimated with a reasonable degree of confidence.

Information gained from the adhesive partition analysis can be applied to the non-partitioned specimens investigated in Chapter 7. Figure 111 reveals FEA calculated surface strains for the partitioned and non-partitioned joints are similar. The estimates of disbond length made in Chapter 7 by the similar method used in this chapter (comparing measured strains with the FEA plots) can therefore be

interpreted with a similar degree of confidence. Further details are included in Chapter 9 Application.

Interpretations made from the comparative RSG, DIC & FEA plots can be transposed to the RSG strain vs applied load curves (Figure 113 - Figure 117). This data is more representative of that provided by SHM enabled joints. Although values reported by the in-situ sensors may be compared to pre-calculated FEA simple direct analysis of available RSG data may provide sufficient data to analysis and management of the structure. A suitable characteristic is that in the event of a disbond progressing up to and including a bond-line partition the RSGs outboard of that partition, as well as the next gauge placed above the leading edge of the following adhesive section, are seen to fall to zero strain (or the non-zero strain configuration discussed in Section 8.3.3). Gauges further into the overlap also show a strain reduction but not to this minima value. At the very least the disbond front can therefore be determined to be between the final gauge showing zero (or non-zero) strain and the next RSG. If no adhesive-partitions are included (or gauges are placed away from such features) the 'lag' between the effective bond edge and the strain experienced at the surface will need to be considered. In the geometries investigated this is approximately 5mm. Further consideration of this is made in Chapter 9; Application.

8.3.2 General observations

The partitioned specimens failed at loads generally lower than the non-partitioned tapered specimens. All partitioned specimens failed via pure 'adhesive failure'. The partitioned test specimens that showed no visible bonding issues however (Partition 4 & 5) failed at loads comparable to the non-partitioned joints which also failed in a pure adhesive failure mode (Taper 4 & 5) as opposed to mixed adhesive/cohesive failure. All specimens revealed some indication of contamination of the bonding surface resulting from epoxy dust being produced when removing high resin peaks in the surface finish produced by the peel ply.

Indicators of damage were evident in all test specimens whist sufficient residual properties remained. Most displayed unambiguous localised drops in strain as disbonds interacted with the adhesive-partitions. The test structure which provided

the least response to damage, and may therefore highlight the limitations of this approach, was that of specimen Partition-3. This joint failed catastrophically even though the disbond was estimated to be only 2.5 – 5mm in length on the side monitored by RSGs and potentially up to 10mm in length (the length of the first adhesive section) on the DIC side. As such there is no defined response resulting from an interaction with an adhesive partition. The earliest signs of deviation from the non-linear strain vs load behaviour can be seen to occur just after 50% of the ultimate load. This is however not highly definable and may therefore be problematic to positively identify in-service, further deviation is however present before failure. Such behaviour may be unlikely when fabrication methods are better controlled. Worst case responses such as this may define thresholds values used to activate maintenance actions. Alternatively simultaneous quality checks of the structure and monitoring system during fabrication may look for such features under the controlled environment of the testing laboratory. Further discussion and recommendations regarding this are included in Chapters 9 & 10; Application and Discussion.

As highlighted in Section 8.2.1 the locations of the bond-line partitions must be considered to avoid influencing joint performance. This feature may however be potentially used as an alternative means to influence progressive bond failure in a similar fashion to / or with the tapered strap, the closer the partition placement to the end the larger the 'magnification' of the stress-strain experienced by the adhesive.

There is evidence disbonds with length extending between bond-line partitions can still show retarded growth within the short sections of adhesive.

8.3.3 Apparent offset of FEA and DIC strain responses and 'Non-Zero strain responses'.

Examination of the responses above reveal some strain gauges (particularly after significant, rapid strain drops) settled at lower, but non-zero strain values until the joint ultimately failed. This is particularly evident in Partition-1 and Partition-2 and to a less obvious extent in Partition-5. In this instance the maximum magnitude of strain reported via DIC was also lower than that of the RSGs. Although these outputs may result from errors or drift associated with the interrogation equipment certain factors suggest this may not be the only potential cause. These include:

- The RSGs on all Partitioned specimens – with the exception of gauges G1, 2, 3 & 6 on specimen Partition-2, which failed dynamically – indicated strain readings of ≈zero after ultimate failure. Some gauges remained in contact with the monitored surface whilst several un-bonded. This suggests the non-zero values reported whilst the structure was still under load may have been based on actual values, the gauges returning to zero when, as a result of structural failure, the applied load was relieved. Those which did not show zero strain values after failure reported very high magnitude tensile or compressive values indicative of damage to the gauges or connecting wires.
- All strain values were zeroed at the start of the tests. The apparent drift was not observed in all tests even though identical equipment was used.
- The strain values presented when gauges – and DIC in the case of Taper-4 in Chapter 7 – all settled at similar values; around 2.5E-4 strains for the RSGs and 5E-4 for the DIC offset seen on Taper-4.
- Each case occurred in joints which appeared to be of a lower fabrication quality. There may be therefore more opportunity for variability in strength between each of the two bond-lines in these joints.

As each interrogation method (RSGs and DIC) monitored opposite faces of the test specimens a brief investigation of strain responses which may occur as a result of different disbond lengths in the two bond-lines was made. The existing taper (non-partitioned) model was adapted to include both bond-lines allowing asymmetric disbond lengths to be introduced. These FEA models, only marginally adapted from those used in previous symmetric investigations with some necessary amendments to boundary conditions, attempt to identify qualitative features which may be present in the event of asymmetric disbonding.

The FEA generated surface strain curves simulating the tapered joint subjected to 10kN of tensile loading with different degrees of damage are shown below. All contain a 30mm disbond in one bond-line. The bond-line connecting the opposite strap to the plate contains no-disbond, a 5mm disbond and a 20mm disbond on the respective cases shown.

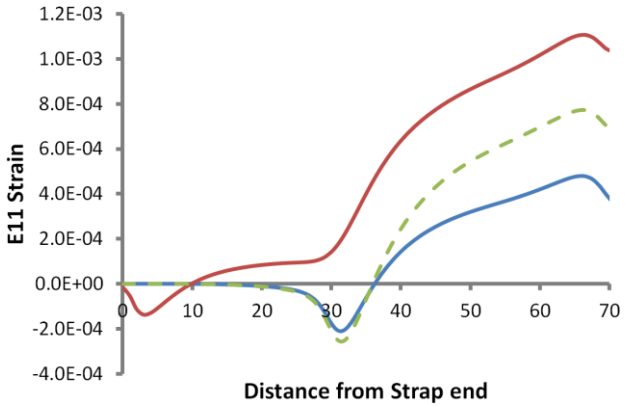

Figure 124: FEA E11 surface strains on a Tapered double-strap joint with a 30mm disbond in one bond-line

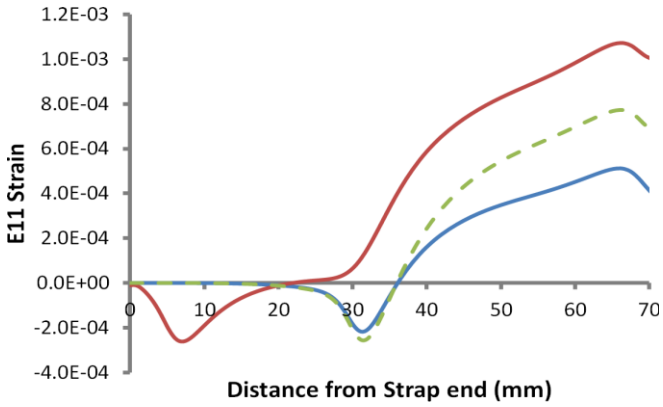

Figure 125: FEA E11 surface strains on a Tapered double-strap joint with a 30mm disbond in one bond-line and a 5mm disbond in the opposing bond-line

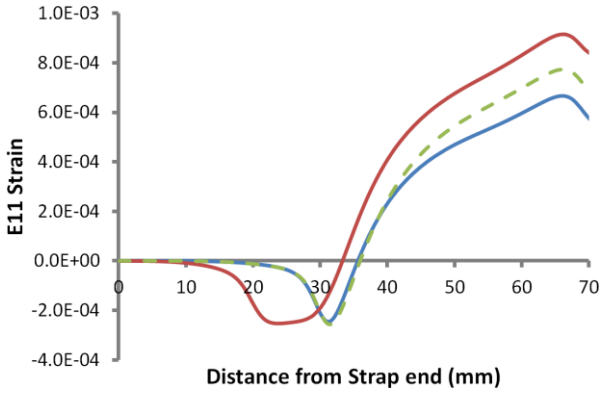

Figure 126: FEA E11 surface strains on a Tapered double-strap joint with a 30mm disbond in one bond-line and a 20mm disbond in the opposing bond-line

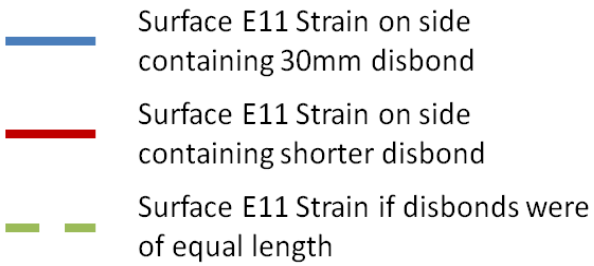

Features of note within the curves presented:

- A region of non-zero strain is present in Figure 124 where a disbond exists in only one bond-line. This is similar (although of a different magnitude, possibly as a result of limitations in the model) to that seen in some physical tests e.g. Partition-2.
- Figure 124 - Figure 126 show the magnitude of strains recorded on the less damage side of the joint (Red) are greater than those on the side with a larger

disbond (Blue). A similar relationship can be seen in the data sets which show evidence of non-zero strain behaviour.

- The strain curve on the joint side containing less damage (Red) contains a region of low strain (in the form of 'non-zero' strain in Figure 124). In regards to location along the joint length this almost perfectly matches the region showing zero strain on the curve describing the strain on the side of the joint with greater damage. Further into the overlap, where both bond-lines are intact, strain rapidly increases (to differing values) on both sides. This feature can be identified in data gained from physical tests, the most recognisable example being that of specimen Partition-2 (Figure 119). If this response is representative the damage on the opposite side of the joint may therefore be inferred from measurements taken from the less damaged side.

Although the statements above suggest the offset values are associated with asymmetric disbond lengths some disparities exist. These may be caused by issues in the FEA models used or other external factors. Potential concerns are summarised below:

- The strain magnitudes calculated via FEA are shifted considerably further from those expected when disbond lengths are identical (dashed green lines) than when observed in the physical tests.
- To produce the curves presented additional boundary conditions were used to prevent excessive bending resulting from loading the now asymmetric structure. These may have over-constrained the model, although deflections were small in this adaption. No visible bending was seen in physical tests.

8.3.3.1 Offset of FEA and DIC strain responses and 'Non-Zero strain responses' summary

The investigation above suggests the observed offset between surface strain measurements may be the result of differing disbond lengths within the test joints two bond-lines. Such asymmetric damage may be related to load alignment or variations in quality, and therefore strength, of the bond-lines. The investigation above used only a modification of FEA models used to simulate symmetrical damage. Although these models show features which can be identified in outputs of

the physical tests significant variation is present. As such, and as the phenomenon has not been directly observed, the presence of differing disbond lengths is only a proposed cause for the strain offset at this time. Future work involving both physical testing and FEA models both tailored towards such an investigation may therefore aid further analysis from in-situ surface strain sensors.

Even though the exact nature of the discrepancies in strain measurement may contain some uncertainty the potential for sensor outputs such as these remains. Any SHM enable joints monitored using the approach investigated will still need to identify damage, and therefore activate appropriate maintenance measures, despite such variations in sensor output.

8.3.4 Continued development

The investigations discussed in this and the previous chapter have shown the approach investigated has potential for use within structures that may be operated under a damage-tolerant regime. The following chapter considers how a system based on this approach may best be included within structure and how information produce by simple strain responses may be presented for interpretation.

9 Application

9.1 Section Introduction

Previous chapters have shown considered design of bonded structure in conjunction with surface mounted strain sensors can prevent bonded joints failing catastrophically as a result of damage initiation (as is usually observed in standards joint configurations) and allow said damage to be reliably identified using simple sensing systems. This Chapter further reviews the responses and results gained from the tapered and tapered-partitioned specimens investigated in Chapters 7 & 8 and suggest approaches how such systems may be used in practical applications.

9.2 Operation and conforming to the current damage-tolerant regime

Section 2.2 describes how composite aerospace structures may conform to damage-tolerance operation. Of the arrested, no-growth or slow growth options available in general composite structure bonded joints must currently be designed to a no-growth philosophy due to their rapid uncontrolled failure. The joints investigated in Chapters 7 & 8 however show behaviour that may be categorised as both arrested and as slow damage growth. Figure 6 illustrates how different categories of damage must be managed in service. Although these figures and recommendations refer to composite laminates subjected to discrete impact events, similar considerations must be made regarding bonded structure which may degrade in strength over time and as a result become overloaded by forces routinely encountered in normal operation. Such demands may also be applicable for bonded metal structure as well as bonded repairs.

Reiterating the means of compliance for composite bonded joints discussed in Chapter 3:

i. *The maximum disbonds of each bonded joint consistent to withstand the loads* [as described in [2] paragraph a.3.] *must be determined by analysis, tests, or both. Disbonds of each bond greater than this must be prevented by design features; or*

ii. Proof testing must be conducted on each production article that will apply the critical design load to each critical bonded joint; or

iii. Repeatable and reliable non-destruction inspection techniques must be established that ensure the strength of each joint."

9.3 Degradation of bonded structure and the consequences of current means of compliance

If the chemical bonds at the interface of the adhesive and adherend are strong, failure of the bond-line will take place within the adhesive (cohesive type failure). As a result the bond strength will be high. If the bonds between adhesive and adherend are weak, or if these become degraded over time, failures will occur at the adhesive-adherend interface (adhesive type failure) and the strength of the bond will be low [191]. Contemporary NDI approaches (as per means of compliance iii) are limited in their capability in identifying such weak bonds. Physical defects such as production voids may be detected which reduce bond-line strength however the presence of such voids may still result in relatively strong cohesive type failure.

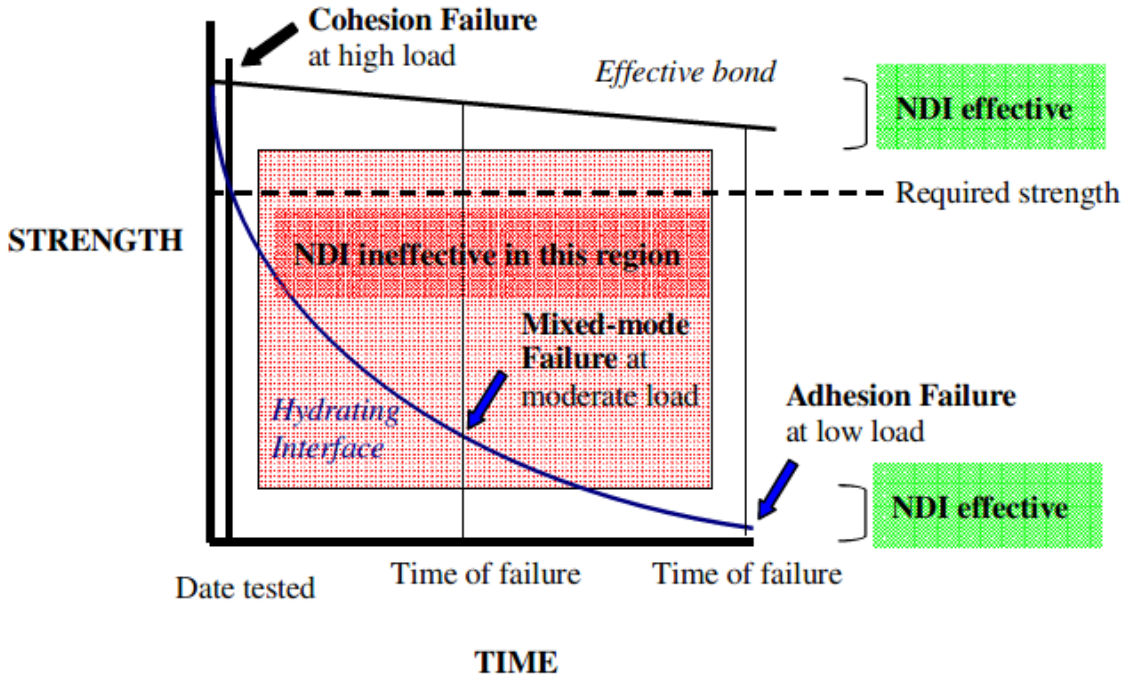

Figure 127: The transition from strong adhesion failure to weaker mixed mode and finally weak adhesion failure as well as the region where NDI cannot detect potential mixed mode failure [191]

NDI approaches are limited in their capability to assess the quality of adhesive-adherend interfaces if no physical defects are present. These approaches therefore cannot identify factors likely to lead to adhesive, or mixed mode type failures [191]. The first moment NDI may recognise such degradation is after a disbond event has occurred. If, as per most bonded structure, catastrophic failure occurs immediately follows (as seen in Chapter 6) there may therefore be no recognition prior to total failure. As such there is a risk a bond which was initially qualified using this approach may degrade to a dangerously weakened condition without recognition by NDI (Figure 127).

The second means of compliance – that of proof testing composite bonded structure – offers the same potential issues, i.e. this may not detect bonds that may require time and exposure to degrade [3,14,140]. Although the structure may at testing present sufficient strengths to qualify (static load testing up to DLL [3]) degradation may again result in structure initially qualified reducing in strength over time to levels inadequate for operation whilst providing no identifiable features to show the part has degraded. AC20-107B [3] does state that adequate demonstration must show processes have long-term environmental durability. This is normally in the form of an environmentally aged sample subjected to a wedge test (ASTM D3762). Surface treatment for bonding is approved if crack growth occurs within the adhesive (cohesive type failure) rather than at the adhesive-adherend interface (lower strength and more subject to environmental degradation adhesive type failure). Although this approach reduces the likelihood there is still the potential for degradation, particularly if despite the rigorous quality controls used in fabrication the bond surface – possibly as a result of contamination or variability during fabrication – differs to that qualified by the wedge test. In such instances the bonded structure may again pass the proof test yet degrade in service in a similar fashion to that shown in Figure 127 and again not be identifiable using NDI.

It is for the reasons highlighted above that most commonly *option I* is used or alternatively proof testing (*option II*) or NDI (*option III*) are used in conjunction with *option I.* This option however results in the inclusion of additional structure or features adding extra mass to the greater structure.

9.3.1 Increased joint strength per unit disbond growth design

Proposed simple models in the potential increases in static strength as disbonds progress along the tapered regions of the modified joints tested are included on Figure 128 & Figure 129 below. Values are based on the simple approaches previously discussed which may possible be used for initial sizing of modified joint geometries. It is recognised that more complex models – e.g. the traction separation approach use with FEA – has previously been used when attempting to model cohesive damage growth.

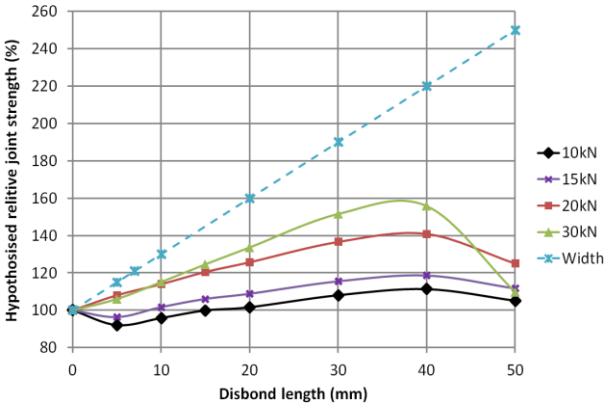

Figure 128: Hypothesised tapered joint relative strength increases based on peak bond-line shear strains and increase in strap width

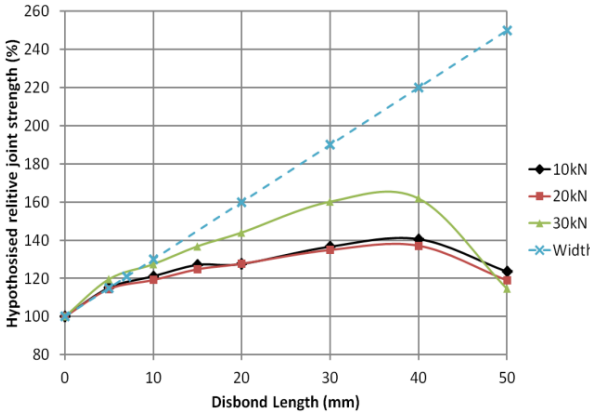

Figure 129: Hypothesised tapered joint relative strength increases based on peak bond-line Peel strains

The values shown on Figure 128 (solid lines) are based on the decrease in peak adhesive shear strains present as a disbond progresses through the tapered joint overlap. Values were calculated in the previously used FEA models. Increases in strength are based on the ratios between the peak strains experienced by the undamaged joint and those of joints containing disbonds of various lengths when subjected to similar loads. Values are taken at the centre-line of the joint along the mid-plane of the adhesive. No account for sharp crack tips or adhesive spew fillets was included as discussed in Chapters 4 and 5. Plots are included for loads ranging from 10kN, where the entire adhesive bond-line is behaving elastically, to 30kN where plastic behaviour is fully established in regions experiencing peak strain. In addition as standard configuration bonded lap type joint strengths are largely

unaffected by the length of overlap but may increase pro-rata with width (Chapter 4) the percentage increase in local strap width from the strap end (distance = 0mm) to the widest part of the tapered region (distance = 50mm) is also included (dotted line).

Figure 129 shows the equivalent strength increases based on FEA calculated peak through thickness or peel adhesive strains. These show a similar distribution to those considering shear. As per Figure 128 strains are selected over stress due to stress values plateauing after plastic yield.

9.3.1.1 Specimen estimated disbond lengths and relative strengths

Below are plots which show the increase in joint strength (load bearing capability) as disbonds initiate and propagate into the overlap of the tested modified, tapered joints. Disbond lengths were estimated by comparing RSG and DIC data with FEA surface E11 strain predictions. Where differences between RSG and DIC values are evident – possibly due to different disbond lengths in the two bond-lines both values are shown. Strength increases are presented as percentages of loads just prior to when initial damage could be detected. This allows the performance of each joint to be assessed in terms of residual strength from the earliest moment of recognisable damage initiation regardless of the joint quality or failure mode. The applied loads for each case are presented on the right-hand Y-axis. Also included are the hypothesised strength increases based on bond-line peak E13 shear strains – based on 10kN (elastic) and 30kN (established plastic) load cases – and those based on increased effective strap width as per Figure 128.

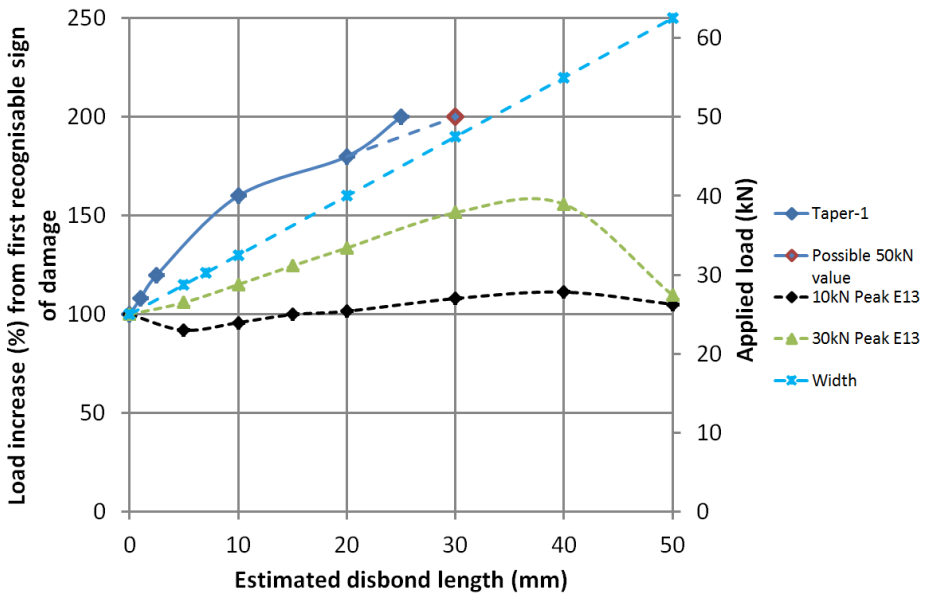

Figure 130: Specimen Taper-1: Estimated disbond lengths and equivalent joint strength as a percentage of damage initiation load plus comparison against hypothesised strength based on peak E13 strains and increased joint width

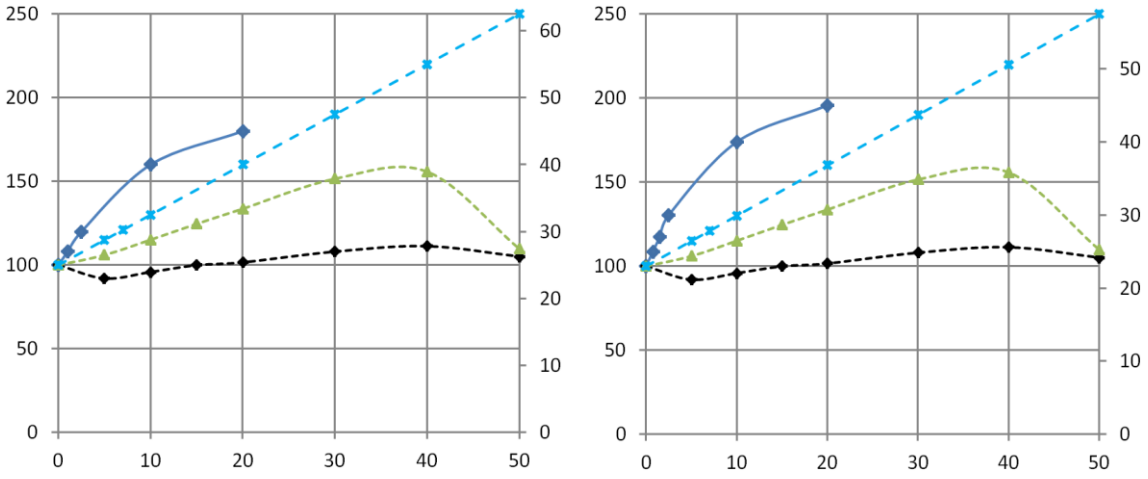

A: Test specimen Taper-2 B: Test specimen Taper-3

Figure 131: Specimens Taper-2 and Taper-3: Estimated disbond lengths and equivalent joint strength as a percentage of damage initiation load plus comparison against hypothesised strength based on peak E13 strains and increased joint width

Specimens Taper-1, 2 & 3 (Figure 130 & Figure 131) all show similar performance in terms of initial and ultimate strength as well as disbond growth. All show first signs of damage at loads greater than the calculated DLL of these joints (13.3kN) as well as the associated DUL (20kN). As such these joints would pass the proof testing

means of compliance discussed in sections 9.2 & 9.3 and in their condition at the time of testing would be considered airworthy. Ultimate failure of these specimens occurred at between 47.6 and 50.5kN at 180-200% of the initial damage load and more than double the selected DUL for these structures. Post testing visual inspection revealed mixed mode failure containing some evidence of adhesive failure (Chapter 8; section 8.2.6.3). As discussed in section 9.3 bonded structures ultimately failing in this mode may be susceptible to strength degradation over time in service. Strength elevations as disbonds propagated were greater than either the simple consideration of peak shear strain or local increase in strap width suggested.

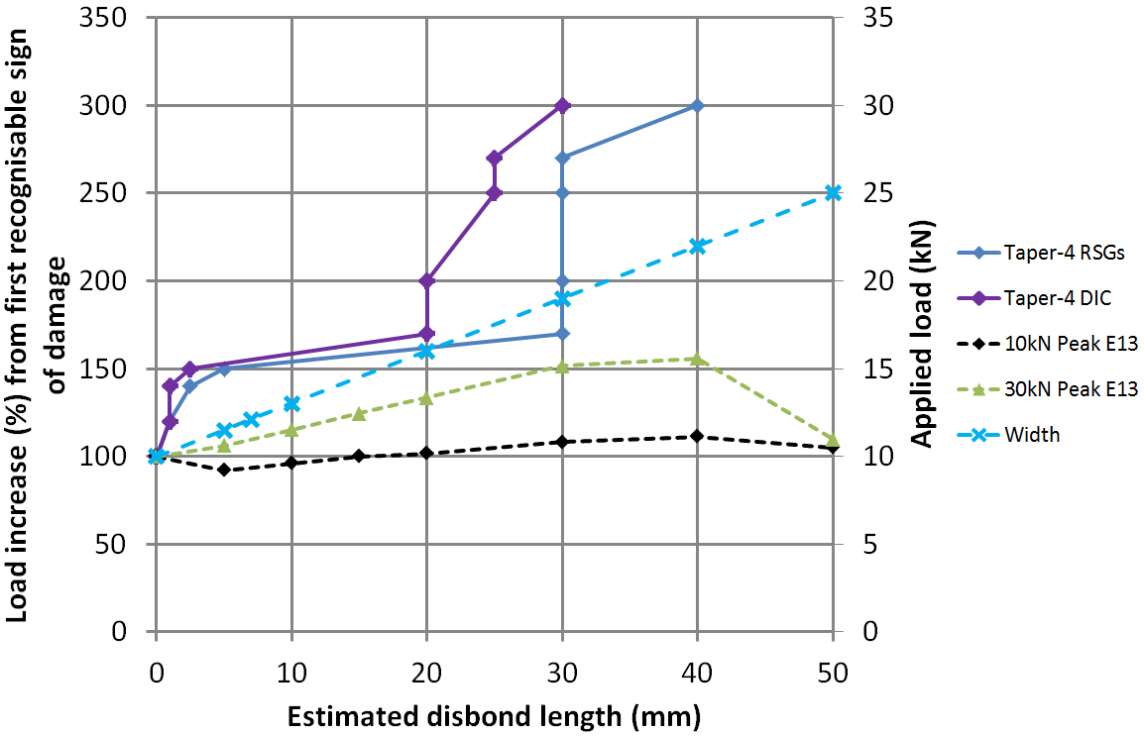

Figure 132: Specimen 'Taper-4': Estimated disbond lengths and equivalent joint strength as a percentage of damage initiation load plus comparison against hypothesised strength based on peak E13 strains and increased joint width

Analysis of RSG and DIC data for specimen Taper-4 (Figure 132), each monitoring opposite faces of the test structure, suggest the disbonds within the joints two bond-line were of unequal length. A rapid disbond event can be seen to simultaneously appear to occur in either bond-line at ≈15kN of load growing to an estimated 20 and 30mm in length as measured by the DIC and RSGs respectively followed by a period of slow growth until ultimate failure. Damage initiation was identified just after 10kN

of applied load and as such this structure would not have passed the DLL proof load test. Ultimate failure however occurred at 300% of this load well above the proposed DUL. If the capacity of the structure as a whole is considered by the greater load per disbond length curve (DIC) the strength increase is again greater than the simple consideration of peak shear strain or local increase in strap width. Damage was in the form of adhesive type failure which can show strength degradation due to environmental ingress over time.

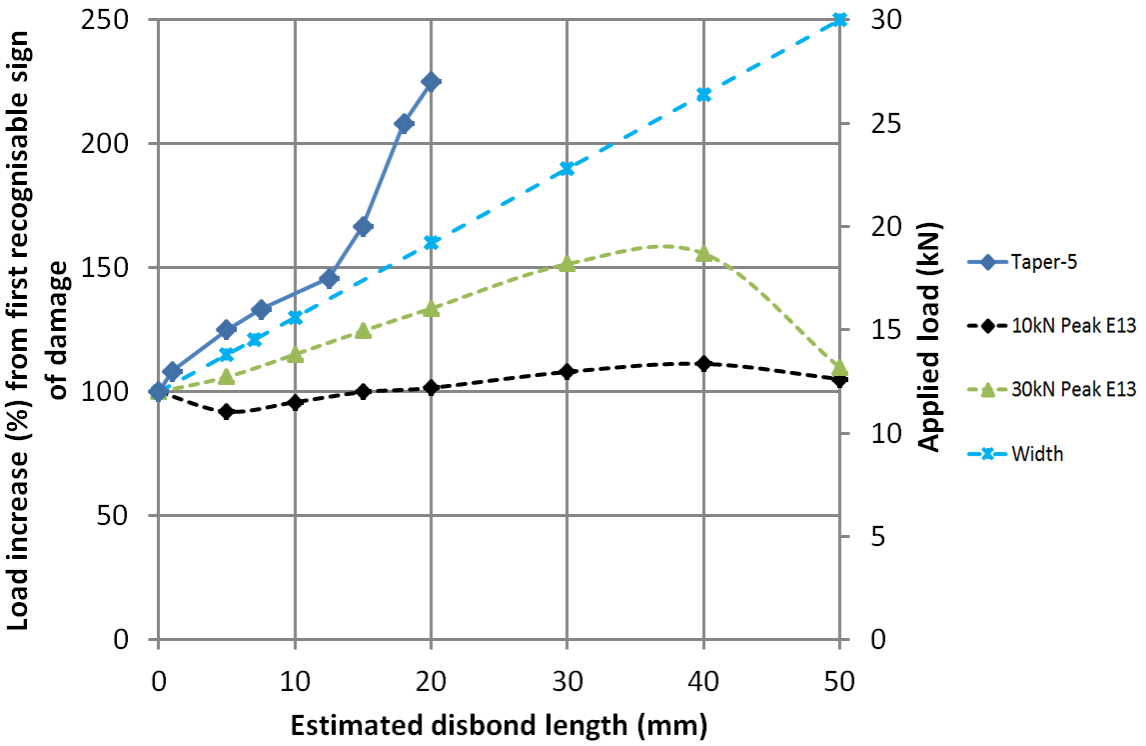

Figure 133: Specimen 'Taper-5': Estimated disbond lengths and equivalent joint strength as a percentage of damage initiation load plus comparison against hypothesised strength based on peak E13 strains and increased joint width

Figure 133 shows the estimated disbond lengths of specimen Taper-5. Although failing as a result of adhesive type failure this was in the form of small arrested events which result in the apparently slow progressive disbond growth seen above. Damage initiation was identified at 12-13kN loading, just below the DLL required of proof load testing. Ultimate failure occurred at 225% of the initial damage load and again above the DUL for this joint. Damage initially grew as may be expected with the increase in strap width; however some further increase can be seen prior to ultimate failure of the joint.

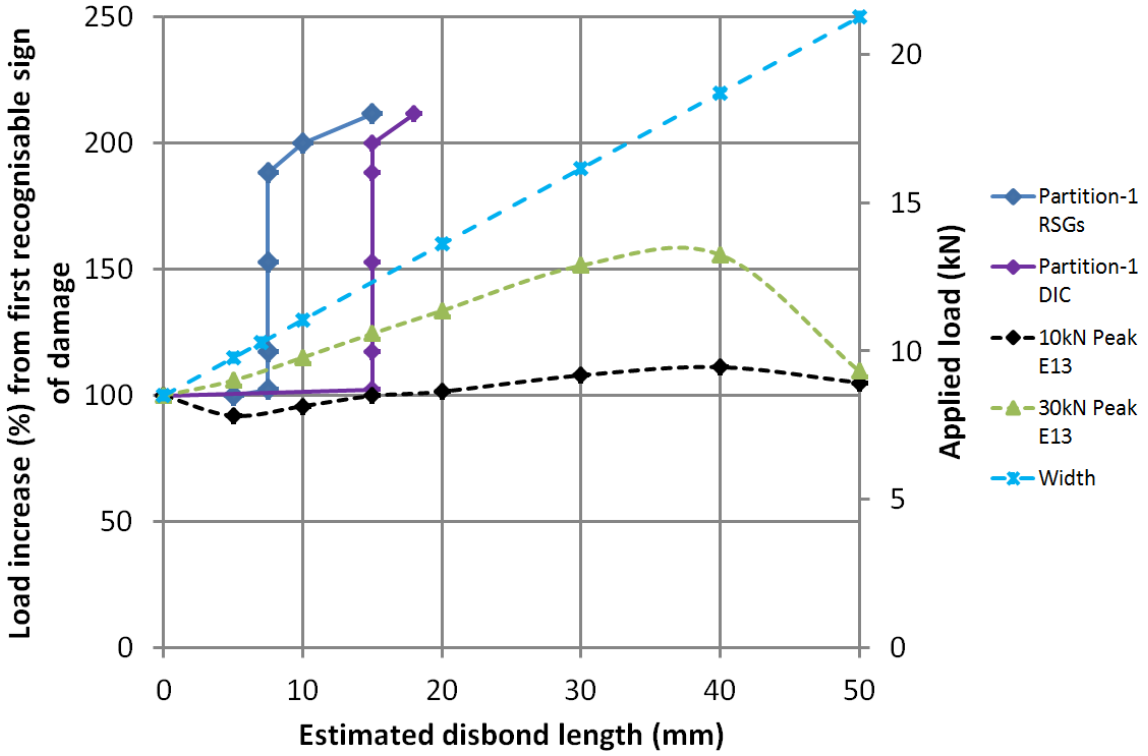

Figure 134: Specimen 'Partition-1: Estimated disbond lengths and equivalent joint strength as a percentage of damage initiation load plus comparison against hypothesised strength based on peak E13 strains and increased joint width

Figure 134 shows the estimated disbond lengths during loading of specimen Partition-1 which contains 5mm bond-line partitions starting at 10 and 25mm from the strap end (Chapter 8; Figure 110). This specimen contained a visually identified non-bonded region for the first 15mm of overlap (10mm plus 5mm partition) on the DIC side bond-line. Initial damage occurred at ≈8.5kN loading in the form of a rapid disbond effect. It is likely this was at least in part due to the small area of bonded adhesive at the strap end of the poorly bonded area failing creating a disbond up to and including the partition in this bond line. Simultaneously a disbond estimated to be approximately 7.5mm in length formed in the opposing bond-line. Both appear to have been arrested until slow disbond growth continued – up to the first partition on the RSG side – before ultimate failure. Ultimate failure occurs at ≈210% of the damage initiation load and at 18kN falls between the DLL and DUL.

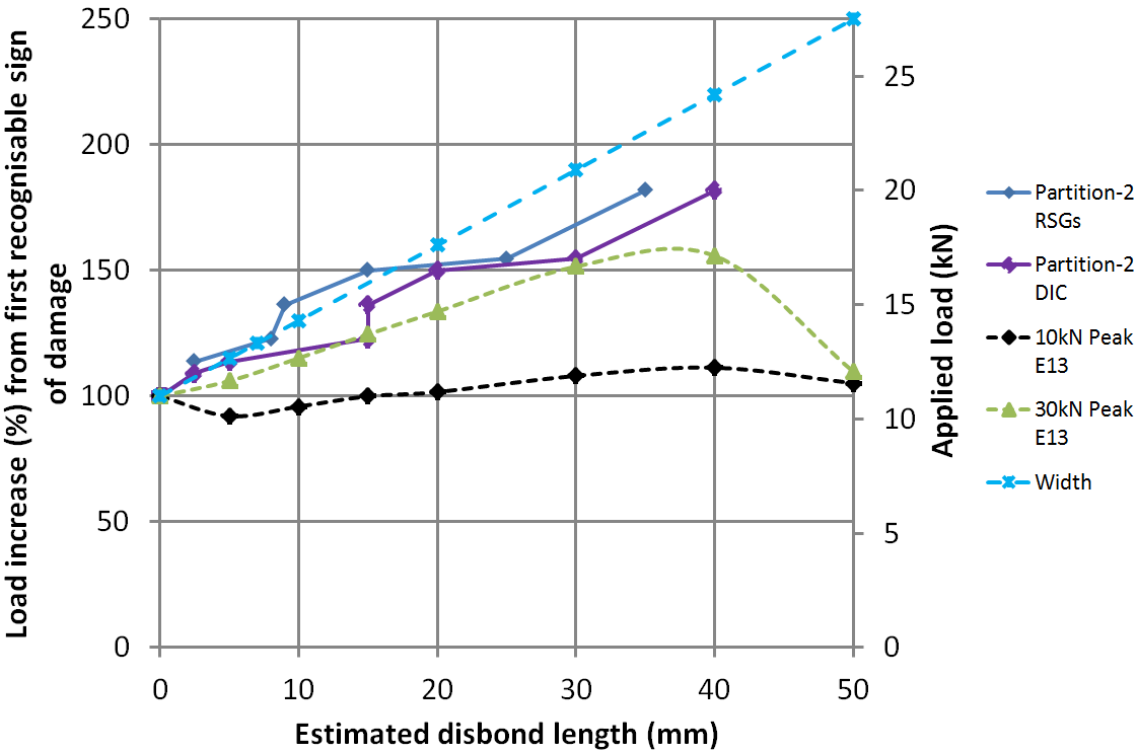

Figure 135: Specimen 'Partition-2: Estimated disbond lengths and equivalent joint strength as a percentage of damage initiation load plus comparison against hypothesised strength based on peak E13 strains and increased joint width

Estimated disbond lengths as load is applied to specimen Partition-2 are shown in Figure 135. Disbonds of marginally differing lengths appear present from data gained by the two interrogation methods. Rapid increases in disbond length, some influenced by the presence of partitions in the bond-lines (10-15 & 25-30mm) can be seen. Damage initiation was identified at ≈11kN, below DLL and current proof testing requirements. Ultimate failure occurred at 20.5kN, over 180% of the damage initiation load and marginally over the DUL. Over the course of the test strength increase per growth in disbond length was marginally lower than the increase in strap width, however still better than that expected from analysing the peak shear strain at the mid-plane of the bond-line. The large disbond length seen in this specimen provides additional opportunity to identify damage from multiple sensors.

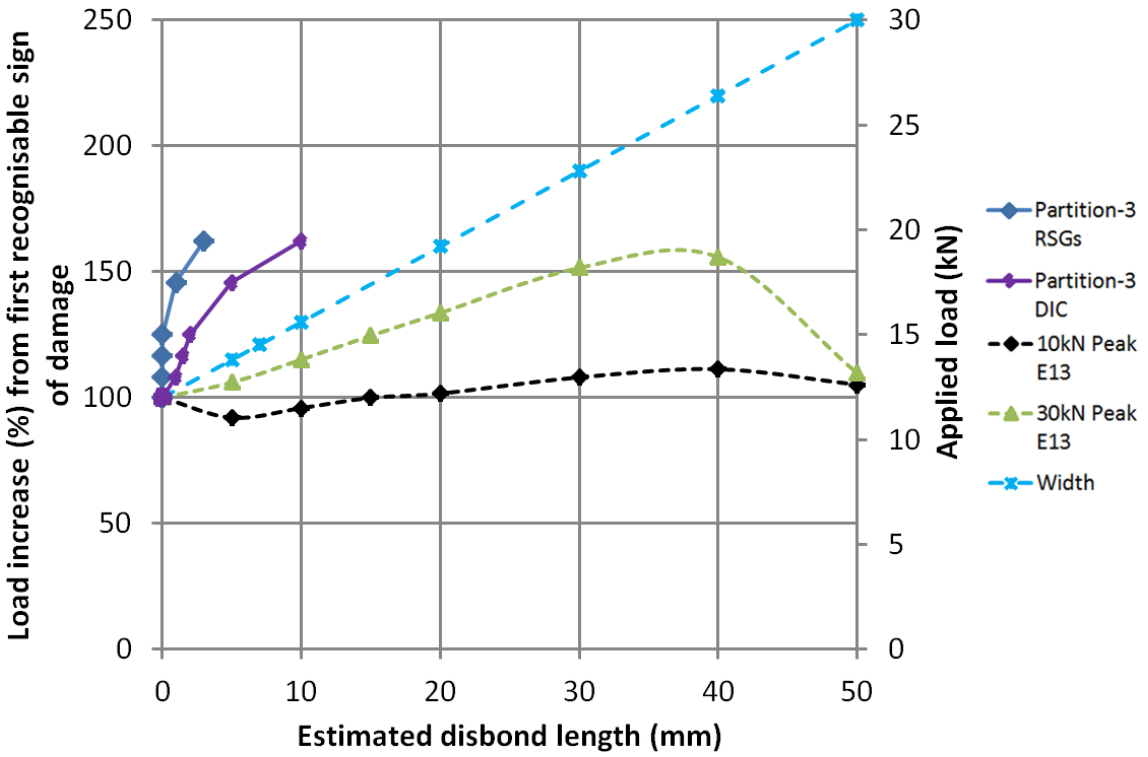

Figure 136: Specimen 'Partition-3: Estimated disbond lengths and equivalent joint strength as a percentage of damage initiation load plus comparison against hypothesised strength based on peak E13 strains and increased joint width

Figure 136 shows the estimated disbond lengths during loading of specimen Partition-3. Some asymmetry between the disbond lengths again appears present. Both disbonds appear to be relatively short at the time of ultimate failure (estimated at approximately 3mm on the RSG side and 10mm on the DIC side), which may not aid confident damage identification prior to catastrophic failure. Damage initiation is identified at 12-13kN on the DIC side (below DLL and therefore a failed proof load) but ≈17kN on the RSG side and therefore above DLL. Ultimate loads for the joint were 19.5kN just below DUL and over 160% of the first identification of damage (DIC side).

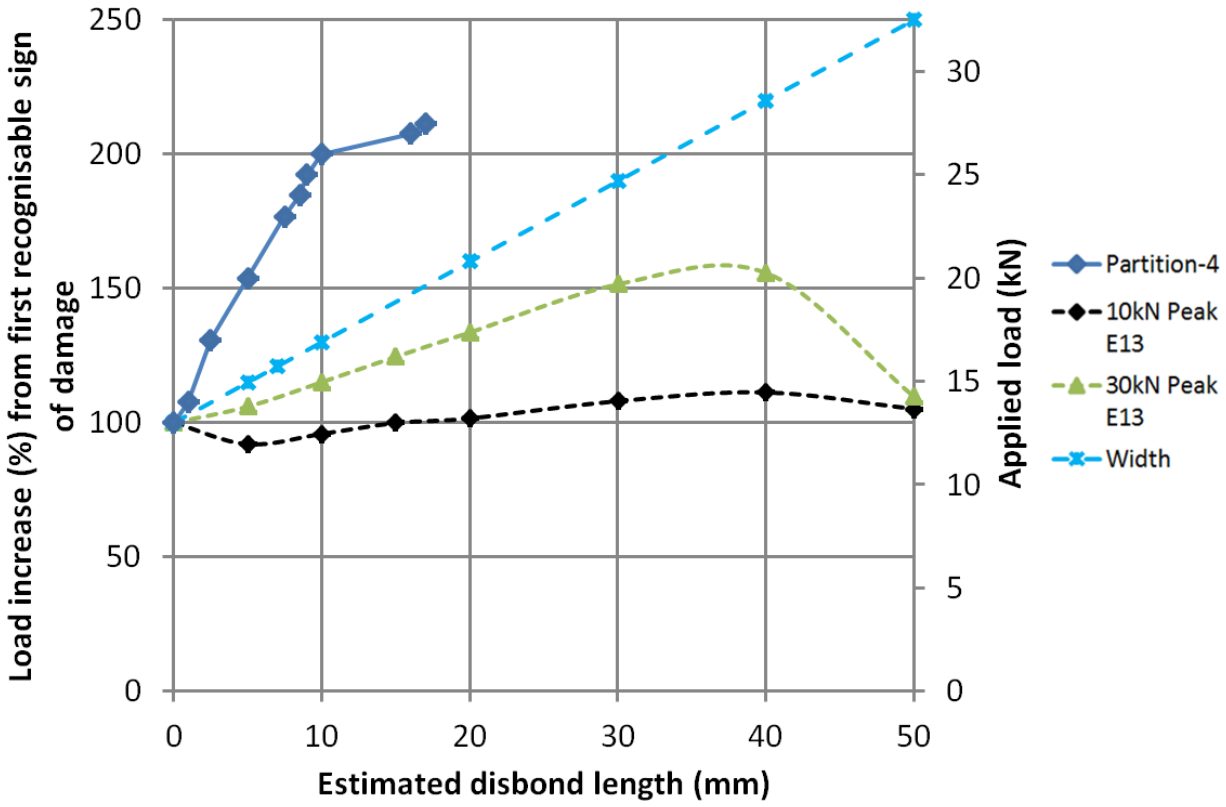

Figure 137: Specimen 'Partition-4: Estimated disbond lengths and equivalent joint strength as a percentage of damage initiation load plus comparison against hypothesised strength based on peak E13 strains and increased joint width

Figure 137 shows the estimated disbond lengths during loading of specimen Partition-4. Damage was identified at 13-14kN so this specimen may have marginally passed a DLL proof test. Slow damage growth, with some interaction with partition 10-15mm into the bond-line, is seen with an apparent strength increase greater than both the proposed peak shear strain values and the increase in strap width. Ultimate failure occurred at ≈28kN, 210% of the load damage was initially identified and greater than DUL.

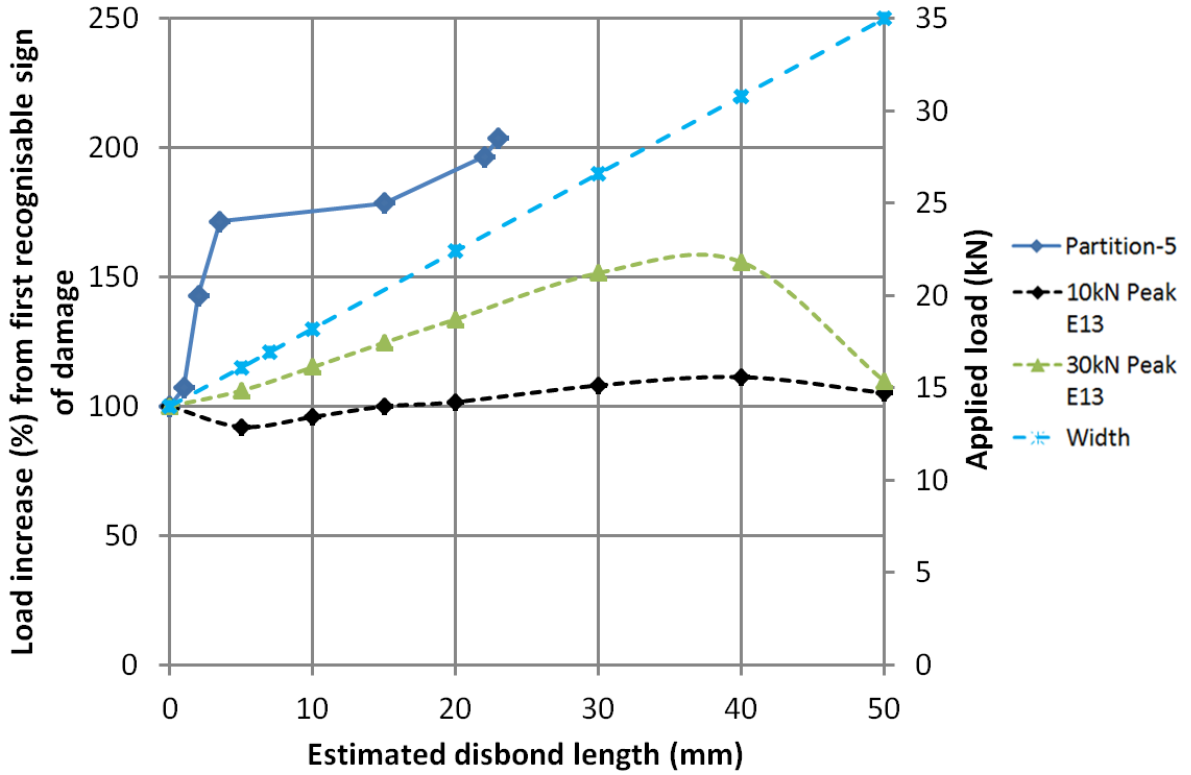

Figure 138: Specimen 'Partition-5: Estimated disbond lengths and equivalent joint strength as a percentage of damage initiation load plus comparison against hypothesised strength based on peak E13 strains and increased joint width

Figure 138 shows the estimated disbond lengths during loading of specimen Partition-5. Damage is initially identified at 14kN load, just above the proof testing DLL requirement of 13.3kN. A small amount of slow damage growth is present with an apparent strength increase greater than that expected by with the peak shear strain assessment of local increase in strap width. A rapid disbond event can be seen to occur which incorporates the first bond-line partition (up to 15mm) followed by a further period of slow growth up to a disbond length of ≈23mm. Ultimate failure occurs at 28.8kN over 200% of the identified damage initiation load.

9.3.2 Increased joint strength summary

Table 20: Summary of characteristic of modified test specimen characteristics

Test Specimen Name	Identified Damage Initiation Load (kN)	% DLL	Ultimate Failure Load (kN)	Ratio of Ultimate Failure Load to Damage Initiation Load (%)	Failure Mode
Taper-1	25	188	50.5	200	Mixed mode
Taper-2	25	188	47.6	190	Mixed mode
Taper-3	23	173	48	209	Mixed mode
Taper-4	10	75	30.6	306	Adhesive failure
Taper-5	12	90	27.5	229	Adhesive failure
Partition-1	8.5	64	18.1	213	Adhesive failure
Partition-2	11	83	20.5	186	Adhesive failure
Partition-3	12	90	19.5	163	Adhesive failure
Partition-4	13	≈100	27.9	215	Adhesive failure
Partition-5	14	105	28.8	206	Adhesive failure

Table 20 above summarises the results from the above analysis. Significant variation can be seen in both the loads identified with damage initiation as well as the ultimate strengths which, as may be expected, appear related to the failure mode and therefore quality of each joint. Variation is also present in the 'percentage strength increase' value although the lowest seen in this data set was that of Partition-3 which still showed an ultimate failure strength of ≈160% of the damage initiation / recognition load.

All specimens ultimately failed with an element of adhesive failure (including mixed mode). As such these joints may degrade over time and are not ideal structure; however purely based on proof tests up to the proposed DLL of 13.3kN most would

have passed this qualification process having shown no initial damage. Several specimens showed initial signs of failure between 10-14kN, around the proposed DLL. As such there is a possibility such joints with barely the required initial strength may have still potentially have qualified. Unlike standard configuration bonded joints however initial damage is not immediately followed by catastrophic failure. All the joints in Table 20 ultimately failed above the proposed DUL (DLL x 1.5) of 20kN with the exception of specimens Partition-1 and 3 which failed at 18.1 and 19.5kN respectively, still significantly greater than DLL. Specimens Taper-1, 2 & 3 which failed via mixed mode failure, and as such may better represent the behaviour of apparently well manufactured structure, ultimately failed at loads approximately 2.5x the DUL values based on DLL values which ensure the adhesive is only subjected to elastic deformation in normal service.

Although all specimens failed in non-ideal failure modes they may be representative of structure that has degraded over time in service (additional work degrading specimens expected to fail from mixed mode and adhesive failure will be required to ensure the progressive damage growth behaviour remains in these instances).

All specimens showed increases in effective strength as any disbond grew within the bond-line. When slow damage growth – or quasi-slow damage growth as a result of multiple short damage events – was present the increase in specific strength relative to the damage initiation load was greater than the proposed models based on either the peak shear strains calculated by FEA or the consideration of the simple strap width increase as a function of increased disbond length. Specimens Taper-4 and Partition-2 which showed some larger scale disbond events still showed significant strength increases, however these were close to or possibly below the predictions made considering local strap width. The strengths were always greater than those based on predictions based on peak strain (note the green peak strain line in the curves above is based on 30kN loading). As such designing to this principle although conservative should produce structure with the appropriate behaviour.

9.4 Proposed approach to operational use

To exploit the benefits of the results and designs discussed a possible scenario incorporating SHM enabled design in aerospace application is proposed.

9.4.1 Inclusion of SHM enabled joints within current means of compliance to allow NDI and Proof testing to be more effective and viable

In general damage-tolerance operation demands that a structure should be capable of maintaining DUL. The minimum capacity to support DLL is associated with category 3 damage (see Chapter 2: lit review chapter, Figure 6). Although these requirements consider discrete impact events on the greater structure the act of proof testing to DLL – the load level required of proof testing of composite bonded joints [3] – therefore does not actually guarantee the required undamaged static strengths are available even under current legislation. The SHM enabled joint concept however allows such a procedure to be used whilst ensuring the airworthiness of the structure by ensuring the bonded component should always have at least DLL capability in service.

The proposed process to initially qualify the bonded structure is outlined below.

- Upon fabrication – and/or a determined time after manufacture – the bonded component is proof loaded (quasi-static loading – which may take the form of tensile and/or compressive loading or bending or a combination depending on application – up to DLL) as per means of compliance *option ii* above. This ensures the component has sufficient strength at the time of initial qualification.
- Readings are taken from the in-situ strain sensors and compared to FEA predicted values and/or values from components previously determined to be sound. This process simultaneously verifies not only the integrity of the test structure but also the sensor array.
- Strain values of individual sensors and there ratios against reference gauges for use with in-service ‘ratio-metric analysis’ as discussed in section 9.4.2 below are recorded for the undamaged structure.
- If deemed necessary additional inspection using NDI may also be performed.

The above process ensures at the time of implementation both the structure and in-situ monitoring array are working to a sufficient standard. In service the structure (and again the sensor array) is ether continuously interrogated using flight loads (requiring storage and/or real time analysis of the sensor output data) or during pre-determined inspection intervals using airframe ground loads. To simplify analysis and to account for variations in load (e.g. wing fuel tanks half-full or empty if ground loads are used) the ratio-metric analysis described in section 9.4.2 below is used. The ratio-metric approach does not depend on absolute load and strain values hence should be invariant to unknown variations in aircraft static loads caused for example by weight variations or changes in configuration. If bond damage is identified further inspection may be performed. As an actual partial disbond would be present this can be identified using standard NDI methods. Appropriate repairs can then be performed. This process is presented in Figure 139 below.

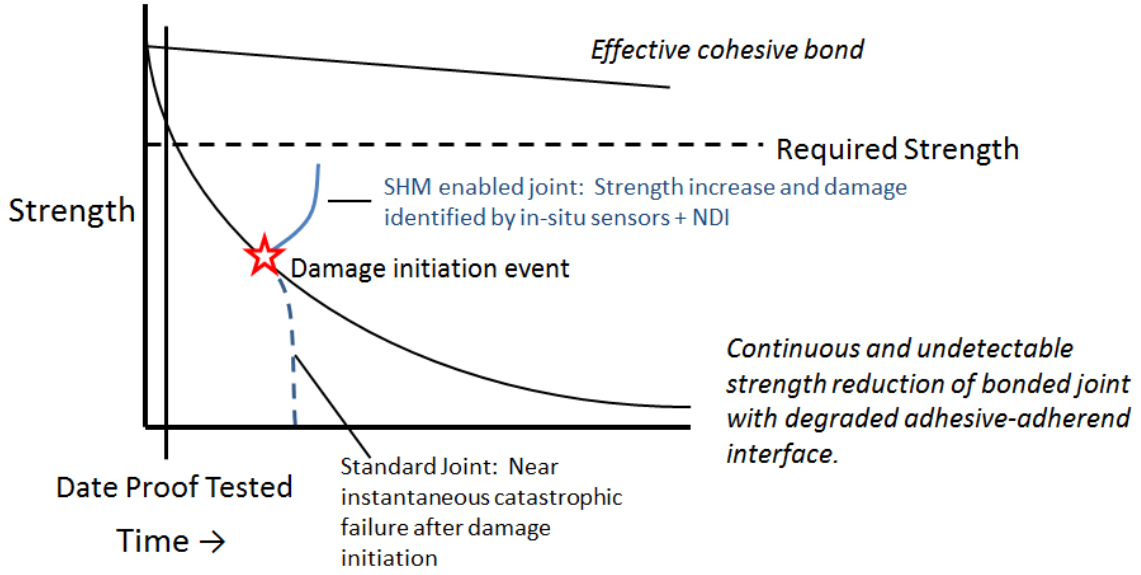

Figure 139: Schematic representation of a joint degrading with time in a standard configuration or operated using SHM enabled design

In the event of a problematic bond degrading eventually a threshold will be passed when the load surpasses the available strength. In a standard joint, as seen in Chapter 6, this results in near-instantaneous catastrophic failure. In the experimental cases where SHM enabled design was used (tapered and tapered-partitioned) ultimate joint strengths ≈160-≈300% of the identified damage initiation load were observed (Table 20) preventing instantaneous failure. Qualified joints

would have adequate strength at the time of certification. Adhesive strength degradation occurs over periods of weeks, months or years [192,193]; much longer than flight durations measured in hours. As such as any degradation reduces the bond strength below the threshold for damage to initiate not only should any damage be identifiable by the in-situ sensor array but the capacity of the joint should, at least temporarily, be raised to a level to ensure continued safe flight until repair.

As per damage-tolerant requirements (Figure 6 and also that proposed by Minakuchi [27] Figure 7 and Figure 13) allowable damage sizes will be influence on the frequency of scheduled inspections although the use of SHM enabled structure should enable inspections to be made faster (and therefore potentially more frequently) than visual or NDI inspections for many, particularly internal, components. If inspections could be reported at very short intervals repairs may be made as and when required under a condition based maintenance program with maintenance actions performed when damage passes a predetermined threshold. The extreme minimum structural condition may be equivalent to that of category 4 damage allowing continued safe flight (80% DLL capability – Chapter 2; Figure 6) upon which the damage will be identified and appropriate repair actions taken directly after that flight (although any scenario in which strength drops below DLL capability should be avoided). The use of SHM enabled structure however does not necessarily need to rely on condition based maintenance. Damage could still be tolerated under the existing schedule based inspection processes. Using the new design principles, it would be assumed that damage would be detected (via the SHM) at those scheduled inspections. This would fulfil the current S-SHM process allowed in MSG-3 revision 2009-1.

9.4.2 Ratio-metric analysis

It is recognised that non-damaged structure shows near linear surface strain responses per unit tensile load. Surface strain values in regions monitored (i.e. in the area of the joint overlap) can therefore be compared to strain values in locations within the same load path but where no damage – and therefore no deviation from the linear strain vs load behaviour – is likely to occur. Deviation from the ratios between these values would indicate shifts from this linear behaviour and indicate

damage independent of the applied load magnitude. Identified deviation from these original ratios greater than predetermined thresholds would initiate appropriate maintenance. Threshold values need to be selected to ensure airworthiness is maintained without generating false indicators of damage. The technique also offers some degree of 'common mode rejection' to sensor errors caused by for example temperature drift provided all the sensors were affected by the drift in the same way.

An idealised ratio-metric plot for a design feature show the following features: An idealised ratio-metric response is shown in Figure 140.

- No change in ratio-metric value if no damage to the bond and no deformation of the structure is present
- A slight change in ratio-metric response if no permanent damage has occurred but some deformation is present possibly as a result of structural bending. As seen in the previously discussed FEA and recorded stain data strap bending resulting in surface compressive strains may be observed towards the end of the strap overlap.
- More pronounced reduction in strain ratio resulting from a disbond event relieving strain from the monitoring gauge. The rate of change will be depended on is the disbond is a slow growth event or a rapid arrested disbond – see fig below.
- Strain ratio values may level off at near zero values if the disbond has progressed far past the monitoring gauge.

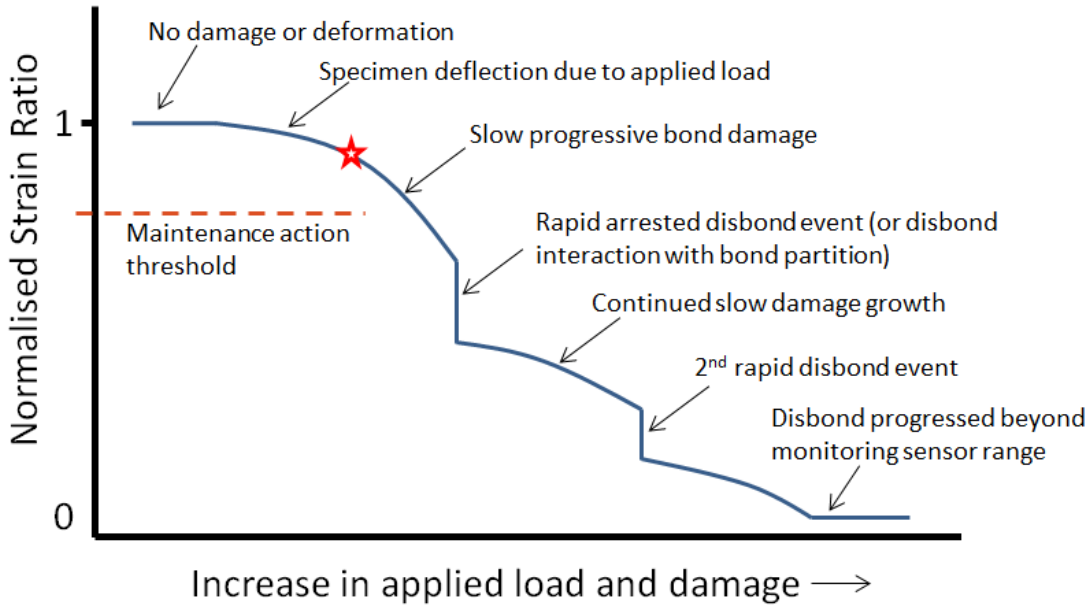

Figure 140: Idealised ratio-metric plot showing expected features of damage growth

9.4.2.1 Location of comparison surface strain sensors

To ensure appropriate placement of comparison reference sensors two factors must be considered. First they must be located within the same load path as the monitoring sensors to ensure all experience the same variations in applied load. Secondly they should be located in areas unlikely to be affected by damage. Within the specimens tested in this research two locations appeared potentially suitable.

Location 1 – On the plate outside of the joint overlap: A gauge placed on the joint plate, close to the straps would be appropriate for strain comparison. Both FEA and the initial tests of the standard configuration bonded joints which included RSGs in these locations (G1: Figure 55, Chapter 6) revealed a linear strain increase with load at these locations as would be expected of the linear elastic composite material. Strains measured at this location (from joint tests and FEA) are ≈1.8E-7 x the applied load (N). No gauges were included at this position on either the partitioned or non-partitioned test specimens.

Location 2 – On the joint strap, away from the strap end: A strain sensor placed a distance sufficiently far from the strap-end where from disbonds initiate and propagate should be suitable. Figure 80 shows FEA surface strains on the tapered strap with different lengths of disbond at 20kN tensile load. It can be seen at a

distance of ≈65mm from the strap edge strains only drop marginally as the disbond progresses. These variations are small when compared to those measured by the RSGs monitoring the tapered region. The tapered-partitioned specimens all had RSGs mounted at this position (Figure 112). Figure 113 - Figure 117 show a near linear strain/load response in all the specimens for this gauge (G6) up to total joint failure. Measured strains at this location are ≈8E-8 x the applied load (N) although greater variability is present compared to the potential reference gauge placed on the plate.

As strain responses at the joint plate are more consistent showing better linearity up to the point of failure this location may be best suited to place any comparative strain sensor. No RSG however was placed in this location in the specimens designed to show progressive failure (Tapered and Tapered-partitioned). As a RSG was present in 'location-2' on the Partitioned specimens this is therefore used for comparison against the gauges spread across the tapered section of joint strap. No RSGs in suitable comparison locations are available on the 'Taper' specimens. To allow further analysis to be made strain values from the RSGs positioned on the tapered region of joint strap are compared to a 'virtual gauge' which produces strains similar to those predicted for those which would be measured at location-2, i.e. 8E-8 x the known applied load (N). This allows comparison, at least in the first stages if disbond (up to ≈30mm) across all test specimens.

9.4.2.2 Examples of ratio-metric outputs from structures investigated

Below are examples of ratio-metric responses of selected specimens each which showed characteristic features linked to damage. Responses not included in the main text are included in Appendix D. Ratio-metric values calculated from strains measured when specimens were subjected to loads <1kN are omitted due to erratic responses associated by the division of two small values largely affected by system noise. Values are normalised against this reference value (ratio at 1kN) to aid comparison of results. Values after component failure are also omitted. In the case of total component or sensor failure the large and erratic nature of the ratio-metric responses would automatically trigger further actions to be conducted to check the condition of the sensor-structure system.

Tapered (non-partitioned) Specimen ratio-metric responses

Strain ratios for the monitoring gauge closest to the strap end (G1) for the 'Taper' specimens (Figure 141, Figure 142 & Figure 143) produce low values which are difficult or impractical to interpret. As such these are not normalised and the original ratio values are shown to illustrate the problematic, close to zero, strain ratios associated with monitoring at this location.

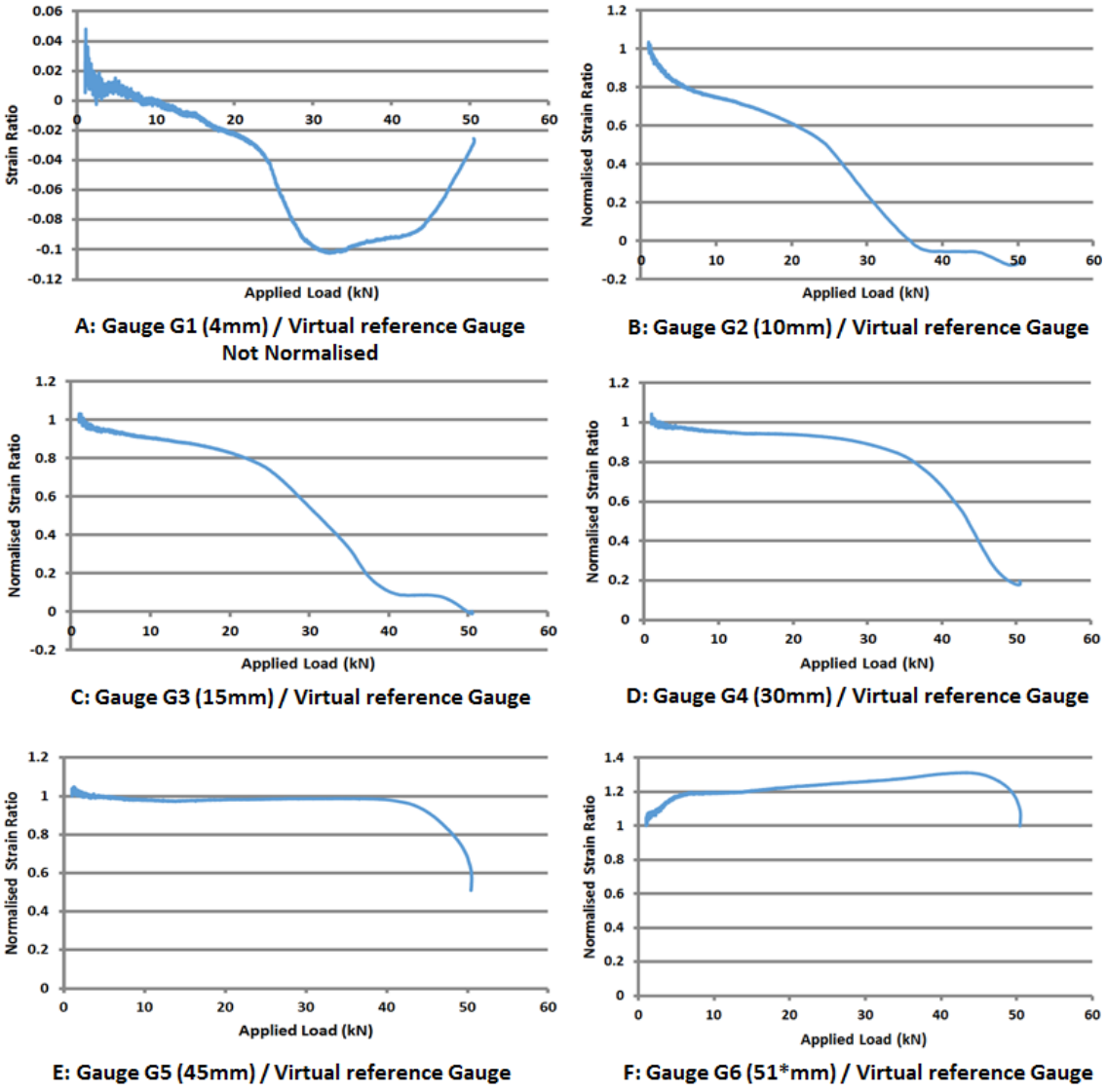

Figure 141: Ratio-metric values for each RSG compared to a virtual reference gauge placed at 'location-2' on test specimen 'Taper-1'

Figure 141 above shows the ratio-metric responses of test specimen 'Taper-1' although near identical responses were observed for specimens Taper-2 & 3. These

were the only specimens to fail as a result of mixed mode failure. As previously discussed the monitoring gauges are compared to a virtual RSG located on the strap 65mm from the strap-end. The curves above show a reduction the ratio values from the moment load is applied. This is most prevalent in the responses of the gauges placed closer to the strap end highlighting the strain response to load is not precisely linear. Assessments of the RSG and DIC outputs against FEA predictions to estimate disbond lengths (see section 9.3.1) suggest no disbonding is present until approximately 25kN loading. It is possible this characteristic may be linked to initial stages of disbonding (therefore showing a more sensitive approach that that used in section 9.3.1) but it may also be associated with bending of the strap introducing an element of compression therefore effectively reducing the tensile strain measured in this region. In the responses from RSGs positioned near the strap end, and therefore close to the region of disbond initiation, an increased change in strain ratios can be seen at the load previously identified as the moment of damage initiation (≈25kN loading). The reduction in strain ratio identifiable from the moment of loading is also present in the specimen Taper-2 & 3 (Appendix D). Any such response which is not linked to significant joint degradation will influence the value of any threshold selected to initiate maintenance actions to avoid unnecessary structural downtime. Deviation from the initial ratio-metric values associated with damage can be seen to occur later in the loading cycle as the location of the monitoring RSGs moved away from the strap-end allowing estimations of the disbond size to be made.

Figure 142 below shows the ratio-metric responses of test specimen ‘Taper-4’. Comparison of DIC and RSG results suggest different disbond lengths may have been present in the two bond-lines of this joint (see Figure 132, Section 9.3.1). Initial damage was previously estimated to occur at ≈10kN loading, below DLL (13.3kN). Major drops in the ratio-metric values can be seen which correspond to rapid disbond events previously identified. Some increases in these values can be seen in the data from G2 and G4 after the major disbond event which occurred just after 15kN load. All values however still remain significantly lower than the initial ratio-metric values. As per specimens Taper -1, 2 & 3 (Figure 141) the values from gauge

G1 are approximately zero and near constant throughout the test providing little data that could be used in service.

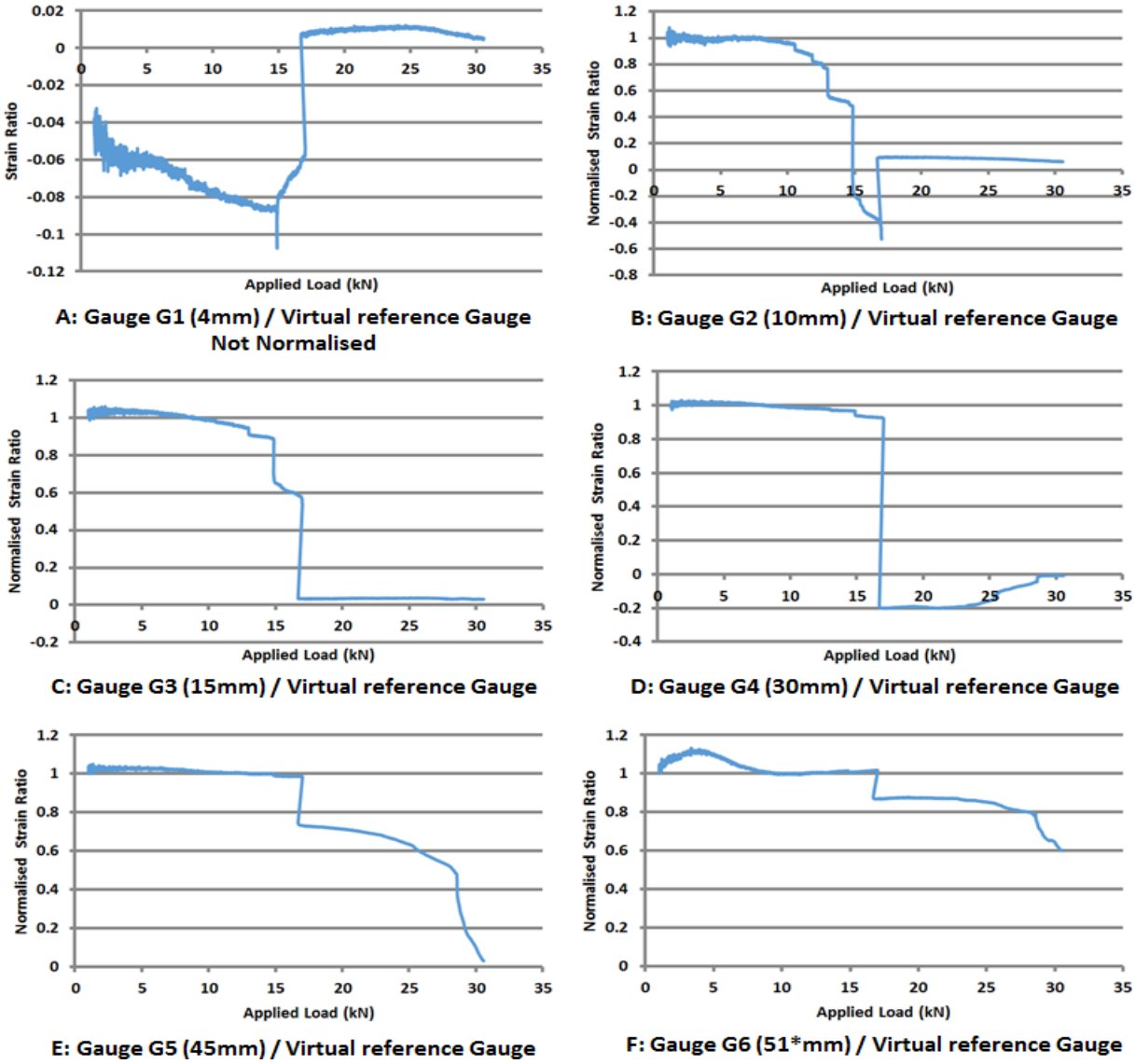

Figure 142: Ratio-metric values for each RSG compared to a virtual reference gauge placed at 'location-2' on test specimen 'Taper-4'

Figure 143 below shows ratio-metric responses of test specimen ‘Taper-5’. This specimen showed progressive damage resulting from small rapid adhesive type failures. An obvious deviation from the initial ratio-metric values can be seen at 13kN (marginally <DLL), primarily from G2 and G3. This is the load previously identified as when identifiable damage initiated. Although estimated disbond lengths are similar to those of specimens Taper 1, 2 & 3 in this case little variation is seen

from G5 and G6 (placed further in-board than the estimated disbond front) although the defined responses from the previous sensors should be adequate to activate a maintenance action. Again ratio values from the gauge placed 4mm from the strap end do not provide practical information for monitoring.

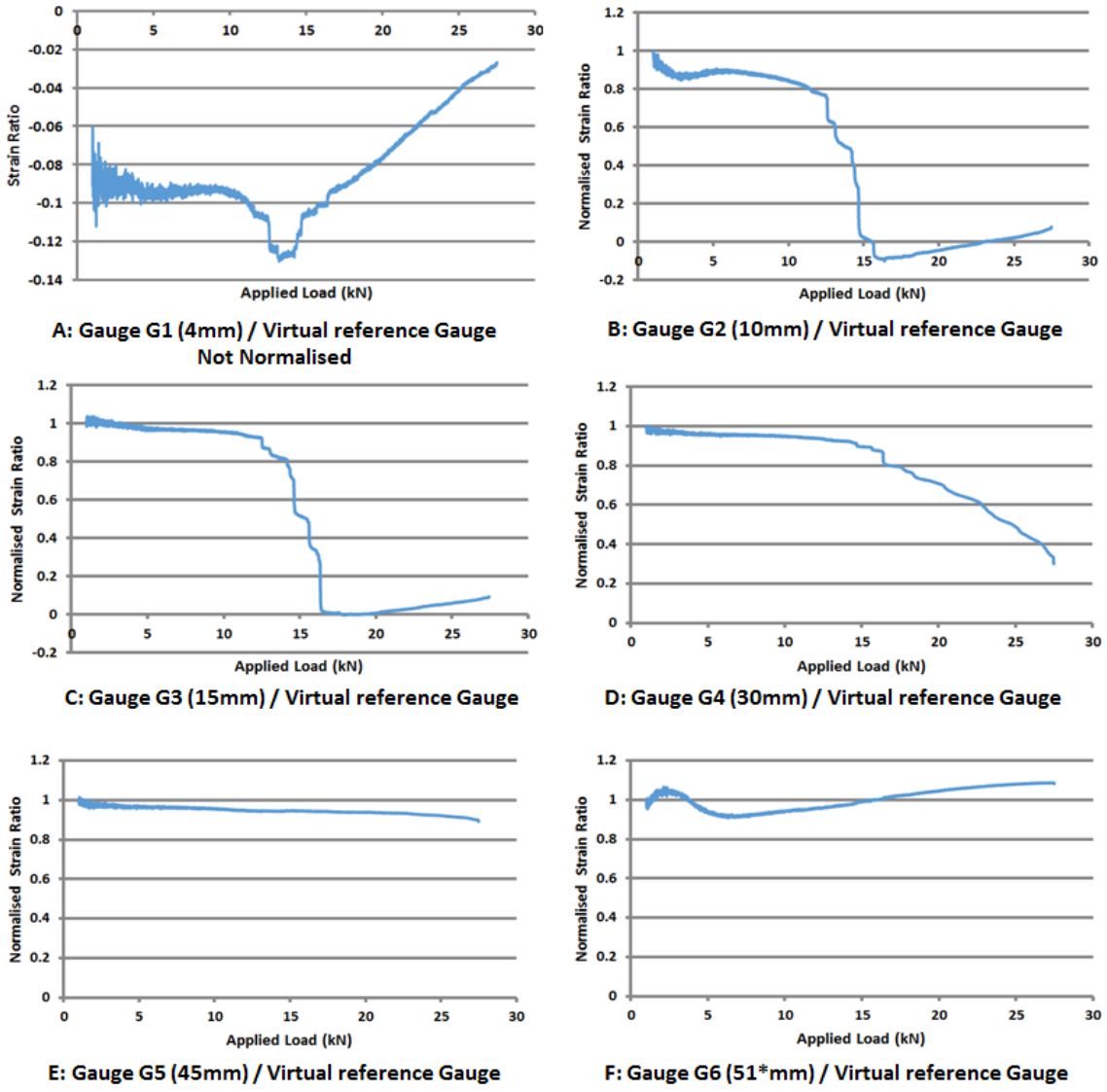

Figure 143: Ratio-metric values for each RSG compared to a virtual reference gauge placed at 'location-2' on test specimen 'Taper-5'

Partitioned specimen ratio-metric responses

Ratio-metric curves below are from partitioned-tapered specimens (RSG array as per Figure 112) which used a real reference RSG placed at ‘location-2’. Information gained from the monitoring gauges closest to the strap end (G1 – 9mm from the end

as oppose to 4mm in the ‘Taper’ specimens) did provide values that could be analysed. As such these ratios, as per the other monitoring/reference gauge pairs, are normalised against the values measured at 1kN of loading.

Test specimen Partition-1 showed evidence of asymmetric disbond growth in the two bond-lines and damage initiation at 8.5kN (below DLL). As previously recognised a significant bond area was visibly not bonded during fabrication. A rapid failure event associated with the first bond-line partition was recognised and in the ratio-metric responses produced a sudden drop in strain ratio in a similar fashion to that seen in Figure 144 below which shows the responses from specimen Partition-2. Due to such similarities the ratio-metric plots for Partition-1 are included in Appendix D.

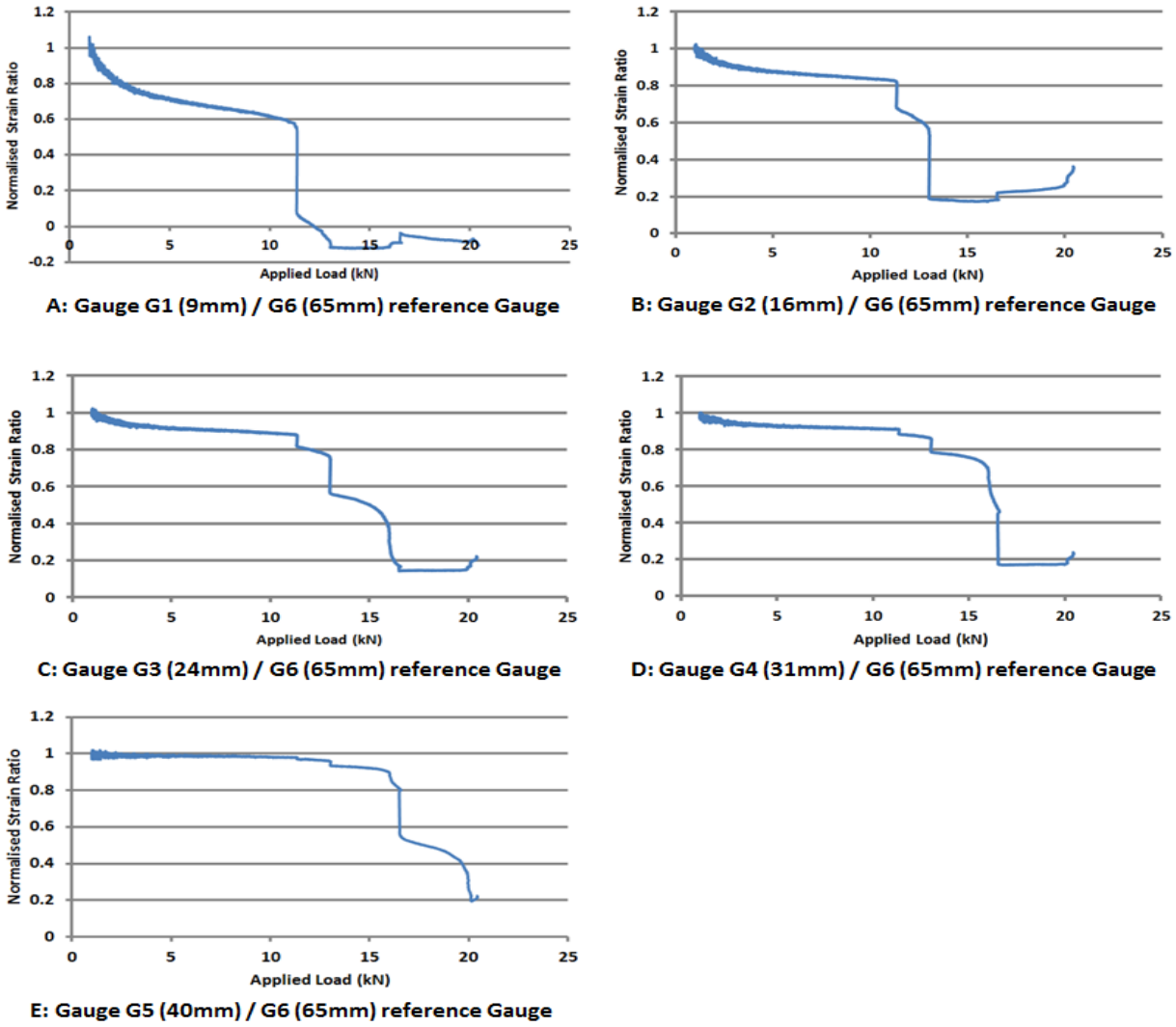

Figure 144: Ratio-metric values for each RSG compared to reference gauge G6: Test specimen 'Partition-2'

Figure 144 shows ratio-metric values of specimen 'Partition-2'. Estimations of disbond lengths (Figure 135) suggest different disbond sizes in the two bond-lines. Initial damage was identified at ≈11kN (<DLL) occurring as an arrested rapid disbond. This is acknowledged by the first sudden drop in the above plots. As the disbond passes under each gauge strain-ratio values can be seen to rise. Although this may need to be considered when analysing ratio-metric responses when interrogated under a static load, therefore producing single values with no recorded history, values are still much lower than those at initial damage and therefore should be lower than any maintenance threshold. Unlike specimens Taper-1 to 5 gauge G1 (9mm from the end rather than 4mm) does produce usable data.

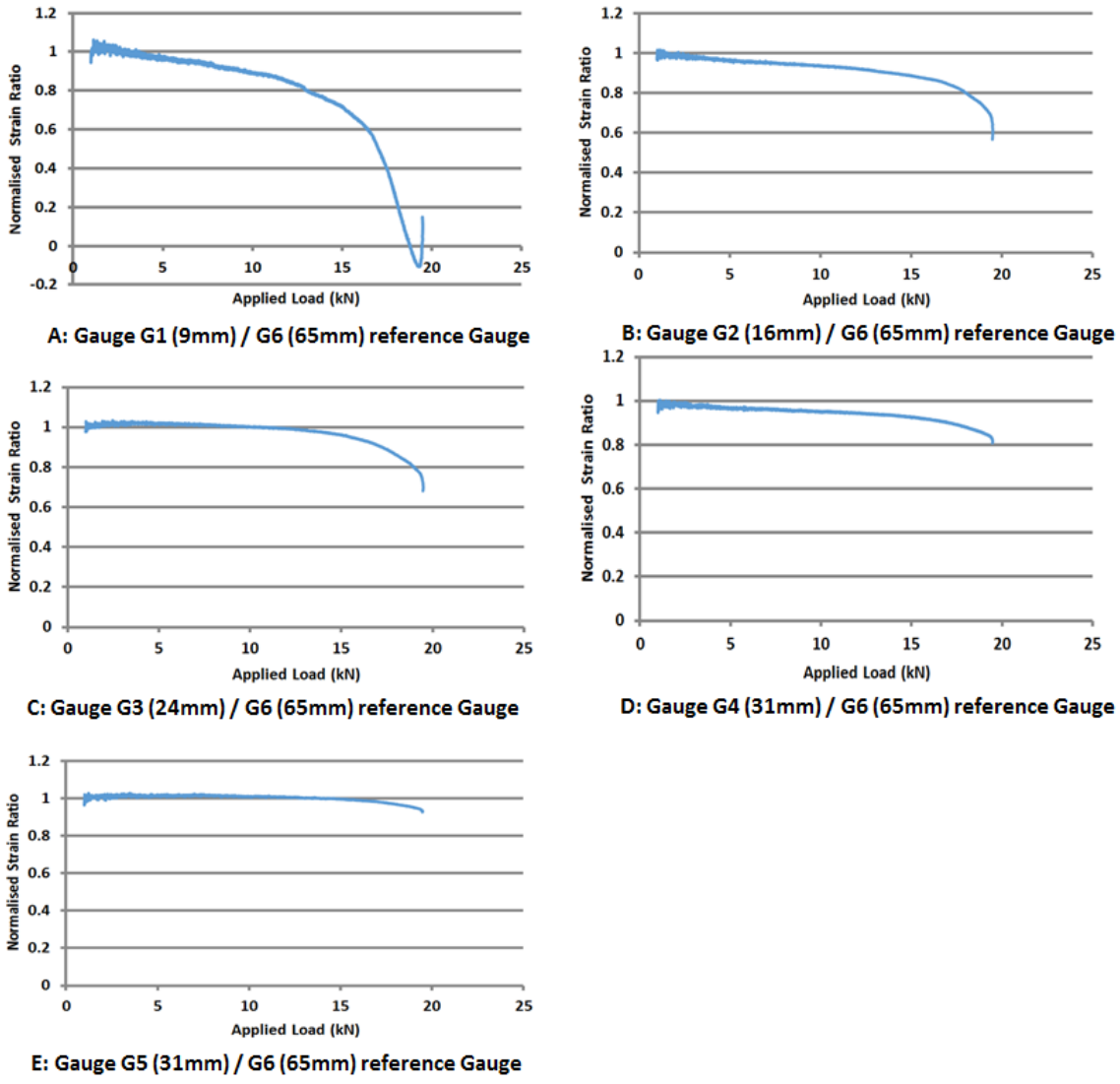

Figure 145: Ratio-metric values for each RSG compared to reference gauge G6: Test specimen 'Partition-3'

Figure 145 shows the ratio-metric responses of test specimen Partition-3. This specimen seemed to have slightly differing disbond lengths in each bond-line (section 9.3.1, Figure 136). This specimen showed initial signs of damage from 12-13kN so would have failed the proof load test but only by a small margin. This and the short disbond length highlight this specimen as showing potentially problematic behaviour. Deviations from the undamaged ratio-metric values at damage initiation load can be seen from gauges placed close to the strap-end in Figure 145. The most prominent and sensitive results are from gauge G1 highlighting the importance of the initial monitoring gauge.

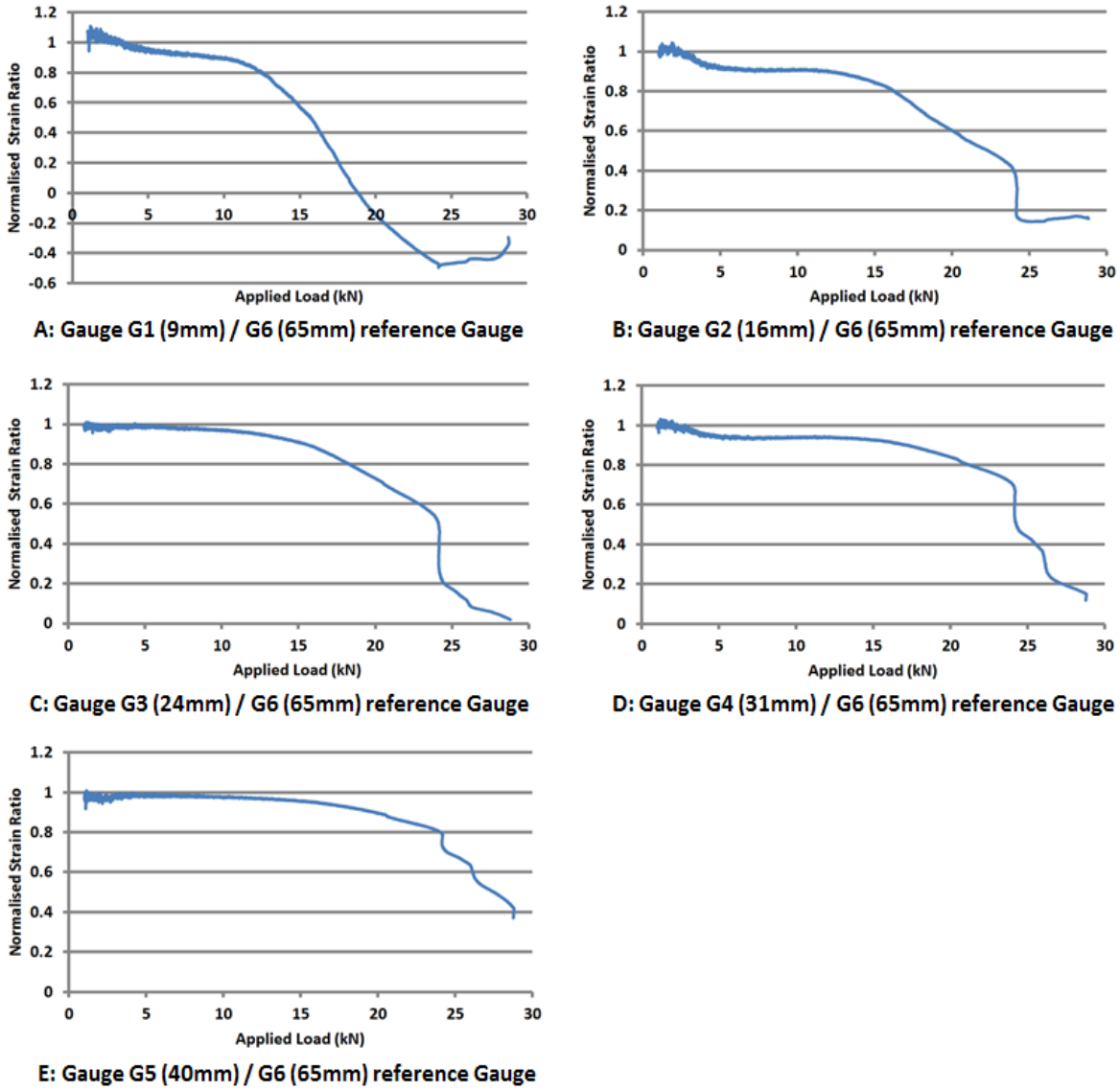

Figure 146: Ratio-metric values for each RSG compared to reference gauge G6: Test specimen 'Partition-5'

Figure 146 above shows the ratio-metric responses of test specimen Partition-5. This specimen exhibited steady progressive disbond growth apart from a rapid event just prior to 25kN of loading associated with the disbond interacting with the first bond partition. Damage was first identified at ≈10kN and as such this joint would have failed the proof testing processes. Deviation from the initial ratio-metric values can be seen at this moment particularly in the ratio values from gauges closest to the strap end. The ratio-metric responses for specimen partition-4 are similar to those shown in Figure 146 and are included in Appendix D although in this instance little evidence of rapid partial disbond events (signified by sudden drops in strain ratio value) is present.

9.4.2.3 Ratio-metric values at zero damage and maintenance action thresholds

Table 21: Ratio-metric values from gauges near the strap end at DLL proof testing loads for test specimens passing proof testing requirements

		Ratio Values at 13.3kN Load		
Specimen name	Initial failure load (kN)	G1(4mm)/Im	G2(10mm)/Im	G3(15mm)/Im
Taper-1	25	N/A	0.414	0.562
Taper-2	25	N/A*	0.437	0.565
Taper-3	23	N/A*	0.487	0.661
FEA			0.378	0.615

		G1(9mm)/G6	G2(16mm)/G6	G3(24mm)/G6
Partition-4	13**	0.305	0.610	0.738
Partition-5	14	0.308	0.768	0.962
FEA		0.310	0.647	0.783

* Ratio values are available that may be interpreted for damage initiation – see Appendix D – however these may be difficult to accurately assess due to their low magnitude (0.005 & 0.07).

** The exact moment of damage initiation is difficult to establish using the comparative method used. As such damage initiation is likely to have occurred at, or very close to 13.3kN and may not be noticed if loading does not continue above this load.

Table 21 summarises non-normalised strain-ratios produced by gauges close to the strap-end. Ratios shown are at 13.3kN of load simulating values during proof testing to DLL. Only specimens that showed no damage up to 13kN are included. In addition comparisons against ratios at these locations are made against FEA

predictions of undamaged joint strain values revealing good correlation between the FEA model and the response of test specimens.

Table 22 presents the data in Table 21 normalised to the initial undamaged condition at 1kN loading as per the curves presented in Figure 141 - Figure 146. This also highlights the change in sensitivity to damage or structural distortion dependent on the sensor location. Information presented in this manner may be easier to interpret in service and enable well defined maintenance thresholds to be defined.

Table 22: Normalised Ratio-metric values from gauges near the strap end at DLL proof testing loads

		Normalised Ratio Values at 13.3kN Load		
Specimen Title	Initial Failure Load (kN)	G1(4mm)/Virtual	G2(10mm)/Virtual	G3(15mm)/Virtual
Taper-1	25	N/A	0.714	0.887
Taper-2	25	N/A	0.796	0.831
Taper-3	23	N/A	0.820	0.965

		G1(9mm)/G6	G2(16mm)/G6	G3(24mm)/G6
Partition-4	13**	0.729	0.813	0.944
Partition-5	14	0.734	0.881	0.938

Although close some variation between the ratio-metric values associated with specific structures can be seen. This may be associated with issues such as the precise location and orientation of the surface mounted strain gauges as well as small effects within accepted tolerances within individual specimens. It may therefore be advantageous to record this data at the time of qualification (proof testing) for comparison or to consider the likely variation resulting from the specific fabrication process when defining any maintenance action thresholds. An alternative would be to use ratios for non-damaged structure based on FEA simulations. Using this approach however would remove the capability to account for the variability discussed. The decision to either record and use values for specific individual components or set values established either by testing or FEA may be based on the number of components to be produced and inspected as well as the variation in ratio-metric response of such components as a result of defined, repeatable manufacturing practice.

Information gained from the sensor system should ideally provide a go (no further action) or no-go (further inspection and possible repair) response. Damage should be positively identified with the minimum disbond size identified defined by the potential for damage growth and time/flight hours between inspections. No-fault-found type responses leading to un-necessary downtime should be avoided. Suitable compromises therefore need to be made regarding appropriate ratio-metric action thresholds and/or sensor placement.

All the specimens tested may represent problematic structure that has degraded in-service. As such lessons may be learned from each test. Specimens Taper-1, 2 and 3 – which failed in by mixed mode failure – may best represent problematic bonded structure that may be produced with slight quality control issues combined with in service degradation (although the specimens tested had not been subjected to environmental degradation). The remaining specimens, which failed by adhesive type failure, may represent structure that has further degraded down the degradation curve shown on Figure 127 or have experienced very poor manufacturing quality control and still marginally passed the proof testing requirement.

Of the specimens tested that which may be of greatest concern may be specimen 'Partition-3'. Not only did this joint fail at the lowest load relative to the first identified sighs of a disbond (163% of the initial damage load) – although the ultimate load at failure (19.5kN) was above the proposed DLL and near the DUL (20kN) – the disbond was of a relatively short length at the moment of failure (estimated as 3mm on the RSG side bond-line and 10mm on the DIC side). This short disbond length limits opportunities to detect damage to sensors placed towards the strap-end.

9.4.2.4 Proposed maintenance action thresholds

Threshold values, based on percentages of ratio-metric values, are matched against the specimens tested. Consideration is made of the ratio values at the proof testing load (DLL 13.3kN) when no physical damage can be identified (i.e. the component passed the proof load test). In the case of specimens Taper-4 & 5 and Partition-2 which failed as a result of multiple, short rapid disbond events at 10-12kN of loading reference is taken from the highest load prior to the rapid drops in ratio-metric values. Specimen Partition-1 is omitted due to the presence of the visibly identifiable

manufacturing defect. Tables containing comparisons of joint residual strengths for various percentages of the ratio-metric values established at DLL are included in Appendix E. Comparisons are made for each monitoring gauge / reference gauge system at ratio values from 90 – 60% of those recorded at DLL.

The joints that would be of major concern in service are those which showed initial failure near or under the DLL as it is possible these such may be encountered in service (Specimens Taper-4 & 5 and Partition 2, 3, 4 & 5 not including specimen Partiton-1 due to visible damage). In summary/discussion of the potential ratio-metric thresholds for each of these joints:

Specimen Taper-4: The presence of rapid failure events - some of which caused significant increases in disbond length – resulted in all sensors (i.e. monitoring and comparative sensor systems) being able to identify degradation whilst the joint still had significant ability to transfer load. The sensors least sensitive to initial damage are those placed furthest from the strap-end (in the Taper specimens G5, 45mm from the strap-end). Even at this location with a maintenance action threshold set to 60% of the DLL reference ratio ≈5kN of load capacity remained (16% of total). This was due to the relatively long disbond (30-40mm) present at the time of full failure.

Specimen Taper-5: Results for taper-5 were largely similar to taper-4. Gauge G4 (30mm) – the second least sensitive gauge – could have potentially raised a maintenance warning using a ratio-metric threshold of 60% of the reference value whilst 4kN of load capacity (15% of total) remained. No useful output can be gained from the gauge furthers from the strap-end – G6 (45mm) – due to the shorter disbond length at failure (≈20mm) in this specimen.

Specimen Partition-2: This had the potential to use ratio-metric thresholds of 60% of the reference values for all sensors. The innermost sensor G5 (40mm) would have indicated a maintenance action while 4kN load capacity (20% of total) remained. Again the ability for sensors to be placed over a wide area of the joint overlap was due to the large disbond size (35-40mm) prior to failure.

Specimen Partition-3: As previously identified Partition-3 may reveal the most potentially problematic response in these tests. The short disbond length up to

failure (3-10mm) means alerts threshold values of 90% or less would be required for all but gauge G1 (9mm) otherwise the joint would have already failed or be close to failure. As such only outputs from gauge G1 (9mm) are of practical use. When ratio-metric thresholds of 90-60% of reference values are used 4.5kN (23%) to 2.3kN (12%) of load bearing capacity remains.

Specimen Partition-4: This specimen showed potential for using various ratio-metric threshold values in most locations with the exceptions of low percentages used with gauges far from the strap-end. Disbond length at failure equalled ≈18mm.

Specimen Partition-5: If damage propagation and failure behaviour as seen on Partition-5 could be assured ratio-metric thresholds as low as 60% may be considered in all gauge locations. At this threshold gauge G5 (40mm) would have indicated maintenance was required while 2.6kN (9%) of the joints strength remained.

Examination of the ratio-metric outputs of the specimens experiencing initial damage near or below the proposed DLL show many possible outcomes may occur. It must be emphasised however that due to such variability and the uncertainty associated with the bonds condition that both the strength remaining after each stage as well as the ultimate disbond length prior to failure may only be known after the joint has failed. Damage therefore needs to be identified while a high probability of suitable residual properties remains. Based on the most problematic case Partition-3 it seem apparent values from the gauge G1 (9mm) is required. Comparisons with the tapered specimens are made using the similarly located gauge G2 (10mm) on these joints. To reduce the possibilities of false damage indicators it is suggested for demonstration purposes – using the SHM enabled joints tested – maintenance actions may be triggered if ratio-metric values on the considered gauges drop to values ≤70% of the ratio established at DLL. The damage size and what ultimately was known to be the remaining load capacity at the moment of this threshold being passed for the joints discussed above is summarised in Table 23.

Table 23: Condition of joints showing evidence of damage initiation around or below Design Limit Load when the effective monitoring gauge closest to the strap-end – G2(10mm) Taper or G1(10mm) for Partition specimens – indicates a ratio-metric value 70% of that of the reference value.

Specimen Title	Proof load at reference ratio	Load when gauge ratio = 70% reference ratio		Disbond length at threshold	Joint specific remaining strength		Ultimate Failure load	
		kN	% DLL		kN	% of total	kN	% DLL
Taper-4	10.1*	13	98% **	1-3 mm	17.6	58%	30.6	230%
Taper-5	12.5*	13.2	99% **	1-2 mm	14.3	52%	27.5	207%
Partition-2	11*	11	83% **	0-1mm	9.5	46%	20.5	154%
Partition-3	13.3 DLL	16.7	126%	1-5mm	2.8	14%	19.5	147%
Partition-4	13.3 DLL	16	120%	2-3mm	11.9	43%	27.9	210%
Partition-5	13.3 DLL	15.5	117%	1mm	13.3	46%	28.8	217%

* Load of partial rapid failure event prior to DLL producing the last moment a reference ratio relating to structure that may be assumed to be undamaged may be assumed.

** Percentages based on 13.3kN DLL not stated reference load.

Table 23 indicates as RSGs positioned 9 or 10mm from the strap-end dropped below the 70% ratio threshold small disbonds were present however reasonable levels of residual strength remained in all cases. Maintenance actions would be activated whist damage sizes were still comparatively low (≤5mm) maximising the chance to identify damage before ultimate failure. Even specimen Partition-3, which ultimately failed with the shortest disbond length, still had the capacity to transfer 2.8kN of load greater than the load to initiate damage. This demonstrates the sensitivity of the technique to damage detection. All the structures discussed ultimately failed at loads close to or exceeding their DUL. These factors, by using the SHM enabled joint design to inspect the structure, fulfil or in some cases surpass the requirements of damage-tolerant structure discussed in Chapter 2; section 2.2.3. Using these threshold values and gauge locations no ‘no-fault-found’ cases would have been reported. This approach appears to provide meaningful results even in cases where disbonds of various lengths within the double-strap configuration are potentially present.

In service it may be advisable to use several gauges in various locations with specific thresholds to confirm damage initiation to avoid false alarms. Evidence that this may be possible can be seen within the tables in Appendix E. Analysis of the ratio-metric values from these additional gauges may also assist determining the severity of the disbond, assuming failure does not occurred with a small disbond as

per specimen Partition-3, although to simplify operation and reduce costs and additional mass overuse of multiple sensors should be avoided.

Although the specimens that showed the greatest capacity (specimens Taper-1, 2 & 3) are most likely to represent actual structures performance setting thresholds to their values if difficult due to the loads being significantly higher than those to be experience in service. Assuming the same but diminished characteristic exist if these joint degrade over time when the ratio produced by gauge G2(10mm) is at 70% this corresponds almost exactly – in a similar fashion to the specimens failing at lower loads – to the moment damage can be identified (Figure 131). Further research will be required to establish if the ratio-metric characteristic change as a result of bond-line degradation (environmental ingress). All specimens tested revealed large amounts of residual strength when damage could be recognised for both adhesive and mixed mode failure. The damage arresting characteristics should therefore prevent further damage growth although further consideration of flight spectral loads must be considered. If the reference ratio-metric values change this may have an adverse effect on diagnosis, either potentially missing damage or activating unnecessary maintenance actions. Such behaviour however is more an issue of global material degradation and not connected to the specific issue being addressed, that of integrity of the bonded joint. Any drift recognised may however aid monitoring such evolution if appropriately analysed however further research would be required to determine if this is the case. If long term analysis does reveal a drift in global structural response the effective ratio-metric reference values to change over time it may be necessary to “re-calibrate” these values possibly with the aid of ground loads and NDI to ensure no disbonds are present.

9.5 Section Discussion

9.5.1 Section summary

Analysis of test results has shown the method based on ratio-metric analysis in combination with current approved certification methods may be used to both simplify the certification and inspection process. It can also eliminate concerns based on the continued airworthiness of the structure due to performance degradation resulting from environmental exposure, at last under quasi-static loading

conditions. The removal of this uncertainty may allow less reliance on additional structural features, such as ‘chicken fastener’ to be realised allowing realistic reductions in mass to be achieved.

Although disbond of various lengths were identified all modified joint specimens showed considerable increases in total load bearing capability compared to the loads where damage was positively identified using either the comparative approach or using appropriate ratio-metric analysis.

Ratio-metric analysis can be used to determine damage severity regardless of applied load and provided usable responses even in cases where differences in the disbond lengths within the joints two bond-lines appear present. The structures capability to prevent total failure at disbond initiation both allows the strain based approach to identify the damage and for actions to be made based on this information.

Taper designs using the simplistic approach of considering peak shear strain values in the mid-plane of the adhesive centre-line appear to show conservative but usable design guides for the degree of taper in such structure. The rate of apparent strength increase would be tailored by the designer for specific structural demands.

The surface strain ratio-metric approach provides a simplistic ‘go – no go’ response to maintenance actions based on predetermined threshold levels allowing for rapid and uncomplicated assessment. This is compatible with the current scheduled inspection and maintenance practices where damage is repaired when detected at scheduled inspections. In this sense, the strain measurement system would fulfil the same function as any other conventional NDT process. The technology in the sensing system discussed is already certified for airworthiness and can be serviced using currently available skills. In the event of sensor system failure the ratio-metric response will be clear and although undesirable would indicate a maintenance action on the system is required. The surface mounted approach to sensor means simple repairs to the sensor array could be made without the requirement to replace the structural component; a necessity for any SHM enabled structure containing damaged embedded sensors. Upon replacement reference ratio values may be re-established using structural ground loads. As the system is activated by physical

disbonds the integrity of the structure at this time, as well as potentially during in depth inspections activated by the in-site sensor system in service, could be assured using standard NDI methods. In service baseline strain ratios may be normalised to values of the undamaged structure at proof testing load (DLL) with reductions from this value of unity being easily interpreted during inspection in a similar manner to that illustrated in Table 23.

Although several sensors on the joint overlap may help ascertain the severity of the damage it is primarily important that damage is identified and repaired before the structure fails. As such the location of the initial sensor is important; particularly as the maximum disbond length at failure may not be known. It has been shown sensors placed too close to the strap-end may produce difficult to interpret data whilst those further into the overlap may be less sensitive to small disbonds and as such not produce differences in ratio-metric values significant enough to avoid 'no-fault-found' type events. Placement and choice of ratio-metric threshold for such a primary sensor must therefore be carefully selected.

Discrete damage events may not be managed using the configurations discussed. As such this form of SHM enabled design may not be suitable in all locations of the greater structure.

10 Research Discussion, Future Works and Conclusions

10.1 Research Discussion

The investigation presented in this thesis presents an alternative approach to composite structural design, enabling more efficient structure to be considered, designed and operated by in-situ sensing of the structures condition. The concept and contribution presented in this thesis has previously not been exploited. Although much research has been made regarding permanent Structural Heath Monitoring sensors and diagnostic systems little research has been conducted to explore how SHM can not only perform automated inspection but also be used to create lighter, less complex and therefore more efficient structural designs. It has been recognised that for such an approach to provide the benefits above, unlike contemporary approaches, the structure and the monitoring system must be regarded as a combined system. Damage tolerance requires the structure to have sufficient residual properties after the initiation of any damage so that appropriate repairs can be made. Without this capacity simply monitoring the structure has no purpose. Damage tolerance design also demands damage should be easily identified. Structures which provide positive damage indicators can be easily inspected by simple in-situ sensors eliminating the requirement of complex sensing systems. Such approaches are likely to be less intrusive within the airframe as well as being easier to maintain and certify for use within aerospace structure. Such approaches may also provide less ambiguous responses therefore providing more defined action thresholds. It is believed that, in this researcher's opinion, with no capability to manage potential damage and provide easily identified damage indicators – as is the requirement for contemporary damage tolerant structure normally monitored using visual inspection – SHM alone cannot provide any benefits.

This work sought to combine the requirement stated above in a considered SHM enabled design primarily aimed at aerospace structures constructed of carbon fibre composite materials. It has been recognised that the application of such an approach to bonded composite structure could provide significant advantages. This is due to difficulties in inspecting such structure – either via visual inspection or via NDI – and the propensity of such features to fail catastrophically almost instantly

after damage has initiated. Currently these issues are resolved by the inclusion of additional, inefficient structure (e.g. additional bolts, fasteners etc,) used in addition to the adhesive bonds to account for the uncertainty associated with such structures condition. The relative low physical dimensionality of bonded structure as well as an understanding of the mechanics of load transfer in such components makes them ideal candidates for adaption with the inclusion of an in-situ monitoring system. In addition the potential to relieve the burden of additional engineering features currently used to account for the uncertainty of the structures condition and the nature of its rapid failure further supports the reasoning for selecting bonded structure for development.

It was recognised to aid the simultaneous design of a combined structure and monitoring system common design consideration should ideally be present. In composite structural design strain is usually considered as a key design parameter over stress (unlike traditional metallic design) due to the differences in modulus of the composite laminates component parts. Adhesively bonded joints also consider strain (or shear-strain) in their design and to define their limit load capability. In this work it was decided therefore to base the SHM enabled design investigation on strain performance (as a design variable) and strain measurement as an SHM technique. Strain is well suited as a measurand to be designed into the structure-sensor network particularly as strain measurement is reliable and already flight certified if sensors are surface mounted. It is also a direct indicator of the instantaneous nature of the load path requiring potentially only little further analysis to analyse the condition of the structure in the region of the sensor. Similar approaches have previously been used under laboratory test conditions to monitor disbond growth in specimens subjected to fatigue conditions used to control damage growth. A new approach was developed in this thesis regarding joint design. In this study a joint design was used which included tapered joint straps. This allowed the magnitude of shear and peel stress/strains, relative to the applied load, experienced by the adhesive bond to be manipulated as a function of the size of any disbond; a concept previously not utilised in bonded joint design or in conjunction with in-situ sensing. The presence of the taper allowed shear (and peel) stresses and strains to reduce in magnitude for a given structural load as a disbond progressed into the

overlap. This ensured in the presence of disbond initiation failure did not rapidly progress as a result of elevated loading – as is seen in most adhesive bonds when not subjected to considered fatigue profiles – allowing the potential for appropriate repairs to be undertaken. A comparison of the effect of the taper on the levels of adhesive shear strain in the presence of a disbond against those in a standard non-tapered double lap/strap joint design is illustrated in Figure 147 and Figure 148.

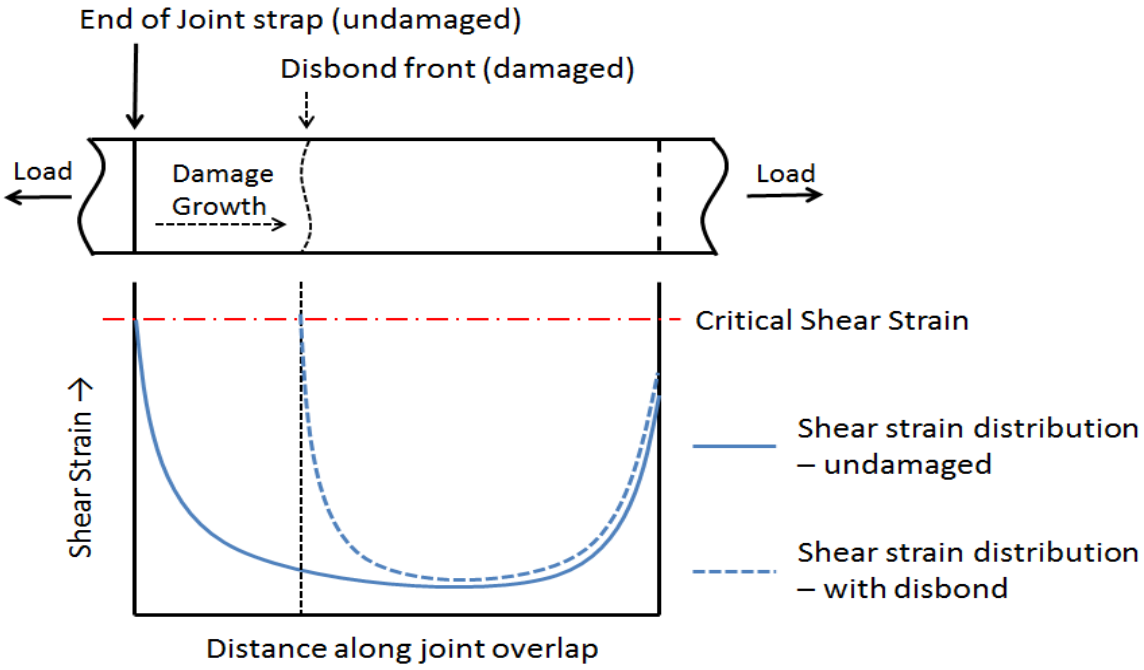

Figure 147: Adhesive bond-line shear-strain distribution comparison of a standard double strap joint (unbalanced) with no damaged and with a disbond

Figure 147 illustrates a bond reaching a critical level of shear strain resulting in adhesive or cohesive failure on an unbalanced (see section 4.3.2.3) standard double strap joint. Exact critical shear-strain values are not only dependent on the particular adhesive and adherend properties but also any degrading factors such as environmental ingress or inadequate surface treatment. It can be seen that as a disbond progresses into the overlap the shear-strain remains above the critical value resulting in continued and rapid damage growth. Variations in the maximum shear strain values at different disbond lengths at 10, 20 & 30kN loading for the standard double strap joints investigate can be seen in Figure 70 - Figure 72 respectively (Blue markers). Further details regarding the strain distributions resulting from flaws in the bond-line are presented in section 4.5.

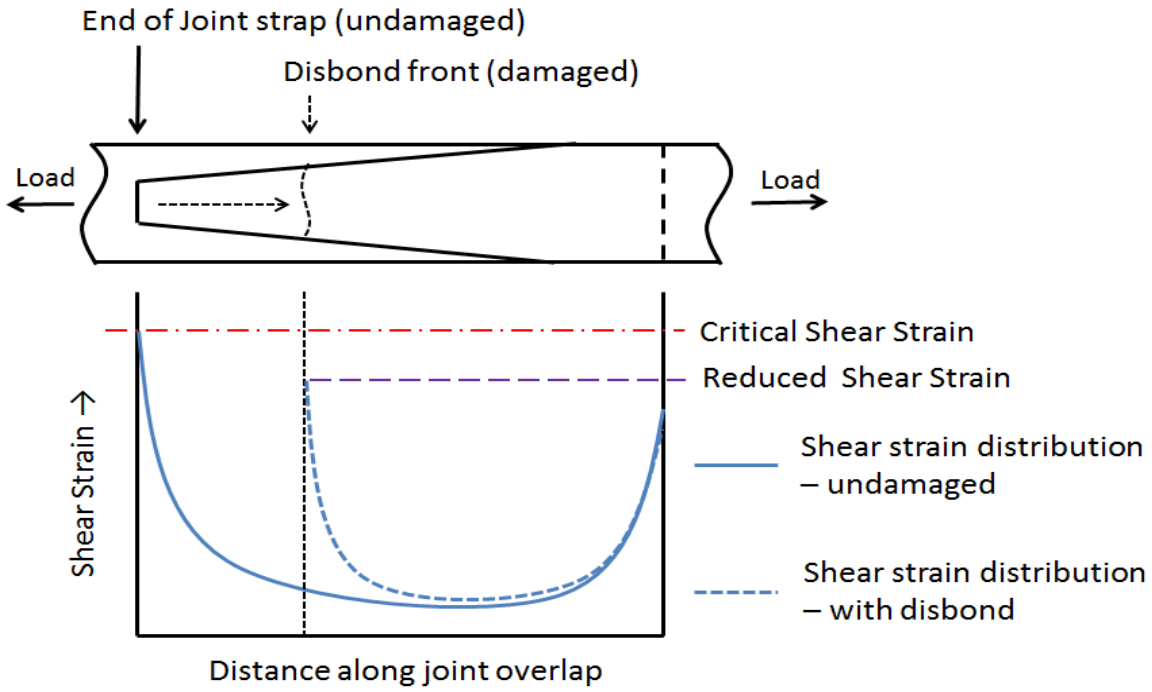

Figure 148: Adhesive bond-line shear-strain distribution comparison of a tapered double strap joint (unbalanced) with no damaged and with a disbond

Figure 148 illustrates a bond reaching a critical level of shear strain resulting in adhesive or cohesive failure on an unbalanced Tapered double strap joint. Again exact critical shear-strain values are not only dependent on the particular adhesive but also any degrading factors such as environmental ingress or inadequate surface treatment. It can be seen that as a disbond progresses into the overlap the shear-strain is reduced to a value below the critical value. The damage is therefore arrested, or alternatively an increase in the required applied load to raise the shear-strain up to the critical value needed to cause further damage. Variations in the maximum shear strain values at different disbond lengths at 10, 20 & 30kN loading for the standard double strap joints investigated can be seen in Figure 70 - Figure 72 respectively (Red markers). Although the geometry raises the shear strain for a given load relative to a standard configuration when no damage is present (maximum strain in tapered geometry tested = 1.28x that for the standard configuration used for comparison), therefore resulting in a joint with lower potential strength (knockdown factor of 78% for the configuration tested), the characteristic of lowering the strain regardless of bond quality allows operation as discussed in Chapter 9 ‘Application’.

The recognition that bond strengths in problematic joints are not known or easily measureable (simply that they are at a value lower than the design strength) must be considered in such a SHM enable joint. The approach used in this research ensured the joint responded to damage in a manner appropriate to damage tolerance and monitoring by ensuring once initiated disbonds were arrested or retarded, the location of this damage could be identified, and that appropriate levels of residual strength remained. These characteristics were present regardless of the quality or failure mode of the bonded joints. The characteristic behaviour was defined as a function of the joint geometry which ensured disbonds initiated and advanced at known locations and the shear and peel stress-strains which drive this damage growth were reduced for a given load as said disbonds increased in size. Any reduction in the quality of the bond affected only the magnitude of loads within these required attributes. The SHM enabled joint and the methods used to operate such structure discussed in Chapter 9 ensure the minimum required strength is present at manufacture and qualification. In the event joint strength degrades, and as a result damage initiates, the reduction in shear and peel stresses which result from the taper design ensure the joint has the required strength to transfer loads likely to be encountered during the remainder of the flight. The novel joint geometry also ensures that damage grows more predictably by initiating at the outer end of the joint strap overlap allowing for efficient placement of surface mounted strain sensors. By using this new approach a slow damage growth characteristic can be engineered into structural joints that would otherwise typically fail in a sudden and catastrophic manner. This allows operation in a way close to and complementing current aerospace legislation. The structure is inherently inspectable by the in-situ sensors and appropriate residual properties remain after damage can be identified as are the requirements for the damage tolerant philosophy. The process shows recognition to all means of compliance for the requirements of bonded composite joints and as such allows operation in reference to these which would otherwise not be possible. Such an approach which uses considered structural geometry (tapered joint straps) to promote appropriate degradation behaviour in the event of damage initiation as well as the capability to use in-situ sensor to monitor such behaviour allowing operation of bonded structure in an inspection/maintenance regime similar to that of

other damage-tolerant structure has not been identified in any previous investigations. In regards to the requirements – stated in Chapter 3, section 3.2.1 – these recognitions and solutions are as follows:

Option I demands the maximum disbonds of each joints must be able to withstand DLLs determined by analysis tests or both. Maximum disbond lengths, although not fully prevented as required in the first option, are controlled by the geometric nature of the structure. This is further reinforced by the fact that repair actions can be prompted via the monitoring system prior to disbonds growing to an unpermitted size and that greater loads than that required to initiate the damage are required to grow the disbond once initiated.

Option ii states proof testing is an acceptable means of compliance. This option does however contain concerns in that problematic bonds may deteriorate during operational lifetimes and as such the proven strength at the time of the test (for example during manufacture and assembly) cannot be guaranteed. Similar reservations over long term performance also exist in the use of adhesively bonded repairs. As discussed in Chapter 9 the approach taken within this study allow this option to be viable by accounting for possible degradation of the joint performance by recognising and containing any damage as a result of degraded properties whist additional adequate strength almost certainly remains.

The third means of compliance – *Option iii*, that of reliable NDI – is also in part addressed. Firstly the in-situ strain sensors have in all cases identified actual damage while adequate strength remains and as such the required strength of the joint (particularly when used in combination with *Option ii*) is assured. As such the SHM enabled structure itself may be regarded as a reliable non-destructive inspection technique. Secondly as damage does not result in spontaneous failure, precursors to such failure are in the form of actual partial disbonds. These features can be positively identified via conventional NDI methods.

As well as closely addressing the current means of compliance of bonds in composite structure all the design processes used in the approach presented in this thesis are familiar to composite structural designers. In addition methods and components used are already flight certified. As such the requirement for expensive

and long duration qualification (possibly up to or surpassing 10 years) of new materials, process or technologies within the aerospace sector – including strategies such as the embedment of technologies such as optical fibres within currently qualified laminates) is effectively eliminated.

The use of ratio-metric analysis, comparing measured strains from sensors in areas where damage may occur to those in regions within the same load path unlikely to deteriorate, provides simple outputs regarding the structures condition based on strain values but independent of actual load magnitude. As such monitoring may be made continuously during flight with data either analysed in real time or recorded for later analysis. Such an approach may however require further in-flight systems which are detrimental to flight performance in terms of both additional mass and power requirements. An alternative would be to interrogate the system during routine 'inspections' using ground loads to provide strain with the sensors still responding to the presence of damage. With the ratio-metric approach discussed in Chapter 9 simple threshold values provide easily interpreted and rapidly produced 'go / no-go' or 'traffic light' responses which if required would result in further inspection of the targeted component, possibly with the aid of NDI and/or repair actions made to the bonded component. Ratio-metric thresholds, as well as structure specific sensor placement, would ultimately be determined as part of the structural elements testing currently performed as part of the building block approach. This approach currently used in the design and certification of composite aircraft [3,14] and could be used with consideration of the SHM enabled structure to define the probabilistic damage growth for each component as well as considering the time interval between inspections in a similar fashion to that currently considered for BVID type damage.

A further potential application for such an approach would be in adhesive bonded repairs made to both composite and metallic aircraft. Currently concerns exist over the long term performance of such repairs. If appropriate repair-sensor array designs can be designed (SHM enabled repairs) such concern would be addressed in the same manner as for structural bonds. Similar benefits may be made as seen with structural bonding as identical considerations have to be included if mechanical fasteners as oppose to adhesive bonds are used in such cases.

An issue with structure potentially certified by many SHM systems is in the event of failure of the monitoring system the entire structure, which is dependent on the SHM to ensure/prove airworthiness, would need to be replaced regardless of its actual condition. The approach investigated in this work has no such issues. Being surface mounted sensors (in the form of RSGs, optical fibres or some other strain sensor) may be easily replaced. In addition the degradation measurand is in the form of a defined arrested/retarded physical disbond. As such this may be detected by conventional NDI methods. In the event of failure of a single sensor or the entire sensor network the structural component can therefore be assessed via NDI. If no disbonds are detected simple sensor replacement can be made. Continued operation should then be able to proceed. It may be required to ensure the ratio-metric behaviour between the reference sensors and those in potential damage locations are still characteristic of that expected by applying loads to the structure and analysing the response to avoid potential false positive indicators during later inspections.

Considered SHM enabled design provides the ability to successfully monitor bonded structure which previously could not be inspected. It is known that appropriately designed and fabricated purely bonded composite structures are capable of transferring demanded loads. Additional design features currently used, such as additional mechanical fasteners, provide no additional strength or stiffness and are likely to introduce additional mass as well as other potential issues such as sites for environmental ingress. The function of such structure is to account for the uncommon event that bonds which cannot be confidently inspected are not or no longer at the desired strength and will fail without warning. Features such as supplementary fasteners are themselves required to be inspected. One of their purposes is that they may be more easily visually inspected than bonded structure. The ability to monitor the bonded joints directly using the robust and easy to interpret approach proposed may significantly reduce downtime resulting from visual inspections. This effect may be particularly relevant in the case of structural joints as many will be inside the aircraft and may therefore require some degree of strip-down to inspect. SHM enabled structure may not only save time, and therefore revenue, by reducing the requirements of such strip-downs but also eliminate other issues

induced by such intrusive maintenance actions. Human error in maintenance activity has been estimated to account for approximately 15% of aircraft accidents [29].

As previously discussed bonded joint designs exploiting adherends with tapered widths in the manner investigated have not been used in contemporary structure or been recognised in published research. This may be due to such joints having lower potential strengths than standard configurations; e.g. the tapered joints in this work had 78% of the potential strength of the standard double strap joints. Such tapered designs may therefore appear less desirable to a designer whose principle goal is that of maximising strength. Such reductions can however be incorporated into the structures overall design. In addition as much of the uncertainty associated with the joints condition is eliminated factors normally used to account for such uncertainties can be reduced. It is unlikely design factors would be completely eliminated, however if a standard adhesive joint was designed with a design factor of 1.5 (equivalent to 67% in service design strength) to account for uncertainties (this is much lower than the civil engineering example described in Table 7 which requires a design factor of 4) the design strength of such a joint would actually be <90% of the tapered SHM enabled joint investigated (78% knockdown factor) if used without a design factor (i.e. design factor = 1).

Just as with current aerospace structure the SHM enabled joints are not deliberately designed to fail. Design strengths are based on the capabilities of the joint at the edge of the monitored region; in the case of the designs investigated at the ends of the tapered overlap. This results in a joint with strength at a multiple factor of the ultimate design strength, as is required in current mandated design practice. The design simply forces the joint to fail in a slow or arrested fashion in the event of degradation as a result of manufacturing defects or environmental exposure which is ideal for monitoring using SHM based on surface strain measurement.

10.1.1 Influence of strain measurement errors

Although it is recognised errors may be introduced by the RSGs themselves which were used as representative in-situ sensors it is believed any influences during these tests were of only minor significance. Expected issues associated with temperature variation have been shown to be minimal (section 5.4.2) due to stable temperature

conditions and the value of strains recorded. Temperature influence may however become significant if larger temperature changes are present in-service in conjunction with SHM enable joint designs reliant on lower strain value measurement. The importance of such factors will need to be considered by the engineer as part of the consideration of each specific design including the choice of strain measurement system (RSGs, FBGs etc). More significant error may be introduced by the precision of placement (both location and angle) of each sensor as well as the quality of sensor adhesion. Some minor variations can be seen in the specimens tested. If the RSG values are compared at the gauges used as monitoring sensors in the ratio-metric analysis (Taper specimens gauge G2, 10mm from strap-end, and Partitioned specimens gauge G1, 9mm from strap-end) at 10kN, before damage is thought to have initiated, strains recorded range from $201x10^{-6}$ to $405x10^{-6}$ (standard deviation $3.24x10^{-5}$). Within this set some difference appears present between the specimens failing by mixed mode failure ($347x10^{-6}$ to $405x10^{-6}$ strains) and those failing by pure adhesive failure ($201x10^{-6}$ to $288x10^{-6}$), additional work may be required to determine if this effect can be used to diagnose bond-line quality. Values from the Partitioned specimens ranged from $220x10^{-6}$ to $256x10^{-6}$ (standard deviation $1.57x10^{-5}$), all failed by adhesive type failure. Variations may in part be due to differences in the fabricated joints themselves. Values in the cases shown are however relatively small and even when present the presence of damage and the means to track its propagation remains highlighting the robust nature of this approach. As with other parts of the joint fabrication process appropriate quality control measures should be made to ensure such factors are minimised. Unlike bond line quality however surface mounted sensors can be inspected visually. As discussed in the application chapter the sensor array may not only be used as part of the monitoring system used to assess the structure during proof-testing but will also be itself scrutinised during this process allowing significant issues with sensor placement or other issues with expected strain outputs to be identified.

The approach used in this research which used surface sensors representing those that may be used in real applications alongside other analysis methods, i.e. DIC and FEA, allowed each method to be compared. As multiple independent methods were used to evaluate the direct or calculated strain experienced by the structure each

can be used to validate the others. As such any significant errors beyond that which would be of use in real applications could, if present, be identified.

10.2 Answers to thesis key research questions

Within Chapter 3, Research objectives questions were asked to enable purely bonded composite structure to be viable via the implementation of an in-situ monitoring or SHM system. These are started and responded to below.

> *How can SHM identify/monitor failure of adhesive bonds? Which methods and techniques are suited to providing easily interpreted responses to damage initiation, with near 100% probability of detection, whist minimising false 'no-fault-found' responses? Which in-situ monitoring methods are best suited for use alongside aerospace structure considering operational and certification requirements?*

This investigation has shown that in order to successfully monitor bonded structure the behavioural response of the joint to damage is at least as important if such a system is to be used in service as the method used to monitor the structure. With suitable response to damage, which must be usable within a damage-tolerance type operational regime, monitoring options are available which can include less complex systems than those that are frequently researched. Monitoring systems need to provide easily interpreted responses and be serviceable if they are to be accepted within the aerospace sector. Surface mounted sensors, although potentially more exposed to damage, are less obtrusive and eliminate the requirement for long and expensive material qualification procedures required of embedded components. Strain measurement presents a direct indicator of the performance of the load bearing structure and in addition (see below) is directly linked to bonded structure design. Such surface mounted sensors – RSGs or optical fibres – are presently flight approved and may also be easily maintained in-service. A surface strain approach, with the aid of ratio-metric analysis between sensors on the same load path used with appropriate maintenance action thresholds, allows simple decision actions to be made by technical personal with no further complex, timely or difficult to analyse diagnostic methods. The application approach discussed in section 9.4 allows assessment of the structure during flight or as part of a land based inspection

program as the ratio-metric response is independent of the applied load. Using this approach, and selecting appropriate maintenance action ratio-metric thresholds as per section 9.4.2, not only allows simple interpretations to be made but in the cases reviewed suggests damage should be detected with near 100% certainty whist providing no incidences of 'no-fault-found' indicators. Figure 141 - Figure 146, as well as additional data in Appendix D, reveal that in 100% of the cases of the Taper and Partitioned specimen tests damage could be easily be identified by considering the ratio-metric threshold value of 0.7 on the selected gauges (Gauge 2 and 1 for the Taper and Partition specimens respectively). This selected sensor / ratio-metric threshold value provides a 'buffer' to ensure no false damage indicators are produced. By examining the direct RSG and DIC data small changes from what would be expected of non-damaged behaviour (deviation from linear load / RSG strain responses, Figure 82 - Figure 86 & Figure 113 - Figure 117, and minor fluctuation in DIC measured strains at the strap-ends) are present at loads which correspond to ratio-metric responses greater than 0.8, therefore not instigating maintenance actions. These observations may be due to damage too small to confirm using the analysis performed or to adherend bending resulting from geometry induced bending moments (see section 4.3.2.5). At the selected maintenance action threshold disbond sizes estimated by comparison against FEA models are ≈1 to <5mm in length, relatively small but within the capability of standard NDI approaches. At the selected ratio-metric threshold, as well as ensuring a minimum of DLL capability was present, the worst performing specimen (Partition-3) still had a ultimate load capacity 16.8% greater than the load at which the ratio-metric threshold was passed; 14% of the total joint strength. All other specimens reported positive damage when an additional 74% of the load at which the ratio-metric threshold was passed was available; 42.6% of the joints ultimate static strength (Table 23 and Appendix E). The ratio-metric value of 0.7 at the appropriate gauges used in this research was selected retrospectively by considering the results of the tests performed. The approach was however consistent and effective in all cases. As previously discussed maintenance threshold values and the sensitivity of the system (which may influence the likelihood of no-fault-found events) will be dependent on the specific joint design (e.g. degree of taper angle) and sensor

placement. Selected threshold values may be made either by multiple specimen testing (as per this work) and/or detailed modelling. Improvements may be made by considering multiple sensors. Compromises between these factors and the maximum potential design strength of the joint will need to be considered by the designer. A system that allows for response to actual macro sized damage (disbonds) can also be backed up using conventional NDI methods either to double check the damage prior to repair or to account for sensor failure and replacement.

> *How can bonded structure be designed to complement the capabilities on the in-situ monitoring system and allow the requirements of the first research question and the previously identified criteria to be enabled? Can such a design in conjunction with appropriate operational and qualification procedure ensure adequate strength is present, ideally to DLL capability?*

The mechanism which results in rapid catastrophic failure once a critical stress/strain level is exceeded within standard configuration strap joints has been previously discussed and is schematically represented in Figure 147 above. As the strain distribution is largely defined by the adherend geometry this lead to the inclusion of the tapered adherend approach presented. In this configuration if damage does initiate – which will occur at the overlap ends and progress inwards as seen in experiment – it is slowed or arrested allowing the monitoring system to identify the partial damage whilst residual strength greater than that of the initially damaged component remains (Figure 148). The adhesive strain profile is defined by adherend geometry, the characteristics of which remain largely unchanged as load increases with only the magnitude of the strain values being affected. As such, a bond-line with lower than designed properties – the nature of problematic joints – would still exhibit the same progressive failure characteristics only at reduced load levels. As previously discussed if required strengths can be established via qualification proof load testing prior to any degradation which will take place over weeks, months or years in-service remaining strengths after damage initiation, even in problematic joints, are likely to be more than sufficient for continued safe flight. The Taper design, used in conjunction with the application method proposed in Chapter 9, showed the SHM enable joint concept could fulfil the requirements of joint

qualification and operation under the conditions of this research. When damage was positively identified with 100% confidence using the ratio-metric approach all the joints remained capable of transferring loads greater than the specified DLL. In the most extreme cases (i.e. specimens 'Taper 1, 2 & 3' where evidence of mixed adhesive/cohesive bond failure was evident) ultimate failure loads ranged from 47.6 - 50.5kN. These values, which are almost 3.8x the DLL and over 2x the DUL, are likely due to better adhesive/adherend adhesion than the other specimens allowing the exploitation of some of the adhesive plastic capability available only at loads greater than DLL. Such joints are as such unproblematic and all easily passed the DLL (13.3kN) proof test by a considerable margin. The joints which represent more problematic structure, i.e. those that revealed possible first signs of damage by retrospective analysis of minor surface strain variation or even confident positive damage identification by the ratio-metric response, also passed the criterion summarised in the research question above. The worst performing of these joints was 'Partition-1', which had visible damage prior to testing. This presented a highly positive ratio-metric maintenance threshold response at 8.5kN, a load ≈64% of the DLL and therefore which may be experience in normal operation. This joint ultimately failed at 18.1kN, over twice the damage detection load and at 136% of the DLL. This joint would therefore be more than capable of carrying the static load required. All other joints exceeded the performance of this example (see Table 20).

> *How can bonded structure be designed to complement SHM; i.e. detectable, predictable and definable damage potentially up to millimetre sale accuracy, aiding operation under an inspection based damage-tolerance regime?*

The experiments with tapered joints showed that the combination of SHM strain measurement and novel joint geometry provide evidence that predictable damage growth and damage tolerance are achievable. This was facilitated by the deliberate engineering of slow damage growth into the joint that could be monitored using surface strain measurement. In an attempt to refine this design to link more quantitatively the actual extent of disbond to the strain measurements, the concept of the partitioned bond was explored and tested. The goal was to contrive a discontinuous, step like response from the sensors once predefined sections of the

bond had failed. In identifying these step features in the sensor response it could be deduced that a disbond of specified length had occurred. This met with limited success with a correlation identified between discontinuities in the strain sensor measurements and bond section failure (as verified by FEA and DIC). Issues for this approach to be used as a diagnostic tool or as a means of ensuring a defined response to damage are however potentially limited due to the restrictions in placing partitions too close to the strap end combined with the potential (as seen in specimen Partiton-3) for total failure to occur prior to the slow growth disbond interacting with the first adhesive partition. RSG values and distribution were seen to closely match distributions of FEA calculated surface strain at various loads and damage sizes, see Figure 87 - Figure 89 (Taper) and Figure 118 - Figure 122 (Partition). In cases where the size of the actual disbond could be estimated with some confidence, i.e. prior to damage initiation (i.e. in the cases considered at 10kN loading), or due to interaction with the bond-line partitions at known locations comparisons could be made. If the gauges as used in the ratio-metric study are considered (G2 for Tapered and G1 for Partitioned joints) the distances from the representative FEA/RSG/DIC curves shown and RSG stain values showing identical strain values are within 2.5mm for the worst case for the Taper specimen set and 1.45mm for the partitioned specimens (excluding specimen Partition-1 which had visible signs of pre-test damage). In cases where defined responses associated with disbond interaction with bond-line partitions were present (e.g. specimen Partition-5 at 25kN) similar levels of agreement between the RSG and FEA data are evident. This suggests the RSG/FEA comparison approach is providing estimates of similar accuracy when disbonds of significant length are present. In addition disbonds can be seen to track across the 10mm bonded regions of the partitioned specimens where disbond lengths must be limited to these regions adding confidence in the use of this approach. The comparisons in FEA data between the Tapered and Partition geometries presented in Figure 111 showed a close correlation in surface strain responses for similar damage and joint load conditions. As such the comparison method, and by association the ratio-metric response approach, should provide similar detail on non-partitioned joint geometries. Minor differences seen between in-situ data and FEA surface strain predictions are likely the result of accuracy of

RSG alignment/placement, natural variation in the specimens due to manufacturing limitations, and the compromise in using the 'engineering constraints' FEA approach over more complex approaches as discussed in section 5.3.1. To further develop this idea, future work could be performed on for example compound strap tapers where the taper angle may change along the monitored section of joint to maximise sensitivity to damage identification whist ensuring further damage is arrested and/or reduce the likelihood of total joint failure when disbonds are comparatively short.

10.3 Future work and development

Within this investigation only a single adhesive, the aerospace approved epoxy resin based film adhesive FM-94, was used. Investigations have been previously made regarding increasing the toughness of epoxy resins. Such approaches aimed at reducing any brittleness effects and enabling more resistance to crack formation by exploiting any plasticity effects via the inclusion of additional nano-particles within the adhesive [194-196]. Inclusion of such materials, and if possible the possible tailoring of their location within the bond, may aid both the performance of the structure and the repeatability of the structures response to damage initiation.

The optimisation of SHM enabled joint designs will be aided by further understanding and refinement of modelling of the shear (and peel) strain responses in regards to desired strength characteristics or damage propagation features. This may include the introduction of FEA modelling methods such as cohesive zone modelling and the traction separation method [197]. It must be remembered however that the strength of problematic adhesive bonds will by their nature be unknown and as such material properties and failure mechanism used in such simulations, as well as any design considerations made from such data, must consider this. Modelling the bond with the desired or expected design properties would simply show the bond would not fail under normal service conditions, assuming the joint has been designed correctly for the expected loads experienced by the structure. More appropriate values would be those for bonds that have degraded so damage initiates at DLL or below. An appropriate experimental plan to determine appropriate shear and peel strengths may therefore be required to establish such degraded properties.

Variation in the joint geometry, such as variable taper dimensions or other approaches may be investigated. Such variations will alter the strain experienced by the bond as disbond lengths increase. Further work which considers this may allow the disbond response to be specifically tailored and aid interpretation of strain data by suitably positioned sensors. Variable or compound tapered designs may be investigated which rapidly reduced the strap width at the end of the overlap to increase sensitivity of damage initiation and detection, this will also result in a greater increase in strap width per unit length of overlap in this region resulting in a more significant 'strengthening' of the joint over this region. The remainder of the overlap may conform to a less severe taper to promote more uniform damage growth characteristics. Taper designs may also be investigated with the goal of producing the joint with the greatest potential properties (in, due to good manufacturing practice, the likely event that the joint will be of good quality and not degrade) whist still allowing SHM enabled joint damage tolerant operation. As previously discussed the tapered geometry has a reduction in potential strength over non-tapered joints; e.g. the design investigated required a knock-down factor of 0.78 compared to conventional geometry. All tested tapered specimens, including those with partitions, which would pass poof testing requirements (loads before damage greater than DLL, i.e. 13.3kN) revealed ultimate failure strengths much higher than the required 20kN DUL, ranging from 28.8kN (144% DUL) to 50.5kN (253% DUL) – Table 20. Considered design may seek to exploit some of this additional strength by reducing taper angles to minimise the performance knockdown of the SHM enabled joint while this significant strength increase after damage initiation can still be exploited for producing appropriate damage growth characteristics. Consideration of factors such as adhesive plasticity will however still need to be considered. Ultimately in actual designs the amount of potential strength and the degree of damage sensitivity/retardation will have to be considered compromised design, dependent on the component and application, by the designer.

During the process of sizing/locating the partitions used in Chapter 8 it can be seen the shear and peel strains magnitude and distribution can be influenced by such features (Figure 104 - Figure 109). Further investigation may use such features to manipulate shear and peel strain distributions in a similar fashion to the tapered

strap geometry used in this thesis. If successful similar results to those produced in this work may be available without the requirement of tapering the joint straps. Identical considerations as those identified for the tapered joints, i.e. adhesive plasticity, knock down factors, damage characteristics and sensor placement will need to be considered.

Future work may also consider the apparent difference (current data set size limits confident conclusions in this regard) between the surface strain measurements prior to damage initiation between specimens failing by pure adhesive and mixed mode failure – see section 10.1.1. If a measurable difference can be confirmed the quality (and possibly susceptibility to future in-service degradation) may be determined at the joint qualification (or as a result non-qualification) stage.

The adhesive bonds presented were subjected to quasi-static loading conditions (displacement control 0.5mm per minute). Further investigation regarding fatigue and dynamic loading (rate of strain based effects) would provide valuable information for designing in-service SHM enable joints.

Continued development should also be made with more complex joint designs such as stepped or tapered joint designs which must be used when bonding structures of greater thickness used to translate greater loads. Peel effects in any bond composite bond must always be considered and are a major reason why joint designs change as thickness increases. If damage has the potential to jump from the adhesive bond-line to within the adherend laminate itself such effects must be considered. Further study should also be made which would apply the design concept to design details which require extended bond-lines.

10.4 Summary and conclusions

The work has provided an investigation into the potential of SHM-enabled design relevant to composite aerospace structures. The work developed novel bonded composite joints capable of progressive failure and that when used with simple surface strain based SHM methods could provide a diagnosis of the structures condition compliant with a damage-tolerant design and operational philosophy. A novel approach to SHM enabled design of adhesively bonded joints based on the

modification of the joint geometry and inclusion of simple surface mounted strain sensors, as well as possible inclusion of the modification of the bond-line architecture itself, has been proposed and demonstrated experimentally. This design approach, particularly when used alongside permitted but currently achievable acceptable means of compliance, promotes appropriate failure modes which can be easily and reliably identified by the in-situ sensors whilst significant residual properties remain. This provides maintenance engineers and technicians with a high probability of detection of initial damage whilst the structure is still likely to possess limit or even ultimate load bearing capability. The result is an SHM enabled joint design which meets the current arrested or slow growth characteristics specified by aircraft regulators as included in the FAA documentation AC20-107B [3].

References

[1] Maintenance Steering Group - 3 Task Force. MSG-3 Maintenance Program development document. Sept 1993;Revison 2.

[2] Federal Aviation Administration. Advisory Circular - Damage tolerance and fatigue evaluation of structure. 2011;AC 25.571-1D.

[3] Federal Aviation Administration. Advisory Circular - Composite aircraft structure. 2009;AC 20-107B.

[4] SAE International. Aerospace Recommended Practice - Guidelines for Implementation of Structural Health Monitoring on Fixed Wing Aircraft. 2013;ARP6461.

[5] Redmond G. From 'safe life' to fracture mechanics - F111 aircraft cold temperature proof testing at RAAF Amberley. 2001; Available at: http://www.ndt.net/apcndt2001/papers/912/912.htm. Accessed 18/07/13.

[6] Baker A, Rajic N, Davis C. Towards a practical structural health monitoring technology for patched cracks in aircraft structure. Composites Part A: Applied Science and Manufacturing 2009;40(9):1340-1352.

[7] Federal Aviation Administration. Determining the Fatigue Life of Composite Aircraft Structures Using Life and Load-Enhancement Factors. 2011;DOT/FAA/AR-10/6.

[8] Schmidt HJ, Schmidt-Brandecker B, Tober G. Design of Modern Aircraft Structure and the Role of NDI. 2013; Available at: http://www.ndt.net/article/ecndt98/aero/001/001.htm#21. Accessed 17/07/13.

[9] TUDelft. Damage tolerant design of composite materials. 2013; Available at: http://www.lr.tudelft.nl/?id=26643&L=1&id=26643. Accessed 26/07/2013.

[10] Ward AP, Parich HE. The choice of fail safe and safe life fatigue philosophies in aircraft design. 1969:238-246.

[11] Tong CT. Literature review on aircraft structural risk and reliability analysis. 2001;DSTO-TR-1110.

[12] Federal Aviation Administration. Advisory Circular - Fatigue, fail-safe and damage tolerance evaluation of metallic structure for normal, utility, acrobatic, and commuter category airplanes. 2005;AC 23-13A.

[13] Irving PE, Buller RG. Prediction of fatigue life under helicopter loading spectra for safe life and damage tolerant design. Fatigue and fracture mechanics 1999;29(ASTM STP 1332):727.

[14] Baker A, Dutton S, Kelly D. Composite materials for aircraft structures. 2nd ed. Reston, Virginia: AIAA; 2004.

[15] Dilger R, Hickethier H, Greenhalgh MD. Eurofighter a safe life aircraft in the age of damage tolerance. Int J Fatigue 2009;31(6):1017-1023.

[16] Federal Aviation Administration. Fatigue evaluation of wing and associated structure on small airplanes. 1973;AFS-120-73-2.

[17] European Aviation Safety Agency. Certification specifications and acceptable means of compliance for large aeroplanes. 2012;EASA CS-25.

[18] Goranson UG. Damage tolerance facts and fiction. 2007;DTAS keynote presentation.

[19] Wilkinson R. Aircraft structures and systems. 2nd ed. St Albans: MechAero; 2001.

[20] U.S. Air Force Research Laboratory. DTD Handbook - Handbook for damage tolerant design. 2011;Online Handbook.

[21] Withey PA. Fatigue failure of the de Havilland Comet I. Eng Failure Anal 1997;4(2):147-154.

[22] Federal Aviation Administration. FARS, Part25, Section 571 - Damage tolerance and fatigue evaluation of structure.

[23] Niu MCY. Composite airframe structures. 4th ed. Hong Kong: Conmilit press ltd; 2005.

[24] Gunnink JW. Damage tolerance and supportability aspects of ARALL laminate aircraft structures. Composite Structures 1988;10(1):83-104.

[25] Federal Aviation Administration. FARS, Part 25, Section 305 - Strength and deformation.

[26] Damage Resistance, Durability, and Damage Tolerance. Composites Materials Handbook, Volume 3 - Polymer Matrix Composites - Materials Usage, Design, and Analysis: SAE International; 2012.

[27] MINAKUCHI S, YOKOTA K, TAKEDA N. Ultra-lightweight Composite Stiffened Panel Designed Based on SHM and Rapid Repair System. Structural Health Monitoring 2015 2015.

[28] The role of advanced numerical methods in the design and certification of future composite aircraft structures. 5th world congress on computational mechanics, WCCM V; Vienna Austria July 7-12; ; 2002.

[29] Scott M, Bannister M, Herszberg I, Li H, Thompson R. Structural health monitoring - the future of advanced composite structures. In: Chang F, editor. Structural health monitoring 2005 - Advancements and challenges for implementation; 2005. p. 107-121.

[30] Harris CE, Starnes JH, Shuart MJ. Advanced durability and damage tolerance design and analysis methods for composite structures: Lessons learned from NASA technology development programs. 2003;NASA/TM-2003-212420.

[31] Structural health monitoring (SHM)–overview on technologies under development. 16th World Conference on NDT, Montreal/CDN; 2004.

[32] Wild G, Hinckley S. Acousto-ultrasonic optical fiber sensors: Overview and state-of-the-art. IEEE Sensors Journal 2008;8(7):1184-1193.

[33] Scruby CB. An introduction to acoustic emission. Journal of Physics E: Scientific Instruments 1987;20(8):946-953.

[34] Cai J, Qiu L, Yuan S, Shi S, Liu P, Liang D. Structural health monitoring for composite materials. In: Hu N, editor. Composites and their applications Rijeka, Croatia: InTech; 2012. p. 37-58.

[35] Bohse J. Acoustic emission characteristics of micro-failure processes in polymer blends and composites. Composites Sci Technol 2000 6;60(8):1213-1226.

[36] de Groot PJ, Wijnen PAM, Janssen RBF. Real-time frequency determination of acoustic emission for different fracture mechanisms in carbon/epoxy composites. Composites Sci Technol 1995;55(4):405-412.

[37] Structural health monitoring for advanced composite structures. Proceedings of the Sixteenth International Conference on Composite Materials. Kyoto, Japan; 2007.

[38] Zhou G, Sim LM. Damage detection and assessment in fibre-reinforced composite structures with embedded fibre optic sensors-review. Smart Mater Struct 2002;11(6):925-939.

[39] Staszewski WJ, Mahzan S, Traynor R. Health monitoring of aerospace composite structures - Active and passive approach. Composites Sci Technol 2009;69(11-12):1678-1685.

[40] Gagar D, Foote P, Irving P. A novel closure based approach for fatigue crack length estimation using the acoustic emission technique in structural health monitoring applications. Smart Mater Struct 2014;23(10).

[41] Grondel S, Assaad J, Delebarre C, Moulin E. Health monitoring of a composite wingbox structure. Ultrasonics 2004;42(1-9):819-824.

[42] Structural Health Monitoring of Composite Laminates Through Ultrasonic Guided Wave Beam Forming. NATO Applied Vehilce Technology Symposium on Military Platform Ensured Availability Proceedings; 2008.

[43] Mariani S, Corigliano A, Caimmi F, Bruggi M, Bendiscioli P, De Fazio M. MEMS-based surface mounted health monitoring system for composite laminates. Microelectron J 2013.

[44] A Review of Energy Harvesting Methodologies for Potential Structural Health Monitoring Applications. Structural Health Monitoring 2005: Advancements and Challenges for Implimentation; 2005.

[45] Tang H-, Winkelmann C, Lestari W, La Saponara V. Composite structural health monitoring through use of embedded PZT sensors. J Intell Mater Syst Struct 2011;22(8):739-755.

[46] Diamanti K, Soutis C. Structural health monitoring techniques for aircraft composite structures. Prog Aerospace Sci 2010;46(8):342-352.

[47] Manka M, Rosiek M, Martowicz A. Piezocomposite Transducers for Guided Waves. In: Stepinski T, Uhl T, Staszewski W, editors. Advanced Structural Damage Detection: Wiley; 2013. p. 109-139.

[48] Fu T, Liu Y, Li Q, Leng J. Fiber optic acoustic emission sensor and its applications in the structural health monitoring of CFRP materials. Opt Lasers Eng 2009;47(10):1056-1062.

[49] Majumder M, Gangopadhyay TK, Chakraborty AK, Dasgupta K, Bhattacharya DK. Fibre Bragg gratings in structural health monitoring—Present status and applications. Sensors and Actuators A: Physical 2008 9/15;147(1):150-164.

[50] Tsuda H. Ultrasound and damage detection in CFRP using fiber Bragg grating sensors. Composites Sci Technol 2006;66(5):676-683.

[51] Gachagan A, Hayward G, McNab A, Reynolds P, Pierce S, Philp W, et al. Generation and reception of ultrasonic guided waves in composite plates using conformable piezoelectric transmitters and optical-fiber detectors. IEEE Trans Ultrason Ferroelectr Freq Control 1999;46(1):72-81.

[52] Pierce S, Philp W, Culshaw B, Gachagan A, McNab A, Hayward G, et al. Surface-bonded optical fibre sensors for the inspection of CFRP plates using ultrasonic Lamb waves. Smart Mater Struct 1996;5(6):776.

[53] Takeda N, Okabe Y, Kuwahara J, Kojima S, Ogisu T. Development of smart composite structures with small-diameter fiber Bragg grating sensors for damage detection: Quantitative evaluation of delamination length in CFRP laminates using Lamb wave sensing. Composites Sci Technol 2005 12;65(15–16):2575-2587.

[54] Lam P-, Lau K-, Ling H-, Su Z, Tam H-. Acousto-ultrasonic sensing for delaminated GFRP composites using an embedded FBG sensor. Optics and Lasers in Engineering 2009;47(10):1049-1055.

[55] De Simio MP, Brown KS, Davies MJ, Olson SE, Derriso MM. Damage detection in composite aerospace structures using elastic waves. Mater Forum 2008;33:143-151.

[56] Van Hoa S, Hubert P, editors. Structural health monitoring (SHM) of composite aerospace structures using Lamb waves. The 19th International conference on composite materials; 28/07/13 - 02/08/13; ; 2013.

[57] Matt H, Bartoli I, Lanza Di Scalea F. Ultrasonic guided wave monitoring of composite wing skin -to-spar bonded joints in aerospace structures. J Acoust Soc Am 2005;118(4):2240-2252.

[58] Lowe M, Challis R, Chan C. The transmission of Lamb waves across adhesively bonded lap joints. J Acoust Soc Am 2000;107(3):1333-1345.

[59] Deng Q-, Yang Z-. Propagation of guided waves in bonded composite structures with tapered adhesive layer. Appl Math Model 2011;35(11):5369-5381.

[60] Ihn J-, Chang F-. Pitch-catch active sensing methods in structural health monitoring for aircraft structures. Structural Health Monitoring 2008;7(1):5-19.

[61] Kessler SS, Spearing SM, Soutis C. Damage detection in composite materials using Lamb wave methods. Smart Mater Struct 2002;11(2):269.

[62] Prasad SM, Balasubramaniam K, Krishnamurthy C. Structural health monitoring of composite structures using Lamb wave tomography. Smart Mater Struct 2004;13(5):N73.

[63] Raghavan A, Cesnik CES. Review of guided-wave structural health monitoring. Shock Vib Dig 2007;39(2):91-114.

[64] SMART layer and SMART suitcase for structural health monitoring applications. SPIE's 8th Annual International Symposium on Smart Structures and Materials: International Society for Optics and Photonics; 2001.

[65] Lin M, Kumar A, Beard SJ, Qing X. Built-in structural diagnostic with the SMART Layer™ and SMART suitcase™. Smart Materials Bulletin 2001;2001(4):7-11.

[66] A new SMART sensing system for aerospace structures. Proceedings of SPIE - The International Society for Optical Engineering; 2007.

[67] Qing XP, Beard SJ, Kumar A, Ooi TK, Chang F-. Built-in sensor network for structural health monitoring of composite structure. J Intell Mater Syst Struct 2007;18(1):39-49.

[68] Habib F, Martinez M, Artemev A, Brothers M. Structural Health Monitoring of Bonded Composite Repairs-A critical comparison between Ultrasonic Lamb Wave approach and Surface Mounted Crack Sensor approach. Composites Part B: Engineering 2012.

[69] Minakuchi S, Tsukamoto H, Banshoya H, Takeda N. Hierarchical fiber-optic-based sensing system: Impact damage monitoring of large-scale CFRP structures. Smart Mater Struct 2011;20(8).

[70] Ferreira L, Santos J, Farahi F. Simultaneous measurement of displacement and temperature using a low finesse cavity and a fiber Bragg grating. Photonics Technology Letters, IEEE 1996;8(11):1519-1521.

[71] Yeo TL, Sun T, Grattan KTV, Parry D, Lade R, Powell BD. Polymer-coated fiber Bragg grating for relative humidity sensing. IEEE Sensors Journal 2005;5(5):1082-1088.

[72] Vishay Precision Group. Strain gages and instruments - Strain gage selection: criteria, procedures, recommendations. 2010;Tech Note TN-505-4.

[73] Efunda. Strain rosette for strain measurement. 2014; Available at: http://www.efunda.com/formulae/solid_mechanics/mat_mechanics/strain_gage_rosette.cfm. Accessed 20/01/14.

[74] Kavitha PE. Strain transformations and rosette gage theory. 2009; Available at: http://www.google.co.uk/url?sa=t&rct=j&q=&esrc=s&frm=1&source=web&cd=1&ved=0CEYQFjAA&url=http%3A%2F%2Fsoliton.ae.gatech.edu%2Fpeople%2Fjcraig%2Fclasses%2Fae3145%2FLab2%2Fstrain-gage-rosette-theory.pdf&ei=AjreUqW8J4a00QWsn4HAAg&usg=AFQjCNGTEVMTOq(TRUNCATED). Accessed 21/01/14.

[75] Vishay Precision Group. Strain gage Rosettes: Selection, application and data reduction. 2010; Available at: http://www.vishaypg.com/doc?11065. Accessed 21/01/14.

[76] Barbero EJ. Introduction to composite materials design. 2nd ed. Boca Raton, USA: CRC Press; 2011.

[77] LeBlanc M, Measures RM. Impact damage assessment in composite materials with embedded fibre-optic sensors. Composites Engineering 1992;2(5–7):573-596.

[78] Structural health monitoring of co-cured composite structures using FBG sensors. Proc. SPIE; 2005.

[79] Lee BH, Kim YH, Park KS, Eom JB, Kim MJ, Rho BS, et al. Interferometric fiber optic sensors. Sensors 2012;12(3):2467-2486.

[80] Structural health monitoring of a composite wind turbine blade using fiber Bragg grating sensors. Sensors and Smart Structures Technologies for Civil, Mechanical, and Aerospace Systems 2010; 8 March 2010 through 11 March 2010; ; 2010.

[81] Canal LP, Sarfaraz R, Violakis G, Botsis J, Michaud V, Limberger HG. Monitoring strain gradients in adhesive composite joints by embedded fiber Bragg grating sensors. Composite Structures 2014;112(1):241-247.

[82] Frövel M, Del Olmo EF, A. Quero F, Carrión G, Pintado J, Güemes A. Damage Detection by Load Path Changes in Reinforced Composite Panels Using Local FBGS and Distributed Sensing. 6th European Workshop on Structural Health Monitoring 2012.

[83] Kronenberg P, Rastogi PK, Giaccari P, Limberger HG. Relative humidity sensor with optical fiber Bragg gratings. Opt Lett 2002;27(16):1385-1387.

[84] Boller C. Next generation structural health monitoring and its integration into aircraft design. Int J Syst Sci 2000;31(11):1333-1349.

[85] Vohra ST. Optical fibre gratings applications. In: López-Higuera JM, editor. Handbook of optical fibre sensing technology Chichester: John Wiley $ Sons Ltd; 2002. p. 475-501.

[86] Murayama H, Kageyama K, Naruse H, Shimada A, Uzawa K. Application of fiber-optic distributed sensors to health monitoring for full-scale composite structures. J Intell Mater Syst Struct 2003;14(1):3-13.

[87] Measures RM. Smart composite structures with embedded sensors. Composites Engineering 1992;2(5-7):597-618.

[88] Qiu Y, Wang Q-, Zhao H-, Chen J-, Wang Y-. Review on composite structural health monitoring based on fiber Bragg grating sensing principle. Journal of Shanghai Jiaotong University (Science) 2013;18(2):129-139.

[89] Kassapoglou C. Design and analysis of composite structures: With applications to aerospace structures. Chichester: John Wiley & Sons, Ltd; 2010.

[90] Comyn J. Thermal Effects on Adhesive Joints. In: Brinson HF, Dostal CA, editors. Engineering Materials Handbook, Volume 3: Adheasives and Sealants: ASM International; 1990. p. 616-621.

[91] Sung N. Moisture Effects on Adhesive Joints. In: Brinson HF, Dostal CA, editors. Engineering Materials Handbook, Volume 3: Adhesives and Sealants: ASM International; 1990. p. 622-627.

[92] Minakuchi S, Yamauchi I, Takeda N, Hirose Y. Detecting an arrested crack in a foam-core sandwich structure using an optical fiber sensor embedded in a crack arrester. Advanced Composite Materials 2011;20(5):419-433.

[93] Minakuchi S, Yamauchi I, Takeda N, Hirose Y. Memorizing and detecting an arrested crack in a foam-core sandwich structure using embedded plastic materials and fiber-optic sensors. Smart Mater Struct 2012;21(5).

[94] Dokos L, Mowlem M, Chambers A, Brambilla G, Pruneri V. Low velocity impact detection and damage assessment in composite materials using fibre Bragg grating sensors. Proceedings of ICCM-13, Beijing,(China) 2001.

[95] Kuang K, Kenny R, Whelan M, Cantwell W, Chalker P. Residual strain measurement and impact response of optical fibre Bragg grating sensors in fibre metal laminates. Smart Mater Struct 2001;10(2):338.

[96] Palaniappan J, Ogin S, Thorne A, Reed G, Crocombe A, Capell T, et al. Disbond growth detection in composite–composite single-lap joints using chirped FBG sensors. Composites Sci Technol 2008;68(12):2410-2417.

[97] da Silva LF, Moreira P, Loureiro A. Determination of the strain distribution in adhesive joints using Fiber Bragg Grating (FBG). J Adhes Sci Technol 2014;28(14-15):1480-1499.

[98] Crocombe AD, Ong CY, Chan CM, Abdel Wahab MM, Ashcroft IA. Investigating fatigue damage evolution in adhesively bonded structures using backface strain measurement. J Adhesion 2002;78(9):745-776.

[99] Solana AG, Crocombe A, Ashcroft I. Fatigue life and backface strain predictions in adhesively bonded joints. Int J Adhes Adhes 2010;30(1):36-42.

[100] Shenoy V, Ashcroft IA, Critchlow GW, Crocombe AD, Abdel Wahab MM. An investigation into the crack initiation and propagation behaviour of bonded single-lap joints using backface strain. Int J Adhes Adhes 2009;29(4):361-371.

[101] An investigation of the crack propagation in a carbon fiber bonded joint using backface strain measurements with FBG sensors. OFS2012 22nd International Conference on Optical Fiber Sensor: International Society for Optics and Photonics; 2012.

[102] LUNA Technologies. Fiber Sensing Solutions. 2013; Available at: http://lunainc.com/products/fiber-sensing-solutions/. Accessed 16/12/13.

[103] Sloan J. High Performance Composites. Nov 2012.

[104] Herszberg I, Li HCH, Dharmawan F, Mouritz AP, Nguyen M, Bayandor J. Damage assessment and monitoring of composite ship joints. Composite Structures 2005;67(2 SPEC. ISS.):205-216.

[105] PIOTROWSKI D, ROACH D, MELTON A, BOHLER J, RICE T, NEIDIGK S, et al. Implementation of Structural Health Monitoring (SHM) into an Airline Maintenance Program. Structural Health Monitoring 2015 2015.

[106] Roach D. Real time crack detection using mountable comparative vacuum monitoring sensors. Smart structures and systems 2009;5(4):317-328.

[107] Comparative vacuum monitoring: a new method of in-situ, real-time crack detection and monitoring. Proceding of 10th Asia-Pacific Conference On Nondestructive Testing; 2001.

[108] Minakuchi S, Banshoya H, Ii S, Takeda N. Hierarchical fiber-optic delamination detection system for carbon fiber reinforced plastic structures. Smart Mater Struct 2012;21(10).

[109] Sbarufatti C, Manes A, Giglio M. Application of sensor technologies for local and distributed structural health monitoring. Structural Control and Health Monitoring 2013.

[110] Poursartip A, Street K, editors. Experimental Investigations of mode I and mixed-mode delamination growth. The tenth international conference on composite materials; August 1995; ; 1995.

[111] Crack detection on composite and metallic aerospace structures. Proceedings of the 4th European workshop on structural health monitoring; 2008.

[112] HBM. RDS Crack Propagation Gauges for Determining Crack Propagation in Componants. 2016; Available at: https://www.hbm.com/en/3453/strain-gauge-rds-crack-propagation-gauge/. Accessed 10/15, 2016.

[113] Pevzner P, Weller T, Berkovits A. Use of heat emitted by broken optic fibers: A new approach for damage detection in composites. Eng Failure Anal 2005;12(6 SPEC. ISS.):860-874.

[114] Yan YJ, Cheng L, Wu ZY, Yam LH. Development in vibration-based structural damage detection technique. Mechanical Systems and Signal Processing 2007 7;21(5):2198-2211.

[115] Structural health monitoring using wavelet transforms. Proceedings of SPIE - The International Society for Optical Engineering; 2001.

[116] Zou Y, Tong L, Steven GP. Vibration-Based Model-Dependent Damage (Delamination) Identification and Health Monitoring for Composite Structures — A Review. J Sound Vibrat 2000 2/17;230(2):357-378.

[117] Doebling SW, Farrar CR, Prime MB. A summary review of vibration-based damage identification methods. Shock Vib Dig 1998;30(2):91-105.

[118] Recent advancements in the electro-mechanical (EIM) impedance method for structural health monitoring and NDE. SPIE 5th International Symposium on Smart Structures and Materials; 1998.

[119] Giurgiutiu V, Zagrai A. Damage detection in thin plates and aerospace structures with the electro-mechanical impedance method. Structural Health Monitoring 2005;4(2):99-118.

[120] An overview of vibrational-based nondestructive evaluation techniques. Proceedings of SPIE - The International Society for Optical Engineering; 1998.

[121] Thermoelastic stress analysis to detect disbonding in a composite patch. Proceedings of the SEM Annual Conference and Exposition on Experimental and Applied Mechanics 2007; 2007.

[122] Ogawa M, Huang C, Nakamura T. Damage detection of CFRP laminates via self-sensing fibres and thermal-sprayed electrodes. Nondestr Test Eval 2013;28(1):1-16.

[123] Swait TJ, Jones FR, Hayes SA. A practical structural health monitoring system for carbon fibre reinforced composite based on electrical resistance. Compos Sci Technol 2012;72(13):1515-1523.

[124] The role of structural health monitoring for future air vehicles. Collection of Technical Papers - AIAA/ASME/ASCE/AHS/ASC Structures, Structural Dynamics and Materials Conference; 2006.

[125] Derriso MM, Olson SE. The future role of structural health monitoring for air vehicle applications. In: Chang FK, editor. Structural health monitoring 2005 - Advancements and challenges for implementation Lancaster, Pennsylvania: DEStech Publications; 2005. p. 17-25.

[126] Structural Health Management and structural design: An unbridgeable gap? IEEE Aerospace Conference Proceedings; 2008.

[127] MacConnell JH. ISHM and design: A new capability perspective. In: Chang FK, editor. *Structural Health Monitoring 2005 - Advancement and challenges for implimentation* Lancaster, Pennsylvania: DEStech Publications; 2005. p. 1293-1300.

[128] Mistry S, Mofakhami MR, Pinsonnault J. Evolving fuselage designs by incorporating SHM technologies. Aeronaut J 2011;115(1174):749-759.

[129] Chang FK, Markmiller JFC. Composite Design with SHM. In: Chang FK, editor. Structural Health Monitoring 2005 - Advancements and challenges for implimentation Lancaster, Pennsylvania: DEStech Publications; 2005. p. 1309-1318.

[130] Design benefits in aeronautics resulting from structural health monitoring. Proc. of the 6th Internat. Workshop on Structural Health Monitoring, DEStech Publ; 2007.

[131] Schmidt H-, Schmidt-Brandecker B, Tober G. Design of modern aircraft structure and the role of NDI. Insight Non Destr Test Cond Monit 2000;42(3):141-147.

[132] Telgkamp J, Schmidt H. Benefits by the Application of Structural Health Monitoring (SHM) Systems on Civil Transport Aircraft. Structural Health Monitoring 2003:285-292.

[133] Assler H, Telgkamp J. Design of aircraft structures under special consideration of NDT. 9th ECNDT, September 2006:25-29.

[134] Broughton W, Crocker L, Gower M. Design requirements for bonded and bolted composite structures. 2002;MATC(A)65.

[135] Structural Behaviour of Joints. Composites Materials Handbook, Volume 3 - Polymer Matrix Composites - Materials Usage, Design, and Analysis: SAE International; 2012.

[136] Hart-Smith L. An engineer's viewpoint on design and analysis of aircraft structural joints. Proceedings of the Institution of Mechanical Engineers, Part G: Journal of Aerospace Engineering 1995;209(2):105-129.

[137] Hart-Smith L. Bolted and bonded joints. In: Henry SD, editor. ASM Handbook - Volume 21 Composites; 2001. p. 271-289.

[138] Banea M, Da Silva L. Adhesively bonded joints in composite materials: an overview. Proceedings of the Institution of Mechanical Engineers, Part L: Journal of Materials Design and Applications 2009;223(1):1-18.

[139] Federal Aviation Administration. FARS, Part 23, Section 573 - Damage tolerance and fatigue evaluation of structure.

[140] The importance of failure mode identification in adhesive bonded aircraft structures and repairs. International Conference on Composite Materials; 1999.

[141] Hart-Smith LJ. BONDED-BOLTED COMPOSITE JOINTS. J Aircr 1985;22(11):993-1000.

[142] Transport Canada. Advisory Circular - Composite Aircraft Structures. 2004;AC 500-009(1).

[143] Olsson R, Asp LE, Nilsson S, Sjögren A. A review of some key developments in the analysis of the effects of impact upon composite structures. ASTM Spec Tech Publ 2000(1383):12-28.

[144] Matthews FL. Load-carrying joints. In: Middleton DH, editor. Composite materials in aircraft structures; 1990. p. 142-155.

[145] Institution of Structural Engineers. Guide to the Structural Use of Adhesives. ; 1999.

[146] Cook L, Boulic A, Harris D, Bellamy P, Irving PE. Safety Regulation Group - Reliability of damage detection in advanced composite aircraft structures. 2012;Paper 2013/03.

[147] Hart-Smith L. Analysis and design of advanced composite bonded joints. 1974;NASA Langley report CR-2218.

[148] Cambell FC. Secondary Adhesive Bonding of Polymer-Matrix Composites. In: Henry SD, editor. ASM Handbook - Volume 21 Composites: ASM International; 2001. p. 620-632.

[149] Adams RD, Wake WC. Structural adhesive joints in engineering. England: Elsevier Applied Science Publishers Ltd; 1984.

[150] Penado FE, Dropek RK. Numerical Design and Analysis. In: Brinson HF, Dostal CA, editors. Engineered Materials Handbook, Volume 3, Adhesives and Sealents: ASM International; 1990. p. 477-500.

[151] Krieger RB. Adhesive Bonding Design and Analysis. In: Brinson HF, Dostal CA, editors. Engineered Materials Handbook, Volume 3, Adhesives and Sealents: ASM International; 1990. p. 459-470.

[152] Anderson G, DeVries K. Predicting bond strength. The Journal of Adhesion 1987;23(4):289-302.

[153] Ashcroft I, Hughes D, Shaw S. Mode I fracture of epoxy bonded composite joints: 1. Quasi-static loading. Int J Adhes Adhes 2001;21(2):87-99.

[154] Johnson WS, Mall S. A fracture mechanics approach for designing adhesively bonded joints. Delamination and debonding of materials: ASTM International; 1985.

[155] Wahab MA, Ashcroft I, Crocombe A, Shaw S. Prediction of fatigue thresholds in adhesively bonded joints using damage mechanics and fracture mechanics. J Adhes Sci Technol 2001;15(7):763-781.

[156] Volkersen O. Die Nietkraftverteilung in zugbeanspruchten Nietverbindungen mit konstanten Laschenquerschnitten. Luftfahrtforschung 1938;15(1/2):41-47.

[157] De Bruyne N. The strength of glued joints. Aircraft Eng Aerospace Technol 1944;16(4):115-118.

[158] Tsai M, Oplinger D, Morton J. Improved theoretical solutions for adhesive lap joints. Int J Solids Structures 1998;35(12):1163-1185.

[159] Hart-Smith L. Adhesive-bonded double-lap joints. 1973;NASA CR-112235.

[160] Goland M, Reissner E. The stresses in cemented joints. Journal of applied mechanics 1944;11(1):A17-A27.

[161] Kim H, Kedward KT. Stress analysis of adhesively-bonded joints under in-plane shear loading. The Journal of Adhesion 2001;76(1):1-36.

[162] Hart-Smith LJ. Adhesive-bonded single-lap joints. 1973;NASA CR-112236.

[163] Hart-Smith L. Adhesive-bonded scarf and stepped-lap joints. 1973.

[164] Hart-Smith L. Further developments in the design and analysis of adhesive-bonded structural joints. Joining of composite materials: ASTM International; 1981.

[165] Potter D. Primary Adhesively Bonded Structure Technology (PABST).Design Handbook for Adhesive Bonding 1979.

[166] Hart-Smith L. Designing to minimize peel stresses in adhesive-bonded joints. Delamination and debonding of materials.ASTM STP 1985;876:238-266.

[167] Chamis CC, Murthy P. Simplified procedures for designing adhesively bonded composite joints. J Reinf Plast Compos 1991;10(1):29-41.

[168] Song M, Kweon J, Choi J, Byun J, Song M, Shin S, et al. Effect of manufacturing methods on the shear strength of composite single-lap bonded joints. Composite Structures 2010;92(9):2194-2202.

[169] ASTM International. Standard Practice for Classifying Failure Modes in Fiber-Reinforced-Plastic (FRP) Joints. 2012;D5573-99 (Reapproved 2012).

[170] Schmid Fuertes TA, Kruse T, Körwien T, Geistbeck M. Bonding of CFRP primary aerospace structures–discussion of the certification boundary conditions

and related technology fields addressing the needs for development. Composite Interfaces 2015;22(8):795-808.

[171] Effects of flaws and porosity on strength of adhesive-bonded joints. Proc. 29th SAMPE Annual Symposium and Technical Conf; 1984.

[172] Hart-Smith LJ. Adhesively Bonded Joints in Aircraft Structures. In: de Silva LFM, Öchsner A, Adams RD, editors. Handbook of Adhesion Technology: Springer; 2011. p. 1103-1149.

[173] Ramkumar R, Saether E, Cheng D. Design Guide For Bolted Joints In Composite Structures. Design guide for bolted joints in composite structures 1986;ADB108123.

[174] Tate MB, Rosenfeld SJ. Preliminary investigation of the loads carried by individual bolts in bolted joints. 1946;NACA Technical Note No.1051.

[175] Anaglyph. CoDA Component Design Analysis User Manual. 13th ed. Teddington, Middlesex: National Physical Laboratory; 2010.

[176] Hart-Smith LJ. Bolted joint analyses for composite structures–current empirical methods and future scientific prospects. Joining and Repair of Composite Structures 2004:127-160.

[177] Hexcel Composites S. HexPly® M21 product data sheet. 2008;FTA002d.

[178] Tsai SW, Wu EM. A general theory of strength for anisotropic materials. J Composite Mater 1971;5(1):58-80.

[179] Tsai SW, Melo JDD. Composite Material Design and Testing - Unlocking Mystery with Invarients. Stanford: JEC Group; 2015.

[180] Rahman N, Roh H, Qian H, Sun C. Prediction of Failure Strength of Adhesive Joints Using Peel Stress and CTOA. 2011:1720.

[181] ABAQUS Documentation. Version 6.11. : Dassault Systemes Simulia Corp; 2011.

[182] Chamis CC. Simplified procedures for designing composite bolted joints. J Reinf Plast Compos 1990;9(6):614-626.

[183] Adams RD, Harris JA. The influence of local geometry on the strength of adhesive joints. Int J Adhes Adhes 1987;7(2):69-80.

[184] Sutton MA, Orteu JJ, Schreier H. Image correlation for shape, motion and deformation measurements: basic concepts, theory and applications. : Springer Science & Business Media; 2009.

[185] Momber AW, Kovacevic R. Principles of abrasive water jet machining. : Springer Science & Business Media; 2012.

[186] Bardis JD. Effects of surface preparation on the long-term durability of adhesively bonded composite joints. 2002;FAA report DOT/FAA/AR-01/8.

[187] Hart-Smith L, Brown D, Wong S. Surface preparations for ensuring that the glue will stick in bonded composite structures. Handbook of Composites: Springer; 1998. p. 667-685.

[188] The Curse of the Nylon Peel Ply. International SAMPE Symposium and Exhibition: SAMPE SOCIETY FOR THE ADVANCEMENT OF MATERIAL; 1996.

[189] Dillard J. Surface Preperation of composites. In: Brinson HF, Dostal CA, editors. Engineered Materials Handbook, Volume 3, Adhesives and Sealents: ASM International; 1990. p. 281-297.

[190] Cytec Engineered Material. FM-94 Adhesive Film Technical Data Sheet. 2010;AEAD-00003.

[191] Assessing adhesive bond failures: mixed-mode bond failures explained. ISASI Australian Safety Seminar, Canberra; 2010.

[192] Brockmann W, Kollek H. Durability Assessment and Life Prediction for Adhesive Joints. ASM International, Engineered Materials Handbook. 1990;3:663-672.

[193] Kollek H. Weathering and Aging Effects on Adhesive Joints. ASM International, Engineered Materials Handbook. 1990;3:656-662.

[194] Singh R, Zhang M, Chan D. Toughening of a brittle thermosetting polymer: effects of reinforcement particle size and volume fraction. J Mater Sci 2002;37(4):781-788.

[195] Nakamura Y, Yamaguchi M, Kitayama A, Okubo M, Matsumoto T. Effect of particle size on fracture toughness of epoxy resin filled with angular-shaped silica. Polymer 1991;32(12):2221-2229.

[196] Argon A, Cohen R. Toughenability of polymers. Polymer 2003;44(19):6013-6032.

[197] Campilho R, Banea M, Neto J, Da Silva L. Modelling of single-lap joints using cohesive zone models: effect of the cohesive parameters on the output of the simulations. The Journal of Adhesion 2012;88(4-6):513-533.

Appendix

Appendix A1 – Bolted standard double strap joint

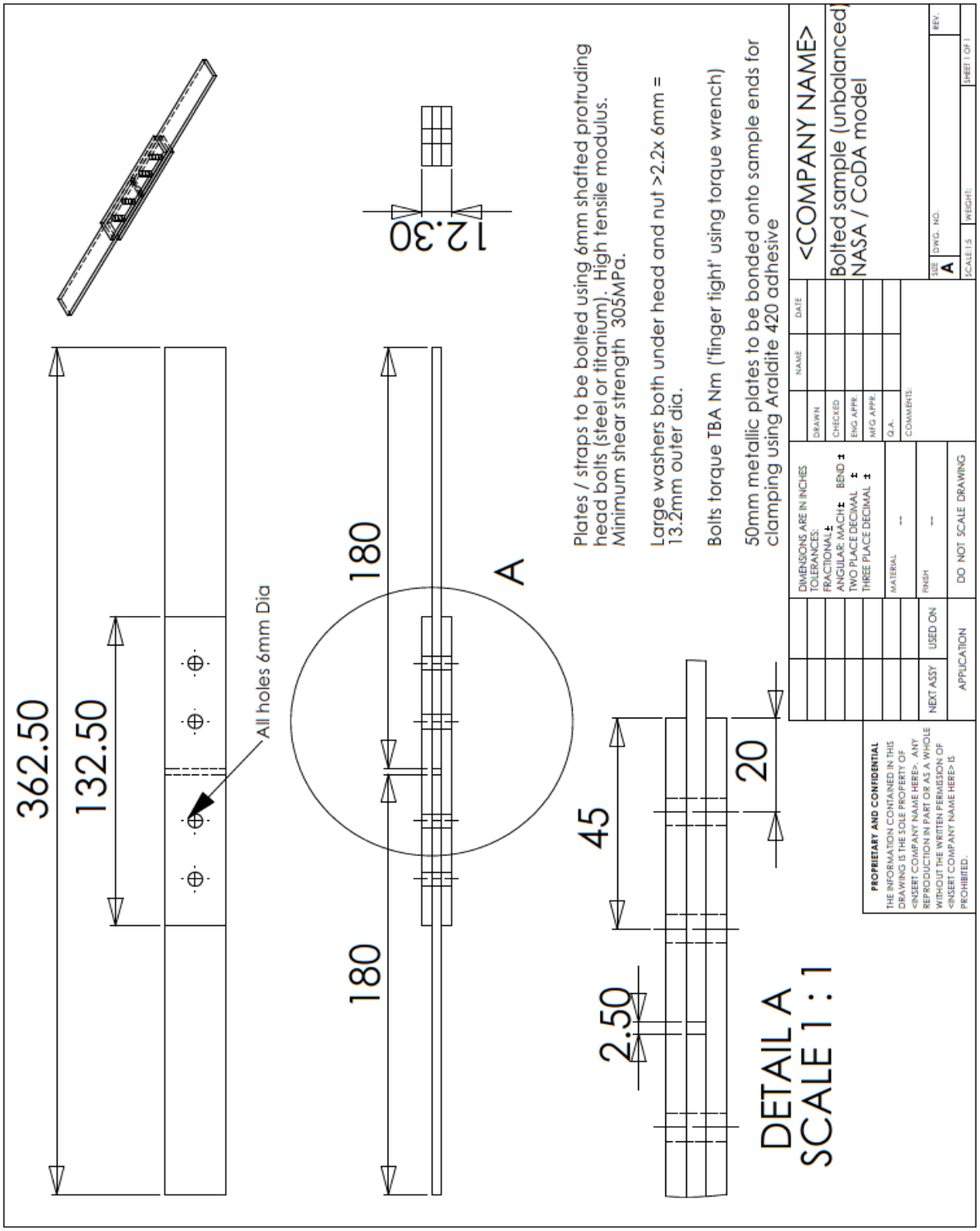

Appendix A2 – 15mm overlap standard double strap joint

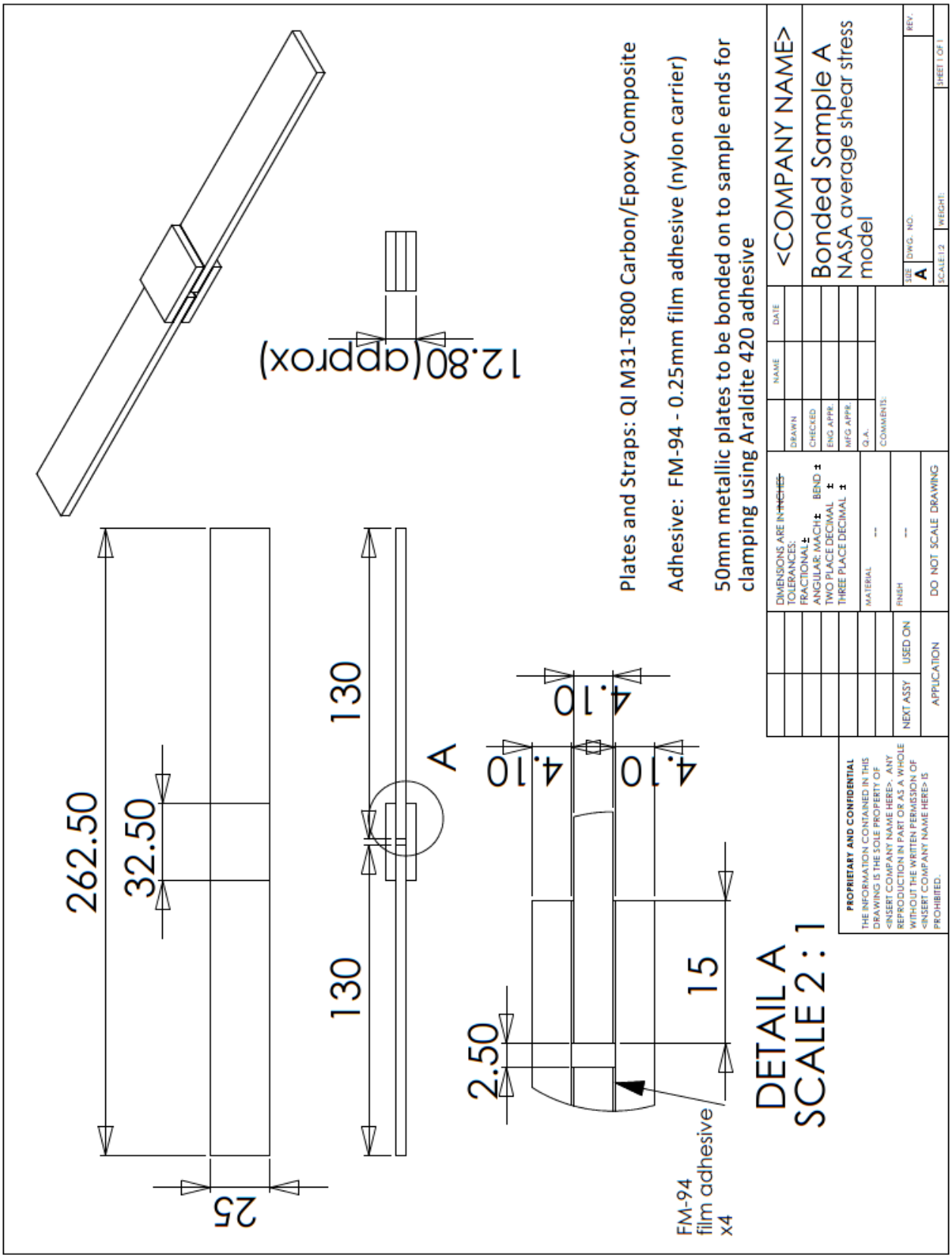

Appendix A3 – 45mm overlap standard double strap joint

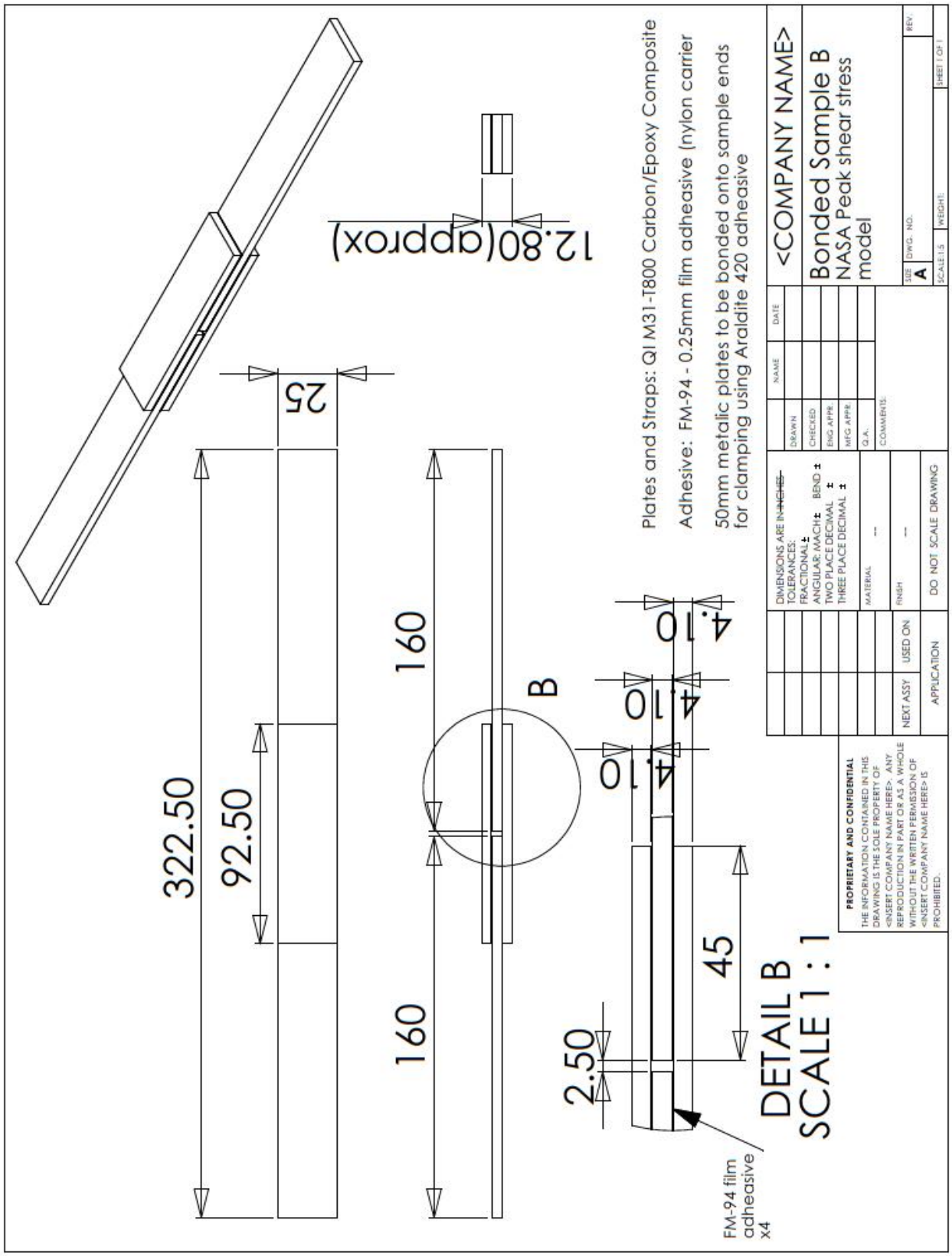

Appendix A4 – 70mm overlap standard double strap joint

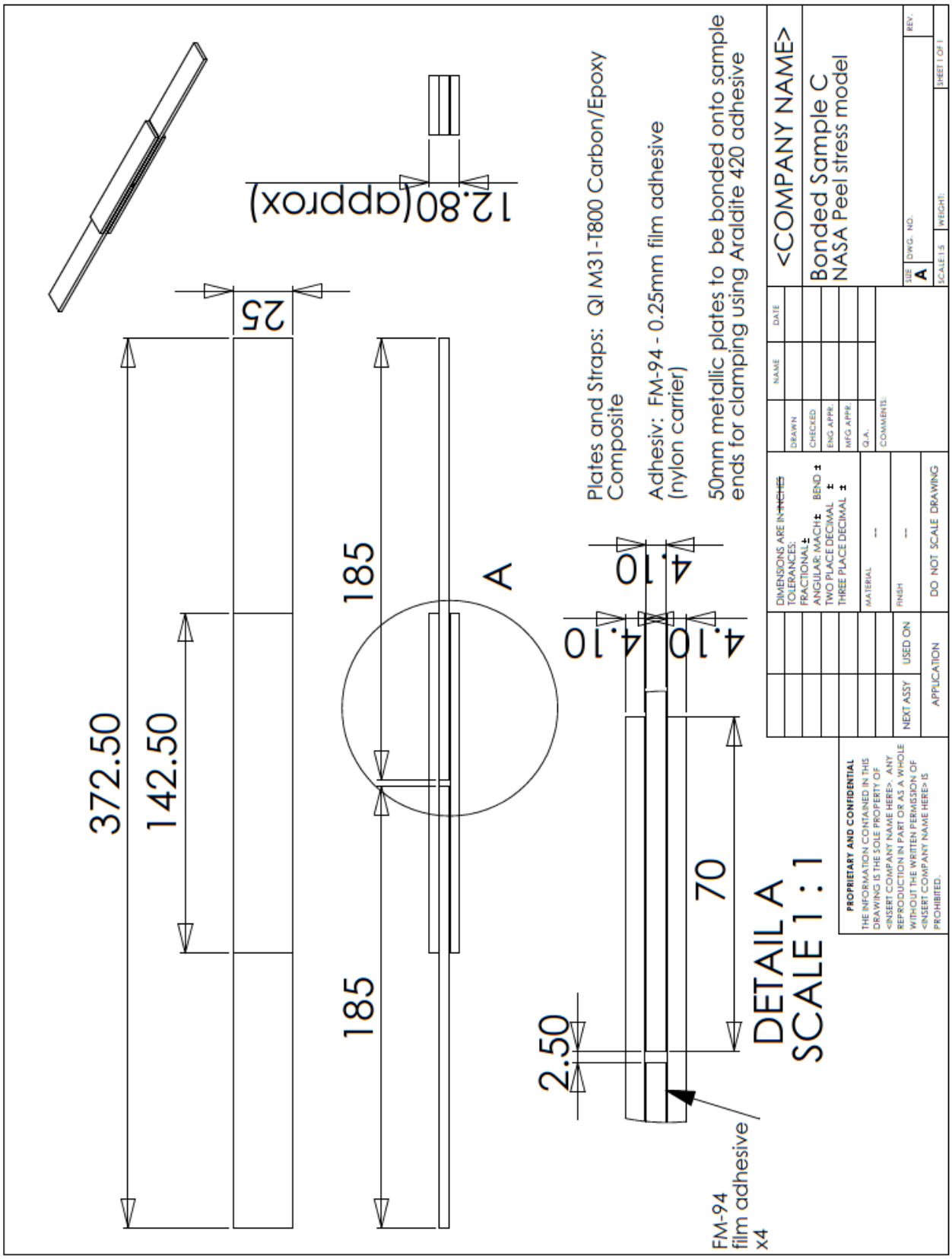

Appendix A5 – ‘Taper’ double strap joint

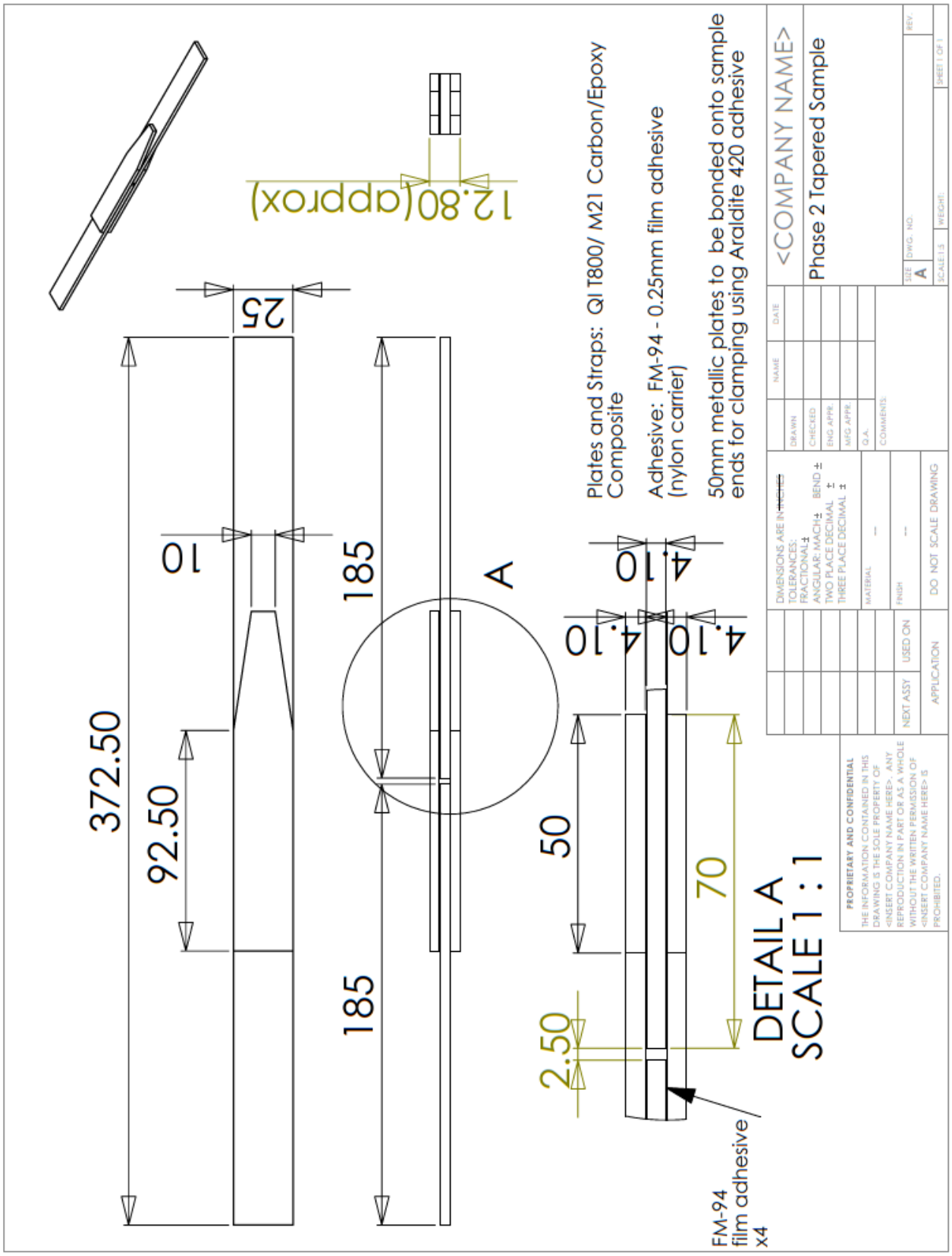

Appendix B – Bond stresses and strains: Standard Joint

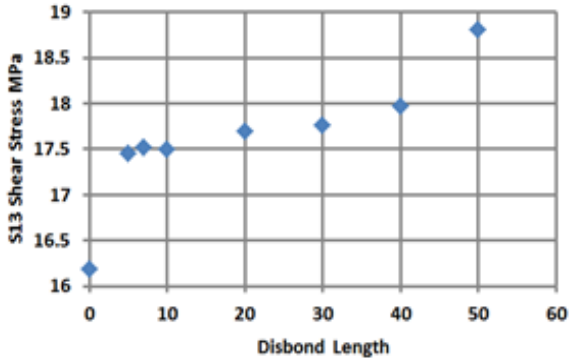

Max Adhesive shear stress values at 10kN loading

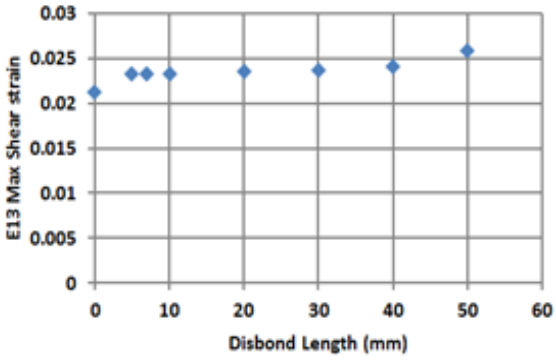

Max Adhesive shear strain values at 10kN loading

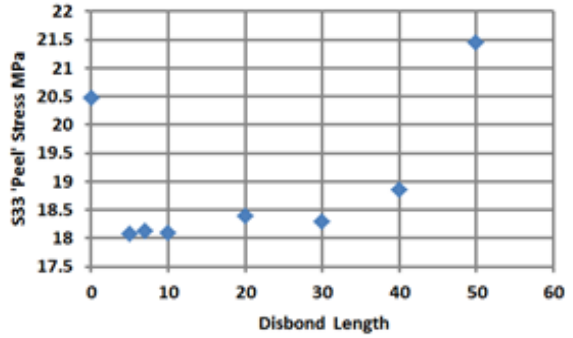

Max Adhesive 'peel' stress values at 10kN loading

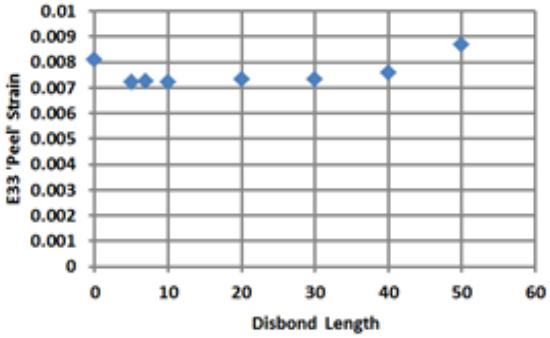

Max Adhesive 'peel' strain values at 10kN loading

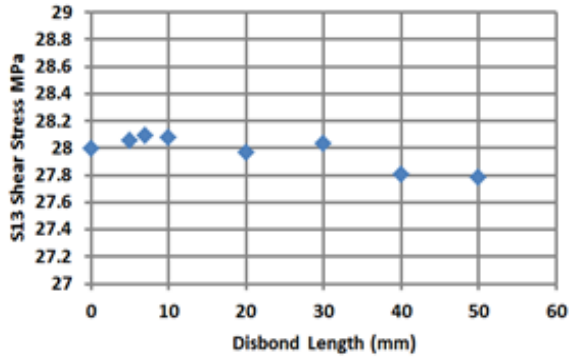

Max Adhesive shear stress values at 30kN loading

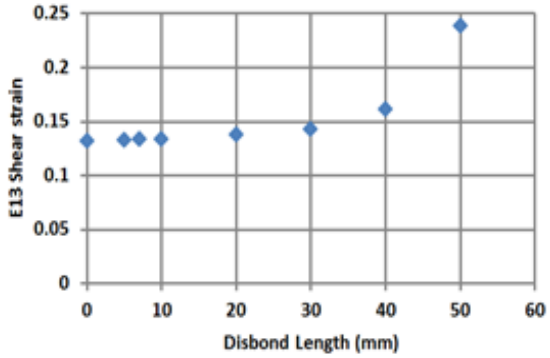

Max Adhesive shear strain values at 30kN loading

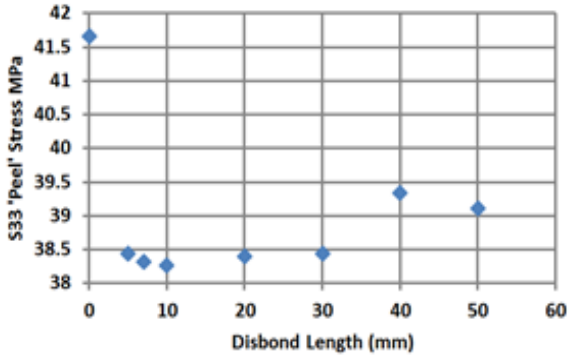

Max Adhesive 'peel' stress values at 30kN loading

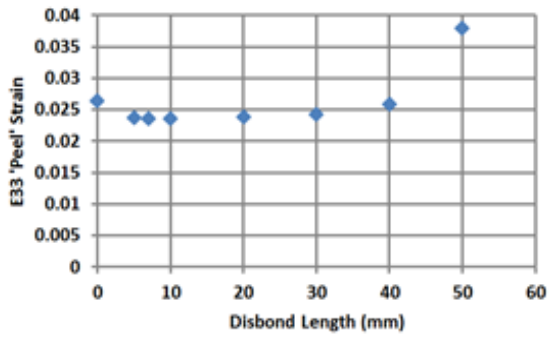

Max Adhesive 'peel' strain values at 10kN loading

Appendix C – Stress / strains: Standard and Tapered joints

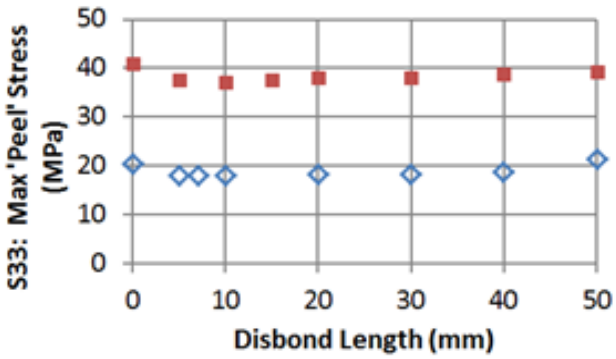

Max FEA Peel stress values at 10kN loading

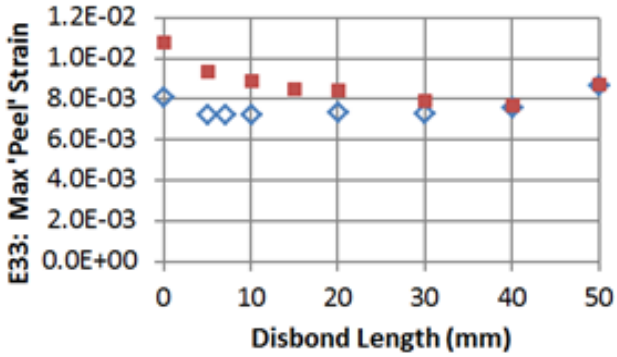

Max FEA Peel Strain values at 10kN loading

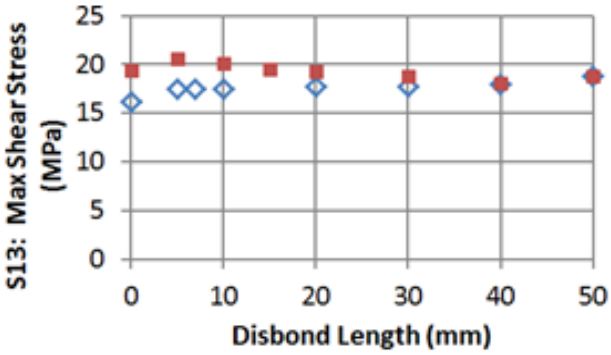

Max FEA Shear stress values at 10kN loading

Blue – Standard Joints (70mm overlap)

Red – Tapered Joints

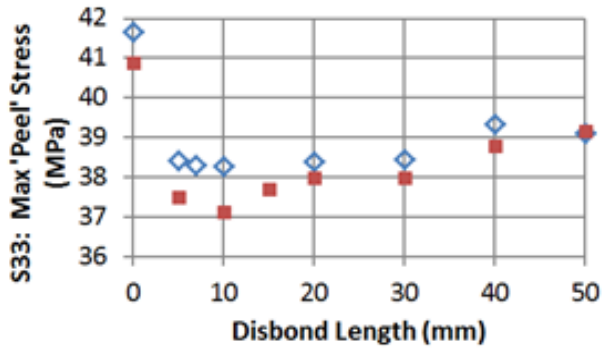

Max FEA Peel stress values at 30kN loading

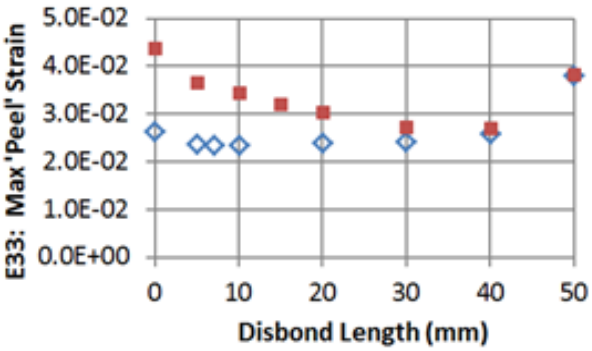

Max FEA Peel Strain values at 10kN loading

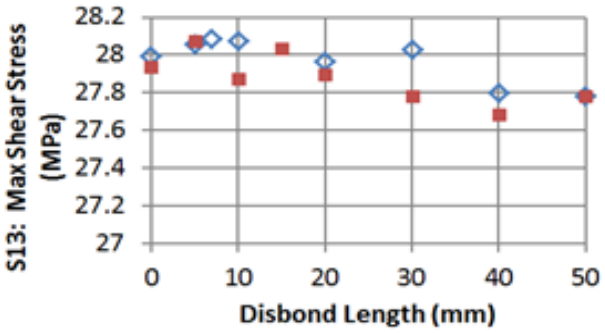

Max FEA Shear stress values at 10kN loading

Appendix D1 – Normalised ratio-metric responses for specimen Taper-2

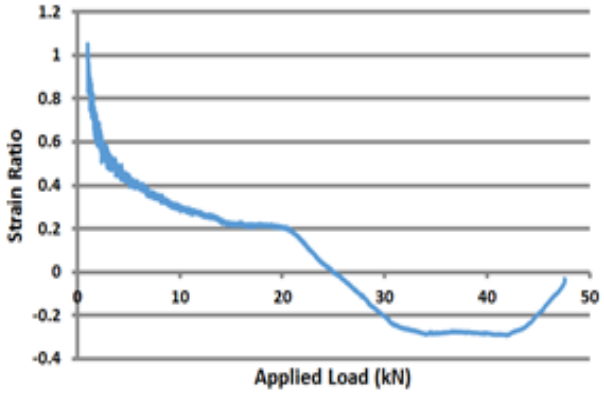

Gauge G1 (4mm) / Virtual reference Gauge

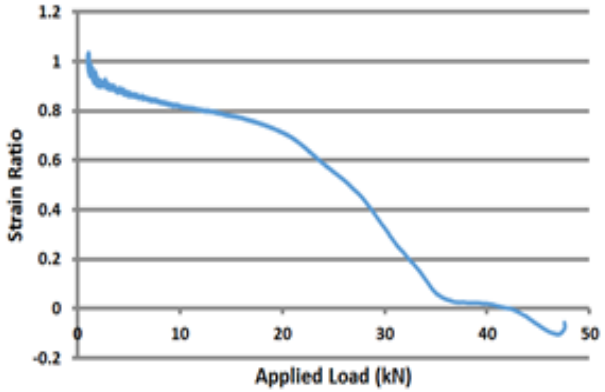

Gauge G2 (10mm) / Virtual reference Gauge

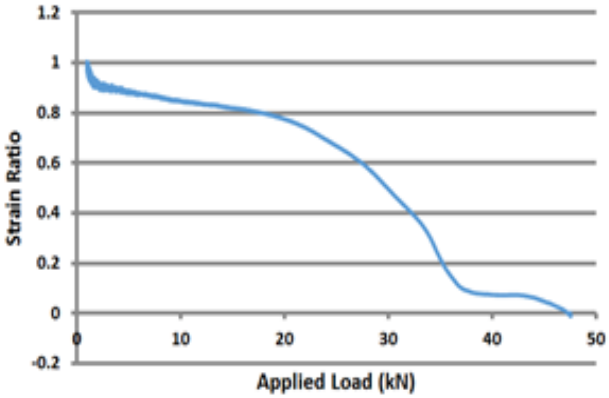

Gauge G3 (15mm) / Virtual reference Gauge

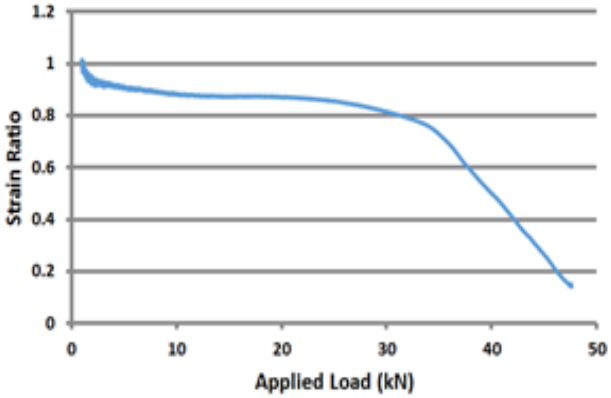

Gauge G4 (30mm) / Virtual reference Gauge

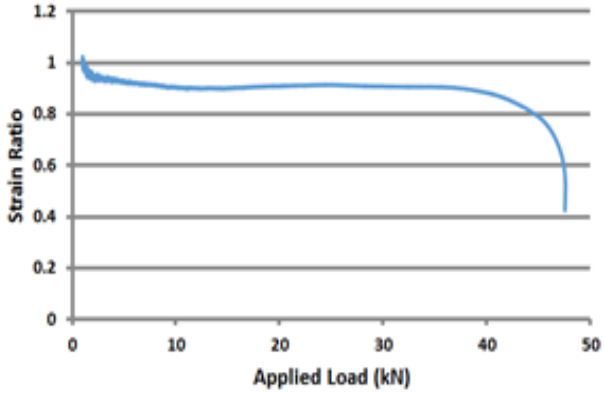

Gauge G5 (45mm) / Virtual reference Gauge

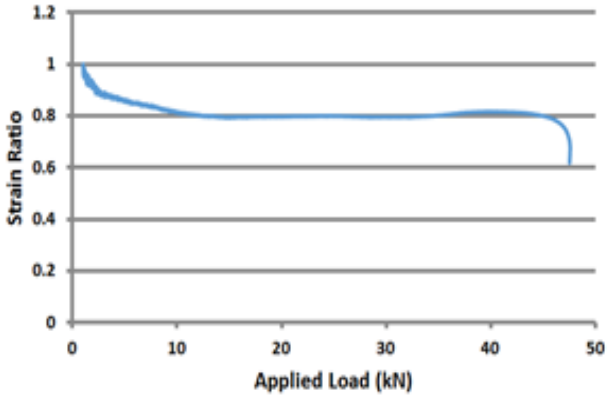

Gauge G6 (51mm) / Virtual reference Gauge

Appendix D2 – Normalised ratio-metric responses for specimen Taper-3

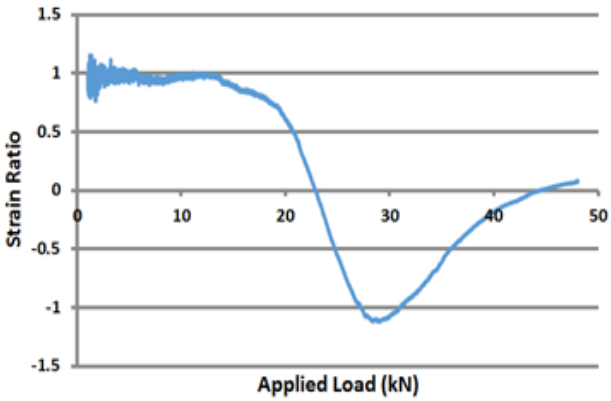

Gauge G1 (4mm) / Virtual reference Gauge

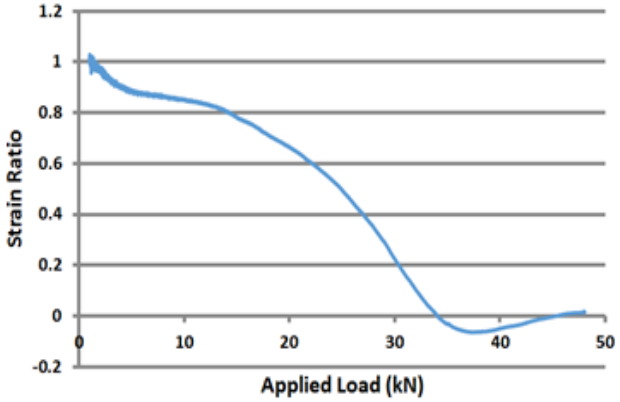

Gauge G2 (10mm) / Virtual reference Gauge

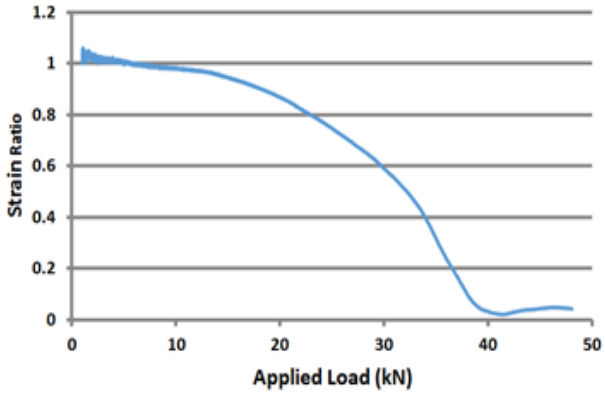

Gauge G3 (15mm) / Virtual reference Gauge

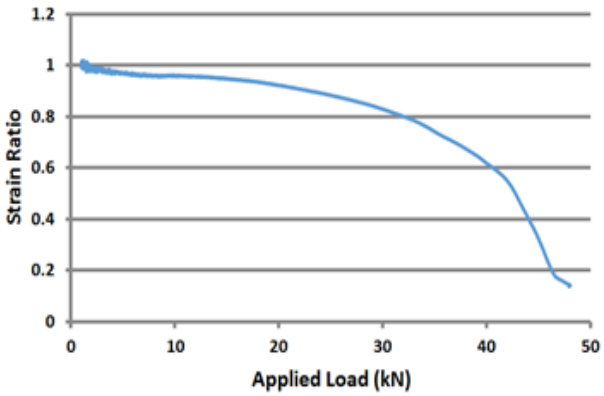

Gauge G4 (30mm) / Virtual reference Gauge

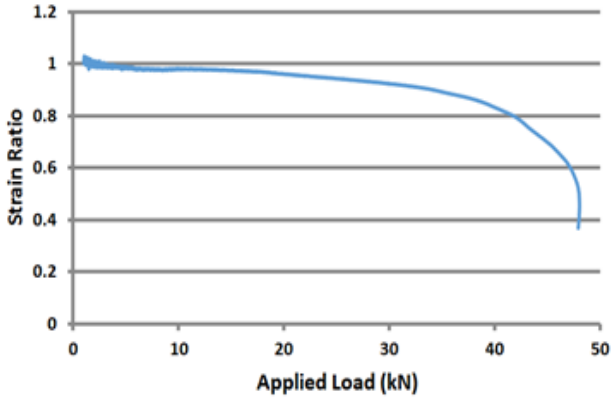

Gauge G5 (45mm) / Virtual reference Gauge

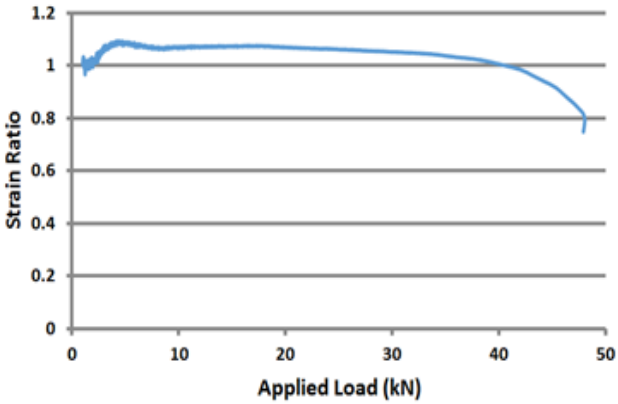

Gauge G6 (51mm) / Virtual reference Gauge

Appendix D3 – Normalised ratio-metric responses for specimen Partition-1

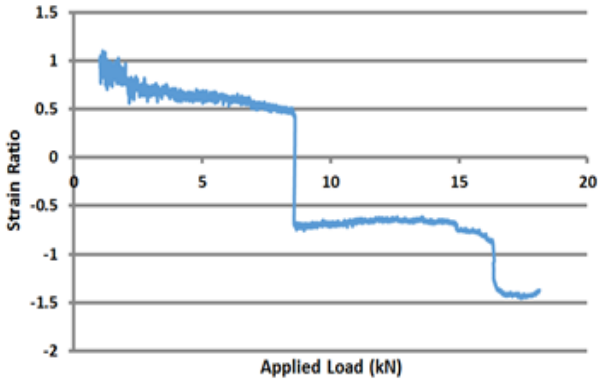

Gauge G1 (9mm) / G6 (65mm) reference gauge

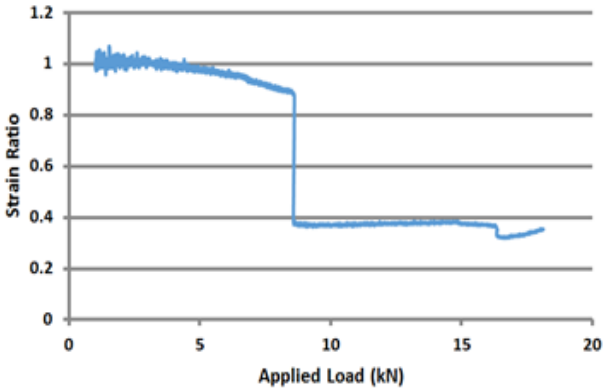

Gauge G2 (16mm) / G6 (65mm) reference gauge

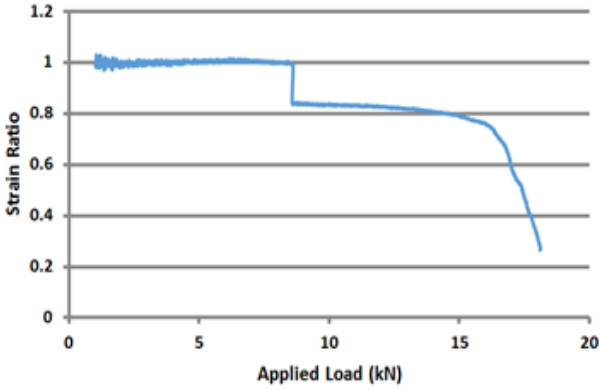

Gauge G3 (24mm) / G6 (65mm) reference gauge

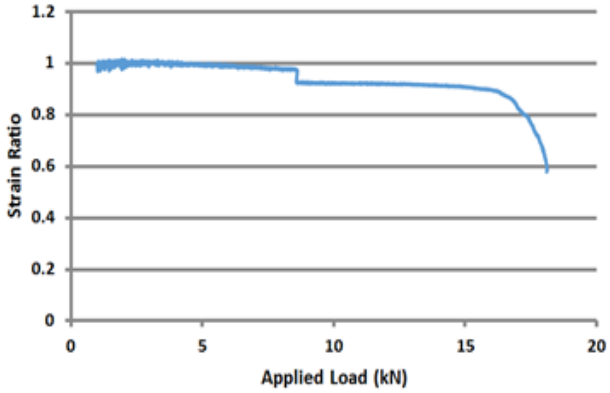

Gauge G4 (31mm) / G6 (65mm) reference gauge

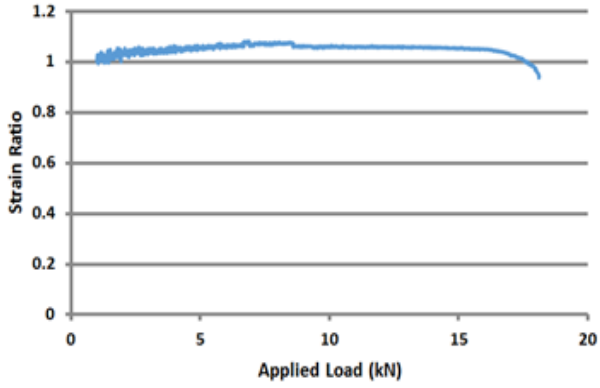

Gauge G5 (40mm) / G6 (65mm) reference gauge

Appendix D4 – Normalised ratio-metric responses for specimen Partition-4

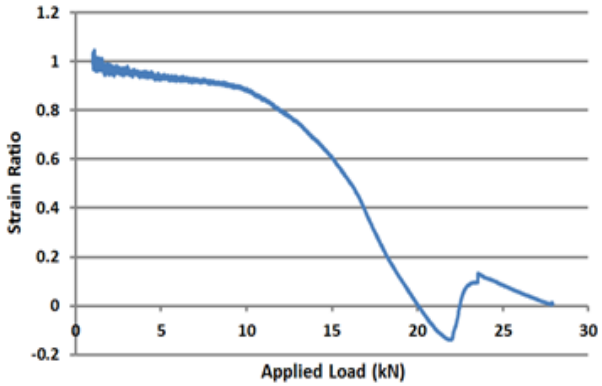

Gauge G1 (9mm) / G6 (65mm) reference gauge

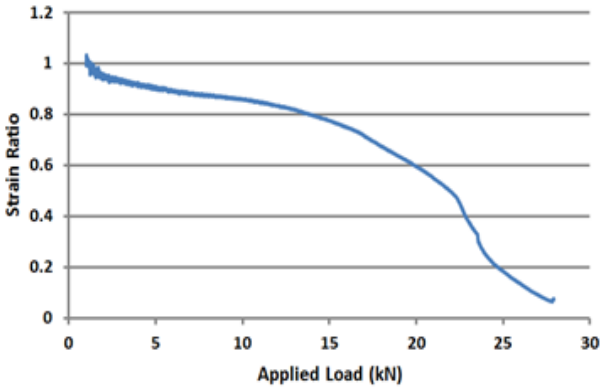

Gauge G2 (16mm) / G6 (65mm) reference gauge

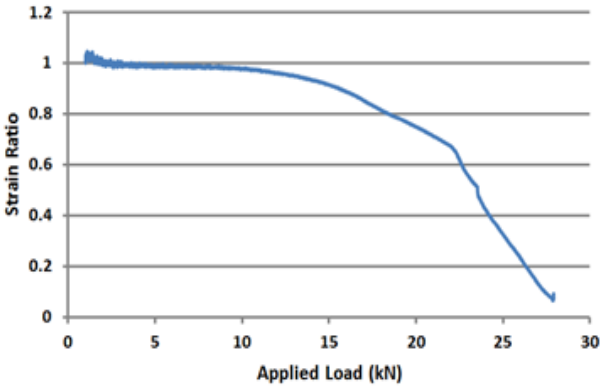

Gauge G3 (24mm) / G6 (65mm) reference gauge

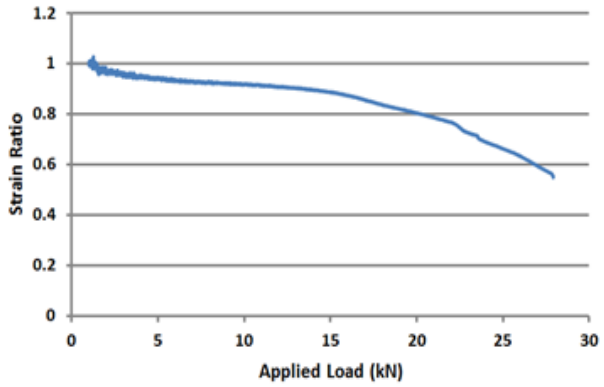

Gauge G4 (31mm) / G6 (65mm) reference gauge

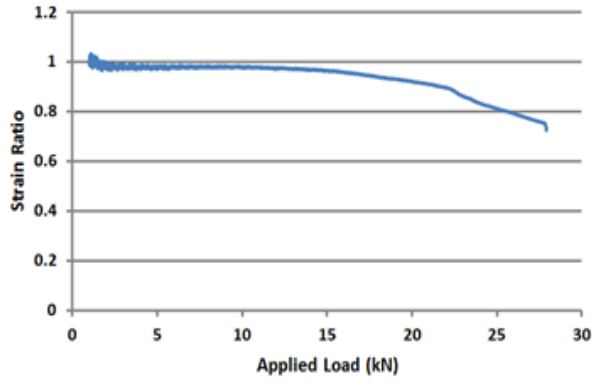

Gauge G5 (40mm) / G6 (65mm) reference gauge

Appendix E – Ratiometric values at each monitoring gauge

Specimen name	Taper-1			G6 not included due to location of RSG				max load (kN)		50.53					
Reference load	13.3 (DLL)														
Monitoring Gauge	Reference Ratio value	90% Reference Ratio		Residual strength		80% Reference Ratio		Residual strength		70% Reference Ratio		Residual strength		60% Reference Ratio		Residual strength	
				kN	% of total			kN	% of total			kN	% of total			kN	% of total
G1 (4mm)	N/A	N/A		N/A	N/A	N/A		N/A	N/A	N/A		N/A	N/A	N/A		N/A	N/A
G2 (10mm)	0.414	0.373		32.47	64	0.3312		28.63	57	0.2898		25.77	51	0.2484		24.38	48
G3 (15mm)	0.562	0.506		28.41	56	0.4496		24.63	49	0.3934		22.33	44	0.3372		20.19	40
G4 (30mm)	0.739	0.665		16.85	33	0.5912		12.72	25	0.5173		10.15	20	0.4434		8.17	16
G5 (45mm)	0.772	0.695		4.24	8.4	0.6176		1.93	4	0.5404		0.54	1	0.4632		0.01	=0

Specimen name	Taper-2			G6 not included due to location of RSG				max load (kN)		47.6					
Reference load	13.3 (DLL)														
Monitoring Gauge	Reference Ratio value	90% Reference Ratio		Residual strength		80% Reference Ratio		Residual strength		70% Reference Ratio		Residual strength		60% Reference Ratio		Residual strength	
				kN	% of total			kN	% of total			kN	% of total			kN	% of total
G1 (4mm)	N/A	N/A		N/A	N/A	N/A		N/A	N/A	N/A		N/A	N/A	N/A		N/A	N/A
G2 (10mm)	0.427	0.384		35.99	76	0.342		25.03	53	0.299		22.74	48	0.256		20.48	43
G3 (15mm)	0.566	0.509		25.86	54	0.453		22.46	47	0.396		19.6	41	0.340		17.63	37
G4 (30mm)	0.733	0.660		15.45	32	0.586		11.9	25	0.513		10.1	21	0.440		8.21	17
G5 (45mm)	0.777	0.699		3.32	7	0.622		1.16	2	0.544		0.31	1	0.466		0.02	=0

Specimen name	Taper-3			G6 not included due to location of RSG				max load (kN)		48.1					
Reference load	13.3 (DLL)														
Monitoring Gauge	Reference Ratio value	90% Reference Ratio		Residual strength		80% Reference Ratio		Residual strength		70% Reference Ratio		Residual strength		60% Reference Ratio		Residual strength	
				kN	% of total			kN	% of total			kN	% of total			kN	% of total
G1 (4mm)	N/A	N/A		N/A	N/A	N/A		N/A	N/A	N/A		N/A	N/A	N/A		N/A	N/A
G2 (10mm)	0.489	0.440		31.1	65	0.391		27.8	58	0.342		25.2	52	0.2934		23	48
G3 (15mm)	0.664	0.598		28.2	59	0.531		24.1	50	0.465		20.7	43	0.3984		17.8	37
G4 (30mm)	0.887	0.798		20.6	43	0.710		14.1	29	0.621		9.9	21	0.5322		6.6	14
G5 (45mm)	0.915	0.824		11.8	25	0.732		5.7	12	0.641		2.7	6	0.549		0.8	2

Specimen name		Taper-4		G6 not included due to location of RSG				max load (kN)	30.6				
Reference load		10.1	Load prior to initial rapid disbond event										
Monitoring	Reference	90% Reference	Residual strength		80% Reference	Residual strength		70% Reference	Residual strength		60% Reference	Residual strength	
Gauge	Ratio value	Ratio	kN	% of total	Ratio	kN	% of total	Ratio	kN	% of total	Ratio	kN	% of total
G1 (4mm)	N/A	N/A	N/A	N/A	N/A	N/A	N/A	N/A	N/A	N/A	N/A	N/A	N/A
G2 (10mm)	0.263	0.237	19	62	0.210	17.8	58	0.184	17.6	58	0.1578	17.6	58
G3 (15mm)	0.485	0.437	17.8	58	0.388	15.7	51	0.340	15.7	51	0.291	14.1	46
G4 (30mm)	0.716	0.644	13.9	45	0.573	13.9	45	0.501	13.9	45	0.4296	13.9	45
G5 (45mm)	0.758	0.682	13.9	45	0.606	13.9	45	0.531	13.8	45	0.4548	4.9	16

Specimen name		Taper-5		G6 not included due to location of RSG				max load (kN)	27.5				
Reference load		12.5	Load prior to initial rapid disbond event										
Monitoring	Reference	90% Reference	Residual strength		80% Reference	Residual strength		70% Reference	Residual strength		60% Reference	Residual strength	
Gauge	Ratio value	Ratio	kN	% of total	Ratio	kN	% of total	Ratio	kN	% of total	Ratio	kN	% of total
G1 (4mm)	N/A	N/A	N/A	N/A	N/A	N/A	N/A	N/A	N/A	N/A	N/A	N/A	N/A
G2 (10mm)	0.324	0.292	14.9	54	0.259	14.4	52	0.227	14.3	52	0.1944	13.3	48
G3 (15mm)	0.53	0.477	14.2	52	0.424	13.1	48	0.371	12.8	47	0.318	12.8	47
G4 (30mm)	0.783	0.705	11.1	40	0.626	9.1	33	0.548	6.4	23	0.4698	4.2	15
G5 (45mm)	0.835	0.752	Fail	Fail	0.668	Fail	Fail	0.585	Fail	Fail	0.501	Fail	Fail

Specimen name		Partition-2						max load (kN)	20.5				
Reference load		11	Load prior to initial rapid disbond event										
Monitoring	Reference	90% Reference	Residual strength		80% Reference	Residual strength		70% Reference	Residual strength		60% Reference	Residual strength	
Gauge	Ratio value	Ratio	kN	% of total	Ratio	kN	% of total	Ratio	kN	% of total	Ratio	kN	% of total
G1 (9mm)	0.26	0.234	9.5	46	0.208	9.5	46	0.182	9.5	46	0.156	9.5	46
G2 (16mm)	0.69	0.621	9.1	44	0.552	9	44	0.483	7.6	37	0.414	7.5	37
G3 (24mm)	0.77	0.693	8.4	41	0.616	7.5	37	0.539	7.5	37	0.462	6.2	30
G4 (31mm)	0.836	0.752	7.5	37	0.669	4.8	23	0.585	4.5	22	0.502	4.3	21
G5 (40mm)	0.867	0.780	4.5	22	0.694	4	20	0.607	4	20	0.520	4	20